SOUTH EAST TECHNOLOGICAL UNIVERSITY

PHD THESIS

Evaluation of the metal additive manufacturing process through the study of the recyclability of metal powders and in-situ monitoring

---

Author:
Paul QUINN

Supervisors:
Dr. Ramesh RAGHAVENDRA
Dr. Jim LAWLOR

March 16, 2024

Declaration of Authorship

I, Paul QUINN, hereby declare that this thesis titled, "Evaluation of the metal additive manufacturing process through the study of the recyclability of metal powders and in-situ monitoring" is entirely my own work and does not contain work work published by any other author, except where due reference or acknowledgement has been made. Furthermore, I declare that this document has not been previously submitted to any other institution for any other academic award.

Signed:

Date:

SOUTH EAST TECHNOLOGICAL UNIVERSITY

Abstract

Department of Engineering Technology

Doctor of Philosophy

Evaluation of the metal additive manufacturing process through the study of the recyclability of metal powders and in-situ monitoring

by Paul QUINN

Laser powder bed fusion (L-PBF) processes are becoming frequently applied within a wide range of industries. Enabling the production of complex, high-value components, within the medical device and aerospace industries where regulations drive the requirement for stringent quality control. Powder material used in the L-PBF process can be costly, and as it is rare for a full batch of virgin powder to be used in one build, it is frequently recycled for subsequent builds. Therefore, it is useful to characterise both the powder material being recycled and the final printed component properties. Characterisation of the recycled powder and the parts allows the feasibility of powder recycling to be assessed. Methods required to extend the utility of a single batch of powder through a process called powder rejuvenation are also investigated. Thus, quantifying the effectiveness of allowing a previously recycled powder to be utilised further in the L-PBF process. With an understanding of the effect of recycling and rejuvenation processes on the powder and the manufactured part properties an empirical model for the prediction of the part density and surface roughness are developed. This allows the user to input the current powder characteristics to predict the manufactured part qualities. Furthermore, the ability to monitor components as they are being built layer-by-layer enables their quality to be assessed. Using in-situ monitoring, the identification of defects as well as measurement of the layers throughout a build allows for greater quality control, as well as a reduction in the requirement for ex-situ measurement. Results from this work provide L-PBF operators with understanding of the effect that recycled and rejuvenating of powders have on the quality of the components produced. Also providing a method to monitor the component layer-wise throughout the process. This will facilitate a more controlled use of L-PBF within the highly regulated industries.

Acknowledgements

I would like to express my gratitude to all those who have been instrumental in the completion of this thesis. This journey would not have been possible without the unwavering support and encouragement of many people.

First and foremost, I am deeply indebted to my supervisors, Dr Ramesh Raghavendra and Dr Jim Lawlor, for their guidance, support, and dedication to my project. Their expertise, patience, and continuous support have been invaluable throughout this PhD.

I extend my appreciation to my colleagues at SEAM Research Centre and South East Technological University, Waterford Campus who have provided resources and offered assistance in various aspects of this research. Your camaraderie and collaboration have made this academic journey not only productive but also enjoyable. I would especially like to thank Dr Sinéad Uí Mhurchadha for her support throughout the project, providing an open-mind to share and prospect ideas.

I would also like to acknowledge the financial support provided by Irish Manufacturing Research, which made this research possible. Their support for this thesis highlights their commitment to remain at the cutting edge of this rapidly developing technology.

I want to thank my, Mam, Dad and sister, Becky, who have always been by my side throughout this project. Your support, understanding and love providing some respite from the pressures of academia and maintaining a level of balance within my life.

Last but by no means least, I want to thank my beautiful girlfriend, Karen, who has always provided me with love, support and encouragement throughout the entirety of my academic career. I am certain I would not have been able to get this far without your support.

Thank you all!

Contents

List of Figures

List of Tables

List of Abbreviations

%wt	Weight Percentage
2D	Two-Dimensional
316L	Stainless Steel (Low Carbon)
3D	Three-Dimensional
AM	Additive Manufacturing
Ar	Argon
ASTM	American Society for Testing and Materials
AUT	Average Use Time
BFE	Basic Flow Energy
CAD	Computer Aided Design
CFD	Computational Fluid Dynamics
CMOS	Complementary Metal Oxide Semiconductor
CNC	Computer Numerical Control
COD	Crystallography Open Database
Cr	Chromium
CT	Computed Tomography
CuCl2	Copper Chloride
DMLD	Direct Metal Laser Deposition
DMLS	Direct Metal Laser Sintering
DSLR	Digital Single Lens Reflex
EBM	Electron Beam Melting
ED	Energy Density
EDF	Empirical Distribution Function
EDX	Energy Dispersive X-Ray
FCC	Face Centred Cubic
Fe	Iron
FEA	Finite Element Analysis
GA	Gas Atomisation
GP1	Stainless Steel
HAZ	Heat Affected Zone
HCL	Hydrochloric Acid
HNO3	Nitric Acid
HR	Hausner Ratio
HRB	Rockwell B Hardness
ICDD	International Centre for Diffraction Data
IMR	Irish Manufacturing Research
ISO	International Standards Organisation
k-s	Kolmogorov-Smirov Test
L-PBF	Laser Powder Bed Fusion

LCI	Low Coherence Interferometry
LSD	Line Segment Detection
MLR	Multiple Linear Regression
Mn	Manganese
MP	Megapixel
MPS	Mean Particle Size
N	Nitrogen
NDT	Non-destructive Testing
Ni	Nickel
O	Oxygen
OM	Optical Microscopy
PBF	Powder Bed Fusion
PSD	Particle Size Distribution
Ra	Arithmetic Mean (Surface Roughness)
RPM	Revolutions Per Minute
Rz	Ten Point Average (Surface Roughness)
SEAM	South Eastern Applied Materials
SEM	Silicon
SLS	Selective Laser Sintering
VIF	Variance Inflation Factor
WA	Water Atomisation
XMT	X-Ray Micro-Computed Tomography
XRD	X-Ray Diffraction
Yb	Ytterbium

Thesis Nomenclature

Parameter	Symbol	Units
Austenite	γ	-
Laser Power	P_P	W
Scan Speed	S_s	mm/s
Layer Height	L_H	μm
Hatch Distance	H_d	mm
Density	ρ	g/cm^3
Variance of Sample Error	σ_{SE}	-
Mean Extreme Diameter	d	cm
Sample Mass	M_s	g
Wavelength	λ	nm
Particle Perimeter	P_P	μm
Particle Area	A	μm^2
Numerical Value for Hardness Scale	N	-
Measure Depth of Indentation	h	mm
Scaling Constant for Hardness	S	mm
Hardness Pre-Load	F_0	N
Hardness Test Load	F_1	N
Build Time	t_i	$hours$
Quantity of Virgin Powder	q_0	kg
Quantity of Recycled Powder	q_i	kg
Standard Deviation	σ	-
Sample Size	n	-
Predicted Response Value	Y_i	-
Predictor Value	X_i	-
Slope Coefficient	β	-
Intercept Value	α	-

1 Introduction

The growing success of additive manufacturing (AM) technologies within industry is due to the opportunity to produce complex components near-net-shape within a single manufacturing process. The conventional subtractive manufacturing methods are challenged and by the process of adding material layer-by-layer, a three-dimensional (3D) model is produced. Subtractive methods are still necessary for production, however, not to the extent that was traditionally required. Additive manufacturing has great potential for the manufacturing industry and extensive research has been put into the technology. The sophistication of AM will develop, as the understanding of the relationships between the material, process conditions and final component properties are investigated.

1.1 Background and Motivation

This research aims to examine the issues emerging from the increasing adoption of the additive manufacturing (AM) process within industry. AM, or more commonly known as '3D Printing', has developed rapidly since its original development in the 1980s. The process was initially developed through the combination of polymer processing with laser technologies and computer aided design (CAD). Initially the focus was to apply the technology for rapid prototyping using polymer materials. As with all developing technologies the range of applications, materials and processes has progressed.

In the short time since its initial development the process has matured in a number of ways. Less-costly, desktop polymer machines are more accessible to the general public, making additive technologies available to both industry and hobbyists. A broader range of materials are available. One of the most significant advancements in the technology was the development of the ability to additively manufacture metallic parts.

As with the development of all new technologies many early challenges emerged, while these are progressively being overcome some still exist. The metal AM process is costly to establish. The feedstock powder material is costly to produce meaning that high level of powder utilisation in the process is extremely important. Another current drawback of the process is the occurrence of in-process defects. These are often not identified until after the products have been fabricated, and even then only after lengthy and costly non-destructive testing (NDT) has been completed. The freedoms of the AM process also results

in challenging products with features and specifications that can be difficult to assess using traditional inspection methods.

The powder material (metal) for the process is produced through atomisation and as a result is expensive, costing up to €500/kg for titanium alloys for example; therefore, recycling the powder for subsequent builds is desirable (Cordova, Campos, and Tinga, 2019). Powder recycling is defined as "the practice of collecting the un-melted powder after a build and reusing it for subsequent builds" (Jacob et al., 2017). The process of recycling leads to changes in the powder characteristics as well as affecting the quality of the parts produced (Sutton et al., 2016b; Jacob et al., 2017). The industries applying laser powder bed fusion (L-PBF) are often required to adhere to stringent quality procedures and standards. Hence, understanding how the feedstock metal powder evolves through the recycling process is required to maintain full traceability within the AM process, while increasing the usable life of a costly consumable (Singh, Ramakrishna, and Singh, 2017; Vafadar et al., 2021).

The ability to monitor the quality of the parts as they are being produced is also a requirement for many of these regulated industries. This area of research has been identified as one in need of significant research attention (Mani et al., 2016). Using in-situ monitoring allows for in-process defects to be identified and quantified during the build process (Everton et al., 2016). Quantifying the defect can allow for a decision to be made on the impact on the integrity of the finished part. The application of in-situ monitoring can also be used to observe the consistency of the powder deposition process in laser powder bed fusion (L-PBF). Consistent and repeatable powder deposition is vital for the successful outcome of the process (Zielinski et al., 2017).

A lack of quality assurance in additive manufacturing is currently a technological barrier for manufacturers to adopt additive processes (Everton et al., 2016; Vafadar et al., 2021). Monitoring the powder material through the multiple stages of recycling and adopting an in-situ monitoring system within the L-PBF process enables quality assurance for the raw material and the final parts.

1.1.1 South Eastern Applied Materials Research Centre

This research is being conducted in the South Eastern Applied Materials (SEAM) Research Centre based in South East Technological University, Waterford Campus. SEAM is an industry focused applied research and development centre, partly funded under the Enterprise Ireland Technology Gateway Programme. The centre provides innovative materials engineering solutions to a wide range of research and industrial partners across Ireland. This ranges from materials characterisation and failure analysis to non-destructive testing as well as having capabilities for metal additive manufacturing and engineering simulation utilising Finite Element Analysis (FEA) and Computational Fluid Dynamics (CFD). SEAM aims to translate the potential of metal AM to Irish companies, through research and development as well as utilising its dedicated AM training centre 3DWIT. SEAM's AM capabilities include an EOS M280 and M100 L-PBF machines and a range of equipment required to compliment the AM

process. A full suite of material and powder characterisation equipment is also present within the research centre.

1.1.2 Irish Manufacturing Research

This research is being carried out in conjunction with (and funded by) Irish Manufacturing Research (IMR) which has identified the AM process as a potentially 'game changing' process for the current manufacturing industry within Ireland. IMR's vision is to enable Irish manufacturing industries to be world leaders in advanced manufacturing through research and development, training and technology enablement. Their establishment of the Advanced Manufacturing Ireland Centre in the National Science Park, Mullingar aims to provide manufacturing companies in Ireland with the support they need to prepare for the next generation of manufacturing processes. IMR's metal AM capabilities include a Renishaw 500M system and a SLM 280 system as well as post-processing equipment such as CNC machining, surface finishing equipment and mechanical testing facilities.

1.2 Project Goals and Objectives

1.2.1 Research Questions

The aim of this research can be summarised into the following research questions;

What are the key factors in powder recycling and rejuvenation processes that influence powder characteristics and resulting part qualities, and how an understanding of these factors can extend the usable lifespan of the costly powder material?

and

Can a defect detection system be retrofitted to a L-PBF machine to identify and monitor emerging part defects resulting from the powder deposition process?

1.2.2 Research Aims

The primary aims of this research project are to evaluate the metal additive manufacturing process of Laser Powder Bed Fusion (L-PBF) through the study of powder recylability and in-situ monitoring. More specifically these aims are:

1. Evaluate the effect of powder recycling on the powder characteristics and resulting part qualities.
2. Evaluate the effect of powder rejuvenation processes for recycled powder material.
3. Develop and test an empirical model for the prediction of L-PBF part properties using recycled powders.

4. Develop and integrate a standalone monitoring system within the EOS M280 machine to identify and monitor emerging part defects within the L-PBF process.

1.2.3 Project Scope

The scope of this research is to evaluate the additive manufacturing process through the study of the recyclability of a common stainless steel powder for additive manufacturing in terms of its affect on the powder characteristics and part qualities. Over the lifetime of the powder these characteristics will be tracked and evaluated. The research will further assess the ability for powder rejuvenation processes to manage and increase the utilisation of recycled powders. The results from these studies will be utilised to build an empirical model to be used by L-PBF users to predict output qualities from a given batch of powder. The models will be built using multiple linear regression, to predict the surface roughness and part density of the parts produced based on the input powder characteristics. The metal AM process will be further evaluated through the use of in-situ monitoring for layer-by-layer monitoring of the powder layering process and parts produced.

1.3 Document Outline

The thesis is structured in the manner shown in Figure 1.1. Chapter 1 details the research aims and goals as well as providing some brief background to the projects and its stakeholders.

Chapter 2 provides the reader with a greater understanding of the metal AM processes that fall within the process category of Powder Bed Fusion. Detailing their operating principals, the raw materials required for this process category and concluding with some current industrial applications. Chapter 3 presents a detailed literature review summarising the current state-of-the-art in the research area of recyclability of metal powders and in-situ monitoring. Chapter 4 reviews the methods implemented throughout the duration of the project. These include the methods for powder and part characterisation, defect detection system and statistical methods. More specific experimental methodologies used in the research are discussed in the relevant chapters.

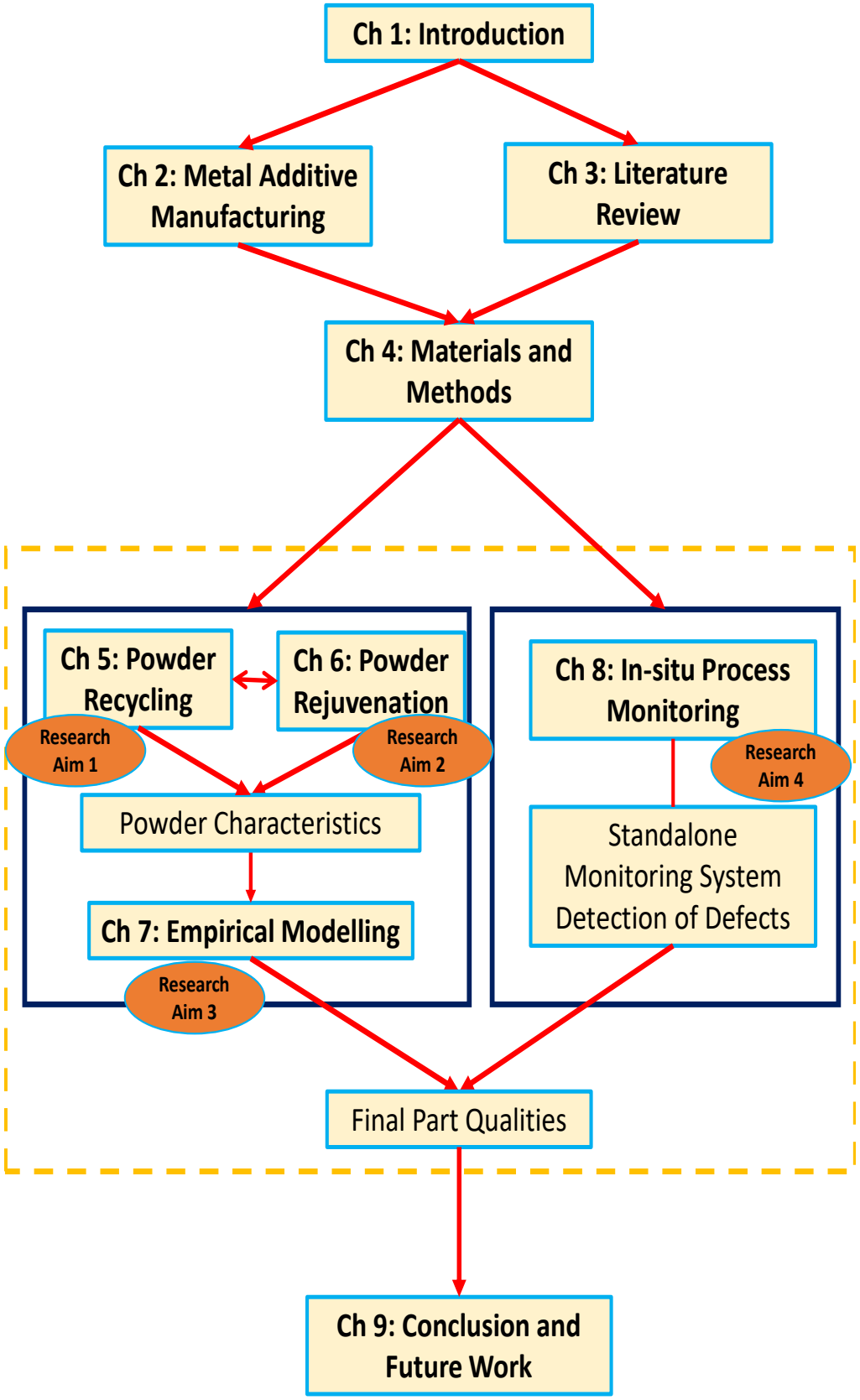

FIGURE 1.1: Flowchart for the structure of the thesis.

Chapter 5 presents an in-depth review of the powder recycling process, which can allow for continued use of a single powder batch. This can also introduce unwanted powder characteristics, thus impacting the manufactured part properties. To develop an understanding of this impact it is essential to characterise both the powder material as it is recycled and the final L-PBF part properties. This allows for the feasibility of powder recycling to be assessed. Powder characteristics, such as particle size and shape, density, flowability and chemical composition, are tracked throughout a series of powder recycling stages. Final part properties, such as hardness, density, surface roughness and dimensional accuracy, were monitored throughout the same process. This ensured that the effect of the powder recycling process on the characteristics and final part properties is understood in detail.

This powder recycling process can continue until the powder characteristics reach an unfavourable level or the remaining quantity of powder is insufficient for future builds. Chapter 6 investigates a common method to increase the utilisation of a single batch of powder material through the addition of virgin powder at a predefined ratio in a process coined "powder rejuvenation". This work also investigates the further recycling process after powder rejuvenation has occurred, for which the same quantity of virgin powder material is added to the remaining recycled powder material. The effect of the process on the powder material, as well as the resulting part properties is defined.

The understanding of the effect of recycling and rejuvenation processes on the powder characteristics and the resulting manufactured part properties can be used to assist technology adopters in the successful use of L-PBF. Empirical models are used in a host of manufacturing processes and routines to allow for outputs to be predicted based on a series of input factors. In Chapter 7 empirical models for the prediction of the part density and surface roughness, based on the observations and results from this work are developed. These models are built using a multiple linear regression allowing for users to input the powder characteristics, such as particle size, shape and average use time, to predict the resulting part density and surface roughness. These models can act as another tool in the AM process to ensure the expected resulting part properties meet the required specifications based on the input powder characteristics.

Furthermore, the ability to monitor the components as they are being built layer-by-layer during the process enables real-time quality assessment. While modern L-PBF machines include advanced monitoring capabilities with additional feedback control loops, older machines do not possess the computing power possible to process such data in real-time. With a vast number of older machines still used in a production capacity today, Chapter 8 presents a standalone "plug-and-play" type in-situ monitoring system and defect detection tool. This system operates independently of the L-PBF machine to ensure there is no impact on the processing of the build instructions. The developed defect detection process enables the operator to be alerted of defects in the process and react accordingly. The standalone system allows for the identification of defects related to the powder deposition process in an EOS M280. Hence, allowing for greater quality control, reducing the requirement for ex-situ testing

of manufactured parts. The system also catalogues the entire build process, assisting regulated industries in the control and validation of L-PBF processes.

Chapter 9 summarises the key findings from the work completed and outlining the conclusions and implications drawn from those findings. Results from this work provide L-PBF technology users with a detailed understanding of the effect that recycling and rejuvenating of powders have on the quality of the manufactured parts. The developed empirical models also assist in moving the L-PBF process towards a zero-defect manufacturing process. The developed in-situ monitoring system provides older L-PBF equipment with a method to monitor the component layer-wise without impacting the operation of the process. The work presented in this thesis provides a depth of knowledge of the L-PBF that will transform the industry by allowing for the prediction of part as well as in-situ part validation, reducing the requirements for large scale round-robin testing of AM parts. Further work to expand the completed research is also presented.

1.4 Project Dissemination

Dissemination of the results presented in this thesis begin in 2018 at the 35th International Manufacturing Conference with a conference presentation and extended abstract presenting the results of an initial study on the effect of the powder recycling process on the powder and part characteristics. This study was continued to produce the results published in the Advances in Materials and Processing Technologies journal paper in 2019. The standalone in-situ monitoring system was designed to elicit data from the process to evaluate real-time performance and was presented at Solid Freeform Fabrication conference in 2019. The initial study of powder recycling was further extended in 2020 to investigate the concept of powder rejuvenation. Attempting to bring the various strands of the work together including recycling, rejuvenation, and in-situ monitoring system development in 2022 an empirical model was developed and validated to predict finished part properties based on the input powder characteristics. This study was published in journal article in MDPI Metals in 2022. The conference publications and journal articles have been subjected to the peer review process, several of the conference publications have been award winning submissions, including the initial powder recycling paper presented at IMC35, in 2018, the thesis summary paper presented at the Sir Bernard Crossland symposium in 2019 and the empirical modelling paper presented at IMC37 in 2021.

1.4.1 Journal Articles

P. Quinn, S.M. Uí Mhurchadha, J. Lawlor, and R. Raghavendra (2022). "Development and Validation of Empirical Models to Predict Metal Additively Manufactured Part Density and Surface Roughness from Powder Characteristics". In: *MDPI Materials* 15, pp. 4707-4722. https://doi.org/10.3390/ma15134707.

P. Quinn, S. O'Halloran, J. Lawlor, and R. Raghavendra (2019). "The effect of metal EOS 316L stainless steel additive manufacturing powder recycling on part characteristics and powder reusability". In: *Advances in Materials and Processing Technologies* 5:2, pp.348-359, https://doi.org/10.1080/2374068X.2019.1594602.

1.4.2 Conference Proceedings

P.Quinn, S.M. Uí Mhurchadha, J. Lawlor, and R.Raghavendra (2021). "Development and validation of empirical models to predict metal additively manufactured part density and surface roughness from powder characteristics", In: *Proceedings of IMC37 – 37th International Manufacturing Conference*. Athlone. pp. 276-284.

Paul Quinn, Sinead O'Halloran, Jim Lawlor, and Ramesh Raghavendra (2020), "Powder Rejuvenation Process Investigation for the Improved Utilization of Powder in Additive Manufacturing" In: *Proceedings of EuroPM2020*. Lisbon/Online.

P.Quinn, C. Ryan, S. O'Halloran, J. Lawlor, A. Parnell, and R. Raghavendra (2019). Development of a standalone in-situ monitoring system for defect detection in the direct metal laser sintering process, In: *Proceedings of 30th Annual Solid Freeform Fabrications conference (SFF)*. Austin. pp. 1390-1399.

P. Quinn, S. O'Halloran, J. Lawlor, R. Raghavendra (2018). "Characterization of recycled powders and resulting properties derived from additive manufacturing". In: *Preliminary Proceedings: 35th International Manufacturing Conference (IMC35)*. Dublin. pp. 8–11.

1.4.3 Conference Presentations

P.Quinn, S. Uí Mhurchadha, J. Lawlor, and R.Raghavendra , "Development and validation of empirical models to predict metal additively manufactured part density and surface roughness from powder characteristics". at IMC37 – 37th International Manufacturing Conference, Athlone, 2021

P. Quinn, S. O'Halloran, J. Lawlor, R. Raghavendra, "Powder Rejuvenation Process Investigation for the Improved Utilization of Powder in Additive Manufacturing" EuroPM2020, Lisbon/Online, 2020

P. Quinn, C. Ryan, S. O'Halloran, J. Lawlor, A. Parnell, R. Raghavendra, "Development of a standalone in-situ monitoring system for defect detection in the direct metal laser sintering process", 30th Solid Freeform Fabrications Symposium, Austin, 2019

P. Quinn, "Evaluation of the metal additive manufacturing process through the study of the recyclability of metal powders and in-situ metrology", 22nd Sir Bernard Crossland Symposium, Belfast, 2019

P. Quinn, S. O'Halloran, J. Lawlor, R. Raghavendra, "The effect of metal additive manufacturing powder recycling on part characteristics and powder

reusability", AMPT21 – 21st International Conference on Advances in Materials and Processing Technologies, Dublin, 2018

P. Quinn, S. O'Halloran, J. Lawlor, R. Raghavendra, "Characterization of recycled powders and resulting properties derived from additive manufacturing", IMC35 – 35th International Manufacturing Conference, Dublin, 2018

1.4.4 Invited Talks

Paul Quinn, Metal Powder recycling Strategies for laser powder bed fusion, Handling metal powders from manufacturing to 3D printing processes workshop, INVIRTA Group, Virtual, April 2021

1.4.5 Academic Awards

Best student Paper Award sponsored by the Society of Manufacturing Engineers (SME) at the 35th International Manufacturing Conference (IMC35) in Technical University Dublin, Bolton Street Campus in June 2018.

3rd Prize in the Paper Presentation Section of the 22nd Sir Bernard Crossland Symposium in Ulster University, Belfast as decided by the Professors of Mechanical Engineers Ireland and sponsored by Engineers Ireland in April 2019.

Best Student Paper Award sponsored by the International Manufacturing Conference at the 37th International Manufacturing Conference (IMC37) in Technological University of the Shannon Midlands Midwest, Athlone Campus in September 2021

2 Metal Additive Manufacturing

Additive manufacturing is a constantly evolving range of technologies used in the manufacture of often high value products. Metal additive manufacturing is one of the many available collections of additive manufacturing processes applied to produce such components. This chapter aims to introduce two metal powder bed fusion (PBF) processes, with a particular focus on the Laser Powder Bed Fusion (L-PBF) process, on which this research will be focused. It will review some applications for metal AM and provide a detailed explanation of its operating principals.

2.1 Additive Manufacturing

Additive manufacturing (AM) is the collection of processes and technologies that take a geometrical model of an object and build it through the continuous addition of material. AM is defined by ISO and ASTM as:

"the process of joining materials to make objects from 3D model data, usually layer upon layer, as opposed to subtractive and formative manufacturing methodologies" (ISO and ASTM International, 2021)

A key element from this definition is the fundamental distinction between additive and subtractive manufacturing processes. AM builds a part layer upon layer, in comparison to subtractive manufacturing processes which remove material to produce a part. AM processes provide new ways to manufacture highly complex geometries and structures (Tofail et al., 2018).

At present the process favours the production of high value complex components in small lots. The benefits of AM are currently being experienced in a range of industries from medical device and implants to automotive and aerospace.

Initially, the AM processes were used for the manufacture of prototypes allowing for concept functionality to be examined early in the product design process. This led the use of the term rapid prototyping. The first metal powder part was additively manufactured in 1990 (Manriquez-Frayre and Bourell, 1990), and in recent times the technology has emerged as a commercially viable manufacturing process (Sames et al., 2016; Frazier, 2014). In 2017, the sales of AM systems increased by 80% with the number of AM system providers set to continue increasing (Wohlers, 2018). According to a recently published report, the AM

industry experienced a growth rate of 18.3% in 2022, maintaining a double-digit growth trend for 25 out of the past 34 years (Wohlers, 2023).

In addition, the ongoing development and increasing sophistication of AM processes has led to their use in the production of end use components for a range of different applications (Herzog et al., 2016). So while at present the process favours the production of high value complex components in small lots (Frazier, 2014) in a range of industries from medical devices to automotive and aerospace (Sutton et al., 2016a; Tan, Wong, and Dalgarno, 2017), the dramatic increase in the use of AM processes means it is vital to understand the advantages and limitations of each process in order to ensure their use is fully exploited.

AM processes are divided into seven separate categories which are distinguished via a process and feedstock material criteria, see Figure 2.1 (ISO and ASTM International, 2021). Processes within these seven categories can then be subdivided using the same criteria where, for example, polymer processes are distinguished from metal powder processes.

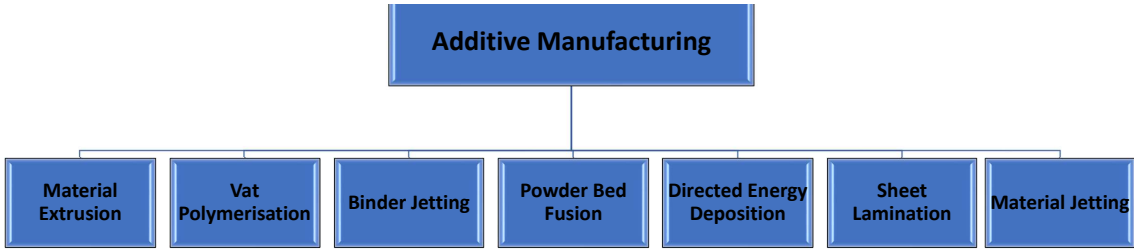

FIGURE 2.1: AM process categories as defined by ISO and ASTM (ISO and ASTM International, 2021).

This research focuses on the Powder Bed Fusion (PBF) process category, further examining the process, its inputs and evaluating the process output. Metal powder is used exclusively in this research and because of this, and to assist the reader in the understanding of this work, the following section will describe in detail the different metal PBF processes. No review of the other processes will be provided in this thesis.

2.2 Powder Bed Fusion

Powder Bed Fusion (PBF) covers the range of processes in which a thermal energy source is used to melt and solidify a bed of powder particles in a selective manner layer-by-layer in order to manufacture a component. In this section the Laser Powder Bed Fusion process and Electron Beam Melting process will be described.

2.2.1 Laser Powder Bed Fusion

The laser powder bed fusion (L-PBF) process consists of a bed of metallic powder being melted and fused selectively using a laser, layer-by-layer, in order to produce a final part. This process was commercialised by EOS GmBH in 1995

when they launched the first commercial L-PBF machine. This went a step further than their previously available selective laser sintering (SLS) machines by fully melting the metal powders. EOS described the particular L-PBF process developed for their equipment as Direct Metal Laser Sintering (DMLS) (Sames et al., 2016). The DMLS and L-PBF processes are the same, but the DMLS process is the licensed name for the specific application of L-PBF on EOS equipment. The term L-PBF will be used exclusively to describe the process in this work, from this point forward. The image below, Figure 2.2 illustrates this L-PBF process.

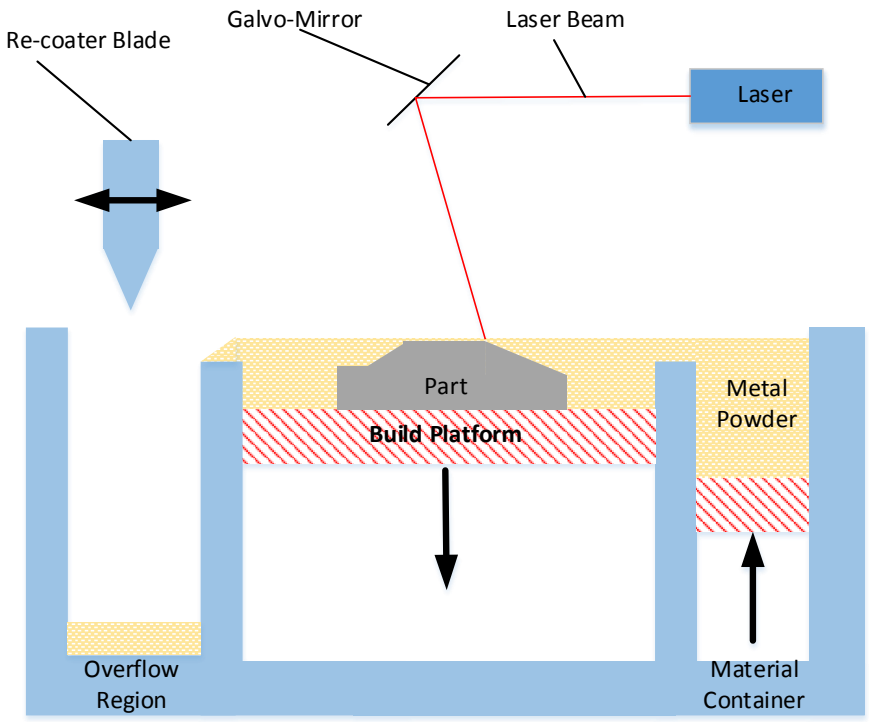

FIGURE 2.2: L-PBF process diagram.

The process begins with the re-coater blade depositing a layer of powder, typically in the range of 20 – 60 μm thickness. This thickness impacts the quality of the parts produced, where thinner layers allows for greater definition of features. Once the layer has been deposited the laser begins to expose and melt the powder bed selectively. The regions in which the laser has to expose are controlled by the layer information loaded into the machine. This layer information controls the galvo-mirror which directs the laser beam across the powder bed. Once the laser has finished melting the layer, the build platform is then lowered by an increment, defined by the layer thickness.

A new powder layer is then added and the process is repeated layer upon layer until the final part is completed. Any powder material which is not deposited on the build platform falls into the overflow region where it can be recycled, along with the un-melted powder from the build platform, for future builds (Jacob et al., 2017). The entire melting process is carried out under an inert environment (Lott et al., 2011), either Argon (Ar) or Nitrogen (N) depending on the powder material

(Gu, 2015). The L-PBF process present within SEAM Research Centre is an EOS M280.

The L-PBF process has a wide range of processing materials and the ability to develop material-specific processing parameters, all while producing near net-shape components. The disadvantages associated with the process include a relatively slow processing time, a high initial capital cost and a rough surface finish produced (Gokuldoss, Kolla, and Eckert, 2017) in comparison to traditional subtractive manufacturing processes.

2.2.2 Electron Beam Melting

Electron Beam Melting (EBM), like L-PBF melts a bed of powder to form a single homogeneous material. However, EBM uses a beam of electrons, as shown in Figure 2.3, to melt the powder bed. Electrons are generated in the electron beam column and projected, at high velocities, towards the powder bed. Multiple lenses are used to ensure the beam of electrons is focused and directed to the correct region of the powder bed, where the electrons cause full melting of the exposed powder bed (Gokuldoss, Kolla, and Eckert, 2017).

The platform then moves down an increment, the depth of movement being defined by the layer thickness and a new layer of powder is added. This process takes place in a near vacuum atmosphere, thus allowing the projected electrons to travel freely from the column to the powder bed. These vacuum conditions in the build chamber also reduce the risk of oxidation on the metal parts during the build process (Gokuldoss, Kolla, and Eckert, 2017).

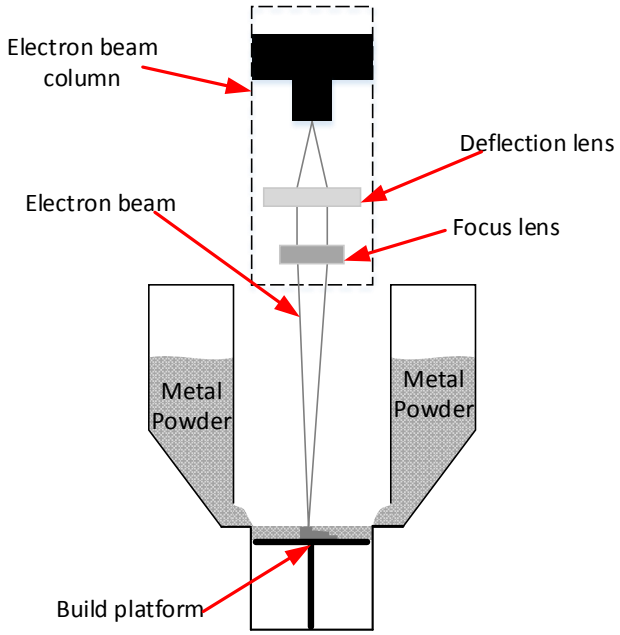

FIGURE 2.3: Electron Beam Melting (EBM) process diagram.

The advantages of the EBM process includes the ability to process brittle materials due to the slower cooling rates as well as the reduction of oxidation due to the aforementioned processing conditions. Disadvantages include the fact that it is a much slower process in comparison to L-PBF, while the development of material-specific processing parameters is also complicated (Gokuldoss, Kolla, and Eckert, 2017). There can also be limitations in the ability to produce some geometries/features in components (Popovich and Sufiiarov, 2016).

2.3 Metal Additive Manufacturing Applications

AM technologies have evolved from being rapid prototyping tools and can now be integrated into full-scale manufacturing processes. For example, metal AM has been successfully implemented within the dentistry, medical device and aerospace industries. These successes are due to the benefits that are afforded by metal AM, including (Manfredi et al., 2013; Tofail et al., 2018):

- Greater customisation of parts with no additional manufacturing cost.
- Reduction in material usage and waste.
- Functional design and overall reduction in product development resource and time.
- Shift manufacturing processes towards on demand manufacturing.

One of the most successful applications of AM is in the production of dental implants. L-PBF is often utilised in this application as it allows for high resolution required for the production of small parts with fine details (Sun et al., 2015). Specifically, L-PBF allows for the production of customised geometries with complicated external surface geometries all within a single manufacturing step.

This ability to produce complex surface geometries creates an increased surface area presented on the implant improving the interface with the bone (Traini et al., 2008) and therefore leading to greater patient outcomes. In addition, porous titanium dental implants, see Figure 2.4, produced using the L-PBF process were shown to exhibit similar mechanical properties to titanium dental implants manufactured traditionally (Traini et al., 2008).

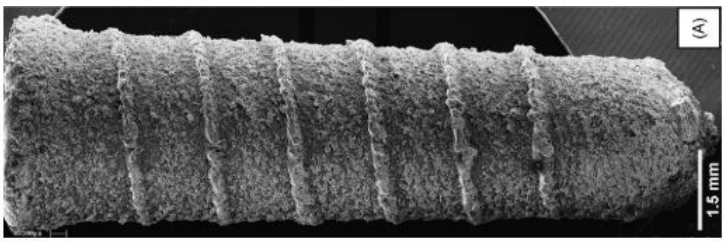

FIGURE 2.4: Porous titanium dental implant produced using L-PBF (Traini et al., 2008).

The medical device industry is another industry where AM technologies are widely applied. The high customisation available in AM allows for bespoke

implants to be produced (Tofail et al., 2018), meeting the exact requirements of individual patients. The AM process allows not only for high customisation but the ability to produce complex surfaces. This intentional porosity and use of lattice type structures within implants can aid bone growth around the implant. Reducing the risks of complications with a patients' acceptance of the implant (Wong and Hernandez, 2012) leading to greater patient outcomes.

An example of this application of AM in the medical devices industry is with Stryker and their Tritanium® spinal implant, seen in Figure 2.5. This implant exploits the ability of AM to produce complex geometries with the inclusion of an external porous structure, mimicking the internal texture and structure of bone. This internal structure aids compatibility of the implant within the patient (Stryker, 2016).

FIGURE 2.5: Stryker's Tritanium® spinal implant (Stryker, 2016).

AM is also successfully applied within the aerospace industry where it facilitates the production of complex components. These can allow for more efficient and effective design. An example is the Leap jet engine, manufactured by General Electric's aviation division, which encompasses 19 additively manufactured jet fuel nozzles, as seen in Figure 2.6.

FIGURE 2.6: GE's Leap fuel nozzle which utilises the benefits delivered by AM (Conner et al., 2014).

The advantage of the AM process means that this single item replaces the previous fuel nozzle, originally a combination of 20 individual titanium pieces assembled and welded together. AM allowed for the redesigned product to be

manufactured within a single process. It also allowed for a total part reduction of 20 to 1, and achieved both a 25% reduction in weight and increased component durability (Conner et al., 2014). The AM process has provided significant improvement to the component in this application (Kellner, 2015).

While the advantages of AM are evident in the examples above, metal AM remains mostly geared towards the production of small volumes of high value components. This is partially due to the high cost of the raw powdered materials compared to those for traditional subtractive methods (Moylan et al., 2013). A general challenge for the technology is the certification and qualification of parts, which is an area requiring significant research (Mani et al., 2016). In general, the fixed costs for conventional manufacturing operations are higher than those of AM. The general approval of AM suggests that manufacturers can be profitable if they adopt the AM process (Frazier, 2014; Vafadar et al., 2021). A 30% cost saving was calculated for the use of metal AM on an Inconel engine casing (Kinsella, 2008). With many others stating the AM processes allows for a greater material utilisation and therefore a reduction in the cost compared to traditional manufacturing processes.

This chapter has presented and described the different metal AM processes which fall under the PBF process category, as well as outlining some of the applications for the L-PBF process within industry. The following chapter will outline the current state of the art in regards to metal powder characterisation and in-process monitoring, relevant to the research questions posed in Chapter 1 of this thesis.

3 Literature Review

Additive manufacturing is constantly evolving and with that the research activities flourish. This chapter will review the theory required to understand the foundations of the different aspects of this research work. It provides the reader with an introduction to the powder material used in the powder bed fusion process, including its, manufacture, characteristics, and their effect on the process. An introduction to the various types of powder recycling methods will be provided, identifying the current state of the art. Following this, some common methods currently applied for in-situ defect detection are presented as well as the means to identify various common defects in the powder bed. This chapter aims to provide foundational knowledge of the state of the art as well as identify potential gaps in the knowledge in which this research aims to address.

3.1 Powder Production

To mass produce the powder feedstock required for the L-PBF process mechanical powder production methods known as powder atomisation are often employed rather than other chemical processes or plasma spherodization (Popovich and Sufiiarov, 2016):

- Chemical Processes - A decomposition of metal under temperature and pressure in order to form metallic powders, most suited to Nickel and Iron powders.
- Plasma Spheroidization - A post-production treatment for non-spherical powders to change the particles shape increasing its sphericity thus, improving the powders flowability (Getto et al., 2023).

While those processes exist, the atomisation process provides the most suited powder properties for AM (Popovich and Sufiiarov, 2016). For this reason gas and water atomisation are the most common production methods and as such are discussed in detail below.

3.1.1 Powder Atomisation

The atomisation process is the most common form of production for large quantities of metal powders for the AM process (Popovich and Sufiiarov, 2016; Hoeges, Zwiren, and Schade, 2017). While other atomisation methods exist, gas and water atomisation are the preferred methods (Džugan et al., 2017). The process of atomisation, as illustrated in Figure 3.1, is achieved by dispersing a thin stream of molten metal, and introducing an inert gas or water at high

pressure. This exposure to the gas or water causes the molten metal to rapidly cool in the form of small droplets which fall and solidify through the atomisation chamber before being collected along the walls or at the bottom of the chamber as a powder material (Upadhyaya, 1996). The two processes produce powders for L-PBF processes, however, they can result in different powder characteristics (Scipioni Bertoli et al., 2017).

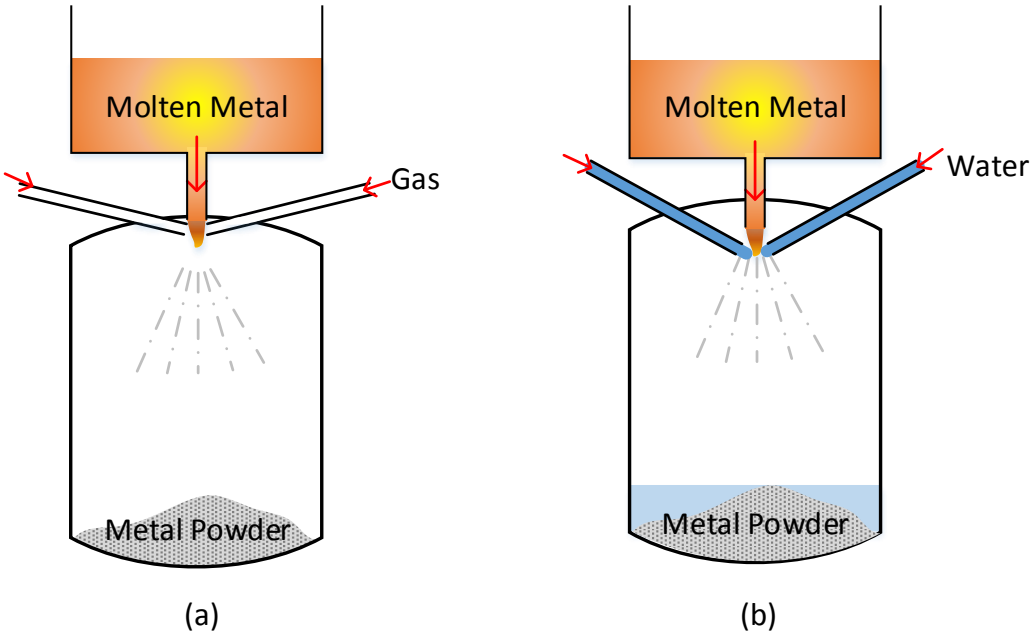

FIGURE 3.1: Atomisation process description (a) Gas Atomisation and (b) Water Atomisation.

Gas Atomisation (GA), as shown in Figure 3.1(a), is a process consisting of two main operations. Firstly the molten metal is forced through an orifice at a flowrate in the range of 45-90 kg/min. A stream of high pressure inert gas either Argon (Ar) or Nitrogen (N), in the range of 0.75-2.6 MPa, is introduced causing the molten stream to disperse and form droplets (Džugan et al., 2017; Klar and Samal, 2007). The droplets fall through the atomisation chamber and cool before being collected in a powder form at the bottom of the chamber (Klar and Samal, 2007). The inert gas that is introduced into the molten material affects the final characteristics of the output powder material and thus the resulting L-PBF parts (Sutton et al., 2016b). Wang et al., 2023a found that when comparing Ar and N as the atomisation gases there was a significant effect on the final properties of the parts produced. Powder atomised with N were found to have a lower elongation due to its effects at the micro-structural level of the powder particle in comparison to GA powders (Wang et al., 2023a). Due to the low solidification rates in GA the powders produced are highly spherical (Hoeges, Zwiren, and Schade, 2017; Boes et al., 2020). In general the particles are spherical in shape with some agglomeration due to smaller particles cooling and adhering to larger particles within the atomisation chamber (Scipioni Bertoli et al., 2017). The composition of the molten metal and atomisation gas used in this process influences the final chemical composition of the powder material produced (Upadhyaya, 1996). To

ensure certain compositions of powder are produced various alloying elements are added to the molten metal before the atomisation process. The powders utilised in this thesis have been produced by gas atomisation.

A common limitation of the gas atomisation process is internal porosity within the particles. A resultant of the atomisation gas becoming trapped within the powder particles. This internal porosity can transfer into the final as-built parts during the L-PBF process (Sames et al., 2016). The particle sizes that are produced from gas atomisation can be controlled by the pressure of the atomisation gas. The gas is typically introduced at a pressure ranging from 0.75-2.6 MPa (Klar and Samal, 2007). Increasing the pressure of the atomisation gas leads to a decrease in the particle size produced. This relationship was investigated by Dungkratok et al., 2005 showing that the higher the pressure of the atomisation gas, the finer the powder particles produced. This ability to control the particle size allows for a high yield of usable powder (Klar and Samal, 2007, p. 26). The scanning electron microscopy (SEM) image in Figure 3.2 shows a typical GA 316L stainless steel powder exhibiting highly spherical particles with a narrow distribution of sizes.

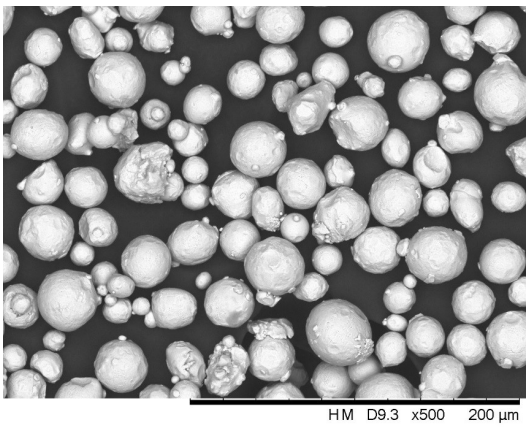

FIGURE 3.2: x500 magnification SEM image of a gas atomised 316L stainless steel powder.

Water Atomisation (WA), as shown in Figure 3.1 (b) is based on the same atomisation principle as GA with the difference being that water is introduced to the chamber at higher pressures than GA, ranging from 11-18MPa (Klar and Samal, 2007). Particles cool up to 100 times faster than GA powder. This is due to the higher solidification rate of water (Hoeges, Zwiren, and Schade, 2017). The particles then fall to the bottom of the atomisation chamber along with the atomisation water. WA requires an additional drying process to complete the powder production (Hoeges, Zwiren, and Schade, 2017; Klar and Samal, 2007).

WA is most commonly used for non-reactive materials such as iron and steel based powders (Dawes, Bowerman, and Trepleton, 2015; Popovich and Sufiiarov, 2016). Due to the increased cooling capacity of water the particles are often irregular in shape (Popovich and Sufiiarov, 2016; Hoeges, Zwiren, and Schade, 2017). These irregularly shaped particles can lead to issues in the packing and flow properties, which are highly influential in the AM process (Dawes,

Bowerman, and Trepleton, 2015). One of the main advantages of WA is that it is a less expensive process in comparison to GA (Pinkerton and Li, 2005; Im et al., 2022).

Similarly to the GA process, the final particle sizes can be controlled. The pressure of the atomising water is adjusted, between the range of 11-18 MPa, to manipulate the final particle size distribution. With an increase in the atomising pressure the finer the particles are produced as the cooling rate is increased. The morphology of the particles can be controlled to a point, through adjustments in the process such as, the re-design of the atomisation chamber and nozzle to allow for slower cooling of the powder. Adjustments in the feedstock molten material can also be used to control the cooling rate of the powder (Klar and Samal, 2007). The SEM image, Figure 3.3, shows a typical WA 316L stainless steel powder, which highlights the irregular particle morphology of WA powders.

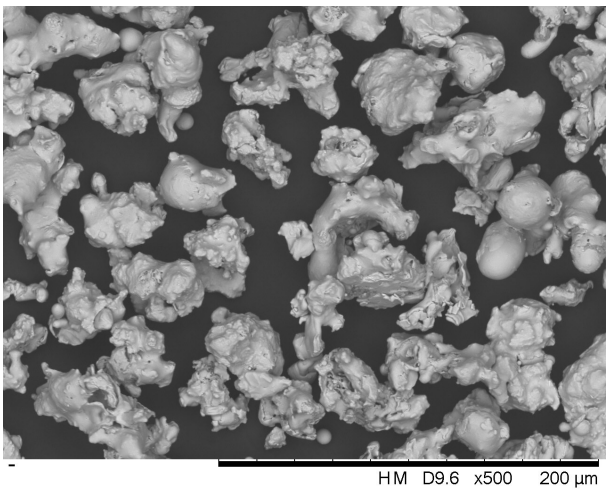

FIGURE 3.3: x500 magnification SEM image of a water atomised 316L stainless steel powder.

Fedina et al., 2020 found that when comparing both GA and WA for low alloy steels, both were capable of producing single tracks, however upon further validation the WA powder samples required some consideration in ensuring a consistent packing density is present in the layering process. This was attributed to the irregular powder morphology (Fedina et al., 2020). L-PBF processes are sensitive to defect incorporation from the powder material. Powder materials that are produced with contamination and or internal porosity will result in parts produced with the same defects internally (Xiong et al., 2022). The processes used to produce the feedstock powders need to be able to provide consistent powders suited to the L-PBF process. The powder atomisation process requires significant research in order to become a precision manufacturing process (Anderson, White, and Dehoff, 2018). This is required to ensure the powder produced meets the specifications required for L-PBF. These research requirements arise due to the lack of fundamental process knowledge of atomisation. The selection of the atomisation method is dependent on the final application of the powder material. For AM the powder needs to be close to spherical and with a specific particle size distribution (Scipioni Bertoli et al., 2017). Gas atomisation offers powders most

suited to the AM process, however, it is a more costly method in comparison to water atomisation (Hoeges, Zwiren, and Schade, 2017).

The powder manufacturing process is vital to the production of powders with the required chemical composition and characteristics for the L-PBF process. Powder characteristics are highly dependant on the atomisation process and the behaviour of the resulting parts are highly dependant on the input powder characteristics, among other factors. The next section looks more closely at these characteristics and the influence they play on the outcome of the L-PBF process.

3.2 Powder Characteristics

The powder production process and its influence on the powder characteristics, was discussed in the previous section. Understanding the characteristics of the powder material used in the L-PBF process allows for an insight into the resulting as-built part properties (Sun et al., 2015). Until now the focus of the research to date in AM powders has been on the process parameters with less attention on the powder characteristics (Cordova, Campos, and Tinga, 2019). The powder characteristics influence the layering process and packing ability of the L-PBF processes thus affecting the final as-built part properties (Spierings et al., 2015; Strondl et al., 2015). These powder characteristics discussed in this section are:

- **Powder Chemical Composition:** The chemical make up of the powder material.
- **Powder Morphology:** The shape of the individual powder particles.
- **Particle Size:** The mean size and size distribution of the powder particles.
- **Powder Density:** The ability for the powder to produce a dense powder layer.
- **Powder Flowability:** The ability for the powder to flow in order to produce a consistent build layer.

The Ishikawa diagram, presented in Figure 3.4, illustrates the different powder characteristics that are discussed in this section and the different terminology used to describe them. The five characteristics listed lead to the required powder properties for L-PBF.

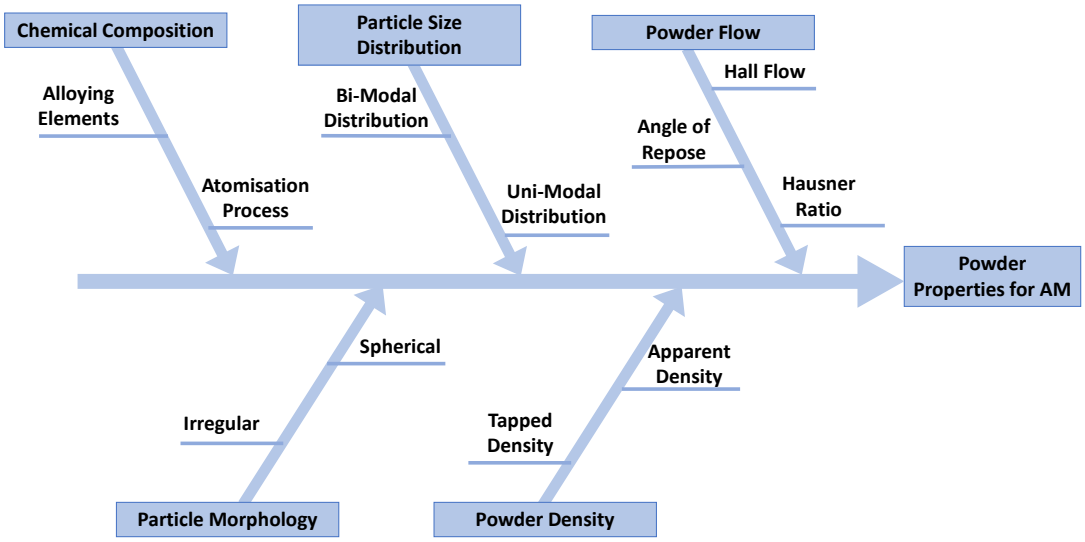

FIGURE 3.4: Ishikawa diagram with influencing characteristics for metal powders.

Understanding the different effects these characteristics can have on the final L-PBF parts is a fundamental requirement for further development and improvement of the L-PBF process. Increasing its applicability to new applications as well as new materials (Moghimian et al., 2021). Lu et al., 2022a identifies that one of the primary constraints preventing the widespread adoption of L-PBF are the expensive raw materials and lack of consistency in their properties.

3.2.1 Chemical Composition

As mentioned previously, the composition of the powder material is determined in the atomisation process. The chemical composition of the molten material used in atomisation is transferred into the final powder composition (Klar and Samal, 2007). The atomisation medium, gas or water, will also influence the final chemical composition of the powder (Wang et al., 2023a). The chemistry of the powder particle is an essential characteristic for metal AM users as it has a significant effect on the final as-built material properties. Various alloying elements are added to the molten metal, in production, to improve the mechanical properties of the resulting powders, enabling the materials application portfolio to be broadened. Different grades of materials are often distinguished by the quantities of the different alloying elements. For example, Table 3.1, shows the composition of two commonly used stainless steel AM powders, 316L and GP1 (EOS GmbH, 2014).

The two materials shown in Table 3.1, are both stainless steel alloys. However, they have different alloy compositions. This is to best suit their individual applications. 316L stainless steel is a commonly used steel in the medical and

TABLE 3.1: Chemical composition of 316L and GP1 steel powders for L-PBF (EOS GmbH, 2014).

Element	**316L (wt%)**	**GP1 (wt%)**
Iron, Fe	Bal.	Bal.
Chromium, Cr	19	17.5
Nickel, Ni	15	5
Molybdenum, Mo	3	0.5
Carbon, C	0.03	0.07
Manganese, Mn	2	1
Copper, Cu	0.5	5
Phosphorus, P	0.025	-
Sulphur, S	0.01	-
Silicon, Si	0.75	-
Nitrogen, N	0.1	-
Niobium, Nb	-	0.45

automotive industries (Sutton et al., 2016b). GP1 is a stainless steel material used for general engineering applications and areas where high sterility is required (EOS GmbH, 2014). The different applications for these two stainless steels determines the alloys required within their chemical composition. Corrosion resistance is achieved in both alloys by the addition of Nickel (Ni) to the molten metal in the alloying stage (Sutton et al., 2016b).

The powder chemical composition is directly translated into the final as-built part composition (Engeli et al., 2016), effecting the performance of the material under different applications. This effect of the powder composition was studied by Engeli et al., 2016. They found that with different Inconel (IN) powder batches, those which contained higher weight percentages of silicon (Si) had a higher susceptibility to cracking in the final as-built parts. This is similar to traditional welding processes where the presence of cracking within welds is often attributed to the presence of silicon (Si) within either the base metal or the welding filler rod (Yoo et al., 2014).

The improper or incorrect storage of metal powders often leads to the formation of oxides and hydroxides on the powder particles. This is an area of concern for the processability of the metallic powder in the AM process. The pickup of oxygen in the powder material and the formation of humidity within the powder batch can translate through into the as-built parts and have an effect on the resulting micro-structure (Tan, Wong, and Dalgarno, 2017). In order to alleviate this issue, silicon (Si) is often added in the atomisation of stainless steels. This higher content of silicon (Si) causes the oxygen (O) content to decrease. This is an important element addition in water atomised powders where the process water is absorbed by the particles leading to high humidity in the powder batch often causing rapid oxidation of the powder (Klar and Samal, 2007).

3.2.2 Powder Morphology

Powder morphology refers to the individual shape of the particles. Powder shape can account for the behavioural characteristics of a given powder material (Benson and Snyders, 2015; Strondl et al., 2015). Ideally particles should be circular in 2D cross section and spherical in geometry. This allows for the powder to perform most efficiently in the L-PBF process, as the powder is able to flow freely. To produce spherical particles strict control of the atomisation process is required (Fedina et al., 2020). A powder batch often will contain a mixture of spherical and non-spherical or 'irregular' particles. These irregular particles can be formed due to the following:

- Powder atomisation process - the method of powder production as discussed in Section 3.1.1 (Klar and Samal, 2007).
- Secondary processing on the powder - secondary processes conducted after the production of the powder in order to achieve the characteristics required, this may include milling or spheroidization (Popovich and Sufiiarov, 2016).
- Powder reuse - the process of collecting the un-melted powder after the process and reusing it for subsequent builds (Jacob et al., 2017).

The assessment of the powder particles morphology is most commonly conducted through measurement of high magnification images of the powder particle cross-sections or X-Ray Micro Computed Tomography and then applying different shape descriptors or form factors to quantify the shape of the particles (Cooke and Slotwinski, 2012; Sutton et al., 2016b; Xiong et al., 2022).

Controlling the morphology of the powder is best achieved in the production stage. As previously mentioned the gas atomisation process typically produces highly spherical particles in comparison to water atomised powders (Scipioni Bertoli et al., 2017). The shape of powder particles is one of the main influences on how the powder material is deposited and layered on the build platform (Sun et al., 2015). Spherical powder material will flow easily and therefore evenly deposit along the build platform thus increasing the homogeneity of each layer. Irregular shaped particles will have a higher resistance to flow and therefore result in an inhomogeneous deposition of powder across the build platform. This is due to the increase in the particle-to-particle friction resisting the powder flow. A uniform layer of powder is required to ensure uniform properties in the as-built parts (Sutton et al., 2016b; Miao et al., 2022). Brika et al., 2019 found that a more spherical powder exhibits far superior flow behaviour and more efficient packing density in the L-PBF process.

3.2.3 Particle Size

The particle size of a powder batch can be described in many different ways, most commonly:

- The particle size distribution which shows the dispersal of particle sizes within a powder batch (Jillavenkatesa, Dapkunas, and Lum, 2001).

- Mean particle size which highlights the average size of the particles measured (Zegzulka et al., 2020).
- D10, D50 and D90 volume distribution values, the point on the distribution curve which 10, 50 and 90 percent of the particles fall under (Vock et al., 2019).

The particle size is determined by the technology used to produce the powder material. The desired range of particles for the L-PBF process is within 10 – 80 μm in diameter with a Gaussian or Normal Distribution. This type of particle distribution is shown in Figure 3.5 below as well as the mean particle size, D10, D50 and D90 values for a typical gas atomised 316L stainless steel powder.

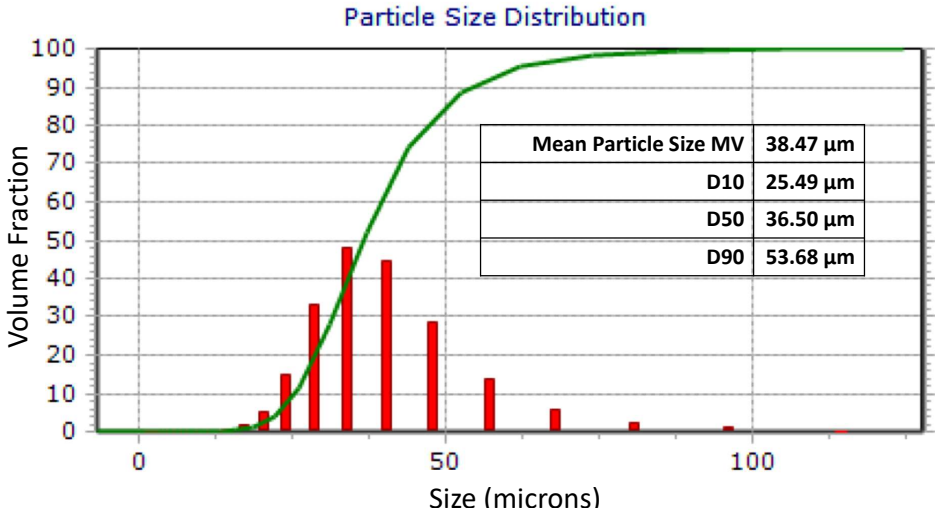

FIGURE 3.5: Particle size distribution for 316L stainless steel powder.

The distribution of particle sizes within a powder batch is a property which impacts the performance of the powder within the AM process (Strondl et al., 2015; Zielinski et al., 2017). The size distribution of particles used should be strictly controlled. Careful consideration for the layer thickness being used in the process is required. This allows for the required detail resolution and surface finish to be achieved, limiting the formation of voids in the as-built parts (Sun et al., 2015). Studies have been carried out which have investigated how the change in particle distribution influences the as-built part density, surface roughness and tensile strength. Spierings, Herres, and Levy, 2011 concluded that a wide particle size distribution as described in Figure 3.6 produced higher density components with a lower surface roughness. They also found that with wider particle distributions resulted in higher elongations at fracture in the tensile tests. The particle size distribution ultimately contributes to how well the powder can flow in the L-PBF process (Liu et al., 2011). Balbaa et al., 2021 presented a study of the dimensional accuracy of the L-PBF parts manufactured from both fine and coarse particle size distributions. This concluded that the samples manufactured with the finer powders had a lower dimensional accuracy due to the noticeable adherence of partially melted particles to the sample

surfaces (Balbaa et al., 2021). Finer particles can often influence the flowability of the powder, discussed in later sections, and cause difficulties in producing uniform powder layer due to increased Van der Waals forces in the smaller particles (Miao et al., 2022).

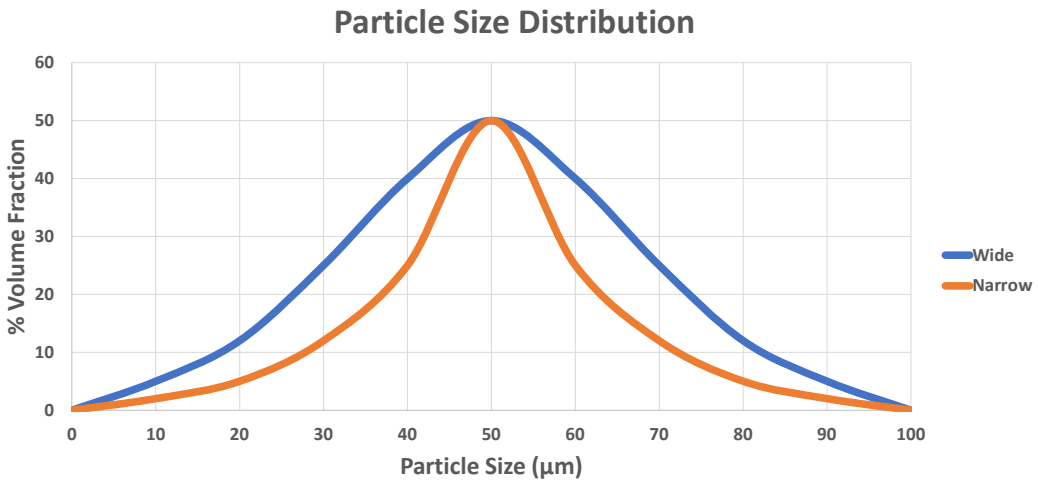

FIGURE 3.6: Example of a wide and narrow particle size distribution.

3.2.4 Powder Density

Powder density, in bulk form, is often described by two characteristics:

- Apparent Density - The powder density in its loose and uncompacted form (Jacob, Brown, and Donmez, 2018).
- Tapped Density - The density of the powder after it has been agitated and compacts (Spierings et al., 2015).

The apparent density of the powder affects the packing characteristics in the deposition of the powder layer (Schade, Murphy, and Walton, 2014; Baitimerov et al., 2018). One of the areas of concern for powder density is in the production of dense and uniform powder layers consistently throughout the build process. The factors that influence the powder density are the particle size distribution and the particle morphology (Jacob et al., 2016). A wide powder distribution, as demonstrated by the blue line in Figure 3.6, allows for a high layer density. The particle size distribution should be made up of smaller and larger particles to enable the highest layer density. The larger particles, enables the powder to flow and smaller particles fill any voids in the deposited layer (Abd-Elghany and Bourell, 2012). This produces a dense powder layer. Powders with a wider particle size distribution provide a higher powder layer density which translates into a higher part density being produced (Liu et al., 2011) as there are significantly fewer voids distributed in the powder layer.

The powder apparent density is not only reliant on the distribution of particle sizes but the morphology of the particles within the powder batch. The

morphology of particles affects how well they can arrange themselves when they are compacted. Particles with a highly spherical morphology will have an increased apparent density translating to a higher tapped density. This is evident through the analysis of apparent and tapped density of gas and water atomised powders. This also affects the powder layer density in the L-PBF process (Schade, Murphy, and Walton, 2014). The irregularly shaped water atomised powders have a significantly lower apparent and tapped density, in contrast to the generally more spherical gas atomised powders (Engeli et al., 2016). This significant variation in the apparent and tapped density is described by the major difference in the morphology of the two types of powders.

3.2.5 Powder Flowability

Flowability, the ability of a powder to distribute an even powder layer for melting, can determine how well the powder will perform in the L-PBF process (Clayton and Deffley, 2014). The flowability of a powder is influenced by the particle size distribution and the particle morphology (Zhao et al., 2021). The different powder layering methods such as scraper blade, roller and slot feed, shown in Figure 3.7, rely on a powder with a high flowability to produce consistent even powder layers during the build process (Schueren and Kruth, 1995).

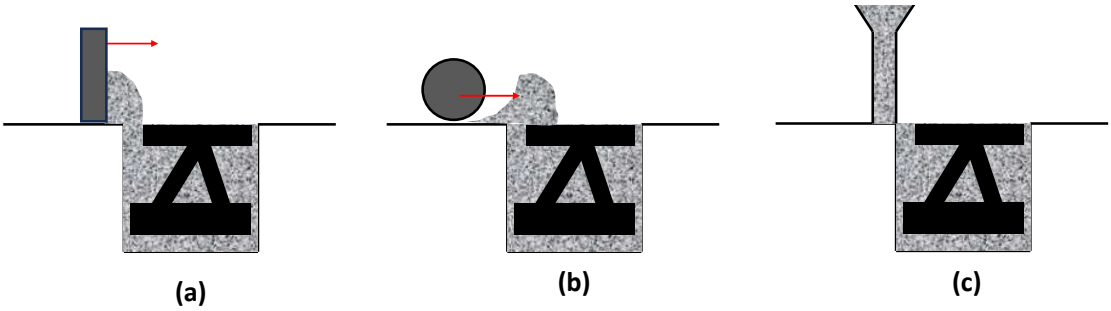

FIGURE 3.7: (a) Scraper Blade, (b) Counter rolling cylinder and (c) Slot feeder powder deposition methods (Schueren and Kruth, 1995).

The flowability of the powder feedstock material is expected to affect the continuity and homogeneity of the powder bed thus affecting the final as-built part properties (Sun et al., 2015; Tang et al., 2015).

Different methods exist for the characterisation of a powders flowability depending on the types of results that are required. Dynamic tests are more suitable for powders in AM as they provide representations of the powder in motion, simulating more closely the layering process. Static methods provide an indication to the flowability of the powder, however, may not directly represent the dynamic behaviour of the powder in the layering process (Spierings et al., 2015).

Some of the most common methods used to characterise powder flowability are the Hall Flow Funnel, Carney Funnel and the Hausner Ratio (Clayton,

Millington-Smith, and Armstrong, 2015). The hall flow meter is a standardised test method covered under ISO 4490:2014 and ASTM B213 and the Carney Funnell is covered under ASTM B417 (Yu and Hall, 1994; Spears and Gold, 2016). The Hauser Ratio is another relationship for describing the powders flow by providing an insight in to the inter-particle friction in the powder batch (Engeli et al., 2016). The Hausner Ratio is the ratio of the uncompacted powder to the compacted powder. These static characterisation methods are less suitable methods to assess the flowability of AM powders, (Spierings et al., 2015) however, due to the ease of testing they are commonly used to describe the flowability of powders for AM (Sun et al., 2015). In order for a good flowability of the powder a particle distribution needs to be balanced between larger and smaller particles. Fine powder particles are detrimental to powder flowability (Kirchner et al., 2016). This is found to be as the larger volume of smaller particles tend to 'lock' together and therefore resist the flow of the powder thus effecting the layering process (Liu et al., 2011). Resulting in a negative impact on the part density, surface roughness and dimensional accuracy (Brika et al., 2019).

The flowability of the powder material is highly dependent on the powder particle size distribution as well as the morphology of the particles (Mussatto et al., 2021). As discussed in previous sections the water atomisation (WA) process produces powder particles that are non-spherical and irregular in shape. This characteristic of the powder means that in flowability tests it is often out performed by the gas atomised (GA) powders. The effect of this was studied in detail and a comparison of the flowability between WA and GA powders was completed (Fedina et al., 2020). The WA powder had a considerably lower Hausner Ratio than the GA powder. This was also correlated to an increases in part porosity, thus, highlighting how the flowability of the powder material leads to an in-homogenous powder layer translating to internal porosity within the as-built parts (Engeli et al., 2016; Abdelwahed et al., 2021). Haferkamp et al., 2021 concluded that the more spherical the powder particles are the better the flowability of the powder. This increased flowability due to being highly spherical resulted in greater powder layer densities.

Powder characteristics play a crucial role in the L-PBF process. The morphology of powder particles can affect the density and flowability of the powder, in turn affecting the quality of the parts. Chemical composition and morphology of the powder impacts the melting behaviour of the powder during the L-PBF process. The choice of powder material and its properties must be carefully considered to achieve high-quality and consistent parts in the L-PBF process. One of the greatest advantages of the L-PBF process is the ability to utilise un-melted powders in subsequent builds, this powder recycling process and its influence on the powder characteristics is discussed below.

3.3 Powder Recycling

Powder recycling is the "practice of collecting the un-melted powder after the process and reusing it for subsequent builds" (Jacob et al., 2017). It is a practice, which until 2015 had not received much attention (Dawes, Bowerman, and

Trepleton, 2015; Cordova, Campos, and Tinga, 2019). The recycling process consists of collecting this un-melted powder after each build, sieving it, and reusing the sieved powder material in the following builds. Figure 3.8 shows a flowchart of this iterative process.

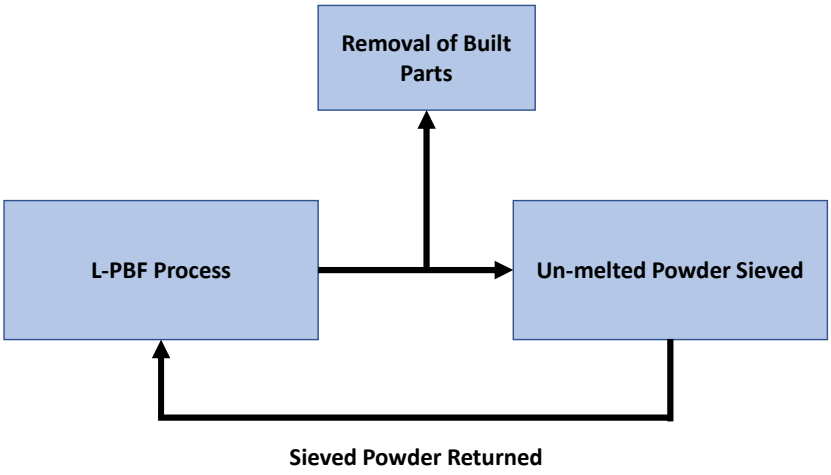

FIGURE 3.8: Powder recycling process.

The above recycling process can continue until:

- The remaining quantity of powder is insufficient for future builds.
- The powder properties have deteriorated to a point which is no longer acceptable.

The volume of the manufactured parts in comparison to the volume of powder dispensed in the L-PBF, results in a large proportion of the deposited powder available for use in subsequent builds (Lu et al., 2022a). Ardila et al., 2014 found that implementing a powder recycling strategy can lead to a 95% utilisation efficiency for the powder material in the L-PBF process. Powder utilisation refers to the amount of powder material in the original batch that is used to produce a component, the greater this value is the more material being used to produce parts in the L-PBF process.

3.3.1 Recycling Process

The powder recycling process means that the powder material has been exposed to the L-PBF processing environment repeatedly. Sartin et al., 2017 has found that the recycling process affects the powder characteristics which in turn affects the resulting as-built part properties (Lu et al., 2022a). It is therefore important to understand these changes in the powder material (Spierings et al., 2015). When powder material reaches the point where it can no longer be re-used in the L-PBF process, due to either of the above reasons, it is common for new virgin powder to be added, this is a practice called powder rejuvenation which is discussed in a later section of this thesis.

The main aim of powder recycling is to improve the overall efficiency of the AM process, ensuring a high rate of utilisation for the originally costly feedstock powder material (Singh, Ramakrishna, and Singh, 2017). The percentage of mass of the powder material that is melted within the machine can be within the range of 3 to 5% per build. This highlights the benefits of recycling powder material for future additive manufacturing (Kellens et al., 2011; Sartin et al., 2017).

3.3.2 Effects of Powder Recycling

Once a L-PBF build is completed the properties of the powder remaining within the build chamber are strongly affected by the interaction with the laser radiation and process environment (Santecchia, Spigarelli, and Cabibbo, 2020). The effects of the powder recycling process on the powder characteristics have been studied by some researchers (Cordova, Campos, and Tinga, 2019; Seyda, Kaufmann, and Emmelmann, 2012; O'Leary et al., 2015). They have looked at the changes in powder characteristics as well as tracking the effect of increased powder use on the as-built part properties. As the recycling process has been found to change the characteristics of the raw material, understanding these changes is vital for industries looking to produce critical components through the L-PBF process.

It has been found that the powder recycling process has an effect on the particle size distribution of the recycled powder. Studies have shown that increased powder recycling leads to the quantity of smaller particles present in the batch decreasing (Seyda, Kaufmann, and Emmelmann, 2012; O'Leary et al., 2015; Tang et al., 2015; Sartin et al., 2017; Cordova, Campos, and Tinga, 2019; Smolina et al., 2022; Cordova et al., 2023). The change in particle size is observed through a shift in the particle size distribution towards to right indicating an increased quantity of powder in the larger particle size ranges. The percentile values (D10, D50 and D90) also support this finding. This increase in turn affects the layering process as the powder's flowability characteristics are changed from those of the virgin powder material. The decrease in smaller particles improves the powders flowability (Sartin et al., 2017). The smaller particles originally in the batch can lock together and restrict the flow of the powder (Liu et al., 2011). He et al., 2022 found a 22% increase in the mean particle size of the powder resulting in a decrease in the porosity of the L-PBF parts manufactured.

This increased flowability causes an improved layering process as the powder is able to flow more freely along the build plate, but the new distribution of powder particles, now including more larger particles, consequently leads to a decrease in the layer density (Haferkamp et al., 2021). This then affects the density of the as-built parts. Popov et al., 2018 have found that the particle size distribution in the L-PBF process is directly related to the as-built part density. The wider the particle size distribution (shown previously in Figure 3.6) the higher the part density. This is because the distribution of smaller and larger particles allows for the smaller particles to fill in the spaces and gaps in the powder later formed by the larger particles (Spierings, Herres, and Levy, 2011). This phenomena as described in Figure 3.9 demonstrates how the particle size distribution affects the powder bed density. The recycling process drives this change in powder

distribution affecting the part density. The powder bed density can be used as an indicator of the density of produced parts from different particle size distributions.

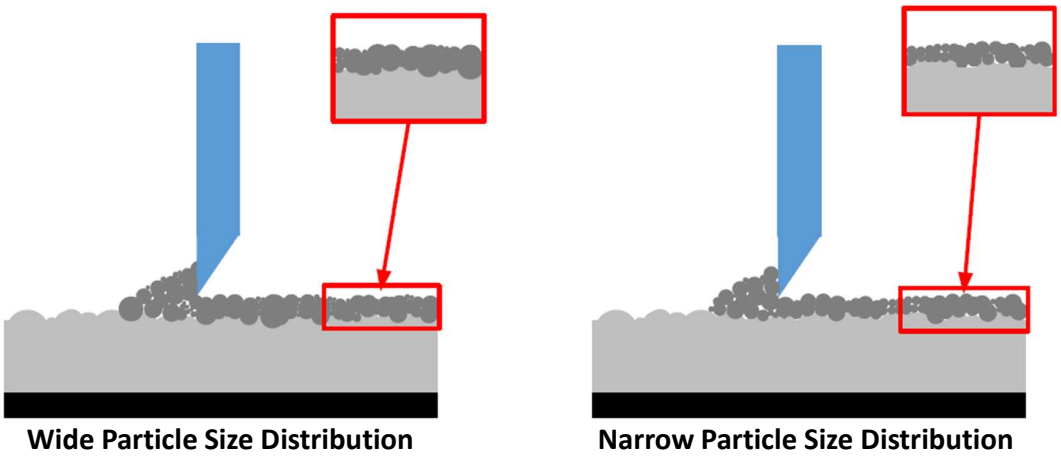

FIGURE 3.9: Narrow and wide particles size distribution effect on bed density.

Powder recycling also effects the morphology of the powder material. This change in morphology when tracked throughout the recycling process shows changes in the shape and form of the powder, thus influencing the powders flow behaviour (Sutton et al., 2016a; Ahmed et al., 2020). The change in the morphology emerges from many different internal processes during the melting of the powder bed. One of these processes is the formation of agglomerates or satellites (Chuang et al., 2021; Beal et al., 2023). Lu et al., 2022b noticed a presence of broken and irregular particles found in the recycled powders which were not in the original virgin powder material. These agglomerates are formed due to smaller particles being fused to larger particles as shown in Figure 3.10 during the L-PBF process (Cordova, Campos, and Tinga, 2019). These agglomerates are still small enough to fit through the sieve (63 μm) for use in the next build. The morphological change in the powder affects the flow behaviour as there is an increase in the particle-to-particle friction (Cordova et al., 2020). This is because of the increased surface area as a result of the irregular particle shape. Figure 3.10 shows some of the non-spherical, agglomerated particles typically associated with recycled powders. Bajt Leban, Hren, and Kosec, 2023 found that the increase in irregularly shaped particles increased as the powder was recycled and re-used. Identifying the impact the L-PBF has on the generation of the morphological changes in the powder. The extent of the non-sphericity and agglomeration increases with the number of recycling processes carried out (Popovich and Sufiiarov, 2016). This was also found to be true for the electron beam melting (EBM) process where powder particles became visibly less spherical with a rougher exterior surface (Tang et al., 2015).

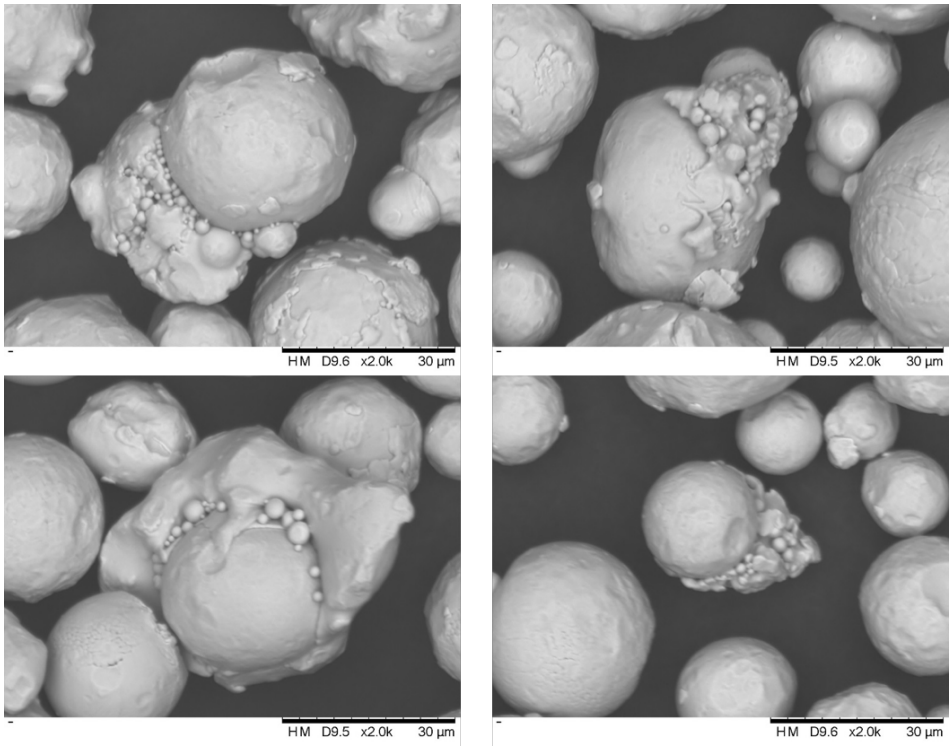

FIGURE 3.10: Non-spherical and agglomerated particles found in recycled powder material.

The change in the physical characteristics in the powder material will affect the powders flowability. This will affect the layering process leading to inconsistencies in the as-built part properties. Consistent and repetitive powder deposition for each layer is vital to controlling the properties of the resulting parts (Foster et al., 2015). As the powder is recycled it has been observed that the powder particle size distribution shifts to the right. The greater quantity of larger particles present leads to increased flowability of the powder. However, this increase in particle size is not the only change, as the morphology has also deteriorated resulting in less spherical particles. This morphological change will impede the flow of the powder. The improvement in flowability due to the increased particle size outweighs the expected decline in flowability due to the deterioration in morphology (Seyda, Kaufmann, and Emmelmann, 2012; Tang et al., 2015; Sartin et al., 2017). It appears that the dominant characteristic in relation to the flowability of the powder is the particle size distribution. The particle size distribution shifted to the right contains a larger percentage of large particles which improves the powder's flow (Liu et al., 2011), due to a reduction of intra-particle friction between smaller particles. Strondl et al., 2015 found an increased flowability for a recycled powder, in comparison to that of the virgin powder material. A similar result was found in the direct metal laser deposition (DMLD) process where, as the powder material was recycled there was an increase in the flowability despite the evident deterioration of the particles morphology (Carroll et al., 2006).

A characteristic which is expected to be affected by the powder recycling process is the powder composition. During the L-PBF process the powder is exposed

to varying environmental conditions. The prolonged and repetitive exposure of powder materials to non-inert environments can trigger oxidation on the surface of the particles (Tan, Wong, and Dalgarno, 2017). This has an impact on the final as-built part properties that are observed. Cordova et al., 2023 determined that the bulk chemical composition of the powder through the recycling process, consisting of 10 builds, remained within their accepted range however the oxygen content did increase. Beal et al., 2023 concluded that after a series of recycling stages of the powder the oxygen content increased. Strondl et al., 2015 found that as the oxygen content within the powder material increased over time the ductility and toughness of the manufactured samples decreased. This contrasted to the findings of Ardila et al., 2014. They found no increase in the oxygen content of the powder after recycling. The difference in the studies could be due to a slightly different recycling methods being applied. Tang et al., 2015 found in the EBM process, the increased powder recycling led to an increase in the uptake of oxygen in the powder which can then translated into the as-built parts. A suggested method to reduce this oxidation in the powder material is to integrate de-oxidising materials such as phosphorous, carbon or graphite into the recycling process to control the levels of oxygen in the powder material (Tan, Wong, and Dalgarno, 2017).

The powder recycling process is a vital stage in advancing the L-PBF process and increasing its viability. Understanding the impact this process has on the powder and therefore the resulting parts produced will facilitate a greater utility of L-PBF. The current state of the art identifies the impacts powder characteristics on the L-PBF process, however, work is required to deepen this understanding. Development of a greater insight into the relationships between characteristics and the L-PBF process in required to establish some guidelines on the powder recycling process.

3.4 Powder Rejuvenation Process

At some stage with powder recycling the quantity of powder within a single batch will be at a level where it is too low to manufacture with or alternatively the powder characteristics have significantly deteriorated. Powder rejuvenation, a practice of mixing virgin powder material with recycled powder material to increase the utilisation of the recycled powder batch (Cordova, Campos, and Tinga, 2019), has received little attention to date. Opposed to powder recycling a rejuvenated powder batch will consist of a mix of both virgin, unused, powder and recycled powder, as demonstrated by the flowchart in Figure 3.11.

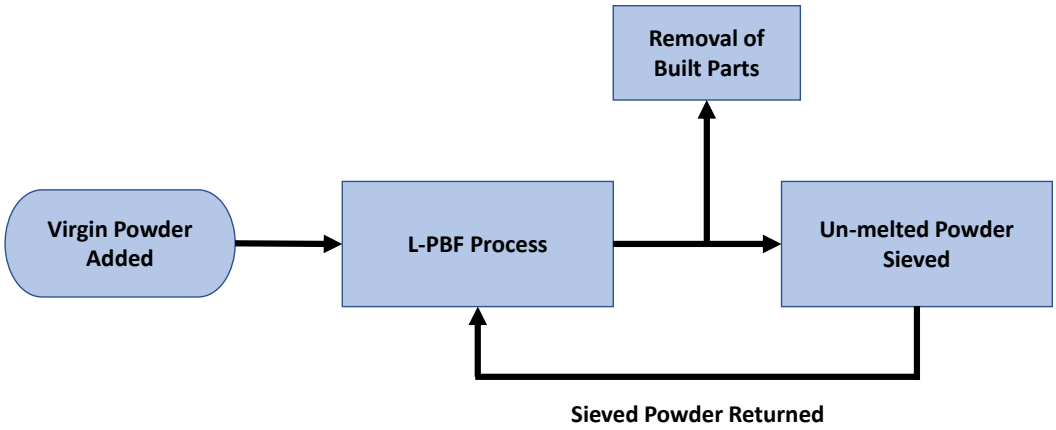

FIGURE 3.11: Powder rejuvenation process.

Powder rejuvenation can be conducted during the recycling process in two distinct ways:

- A continuous addition of material throughout the life of the powder to ensure the powder quantity and quality remains at an adequate level for further utilisation.
- A "top-up" process, where, a recycled powder batch is mixed with a virgin powder in a pre-determined ratio (Lutter-Günther et al., 2018).

This "top-up" process can be applied in a similar manner as presented by Harkin et al., 2020, where a proportion of the original batch is withheld from the build process and used to top up the powder as and when required. This is the preferred method, as conducting the top up process with dissimilar batches can create issues with traceability of the powder feedstock material (Lutter-Günther et al., 2018).

Strondl et al., 2015 presented a method of mixing recycled powder material with virgin powder material through the small additions of virgin powder, after each recycle of the powder. This method ensures the quantity of powder remains consistent, but the ratio of recycled powder to virgin powder is constantly changing. Strondl et al., 2015 found that there was an increase in the flowability of the recycled powder in comparison to the virgin powder. This study clearly shows the addition of small amounts of virgin powder allows for characteristics such as the particle size to remain within their specifications while improving the flowability of the powder (Strondl et al., 2015). This procedure was also applied by Cordova, Campos, and Tinga, 2019 with a batch of Inconel 718. Yánez et al., 2022 conducted a similar study where a continuous addition strategy was applied to the recycled powder. The method they applied consisted of the recycled powder being consistently supplemented with virgin powder after each L-PBF build. This ensured that a consistent quantity of powder was available for the L-PBF process. They repeated this process for a total of 12 builds. The published results were limited, stating that there was an increase in the oxygen content of the recycled powder samples. Further testing of the sample produced

from the L-PBF process with this powder conveyed that there was a significant increase in the surface roughness of the samples. This increase is likely due to a morphological change of the recycled powder used.

Harkin et al., 2020 presents an alternative method to the above where initially a percentage of the powder batch is withheld from being used in the L-PBF process. This proportion is then used to "top-up" the powder quantity as and when required in the powder recycling process. Harkin et al., 2020 continued this study of a Titanium powder for a total of nine L-PBF build processes. The oxygen content of the powder increased by 0.031% over the nine cycles with the levels exceeding the acceptable level after 7 cycles. These results are similar to those found in powder recycling studies previously shown. The authors found no changes in the size and shape characteristics of the powder particles. The flowability of the powder showed an increase as the recycling increased and the powder remained within the free flowing state a desirable property for L-PBF powders. This study shows that regardless of the recycling process and rejuvenation method applied for some materials the absorption of oxygen due to exposure to the L-PBF process is considered the critical factor. Other methods applied may not result in the same powder degradation and its typically driven by the material being used and its ability to withstand oxygen absorption. Further studies from the authors focused more on the mechanical properties resulting from these observed oxygen changes. It was shown that the mechanical properties did change as a result of this increased oxygen content, however they also cite that it may be influenced by the nitrogen within the build process (Harkin et al., 2022). Wang et al., 2023b presents a similar method or powder rejuvenation where a percentage of the original powder batch is maintained for the process. In this study a total of 14 build cycles were completed and after every five cycles this virgin powder was mixed in to the recycled powder. The resulting experiments determined that the process led to an increase in the mean particle size as well as the flowability improving, in agreement with other studies presented. The oxygen content gradually increased however, there was no phase change observed in the microstructure of the samples. A similar result was found by Lanzutti et al., 2023.

The above studies from (Clayton, Millington-Smith, and Armstrong, 2015; Strondl et al., 2015; Harkin et al., 2020) show the effect of the addition of virgin powder material to the recycled powder. The flowability results for both studies were acquired through the use of powder rheology. This is a dynamic test method of determining the flow characteristics of powders. This may provide a indication into why the findings are contradictory to those previously found by Seyda, Kaufmann, and Emmelmann, 2012; Tang et al., 2015; Sartin et al., 2017; Liu et al., 2011 who employed the standard static method of flow characterisation. The rheology method used by Strondl et al., 2015; Clayton, Millington-Smith, and Armstrong, 2015 gives a reading of the powders basic flow energy (BFE) which is a dynamic measure of the powders resistance to flow. The higher the BFE the more resistance to flow within the powder (Clayton, Millington-Smith, and Armstrong, 2015). These contradictory findings may be due to the effect of the additions of virgin powder to the recycled material or the different

characterisation method employed.

Powder rejuvenation allows for a further utilisation of the powder material used within the L-PBF process. The process leads to in general an increase in particle size and a narrowing of the particle size distribution. The morphology of the powder material deteriorates as the quantity of agglomerates increases and the flowability of the powder material has been found to improve. The chemical composition of the powder changes affected by the process of oxidation throughout the rejuvenation processes.

3.5 Defect Detection

Defects are undesirable occurrences in all manufacturing processes whether they be additive or subtractive. The additive manufacturing process has many different types of defects which often occur due to the following reasons:

- inconsistencies in the processing parameters
- changes in the operating environment
- inconsistencies in raw materials
- sub optimal build preparation

The defects which occur as a result of the above reasons include the following:

- Insufficient fusion - lack of inter-layer bonding between the successive layers in the process (Abdelrahman et al., 2017).
- Balling - molten metal solidifies into balls instead of solid layers thus affecting the layer bonding (Li et al., 2012).
- Internal porosity - formation of voids or pores within a part (Grasso and Colosimo, 2017).

The aforementioned defects can occur at various stages throughout the L-PBF process such as during laser exposure or in the powder deposition process. The aim of the powder deposition process is to ensures that there is a suitable layer of powder deposited for the laser exposure process.

Defect detection in the AM process has received significant research focus (Kanko, Sibley, and Fraser, 2016; Grasso et al., 2016; Everton et al., 2016; Sturm et al., 2016; Abdelrahman et al., 2017; Colosimo and Grasso, 2020; McCann et al., 2021) due to the realisation of the potential for the AM technology within industrial environments. The ability to produce high value complex components that were previously unattainable due to limitations in materials and manufacturing has led to increased attention. A move towards "*defect free*" manufacturing can increase the applicability of the L-PBF process (Dejene and Lemu, 2023; Colosimo and Grasso, 2020). Presented below is a series of classifications for the defects typically observed in the powder deposition process in powder bed fusion additive manufacturing and details of the previous research efforts in monitoring the AM process.

3.5.1 Definition of Defects

Defects in the process of powder deposition is of greatest concern to this research and as such the main defects experienced in that area are listed and detailed here. The powder deposition process is critical to the outcome of the process due to the high dependency of many mechanical properties on the even distribution of a powder layer (Miao et al., 2022). Defects often emerge during two distinct L-PBF operations:

1. Re-coating of the powder bed.
2. Laser interaction.

The occurrence of defects in the build process can be limited through ensuring homogeneity of the deposited powder bed. A homogeneous layer of powder on the build plate will ensure that the melting process will be evenly distributed and consistent for each layer (Lu et al., 2022a). Deposition of powder across the build plate is one of the most vital stages of any powder bed fusion AM process (Zielinski et al., 2017). An evenly deposited layer of powder on the build platform is essential for ensuring that a build is successful, reducing porosity in the final parts (Averardi et al., 2020). The powder, once it is within the process chamber, is only ever in direct contact with the re-coater blade and the build plate. This, powder contact only occurs during the re-coating stage of the process. A good quality deposition process means that there is a consistently even layer height across the entire build plate throughout the process. A powder layer which is deemed to be good quality is one which is free from gaps in the powder deposition. These gaps in the powder bed are often caused in the deposition stage by a damaged re-coater blade or if large particles become stuck in the re-coater. The quality of the layer of powder on the build plate fundamentally influences the extent of fusion between adjacent particles during laser melting. If the layer of powder is too thin on the build plate the laser power may begin to travel through previously melted particles and cause re-melting of previous layers. If the layer is too thick then the laser may not have enough power to fully melt through the entire layer height, therefore creating a lack of fusion between adjacent layers. Imperfections in the powder bed can often occur in one layer and then later correct themselves with future depositions of powder. Ensuring the first layers of powder are evenly distributed across the build plate provides a strong foundation for the building process providing adhesion between the first layers and the build surface (Tan, Wong, and Dalgarno, 2017).

3.5.1.1 Re-coater Hopping

This is a defect in the distribution of a powder layer, caused by the re-coater blade striking a part in the powder bed causing the re-coater to vibrate. This vibration therefore leads to ripples across the powder bed, perpendicular to the direction of the re-coater, creating small ridges of powder deposited across the build platform (Scime and Beuth, 2018), as demonstrated in Figure 3.12. The ridges can result in inconsistent deposition of the new powder layer and lead to defects in the resulting laser exposure process.

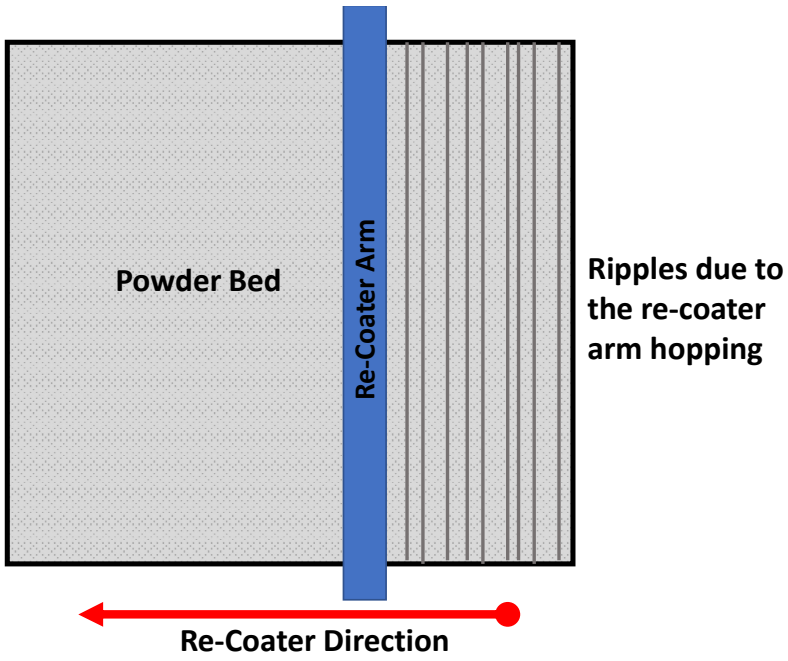

FIGURE 3.12: Re-coater hopping in the powder bed.

3.5.1.2 Re-coater Streaking

A defect caused in the deposition of the new powder layer, often when the re-coater blade drags a piece of debris across the build platform, or if the re-coater blade is damaged. Both result in a disruption to the deposition of the powder bed in the form of lines or ridges (Craeghs et al., 2011) created parallel to the re-coater blades direction of travel (Scime and Beuth, 2018; Foster et al., 2015), shown in Figure 3.13. The can result in inconsistent powder melting during the laser exposure phase.

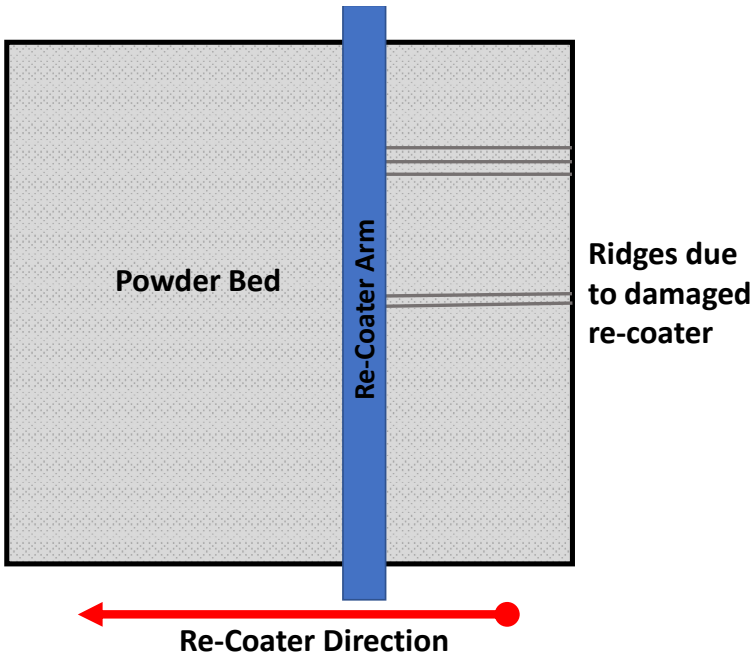

FIGURE 3.13: Re-coater Streaking in the powder bed.

3.5.1.3 Super Elevation

This is a defect which is mostly caused by sub-optimal build preparation. In some parts, where there are thin overhanging regions the part may curl or warp as a result of the residual stresses developed during the build process (Jacobsmühlen et al., 2013). This creates a region of the part that will protrude above the powder layer. This warped material is often hit by the re-coater in the powder layering process and can cause some of the previously discussed defects like re-coater streaking or hopping. This defect can be avoided through process parameter optimisation, build orientation or support material (Grasso and Colosimo, 2017). Detection of elevated edges in a timely manner can also prevent damage to the re-coater blade, leading to re-coater streaking and the effects that may result from that

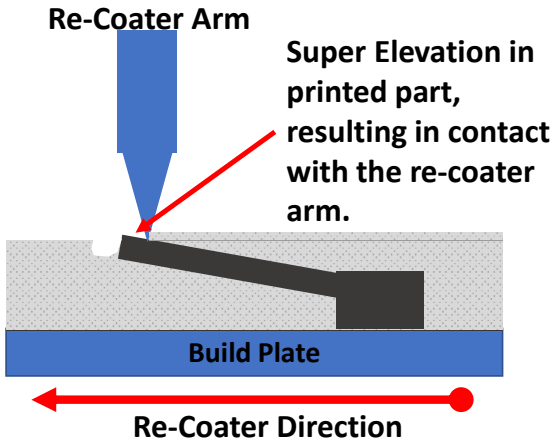

FIGURE 3.14: Super elevation demonstrated in a cross section of the powder bed.

3.5.1.4 Incomplete Spreading

This defect occurs when there is insufficient powder deposited, shown by the regions in white in Figure 3.15. This leads to a proportion of the build plate, typically towards the end of the re-coater travel, that does not receive enough powder material (Scime and Beuth, 2018). The defect is a result of incorrect re-coater parameters being selected but can also occur when there are other defects present within the build platform that may disturb the distribution of powder (Scime et al., 2020).

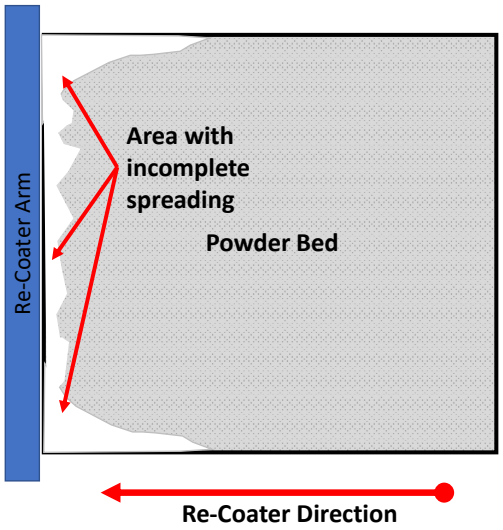

FIGURE 3.15: Incomplete spreading demonstration in the powder bed.

3.5.2 Platform Monitoring

Ensuring the advancement of the L-PBF process in the industrial sector is a top priority, and one way to achieve this is by prioritizing the development and deployment of in-situ monitoring systems capable of effectively monitoring the build platform (Colosimo and Grasso, 2020). The build plate is where the laser interaction occurs with the powder material. The quality of the deposited powder material will determine the quality of each of the layers melted. Monitoring of the build plate and the powder bed can take a static or dynamic approach (Neef et al., 2014; Foster et al., 2015; Land et al., 2015; Abdelrahman et al., 2017). A static monitoring approach captures data at various stages through the L-PBF process to be analysed, conversely a dynamic approach captures continuous data from the process for analysis. The multiple influences on the L-PBF process and effect local deviations in the powder layer distribution can have in the quality of the manufactured samples highlight the importance for monitoring systems to be in place (Fischer et al., 2021).

The first powder layer is deposited by the operator manually and as such this leads to a range of different first layer thickness's. This is due to inconsistencies in set-up procedures between different operators. This defect was noted by Neef et al., 2014 who applied the use of Low Coherence interferometry (LCI) to monitor

the homogeneity and layer height of the first powder layer. LCI is a non-contact optical sensing tool. The sensor sends out a light signal to a surface which is reflected back and detected by the interferometer. The method measures the distance to the build platform without a layer of powder and then also after the first powder layer has been deposited this is then used to establish the thickness of the deposited layer. The tool can be used by the operator to decide whether or not to change the layer height or to begin the build process. The researchers suggest this method could be used to ensure the level of the build plate within the chamber. The application of the LCI set-up allows for measurements to be taken across the build platform. Allowing for features of interest to be monitored i.e. the level of the build plate or homogeneity of the layer thickness. The speed at which this method can provide the information required is dependant on the area being scanned, the larger the area the longer this method will take. The method allows for the consistent deposition of the first layer of powder as well as allowing the level of the build plate to be confirmed. Both of which will enable a consistent powder bed deposition and improve the quality of the components produced, removing the element of inconsistency with operator set-up.

Monitoring the powder bed through the build process was achieved by Abdelrahman et al., 2017 with a set-up in which a standard digital single-lens reflex (DSLR) camera was used to take an image after each layer of powder had been deposited. This method produces a range of images that represent each of the powder deposition stages throughout the build process. Through post-processing of the acquired images any defects observed in the powder deposition process can be identified and then later translated into the affected part. This method allows for a map to be created of the locations of the imperfections, as seen in the images. Due to the often occurrence of flaws in a single layer and then for them to correct themselves in subsequent layers, caution is required in this method. To address this issue in the image post-processing a flaw must be present in greater than two successive layers for it to be considered an issue to the integrity of the build. The number of layers a defect needs to be present in a build before it becomes detrimental to the final part properties will be highly dependant on parts manufactured and the industry for which those parts are being made. For some industries a zero-defect manufacturing ethos may be employed and as such any identified defects would result in a failed part.

Land et al., 2015 present a similar method of imaging each layer of the build to Abdelrahman et al., 2017, however they collected images by imaging from multiple angles over the build plate. This allows for the development of the features on a part through each layer of the build to be continuously observed. This differs from the previous method as the part is being observed in comparison to the powder deposition. The method described utilises three cameras mounted above the build plate allowing for the required images to be taken. Imaging the build plate from multiple angles allows for more information to be retrieved, details that may not appear in one angle could present themselves in another due to the inconsistency of the lighting within the build chamber. The strength that this method allows is the full part and the development of the different features are being observed instead of the powder bed being observed. However, due

to this set-up there is a large quantity of images and data collected meaning processing time can be quite high. This can be an issue in terms of the quantity and speed of data that is transferred especially for high resolution images of the process. At present this is the extent of their work with their future aims to use this information to provide a system of real time in process closed loop control. Pagani et al., 2020 presented a method of in the same manner as both Foster et al., 2015; Abdelrahman et al., 2017. Their images are fed into an algorithm which identifies the edges of the components printed and compares the results with the input data for comparison and validation.

The deposition of powder is often affected by the previously melted layers. Some components will become distorted through the build process due to the multiple cycles of rapid heating and cooling, creating residual stress, inherent with L-PBF processes (Park, Tran, and Nguyen, 2017). This thermal distortion will cause the component to break away from support material to super elevate, as described earlier, causing contact with the re-coater. This can cause a build to be aborted if the protrusion is significant enough to stop the re-coater arm or if the contact with the re-coater causes the powder to be "flicked" away, leading to a non-homogeneous powder bed. This is observed by Foster et al., 2015 where the lack of powder due to this "flicking" is likely to produce further defects in the build due to the non-homogeneous layer of powder material. Imaging the build area allowed for the development of this issue to be observed. This causes a hollow in the powder bed behind the protruding part. A standard DSLR camera was installed into the build chamber of an EOS M280, with the support of multiple light modules to aid with lighting of the imaged area. The method was tested through imaging a build that would generate defects, due to the inefficient positioning on the build platform. This would allow for the defect detection capability of the system to be assessed. The lighting is a key element to this set-up with the multiple flash modules allowing for different defects to be observed in each image. The post-processing of the acquired images allow them to be stacked to form a 3D model. This can then be used to correlate to the defects detected by X-ray CT of the solid components. This system allows for documentation of the entire build process through imaging each build layer. A defect within a part can be traced back to the layer in which it began to occur, allowing decisions on the integrity of the built parts to be made.

These discussed methods provide an insight into the quality of each powder layer at the beginning and during the process. The aim of this is to ensure the quality of the powder deposition process has minimal negative impact on the quality of the output component. A homogeneous powder bed will ensure that the laser melting process is consistent throughout the build platform (Cordova, Campos, and Tinga, 2019). If there was a powder deposition issue in one area of the build platform then that location can be translated into a part and the extent of the issue can be assessed further in ex-situ examination processes. A common issue that is presented in the above methods is the data acquisition in terms of speed and quantity of data that is acquired for a build.

3.6 Summary

The following points are a brief summary of the main findings from the literature review:

- L-PBF is an additive manufacturing process which is gaining popularity for the production of high value complex components for the medical devices, aerospace and automotive industries. These industries can utilise the L-PBF process to increase the complexity and functionality of the components.
- Metal powders are the feedstock material for the L-PBF additive manufacturing method. These powders are produced through an atomisation process, which heavily influences the powder characteristics. The characteristics of the powder material along with the L-PBF process parameters control the final as-built part properties. Understanding the relationships between the powder characteristics, the recycling process and rejuvenation process can enable a greater utilisation of the powder.
- Powder recycling is a process to gain a greater utilisation from L-PBF powders, however this process impacts the characteristics of the powder particles and the outcome of the L-PBF process.
- Powder rejuvenation enables a further utilisation of recycled powder, attempting to restore some of the original bulk powder properties to make it suitable for the L-PBF process.
- The detection of defects throughout the additive manufacturing process is an area where a lot of research to date has been focused in particular on the monitoring of the build platform and powder deposition process. In-situ monitoring of the additive manufacturing process has been highlighted as an area for research to allow the technology to develop further.

4 Materials and Methods

The aim of this chapter is to introduce and describe the materials and methods that were applied during the studies presented in this thesis. The 316L powder for the project is presented and its key properties identified. This is followed by a description of each of the methods applied throughout the studies conducted in this body of research, these include the powder characterisation methods, part characterisation methods, defect detection system and finally statistical methods used to quantify the data collected. The methods outlined will be referred to throughout the remaining chapters of this thesis.

4.1 Materials

The powder material central to this project is Stainless Steel 316L. This powder is supplied by EOS GmBh. This material has a range of applications across multiple industrial sectors including medical device, aerospace and automotive.

4.1.1 Stainless Steel 316L

316L stainless steel is a gas atomised, corrosion resistant iron-based alloy powder supplied by EOS GmBH. The chemical composition of this powder is quantified in Table 4.1 and corresponds to ASTM F138, a standard for the composition of steel surgical implants (EOS GmbH, 2014). This alignment with the ASTM standard, allied to the materials corrosion resistance, is why this material is used in the medical device and surgical implants industry (Sun et al., 2016). 316L has a Face Centre Cubic (FCC) structure consisting of a single Austenite γ phase (Yan et al., 2019).

TABLE 4.1: Chemical composition of Stainless Steel 316L (EOS GmbH, 2014).

Element	Content (%wt)
Iron, Fe	Bal.
Chromium, Cr	17.00 - 19.00
Nickel, Ni	13.00- 15.00
Molybdenum, Mo	2.25 - 3.00
Carbon, C	0.03
Manganese, Mn	2.00
Copper, Cu	0.5
Phosphorous, P	0.025
Sulphur, S	0.010
Silicon, Si	0.75
Nitrogen, N	0.1

4.2 Laser Powder Bed Fusion

As introduced in Section 2.2.1 of this thesis the L-PBF process is a process of melting a metallic powder selectively using a laser to produce a metallic components. The EOS M280 process used in this research consists of a 200W Ytterbium (Yb) fibre laser and a build envelope of 250 x 250 x 325 mm.

The L-PBF process is depicted in Figure 4.1. The process begins with a re-coater blade depositing a new layer of powder across the build platform. This layer of powder can be anywhere from 20 - 60 μm in thickness depending on the material being processed and quality required. In general smaller layer thickness's result in finer details. With the deposited layer of powder material across the build platform the laser then exposes the regions of the build plate according to the layer information or slice data. The laser melts the powder particles to form solid metal. Once the laser has finished exposing the layer a new powder layer is deposited and the process is repeated. This laser processing is conducted under an inert atmosphere using either Nitrogen or Argon.

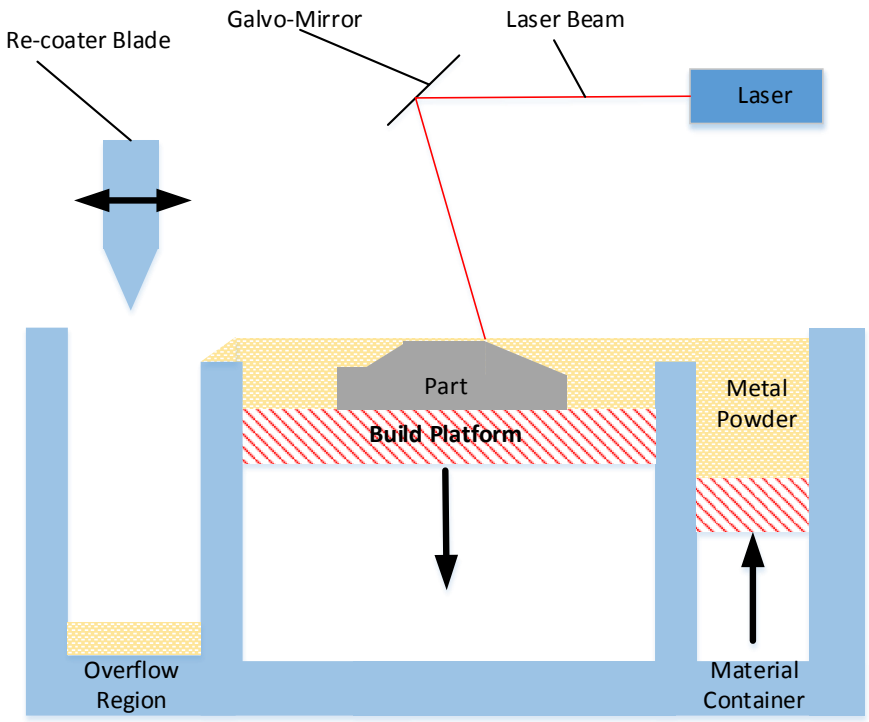

FIGURE 4.1: L-PBF process description.

Before processing any build files the selected CAD file needs to be converted to a slice file, a layer-by-layer file of the parts, which the laser can follow. The slice file contains all of the information about the part including the processing parameters, support structures and its location within the build envelope. This file was imported to PSW a machine specific software allowing for the final build parameters to be defined. For this project the default material specific parameters, as specified by EOS, were applied. The laser parameters determine how much energy is applied to the powder layer to melt the adjacent powder particles to form the solid metal. The parameters of interest are the Layer thickness, Laser Power, Scan Speed and Hatch Distance. The default scan and laser parameters for 316L are shown below in Table 4.2.

TABLE 4.2: Default Scan and Laser Parameters for SS316L.

Parameter	**Value**	**Units**
Laser Power, P	195	W
Scan Speed, S_s	1100	mm/s
Layer Thickness, L_H	20	μ m
Hatch Distance, H_d	0.09	mm

The resulting energy density (ED) for the default build parameters has been calculated to be 98.48 J/mm^3. This was calculated using Equation 4.1 as shown

below (Thijs et al., 2010).

$$ED = \frac{P}{S_s H_d L_H} \tag{4.1}$$

4.3 Powder Characterisation

Powder characterisation is the determination of the fundamental characteristics of the powder particles and the subsequent powder batch. These characteristics have a significant impact on how the powder will perform within the L-PBF process. Powder characterisation methods that are applied to AM powders are typically adopted from traditional powder characterisation processes (O'Leary et al., 2015). The powder characterisation methods that are explained in this section are those, employed in Chapter 5 and Chapter 6 of this thesis.

4.3.1 Powder Sampling

There are three commonly applied powder sampling methods:

- Stream Sampling
- Chute Sampling
- Scoop Sampling

Due to the fact the powder being evaluated here is stored in a container, machine hopper or overflow, the first two methods are less suitable, with scoop sampling the most effective method. This method allows for a sample of bulk powder material which is stored within a container to be assessed.

The method consisted of a scoop being plunged into the powder and removing a sample. Prior to sampling, the powder within the powder dispenser was mixed using a scoop to achieve a good mix in the batch and to ensure powder has not settled. One of the common errors associated with this method is that sampling in one scoop may lead to a non-representative sample of the entire powder batch (Allen, 1997). This error was ameliorated by taking multiple smaller scoop samples throughout the powder container. Jillavenkatesa, Dapkunas, and Lum, 2001 found that the standard deviation when sampling by Scoop was 5.15% when compared to other powder sampling methods. In order to ensure a representative sample of powder is taken the minimum sample mass is calculated using Equation 4.2 (Allen, 1997).

$$M_s = \frac{1}{2}\left(\frac{\rho}{{\sigma_{SE}}^2}\right)\left(\frac{1}{w_1} - 2\right)d^3 x 10^3 \tag{4.2}$$

Where (Allen, 1997):

- ρ is the apparent density of the powder material in g/cm^3.
- σ_{SE} is the variance of the sampling error.

- w_1 is the percentage fractional mass of the coarsest size class being sampled.
- d is the mean of the extreme diameter within the maximum size class in cm.

Powder was sampled twice per build. The first sample was taken before the building process and the second sample after a build was complete. Samples of approximately 150g in weight are required to conduct the chosen range of tests and analysis described in the following sections. A sampling scoop of approximately 15g was used to sample ten locations in the powder dispenser of the EOS M280, as shown in Figure 4.1. The ten sampling locations were distributed across the entire volume of the dispenser. Once sampled the powder remained within an airtight container, to limit the absorption of any moisture and oxidation, until testing was conducted.

4.3.2 Chemical Composition

Powder bulk chemical composition refers to the chemical make-up of the powder. As presented in the literature review, Section 3.2.1 and 3.3.2, the composition of the powder is heavily influenced by the atomisation process used but subsequently can also be affected by the recycling of the powder.

4.3.2.1 Energy Dispersive X-Ray

The composition of the powder was analysed through the use of a Scanning Electron Microscope (SEM) with an Energy Dispersive X-Ray Analyser (EDX) attachment (Pinkerton and Li, 2005; Sutton et al., 2016b; Cordova, Campos, and Tinga, 2019) on a Hitachi TM3030 Plus table top SEM.

For EDX analysis the surface of the powder particles is excited by a beam of electrons, the ejected x-rays are then detected, and their peak values are assigned to a known value for each chemical element, as seen in Figure 4.2. This method is semi-quantitative due to the assignment of peak values with a known value for a given element, and as such is generally used as an estimation tool for the composition of the powder (Slotwinski et al., 2014).

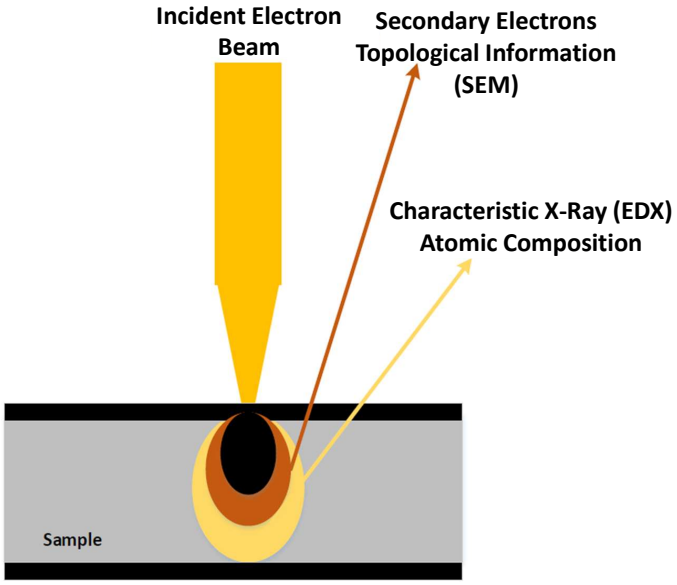

FIGURE 4.2: Scanning Electron Microscopy operating principals.

Powder was deposited in a thin layer on top of a carbon conductive tab before being mounted onto Ø15 mm aluminium specimen mounts for the SEM. For each sample of powder three EDX maps of the surface were conducted at a magnification of x250, allowing for a larger area of the deposited powder to be assessed. The resulting chemical composition were then determined and averaged over the three tests.

4.3.2.2 X-ray Diffraction

X-ray diffraction (XRD) is a non-destructive characterisation method that can be used to determine and analyse the crystalline phase structure of materials. The crystalline phase structure of materials corresponds to the specific chemical and atomic arrangement within the material. XRD analysis of a material allows for the determination of the:

- Nature of the crystalline phases present in the powder.
- Quantity of each phase present in a material.
- Presence of amorphous material.

In XRD a beam of X-rays are fired on to the surface of a sample, as described in Figure 4.3. A detector is rotated around the sample to detect the diffracted X-rays from the sample. These scattered X-rays produce a diffraction pattern, which contains the relevant information of the atomic arrangement within the crystalline structure. Each diffraction pattern is a product of the unique crystal structure of a material.

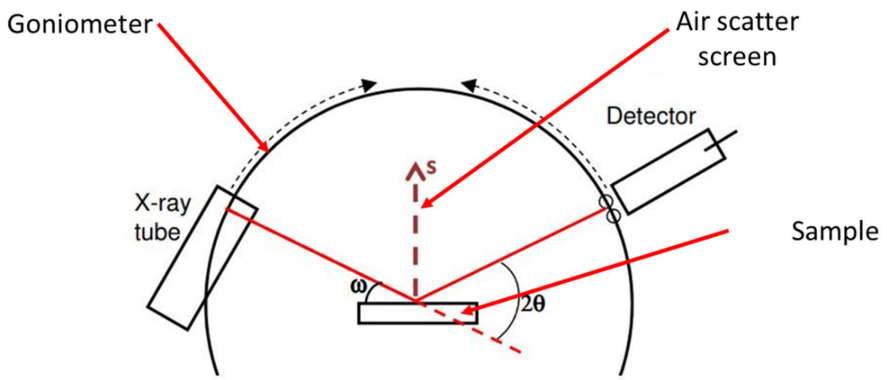

FIGURE 4.3: Description of the XRD analysis method and test setup.

Diffraction peaks, as shown in Figure 4.4 are used to describe planes of atoms. The miller indices (hkl) were used to describe these planes of atoms. These planes of atoms assist in the analysis of the atomic structure and microstructure of the sample. The position of the diffraction peaks are determined by the distance between the parallel planes of atoms. Bragg's law is used to calculate the angle between parallel planes of atoms. This is then used to produce a diffraction peak required to determine the spacing of the internal material lattice spacing of the crystal structure. The law states that scattered X-rays from a crystal lattice corresponds to the angle of incidence (Cantor, 2020). The law provides a simple model to understand what conditions are required for the diffraction of the X-rays.

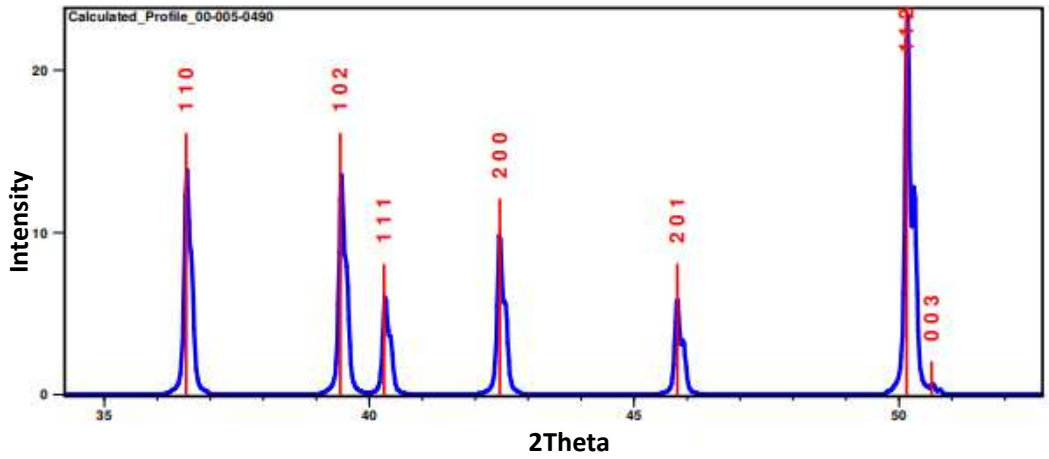

FIGURE 4.4: Example of the detected XRD peaks with the associated miller indices, shown in red.

XRD was conducted on the powder samples to assess the effect of the rejuvenation and recycling processes on the microstructure of the powder, specifically, the primary phases. The phases present within the 316L powder were

assessed at different stages in the powder recycling and subsequent rejuvenation process. The phase analysis was conducted using XRD using a Bruker D8 Advance X-ray diffractometer with a Cu-Kα radiation (λ = 0.154 nm) operating at 40 kV and 40 mA.

The metal powder samples were poured into a cavity mount which ensured that the exposed powder surface was spread flat. A step size of 0.01° and a dwell time of 0.2 seconds per step was selected. The XRD data was assessed using International Centre for Diffraction Data (ICDD), Crystallography Open Database (COD) and Bruker Eva® software. The primary phases from each of the powder samples were compared.

4.3.3 Powder Morphology

The morphology or shape of powder particles was analysed both qualitatively and quantitatively by Scanning Electron Microscopy (SEM). Sample preparation and test methods were developed to allow for the morphology of the powder particles to be assessed. A thin layer of powder was deposited onto of a carbon conductive tab and mounted upon a Ø15 mm aluminium specimen mount for the SEM. SEM images at x100, x250, x500 and x1000 magnification were then captured. The increasing magnification allowed for the morphology of the individual particles to be observed. Qualitative analysis was initially conducted through visual observation of the captured SEM images, this provided a visual reference to the morphology of the powder particles.

Quantitative analysis was conducted using the images acquired from the SEM at x250 and x500 magnification. The images were imported and further analysed within ImageJ. ImageJ is an open source image processing software (Abràmoff, Magalhães, and Ram, 2004). Image analysis is required to determine the area, A, and perimeter, P, of individual captured particles. The image analysis procedure, as outlined in Figure 4.5, required the images to be converted to binary allowing for individual particles to be selected and their area and perimeter to be extracted.

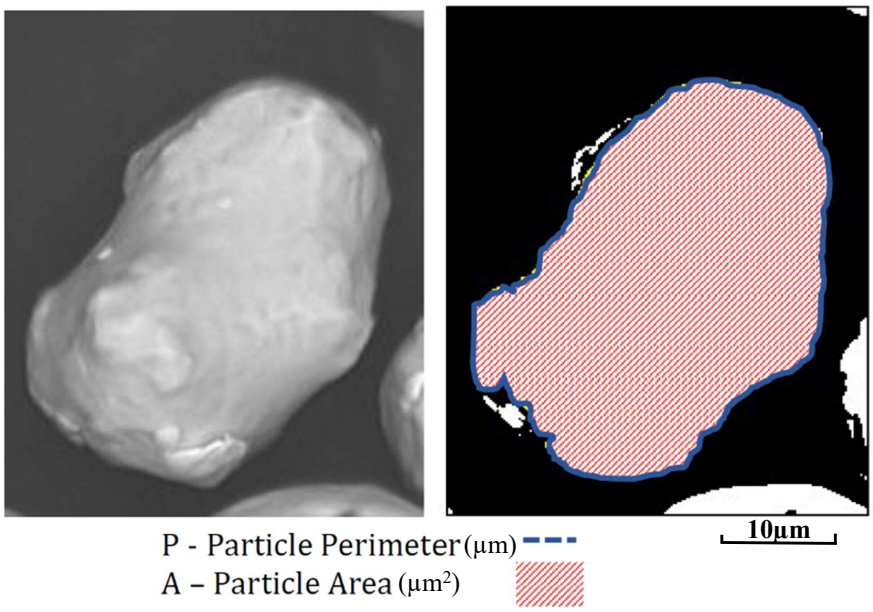

FIGURE 4.5: Quantitative powder morphology procedures.

This provides the data for the circularity of the particles to be calculated using Equation 4.3 (Cox, 1927; Sun et al., 2015). A perfectly circular particle will have a circularity value of one where as non-circular particles will have a value less than one.

$$Circualrity = 4\pi(\frac{A}{{P_p}^2}) \tag{4.3}$$

Where (Cox, 1927):

- A is the projected area of the particle in μm^2.
- P_P is the perimeter of the measured particle in μm.

Other shape descriptors, such as the particle convexity, aspect ratio and solidity can also be used to represent the powder morphology. These descriptors are, like the circularity descriptor used, based on a 2D representation of the particle and typically quantified by an image analysis process similar to the one deployed in this thesis. For this work the circularity descriptor was used.

4.3.4 Particle Size

Powder particle size was investigated through the use of Laser Diffraction. This was conducted using a Microtrac S3500 Dry Dispersion Laser Diffractometer. This method utilises a laser beam to illuminate a sample of powder which is dispersed in front of a series of detectors. The detectors measured the intensity of the scattered light caused by interference with the dispersed particles. The interference pattern measured by the detectors was then used to calculate the individual particle sizes (Slotwinski et al., 2014), as shown schematically in Figure

4.6. The test methodology for laser diffraction method is defined in the ASTM B822 and ISO 13320 standards.

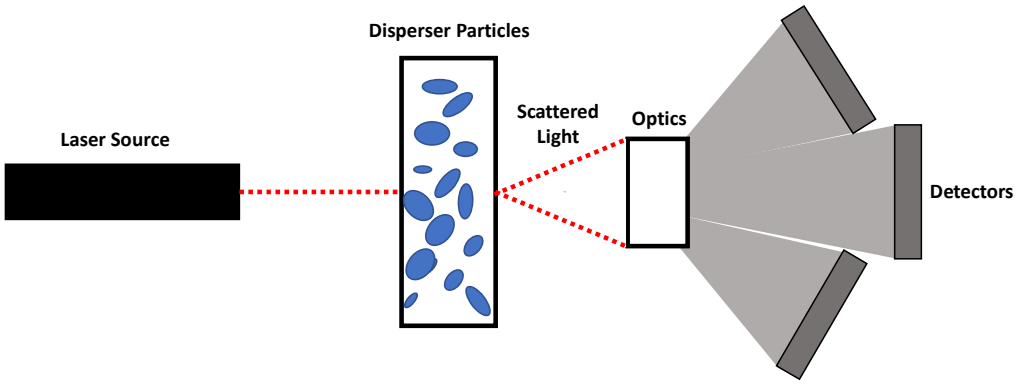

FIGURE 4.6: Laser diffraction operation.

Prior to analysis the powder was mixed with a small sampling spoon in order to prevent the effects of settling which may have occurred in storage. A volume-based particle size distribution of the sample was then obtained. Each powder sample was tested three times with the mass of the sample ranging from three to five grams. The individual results from each test are obtained and an average for the batch was produced.

The values of interest extracted from the laser diffraction test for this study are as follows:

1. Mean particle size - average particle size in the tested batch.
2. Volume particle size distribution - The distribution of particle sizes in the batch.
3. Span of the particle size distribution - the width of the distribution of the particle sizes.

These values allowed for comparison with other powder samples from different manufacturers as well as the relevant literature. Some qualitative analysis of the powder particle size can also be conducted when assessing the morphology of the powder particles. However, the laser diffraction method then ensures a quantitative value can be associated with each powder sample.

4.3.5 Powder Density

Powder density refers to the mass of powder per unit volume. As defined by the Equation 4.4.

$$Density = \frac{Mass}{Volume} \tag{4.4}$$

The powder density was determined by three different methods allowing for the Apparent Density, Tapped Density and Skeletal Density to be quantified. Each of these measurements were used to provide a greater understanding of how the powder may perform in the L-PBF process. These methods are explained in the subsequent sections and can be seen in Figure 4.7 below.

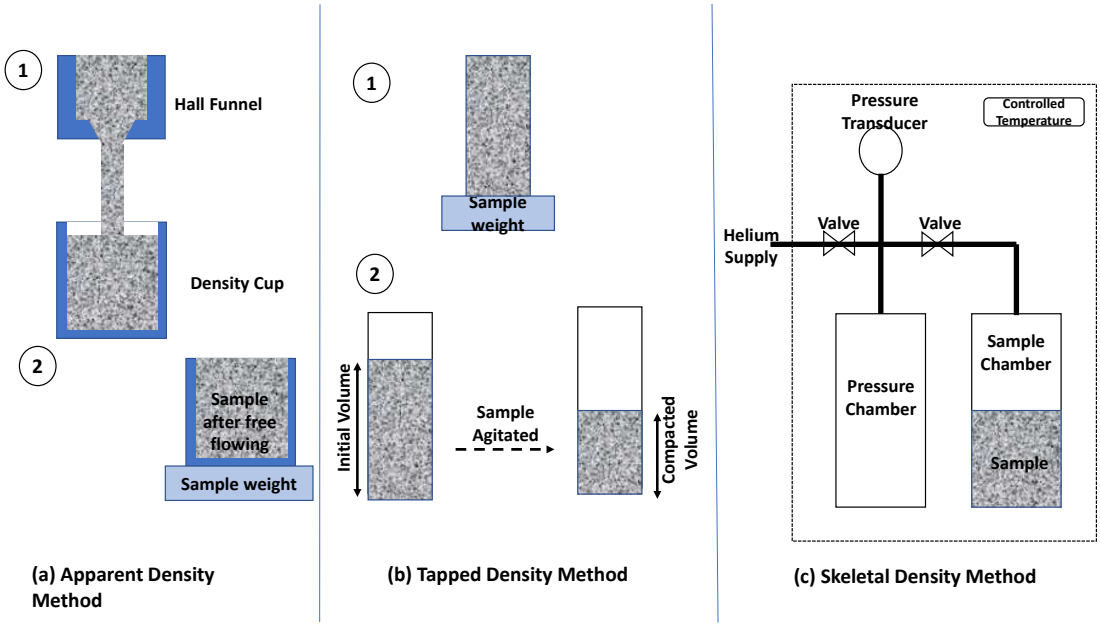

FIGURE 4.7: Powder density determination methods for (a) Apparent Density, (b) Tapped Density and (c) Skeletal Density.

4.3.5.1 Apparent Density

The apparent or bulk density of a powder is defined as being the mass per unit volume of the powder after free-falling. It is the density of an un-compacted sample of powder (Schueren and Kruth, 1995; Popovich and Sufiiarov, 2016). The determination of apparent density of powder material is covered by standards ASTM B212 and ISO 3923-1 (Kirchner et al., 2016; Slotwinski and Moylan, 2014).

The methodology to determine the apparent density is as follows; an empty density cup of a known fixed volume was weighed. A powder sample was then loaded into a Hall Funnel above the empty density cup. The powder was allowed to fall freely into the cup until it overflows the density cup. The excess powder was then scraped from the top of the cup. This ensured that only the mass of powder within the density cup was being measured. The mass of the filled cup was then measured to the nearest 0.01g and the initial mass of the empty cup subtracted to determine the mass of the powder. This process is shown above in Figure 4.7(a). The apparent density was then calculated using a modified version of Equation 4.4, as shown below in Equation 4.5.

$$Density = \frac{Mass_{FullCup} - Mass_{EmptyCup}}{Volume} \tag{4.5}$$

4.3.5.2 Tapped Density

The tapped density is defined as the mass per unit of volume of a powder after the powder it has been vertically agitated until no more visible settling occurs. That is the mass per unit volume after the powder has been fully compacted through an agitation process. The tapped density of powder material is covered by standards ASTM B527 and ISO 3953 (Engeli et al., 2016).

The methodology for the tapped density as shown in Figure 4.7 (b) is as follows. A sample of 50g of powder was introduced into a graduated volumetric cylinder of 25ml. The volume the powder occupies in the cylinder was noted. It is important that in this process the powder was poured freely into the graduated cylinder so as to avoid any possible compaction prior to the agitation stage. The cylinder was then placed into the tapping apparatus and operated until no more visible settling has occurred. Volume readings were recorded every 100 taps. The volume of the powder after the tapping was then recorded. The tapped density was calculated using Equation 4.4. The test was repeated three times using fresh, untapped powder for each test, an average tapped density value was then obtained.

4.3.5.3 Skeletal Density

Skeletal density is assumed to be the density of a fully dense part with no discernible porosity (Slotwinski et al., 2014). An AccuPyc II 1340 Helium Pycnometer is used to determine the skeletal density of the powder sample. A schematic of this apparatus is presented in Figure 4.7 (c).

A sample of known mass was placed into one of two chambers of known fixed volume. These chambers are maintained at a constant temperature throughout the tests. Helium gas was then added to the sample chamber. Helium is chosen as it is light enough to access the open pores within the powder sample. The pressure of the helium in the cell was then recorded. Once equilibrium in the sample chamber has been reached the helium is released and flows into the second empty chamber and equilibrium is reached. The ideal gas law was then applied between the two chambers with the recorded equilibrium pressures and temperatures allowing the volume of the powder to be quantified. The density measurement was repeated ten times or until the difference after five consecutive readings is less than 0.005 g/cm^3. With the volume and mass known, Equation 4.4 was applied to calculate the skeletal density of the powder (Slotwinski et al., 2014).

4.3.6 Powder Flowability

Powder flowability is one of the key characteristics for AM powder materials. The flowability of a powder will determine its performance within the AM process (Clayton and Deffley, 2014). A good flowability allows for a consistent layering process and therefore a good overall process performance. Poor flowability will lead to inconsistency in the powder layering process. The Hausner Ratio was

used in this research to provide an indication of the flowability of the powder tested.

The Hausner Ratio is the ratio of the tapped density to the apparent density, discussed in previous sections. This gives an indication to the flowability of the powder material. Due the ease in which it can be determined it is one of the most common ways to determine the flowability of a powder (Sutton et al., 2016b). It provides an indication into the inter particle friction in the powder sample.

$$HausnerRatio = \frac{TappedDensity}{ApparentDensity} \tag{4.6}$$

A low value for the Hausner Ratio is an indication of good flowability in the powder sample as there is low particle to particle friction. This means that the powder can be compacted more as the tapped density will be significantly lower than the apparent density. A value lower than 1.25 is determined to have good flowability (Kirchner et al., 2016). With an ideal Hausner Ratio of 1.00 to 1.11 being classed as excellent flowability (Sutton et al., 2016b) as shown in Table 4.3.

TABLE 4.3: Powder flow descriptions in terms of the Hausner Ratio (Sutton et al., 2016b).

Hausner Ratio	Flow Description
1.00 - 1.11	Excellent
1.12 - 1.18	Good
1.19 - 1.25	Fair
1.26 - 1.34	Passable
1.35 - 1.45	Poor
1.46 - 1.59	Very Poor
>1.60	Non-flowable

4.4 Part Analysis

The following methods were used to characterise the as-built parts produced by the L-PBF process. The analysis of the parts allows for the effect of the powder characteristics on the as-built parts to be quantified. Thus, enabling the relationships between the input powder and output part quality to be inferred.

4.4.1 Sample Design

In order to assess the impact of the powder recycling and rejuvenation process on the as-built part qualities, a series of parts were designed for test methods, described in the following section, to be conducted. The parts designed can be seen in Figure 4.8 below.

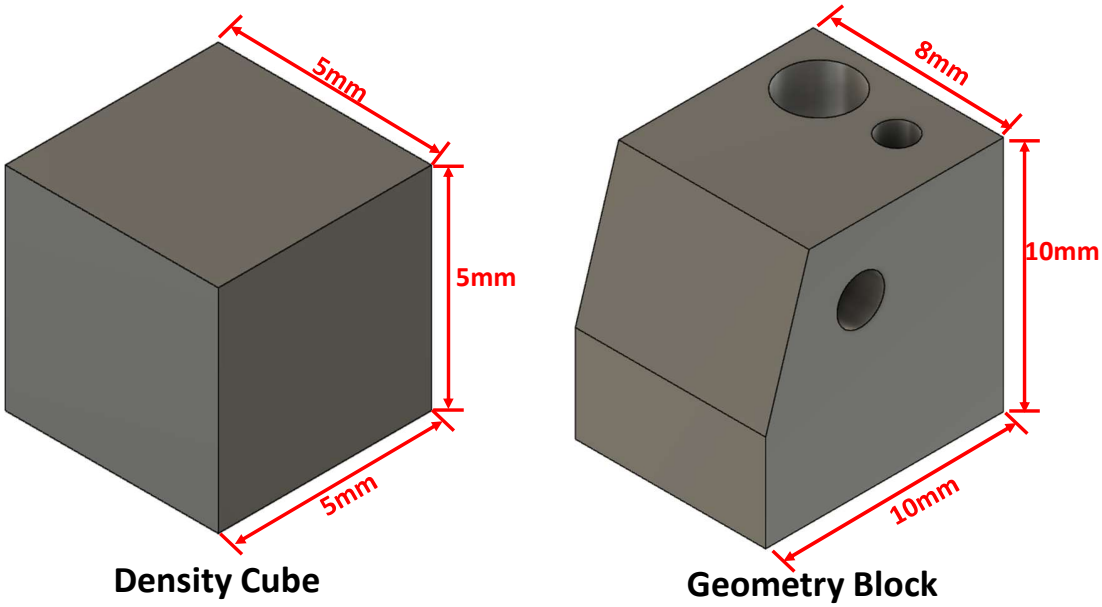

FIGURE 4.8: Designed and printed test parts.

Each of the designed parts shown above allow different qualities to be assessed. The first of the parts designed were density cubes which are $5\ x\ 5\ x\ 5\ mm^3$ in dimension. These cubes were mounted and sectioned in order to reveal the cross-section allowing the porosity content to be analysed. Three cubes were required in order to assess the cross-sections corresponding to the different orientations to the re-coater system within the machine.

The final part is a geometry block. This allowed for multiple characteristics to be assessed. Firstly the surface roughness of the faces was determined though focus variation. The incorporation of different hole diameters and orientations allowed for the dimensional accuracy of the parts and features to be quantified. The flat surfaces allowed for the hardness to be assessed in both the horizontal and vertical planes. As the parts were tested for hardness some design testing rules regarding the distance from previous test locations must be observed and were incorporated into the design of the part.

As discussed earlier a slice file needs to be generated for the build to be completed. For this the parts were exported from the CAD software and imported into Materialise Magics. In Magics the parts were orientated to their positions within the build envelope and support structures applied as required. Once the parts were correctly orientated and supported in Magics a slice file was exported as a .sli file, which can be read by PSW on the EOS M280. Figure 4.9 below shows the orientation of the parts and assignment of support material.

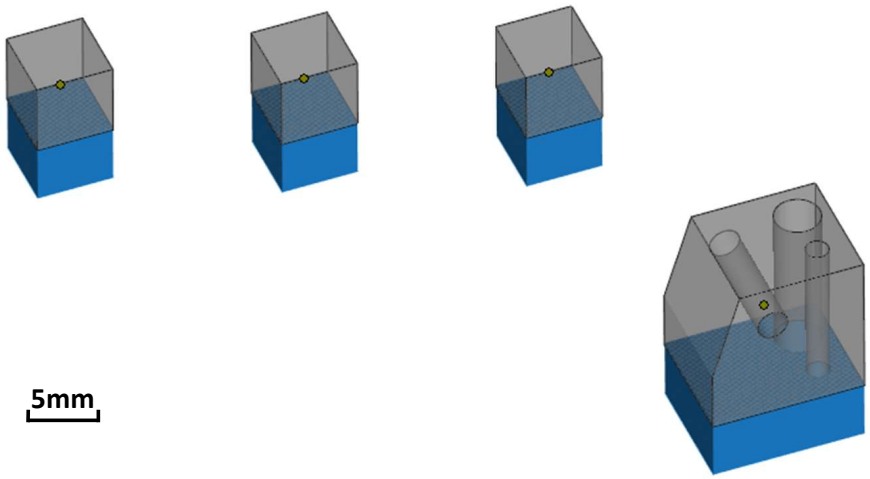

FIGURE 4.9: Test parts with assigned support geometry (blue) and orientation.

4.4.2 Surface Roughness

Surface roughness provides an understanding into the condition of the surfaces produced by the L-PBF process. Focus variation, as shown in Figure 4.10 was utilised to measure the surface roughness of the as-built parts. A Bruker Alicona Infini Focus SL was used to measure the arithmetic mean (Ra) and ten-point measure (Rz) values of the tested surfaces. This method is a non-contact surface measurement.

Focus variation operates by capturing a series of images of the surfaces at different focus heights. These images are then compiled utilising the areas of the captured images in focus to complete a representation of the surface condition. The images are captured using a x5 magnification providing a vertical resolution of 460 nm and a total measurement area of 13 mm^2. The surface roughness of the parts were measured without any prior surface treatment to represent the surface finish as produced directly by the L-PBF process. Each measurement consisted of five regions across the sample surface and then averaged to ensure a greater representation of the surface.

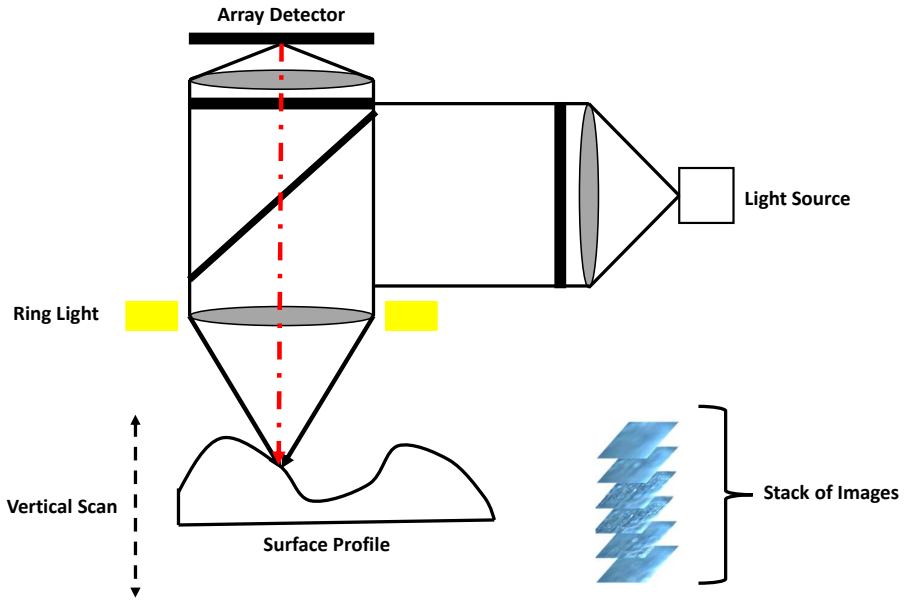

FIGURE 4.10: Focus variation surface roughness measurement method.

Ra is one of the most commonly used roughness parameters (Townsend et al., 2016). Ra is developed by measuring the area of the peaks and valleys in the surface over a given length and then the average is used to produce the Ra value, see Equation 4.7. One of the main limitations of the Ra value is that it does not differentiate between the peaks and valleys of the measured surface. Therefore, Ra can be insensitive to extreme values in measured peaks or valleys as the average over a measurement length is used (Bhushan, 2000).

$$Ra = \frac{\Sigma A}{L} \tag{4.7}$$

Rz is another commonly used roughness parameter which looks at the average distance between the highest peak and lowest valley in the sampling length (Whitehouse, 2002, p 54). This is shown in Figure 4.11. This method calculates the surface roughness by taking the five highest peaks and five lowest valleys within the sampling length and finds the average distance between them, shown by Equation 4.8. It is known as the maximum height of the assessed area. In contrast to Ra, Rz can be insensitive to smaller features present within the measured surface.

$$Rz = \frac{\Sigma Rp + \Sigma Rv}{5} \tag{4.8}$$

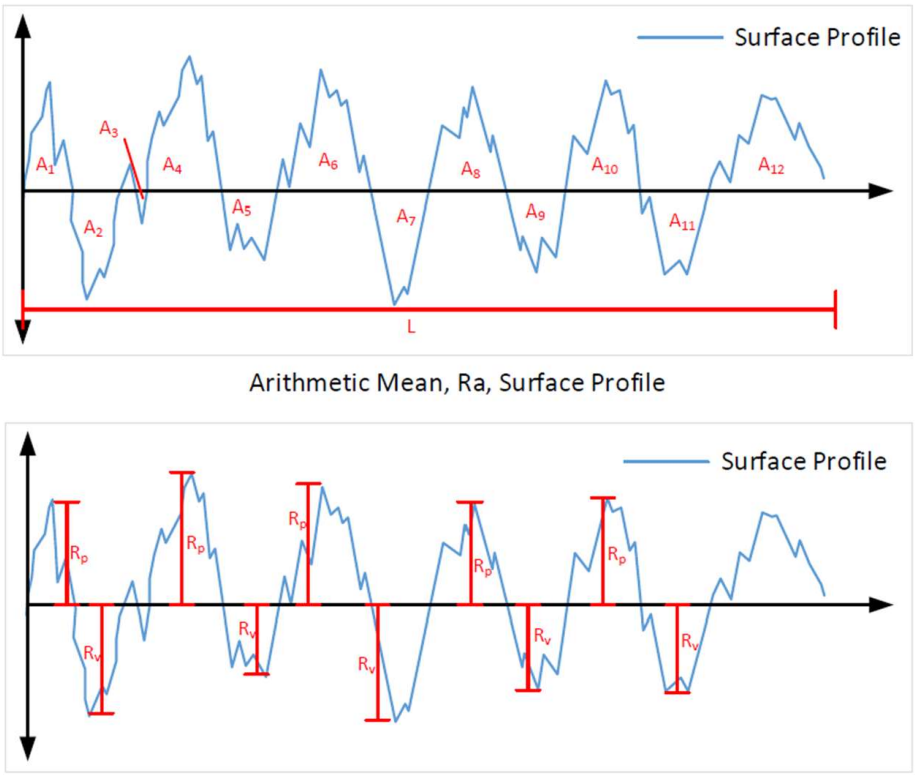

FIGURE 4.11: Surface roughness Ra and Rz profiles.

Three measurements across the surface on each of the tested parts were recorded and an average obtained. This enabled a greater representation of the overall surface of the part despite the total measurement area of 13 mm^2 achieved by the applied magnification.

4.4.3 Hardness

Hardness testing provided the hardness of the as-built parts, this is a mechanical property often stated on material data sheets. The material data sheets provide an expected hardness value for each material.

4.4.3.1 Sample Preparation

Prior to hardness testing the surface was ground down to prevent the surface roughness interfering with the indentation process and resulting measurement. A manual grinding procedure was required to produce a smooth surface for the indenter to test as outlined in the ISO standard for Rockwell Hardness Testing (ISO, 2016). The grinding process allows for the higher points in the rough surface to be removed producing a more uniform surface finish for testing.

This was achieved by holding the sample on to a sheet of 1200 grit silicon carbide paper mounted in a grinding machine rotating at 300 RPM. Allowing for a more

uniform surface for the indentation and resulting measurement. The original surface finish and the test surface finish are shown in the microscope images in Figure 4.12 below.

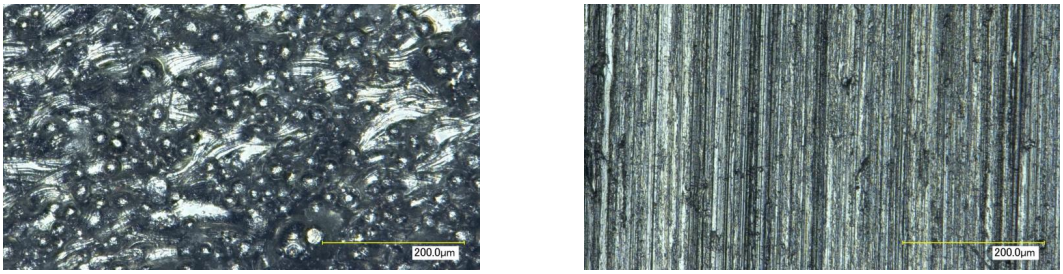

Before Grinding procedure

After Grinding procedure

FIGURE 4.12: x500 optical microscope images of the test surface before and after conducting the grinding procedure.

4.4.3.2 Hardness Measurement

Part hardness was measured on a Zwick Roell Indentec Hardness Tester. The hardness test measures the bulk hardness of the material. Described by Figure 4.13, the hardness test was conducted by applying a pre-load, *F0*, to the surface of the part. The depth of this indentation was then taken as the reference point for the depth measurement. The test load, *F1*, was then applied and removed.

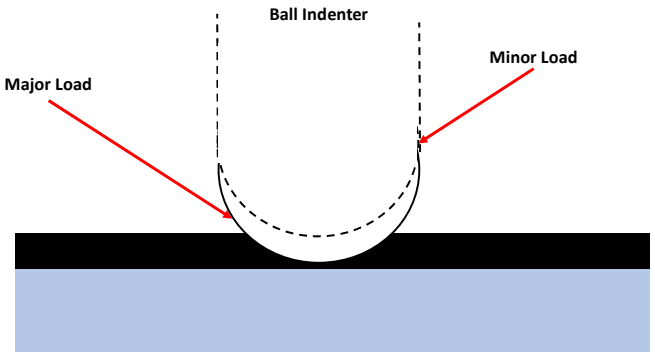

FIGURE 4.13: Rockwell hardness testing schematic (Herrmann, 2011).

The resulting depth of indention was then recorded. A hardness is then calculated using Equation 4.9 below.

$$HRB = N - \frac{h}{s} \tag{4.9}$$

Where:

- N is the numerical value for the applied hardness scale.

- S is the scale division, this represents the resolution of the measurement scale.
- h is the measured depth of indention.

The HRB Rockwell hardness scale was chosen as it is suited to steel and stainless steel materials. The resulting part hardness was recorded on the Rockwell Hardness B scale with the following testing procedures, Table 4.4, applied (Herrmann, 2011).

TABLE 4.4: Rockwell B hardness scale (Herrmann, 2011).

Harness Scale	**B (HRB)**
Indenter Type	Ball Indenter Diameter 1.5875mm
Pre-Load, F_0	98.07 N
Test Force, F_1	980.7 N
Numerical Value, N	130
Scaling Constant, S	0.002mm

The hardness measurements were taken five times for each part on both test surfaces and the hardness values are then averaged. The locations of the indentations for each measurements must be spaced at a minimum of 2 mm from any each previous indentation as well as 2 mm from any edges as recommended by ISO 6508 (ISO, 2016). This is to ensure that the measurement was not influenced by the previous indentation or variations in the hardness near an edge.

4.4.4 Part Density

Density analysis of the as-built parts is conducted through micro-sectioning the specimens and then imaging the different cross sections to analyse the quantity of pores present. The micro-sectioning method allowed for an assessment of the quantity of internal pores present in the part (Spierings, Schneider, and Eggenberger, 2011).

4.4.4.1 Sample Preparation

Sample preparation included mounting the samples in three separate orientations to allow for cross sections of different planes to be measured. The samples were mounted in Buehler Epoxicure 2™ resin. Samples were then left overnight at room temperature to cure and harden. Once cured, the samples were ground and polished, using the Buehler AutoMet 250 Pro System. Grinding allows for the required cross section to be revealed and the following polishing steps are used to remove any scratches in the cross section. The grinding routine, shown in Figure 4.14, is used to reveal the cross section. Grinding of the samples is conducted using silicon carbide paper with water. Parts were ground in three separate stages with finer grit paper being applied at each successive step. The initial two grinding stages allow for the bulk material to be revealed and the final stage removes any surface scratches and prepares the micro-section for polishing.

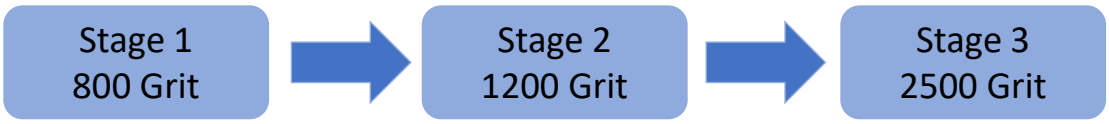

FIGURE 4.14: Sample grinding stages.

Once grinding was completed the polishing of the samples, shown in Figure 4.15 was conducted to produce a micro-section free of scratches. Polishing is completed using a diamond suspension fluid fed onto a polishing cloth in steps of decreasing abrasiveness.

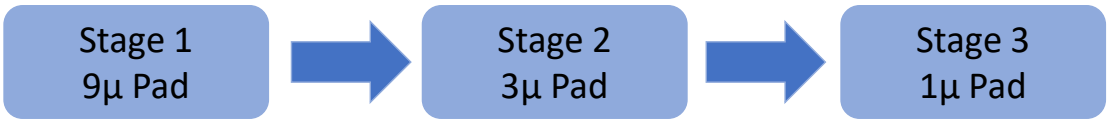

FIGURE 4.15: Sample polishing stages.

4.4.4.2 Image Analysis

Images of the micro-section were taken at a magnification of x200, using a Keyence VH-Z 100R digital microscope. Ten images of each cross section were required to allow for the greatest representation of the overall cross section of the sample.

Images were then imported into ImageJ, an image processing software for analysis (Abràmoff, Magalhães, and Ram, 2004). Within the software the steps outlined in Figure 4.16 were completed. Theses steps are described as:

1. The micrograph was imported into ImageJ for analysis.
2. The scale of the image was set using the scale bar on the acquired micro-graph.
3. The images were then converted to binary to produce a clear definition between the pores and bulk material.
4. The measure particles tool was then deployed to output the percentage of black space (pores) to white space (bulk material) in the micrograph.

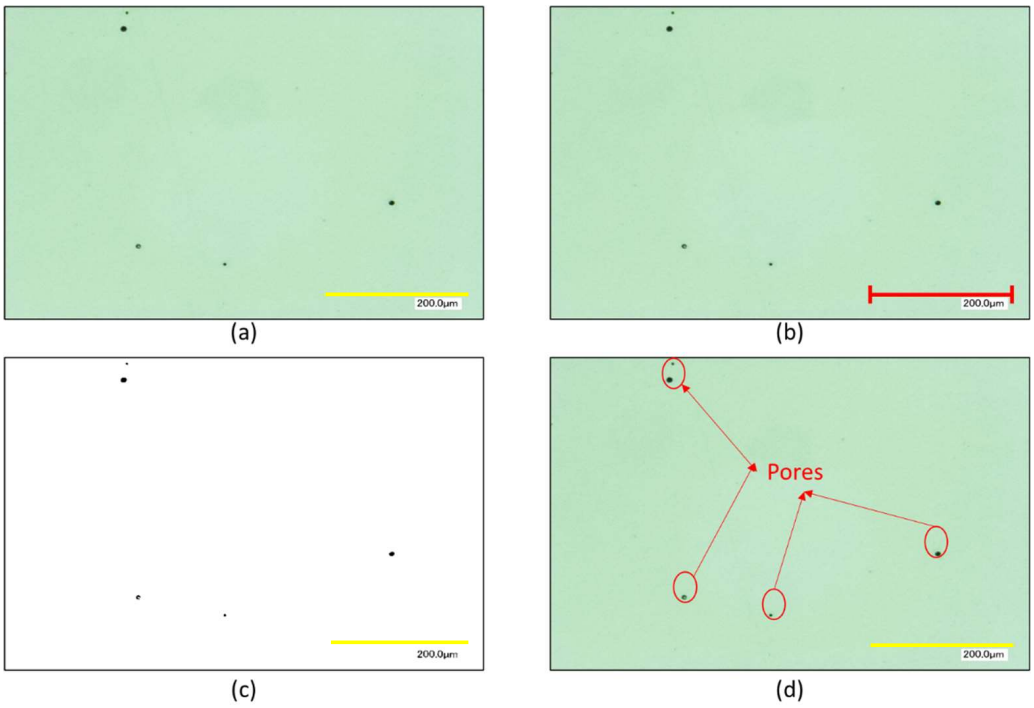

FIGURE 4.16: ImageJ porosity analysis process.

An average percentage porosity was then calculated from the ten analysed images. This average porosity was subtracted from the stated as-built density of 100% (EOS GmbH, 2014) to provide the resulting part density. Samples were then re-ground and polished to assess the presence of pores in a secondary cross section. two cross sections separated by approximately 2mm were analysed. This provides a greater representation of the overall porosity within the part. The cross section with the lowest measured density was used to represent that sample.

4.4.5 Dimensional Accuracy

The dimensions of the printed parts were assessed to see if there is any significant deviation from the originally designed part dimensions. Parts were measured using a CNC coordinate measuring machine, an OGP Smartscope 500. This is a computer numerical control driven machine allowing for accurate measurements, to four decimals places, to be recorded (Mani et al., 2016). The different measurement orientations are shown in Figure 4.17.

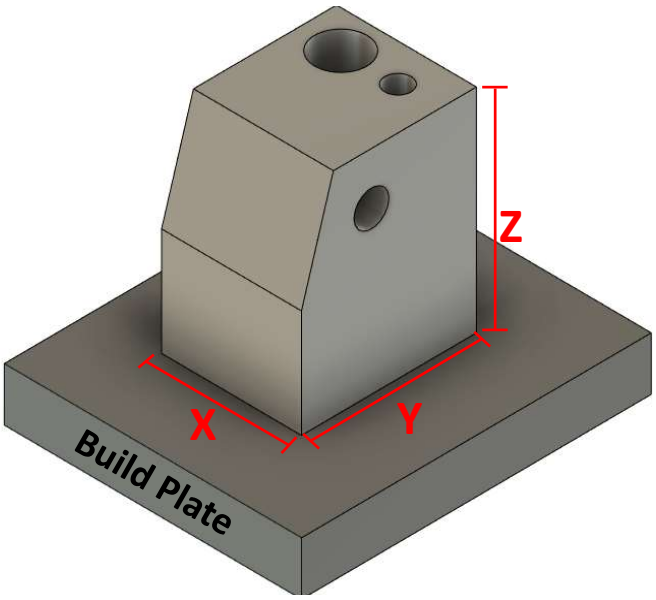

FIGURE 4.17: Example of dimensional accuracy measurement orientations.

The dimensions of the parts along the X and Y plane were measured with this process prior to removal from the build plate so as to avoid the part removal process affecting the resulting part dimensions. The vertical height or Z plane dimension was measured using a calibrated set of Mitutoyo digital vernier callipers. The measurement process was carried out five times for each part and averaged. The maximum deviation from the designed dimension is the metric of interest in this case. This was compared to the stated dimensional accuracy for the material, outlined in the material data sheet (EOS GmbH, 2014).

4.4.6 Phase Analysis Characterisation

The samples manufactured for the density measurement process were used to assess the potential impact of the powder recycling and subsequent rejuvenation process on the phase composition of the L-PBF parts.

The polished micro sections of the density cubes, produced using the method shown in Figure 4.14 and Figure 4.15, were etched using Fry's reagent (150ml water, 50ml HCL, 25ml HNO3, 1g CuCl2) by swabbing the polished surface in the etchant for a total of three minutes. The samples surface was then cleaned using de-ionised water. The microstructure melt pool and grain boundaries were captured using optical microscopy on the Keyence digital microscope VH-Z 100R digital microscope at a magnification of x500. Further SEM imaging was also completed to observe the phase structure and orientation present within the microstructure.

4.5 Build Hours Calculation

In order to monitor the use of a particular powder batch the build hours were recorded. The Average Use Time, *AUT*, as proposed by Denti et al., 2019 was used to represent the increased exposure of the powder material to the L-PBF process. For a standard powder recycling procedure where the same batch of powder is being recycled without the addition of any new powder the hours can be counted sequentially, as shown by the equation below.

$$AUT(i) = AUT(i\text{-}1) + t_i \tag{4.10}$$

where *AUT(i)* is the average use time of the i-th build, *AUT(i-1)* is the average use time accumulated at the (i-1)-th build and t_i is the build time of the i-th build.

With powder recycling as previously discussed in the literature review there will be a stage where a powder rejuvenation process will need to be conducted. This process adds complications to the above equation as there is now two batches of powder with varying *AUT* being mixed. To account for this Denti et al., 2019, proposed the following equation when one of the powder batches being mixed is virgin, unused, powder.

$$AUT(i) = \frac{q_1[AUT(i\text{-}1) + t_i]}{q_0} \tag{4.11}$$

where *AUT(i)*, *AUT(i-1)* and t_i are as previously described. q_1 is the quantity of powder remaining the i-th build and q_0 is the quantity of virgin powder being added to the recycled powder as a part of the powder rejuvenation procedure. The *AUT* was used throughout this thesis to represent the increased exposure of the powder to the L-PBF process. In the case of the Powder Recycling study presented in Chapter 5 Equation 4.10 is used and the Powder Rejuvenation study in Chapter 6 Equation 4.11 is used.

4.6 Monitoring System

It was determined that the monitoring system installed into the chamber of the EOS M280 should be a standalone system. This means that the operation of the monitoring system was to be separate, or standalone, to the operation of the EOS M280. This is required due to the relatively low computing power currently available on the EOS M280. The addition of such monitoring system may interfere with the general computing processes required to complete a build. This is a resultant of the age of the M280 system. As such the system installed is operated completely separately to the M280's computer and can be removed or installed from the machine without impacting the operation of the machine. In addition to the system being standalone there are other constraints regarding the operational environment of the M280 chamber that need to be considered, these are discussed in detail in the following sections. The general operation for the

installed monitoring system is presented in Figure 4.18, the components of which and their selection is discussed further in this section.

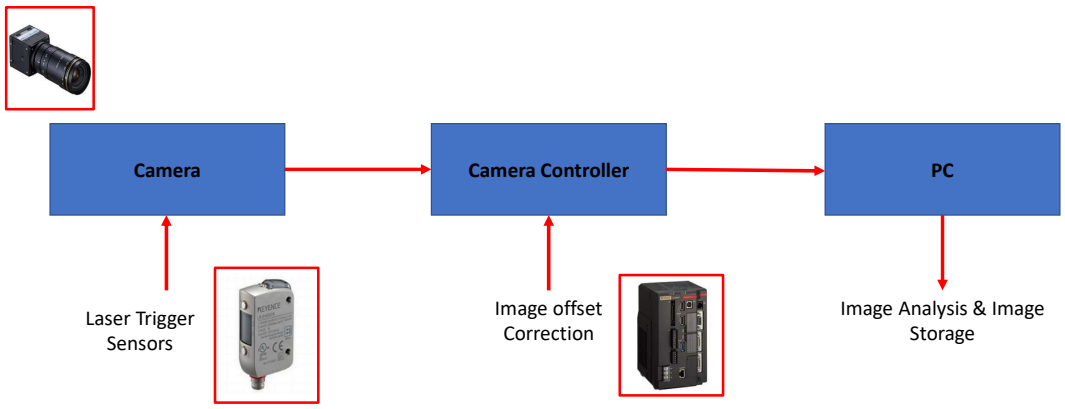

FIGURE 4.18: General operation and components of the installed monitoring system.

At a very high level the system operates by a camera capturing an image which was triggered by one of the laser trigger sensors mounted inside the build chamber. The captured image was then passed to the controller unit which applies a correction, due to the requirement for off axis mounting. This corrected image is then sent to a computer where the images are stored and analysed. The following sections detail the individual aspects of the system shown in Figure 4.18.

4.6.1 Build Chamber Environmental Constraints

The selected monitoring system must be capable of operating within the build chamber of an EOS M280 DMLS machine. During a build the camera in the monitoring system was subjected to an inert atmosphere (Argon or Nitrogen), elevated temperatures and low humidity. The inert atmosphere is required by the laser melting process to shield the melt pool during the build process (discussed previously in Chapter 2). During a build the build platform is also raised to a temperature between 40 and 100°C depending on the material being processed and as such the relative humidity in the chamber reduces as the build progresses. Figure 4.19 shows a plot of the environmental conditions of the M280 build chamber during a 316L stainless steel build, when the build plate is maintained at 80 °C for the duration of the build.

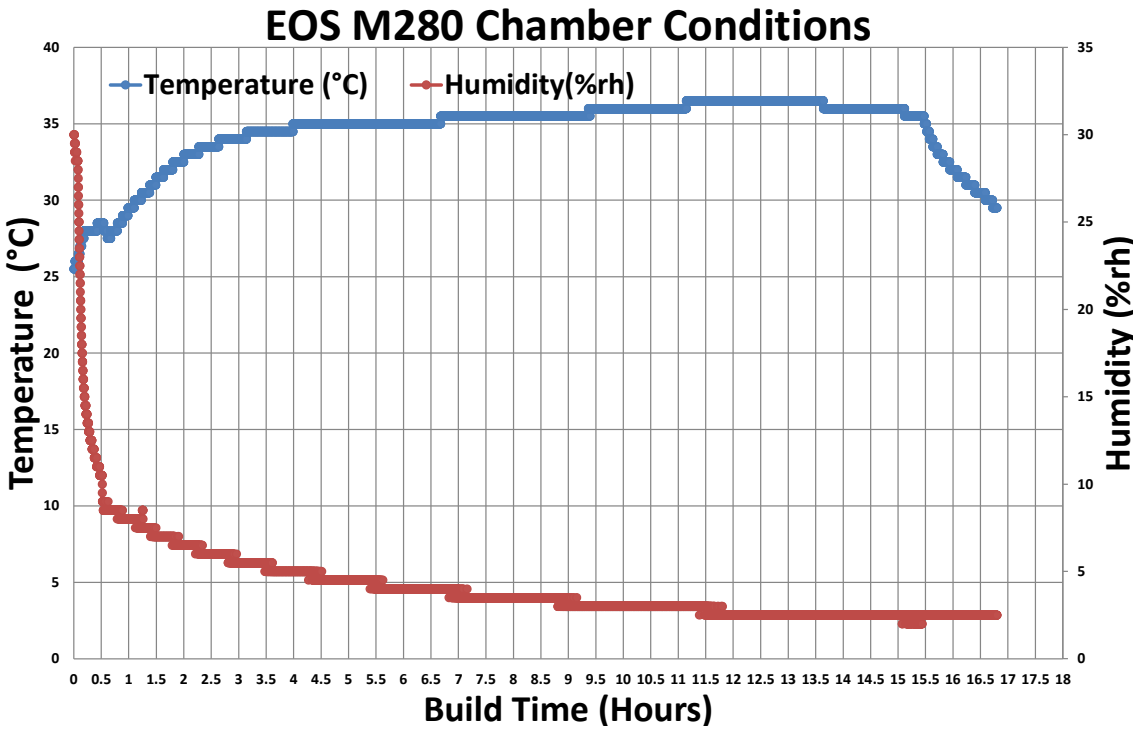

FIGURE 4.19: EOS M280 Build chamber temperature and relative humidity over the course of a 17 hour build.

4.6.2 Camera and Controller

With the constraints for the monitoring system in mind the aspects of the monitoring system were selected to suit. A Keyence complementary metal oxide semiconductor (CMOS) monochrome 21MP camera with a 16 mm lens attached was selected. This camera and lens combination results in an image pixel size of 3.5 x 3.5 microns. Two laser trigger sensors (Keyence LR ZH500CP) are installed within the chamber to trigger when the system captures an image. The location of the re-coating arm was utilised to trigger when the system should capture an image. The camera and sensors are required to be mounted within the build chamber of the EOS M280 and as such the camera and triggers are IP64 and IP68 rated respectively. As the controller system sits outside of the build chamber no IP rating is required for it. Finally a camera controller module, the CVX500 from Keyence, was used to control the trigger sensors and camera system.

Due to the off centre axis mounting of the camera in order to avoid its interference with the laser window, a correction must be applied to the images captured to remove the inherit distortion in the image demonstrated in Figure 4.20.

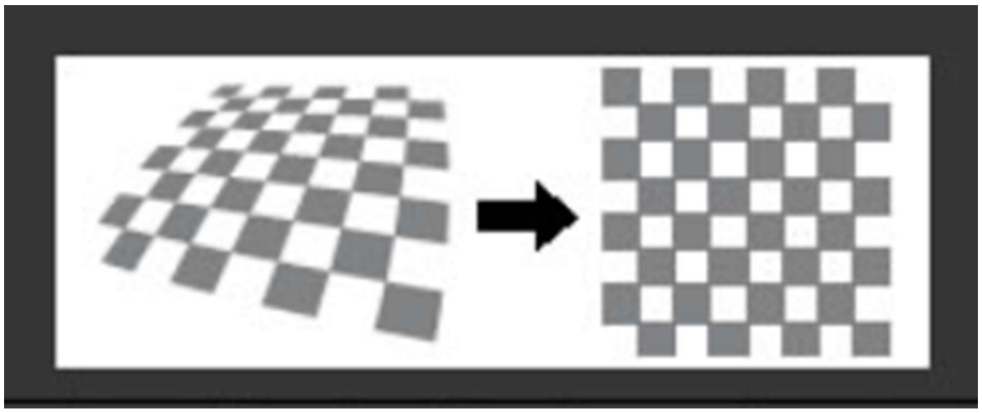

FIGURE 4.20: Example of distortion correction due to the off axis placement of the camera system.

This correction enables any potential distortion in the captured images due the off axis mounting position, to be eliminated in the saved images. A chequerboard pattern was used to complete this process, and ensure the off-axis captured images has the distortion removed.

4.6.3 System Installation

The previously described camera, trigger sensors and controller unit were installed into the EOS M280 in order to complete the system. The trigger sensors were located behind the panel at the rear of the build chamber. Once the re-coater arm was at either of its furthest most left or right position the camera was triggered to capture an image.

The operational work flow is discussed further in Chapter 8. The controller unit was mounted in the rear of the machine where it could be accessed in order to connect storage drives and an external monitor. The controller was also connected to an external computer. Images were saved to the computer and the developed code analyses the saved images as well as displaying the output of the analysis in real-time.

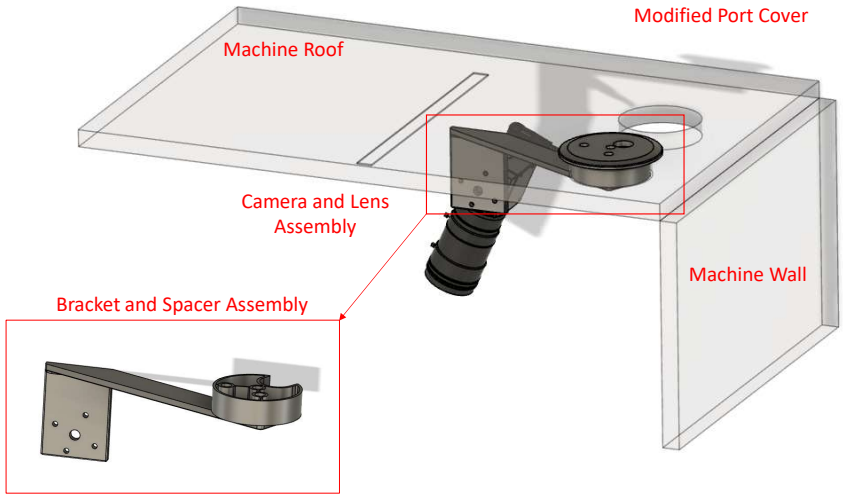

FIGURE 4.21: CAD design of the camera system mounting bracket and location within chamber.

The camera is mounted via one of the chamber access ports in the roof of the build chamber as shown in Figure 4.21. These ports are typically used for testing and servicing. A modified port cover was used to allow for the pass through of the necessary cables to the camera assembly. A bracket and spacer allows the camera to be connected to such port and located in the centre of the build chamber was designed and additively manufactured in 316L stainless steel on an EOS M280. The bracket is shown in Figure 4.22 below.

FIGURE 4.22: Designed and manufactured camera mounting bracket and access port spacer.

This bracket allows the camera to be mounted via the front access port and remain in the centre of the build chamber in order to capture the images of the build plate. Figure 4.23 shows the installed standalone monitoring system in the EOS M280.

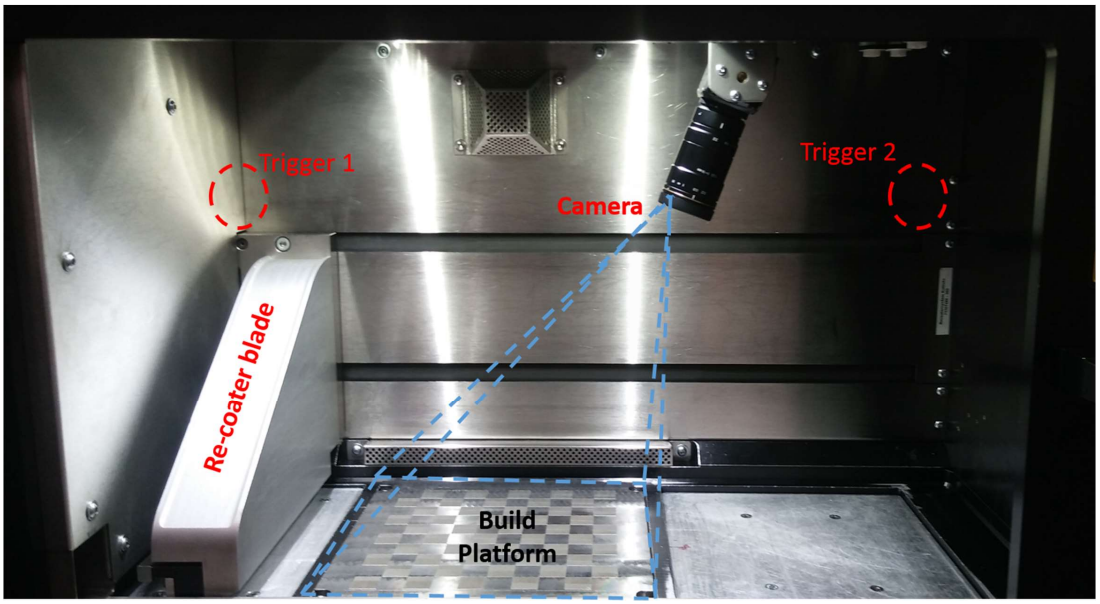

FIGURE 4.23: Installed Camera system and location of components within the build chamber.

4.7 Statistical Methods

In order to analyse the data collected a series of statistical methods was applied. The standard error of the means was used to calculate the standard error of the measurements recorded and multiple linear regression was used in the development of the empirical model. These methods and the theory supporting them are presented below.

4.7.1 Standard Error of the Mean

The error associated to a data set which fits a normal curve can be described by the use of the standard error of the mean (Lee, In, and Lee, 2015). In order to increase the accuracy of the measurements made by the methods previously discussed, each test method was conducted multiple times, as shown in Table 4.5.

TABLE 4.5: Test method number of repetitions.

Test Method	Number of Repetitions, n	Section
EDX	3	4.3.2.1
XRD	3	4.3.2.2
Powder Morphology	3	4.3.3
Particle Size	3	4.3.4
Apparent Density	3	4.3.5.1
Tapped Density	3	4.3.5.2
Skeletal Density	5	4.3.5.3
Powder Flowability	3	4.3.6
Surface Roughness	5	4.4.2
Part Hardness	5	4.4.3
Part Density	5	4.4.4
Dimensional Accuracy	5	4.4.5

A mean value and standard deviation for each of the measurements was obtained. The error associated with this mean value can be described as the Standard Error of the Mean (SE). This given by Equation 4.12 shown below.

$$SE = \frac{\sigma}{\sqrt{n}} \tag{4.12}$$

Where:

- SE is the standard error of the sample mean.
- σ is the standard deviation of the measured values.
- n is the sample size.

The standard error of the mean shows that the error for a sample means is less variable then individual means. The larger the sample size, n, the smaller the variability in the results (Reilly, 2006). The standard error of the mean provides an estimate as to how well your sample data represents the sample population.

4.7.2 Normality Testing

The test for normality is a check on how well a data set fits a normal distribution. This is an important statistical check because methods such as regression analysis, t-tests and analysis of variance rely on the data being normally distributed. The assumption of normality is rarely violated on large sample sizes (n > 30). For samples sizes in the hundreds the distribution of the data can be ignored. Normality can be tested using visual analysis and comparing the distribution to a normal distribution.

Normality tests are supplementary to the visual methods above. A common normality test is the Kolmogorov-Smirov (K-S) test. The test compares the scores in the sample to a normally distributed set of scores with the same sample mean

and standard deviation. The K-S normality test is an empirical distribution function (EDF). The test compares the theoretical cumulative distribution function of the test distribution to the EDF of the data set. Smaller samples sizes often pass the normality tests. A limitation of the K-S method is that it an be highly sensitive to extreme values (Ghasemi and Zahediasl, 2012).

Normality tests were conducted on all results in order to ensure that the correct regression model is being applied in the statistical analysis of the results.

4.7.2.1 Multiple Linear Regression

Multiple linear regression is one of the most common forms of regression analysis. It is used to describe the relationship between one dependent variable and two or more independent variables. A multiple linear regression (MLR) analysis has the task of fitting a single linear line between a multi-dimensional cloud of data points as described in Figure 4.24. The independent variables are also known as predictors as they are used within the MLR model to predict the dependent variable.

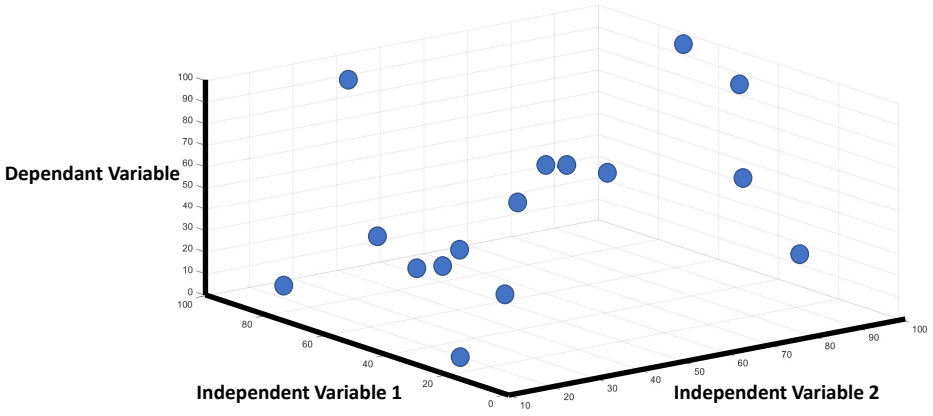

FIGURE 4.24: Example of a multi-dimensional data cloud.

A MLR model can be given in the following equation format:

$$Y_i = \alpha + \beta_1 X_1 + \beta_2 X_2 + ... + \beta_n X_n \tag{4.13}$$

Where:

- Y_i is the predicted response.
- α is the intercept value.
- β is the slope coefficient.
- X_i is the predictor value.

In the development of a MLR model there are four main assumptions upon which the model is based. These assumptions are as follows:

1. There must be a linear relationship between the dependent variable and independent variables i.e. a change in the dependent variable can be explained by a change in the independent variable.
2. The residuals created from the developed model are normally distributed, centred around a mean of zero and lie within a single standard deviation of the mean.
3. The independent variables are not highly correlated with each other i.e there is no multicollinearity in the data.
4. The observations are selected independently and randomly from the entire population.

Prior to the development of the empirical model, the range of variables to describe the dependent variables are analysed in an exploration matrix plot. This plot was used to determine the strength of the relationship between the independent and dependent variables. The Pearson's correlation coefficient was used to quantify the strength of these relationships. The coefficient indicates the strength of relationship between the plotted values. A high Pearson Correlation coefficient, i.e., closer to 1, indicates a strong linear relationship between the independent and dependent variables explored. Those with a strong linear relationship shown in the matrix plots are likely to contribute significantly to MLR model; however, their significance to the developed model is tested further in the next stages of the model development.

Those variables with a high Person coefficient were then used in the development of the MLR model. The MLR tool within Minitab Statistical Software generates the MLR model using 70% of the input data with the remaining 30% being withheld for validation of the empirical model. The 30% of data that was withheld was used to confirm the fit of the developed model with measured data.

The first stage of testing the developed MLR models is to ensure that the inclusion of the previously selected independent variables contribute significantly to the developed model. This significance was given by the test statistic, the p-value. If the p-value is smaller than 0.05, it indicates the inclusion of the variable is statistically significant to the model. All variables require a p-value of less than 0.05 to be included in the final developed model.

With the included variables deemed significant to the model, the coefficient of determination or R-Squared value was used to determine how much of a change in the dependent variable can be explained by the developed model. A higher R-Squared value indicates that more of the change in the dependent variable is explained by the model. A R-Squared value of 1 indicates a perfect linear relationship between the model and dependent variable. With the inclusion of the independent variables and the model tested the final tests to confirm the assumptions of a MLR model are tested.

The variance inflation factor (VIF) was also used to confirm how significant the developed MLR model is. The VIF is a measure of the multicollinearity of the variables within the model, i.e. how independent they are from one another.

This would be shown by the return of the value greater than 4, indicating that the variables are dependent on one another. The VIF value should be as low as possible to ensure that there the selected variables are not collinear in the model.

Testing the validity of the developed model was required to ensure that the selected model can represent the relationship with a high degree of accuracy and repeatability. To do this, the predicted values of the model are compared to the original measured values. The difference between these values is known as a residual. The testing of the model revolves heavily around these residuals and how they react with the independent variables used. These tests require four interactions to be analysed, as follows:

- A plot of the residuals against the predicted values is normally distributed.
- The residuals are normally distributed.
- A plot of the residuals and the input variables (powder characteristics in this study) displays no significant trends.
- A plot of the residuals and the possible input characteristics omitted from the model displays no significant trend.

Once all the above conditions have been confirmed, the assumptions for the validity of an MLR model have been met, and the accuracy of the developed model can be established based on the largest residual generated.

4.8 Conclusions

This chapter has presented the materials and methods that are required to complete the studies presented in this thesis. The chapter begins by outlining the material used in this project a 316L Stainless Steel powder. The L-PBF process is then explained in detail including the process of assigning print parameters, later in the chapter the process of preparing the file for L-PBF is presented. The methods required to characterise the powders and the resulting parts, manufactured by the L-PBF process, are explained in detail. The setup and installation of the monitoring system for the detection of defects in the L-PBF process is introduced providing an understanding of some of the constraints assessed in its development and installation. Finally the chapter concludes with an explanation as to some of the statistical methods that are required to analyse the results from the powder and part characterisation processes presented.

5 Powder Recycling

Powder recycling allows for the costly powder material to be utilised beyond a single build. This is a process widely adopted without a great understanding of the effects on both the powder and parts produced. A study has been designed to measure this potential impact. The aim of this chapter is to assess the effect of powder recycling on the powder characteristics and the qualities of the parts produced. The methods applied and results from the study will be presented before being discussed in detail in the later sections of the chapter. The results highlight the effect of the powder recycling on powder characteristics and the resulting affect on the quality of the parts produced.

5.1 Materials and Methods

The material for this study was a Stainless Steel 316L powder as outlined in Section 4.1.1. This powder is a commonly applied stainless steel powder for the medical device, aerospace and auto-mobile industries (EOS GmbH, 2014).

The methodology for this project is split into two sections; powder characterisation methods and part qualities methods. Table 5.1 and Table 5.2 below identify the methods applied for powder characterisation and part qualities respectively. The statistical methodology discussed in Section 4.7, were applied to the presented results.

TABLE 5.1: Powder Characterisation Methods

Characteristic	**Method**
Powder Chemical Composition	Scanning Electron Microscopy (SEM) and Energy Dispersive X-Ray (EDX)
Powder Phase Analysis	X-Ray Diffraction Analysis
Particle Size	Laser Diffraction
Particle Morphology	SEM Imaging and Morphology Analysis
Powder Density	Pycnometry
Powder Flowability	Hausner Ratio

TABLE 5.2: Part Quality Assessment Methods

Part Quality	**Method**
Dimensional Accuracy	CNC Coordinate Measuring Machine
Hardness	Rockwell Hardness
Surface Roughness	Focus Variation
Part Density	Micro-sectioning and Image Analysis
Part Microstructure	Etching and SEM imaging

5.2 Powder Recycling

The powder recycling process, as previously defined in Chapter 3.3, is the "practice of collecting un-melted powder after the L-PBF process and reusing it for subsequent builds" (Jacob et al., 2017). It increases the usable life of a powder batch for the L-PBF process. The process for powder recycling is outlined in Figure 5.1, consisting of a series of stages where the powder surrounding the part is sieved then added back into the material container ready for the next build process.

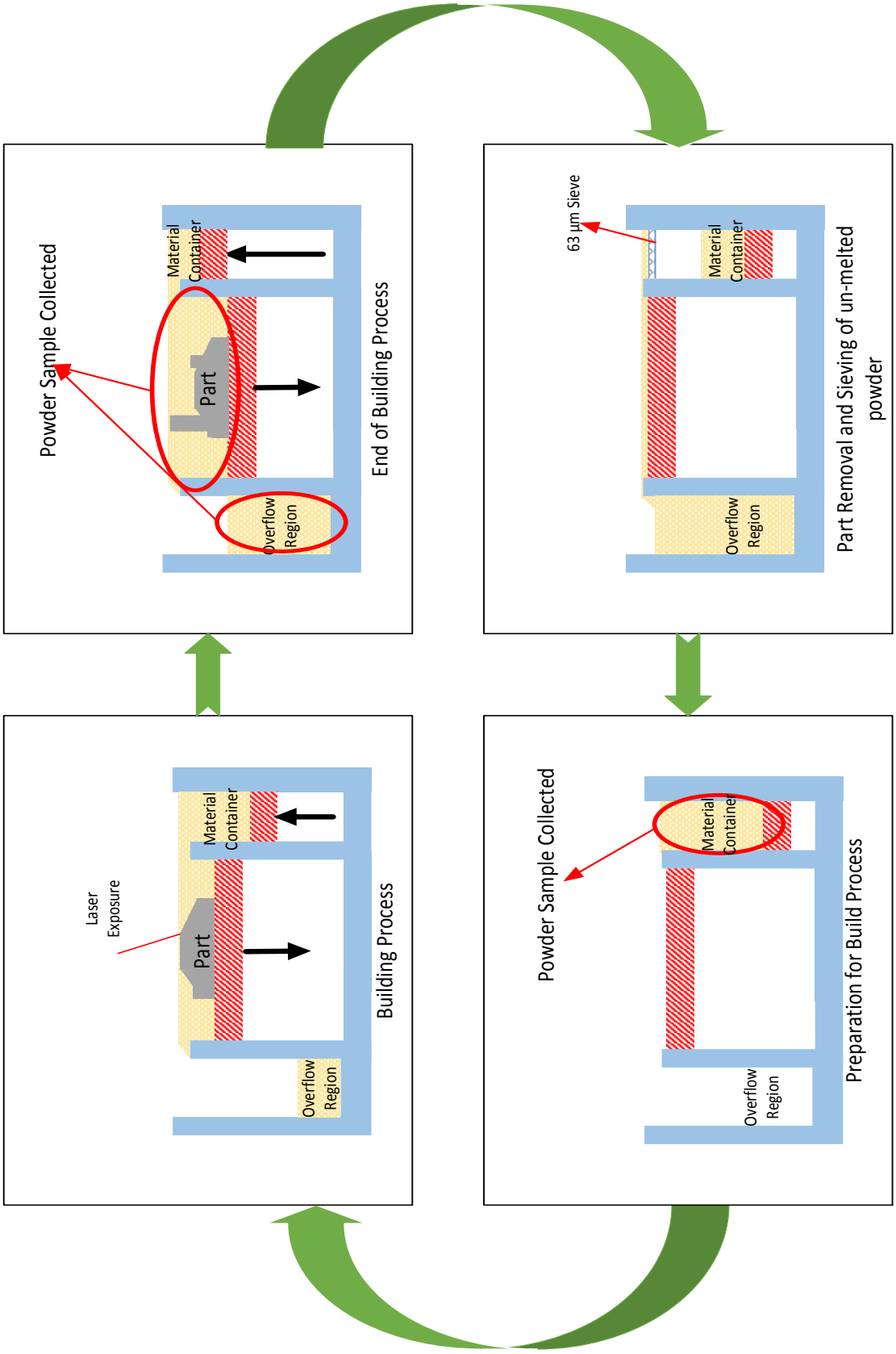

FIGURE 5.1: Schematic of the powder recycling process.

5.3 Powder Sampling

As described in section 4.3.1 the scoop sampling method was employed to sample the powder material. In order to ensure the powder sample size was representative of the batch of powder the minimum sampling mass to represent the batch of powder was calculated using Equation 4.2 (Allen, 1997). Prior to the calculation of the minimum sample size some of the powder parameters are required for the calculation. These parameters and associated values were as follows(EOS GmbH, 2014)

- Powder Bulk Density, ρ, 4.8 g/cm^3.
- Fractional mass of coarsest size class, w_1, 0.52%.
- Extreme diameter within the maximum size class, d, 233.129 x 10^{-9} cm^3.

The above listed values are dependant on the powder assessed. The variance in the sampling error, σ was chosen to be 5%. The minimum sample mass was calculated as shown below.

$$M_s = \frac{1}{2}(\frac{\rho}{\sigma^2})(\frac{1}{w_1} - 2)d^3x10^3 \tag{4.2}$$

$$M_s = \frac{1}{2}(\frac{4.8}{0.05^2})(\frac{1}{0.52} - 2)0.000000233x10^3 \tag{4.2}$$

The minimum sample mass calculated was 37.3g. The required sample mass, 150g, for the series of characterisation tests greatly exceeds that of the minimum sample mass calculated. Powder samples were collected at different stages in the process as outlined in Figure 5.1.

5.4 Results and Discussion

The aforementioned experiments were conducted over a period of 6 months which resulted in a total of 12 separate L-PBF builds, of varying lengths, accumulating a total of 120 build hours on the powder material as calculated using Equation 4.10. After each build a sample of powder was extracted from the EOS M280 and stored in sealed container prior to characterisation. The sealed container ensured that the exposure to oxygen and moisture was minimised. Testing was then conducted in the order presented by the results sections below.

The results presented below show the effect of powder recycling (i.e. Average Use Time (AUT)) on the powder characteristics and the part qualities. Each data point on the following graphs represents a powder sample, taken at the end of a L-PBF build. The error bars presented in all graphs are representative of the standard error of the mean, calculated using Equation 4.12.

5.4.1 Powder Characteristics

The characterisation of the powder material allows for the characteristics of the feedstock material to be quantified. Any changes in these characteristics are then compared to the original characteristics of the virgin powder material.

5.4.1.1 Powder Chemical Composition

The chemical composition was determined using Scanning Electron Microscopy (SEM) with Energy Dispersive X-Ray (EDX) analysis. The bulk powder chemical composition primarily consists of Iron (Fe), Chromium (Cr), Nickel (Ni) and Molybdenum (Mo) with smaller quantities of other elements present (EOS GmbH, 2014). Throughout the powder recycling process, the EDX map results showed no significant change in the powder chemical composition. The graphs, Figure 5.2, below show the composition of the main elements, as listed above, throughout the recycling process.

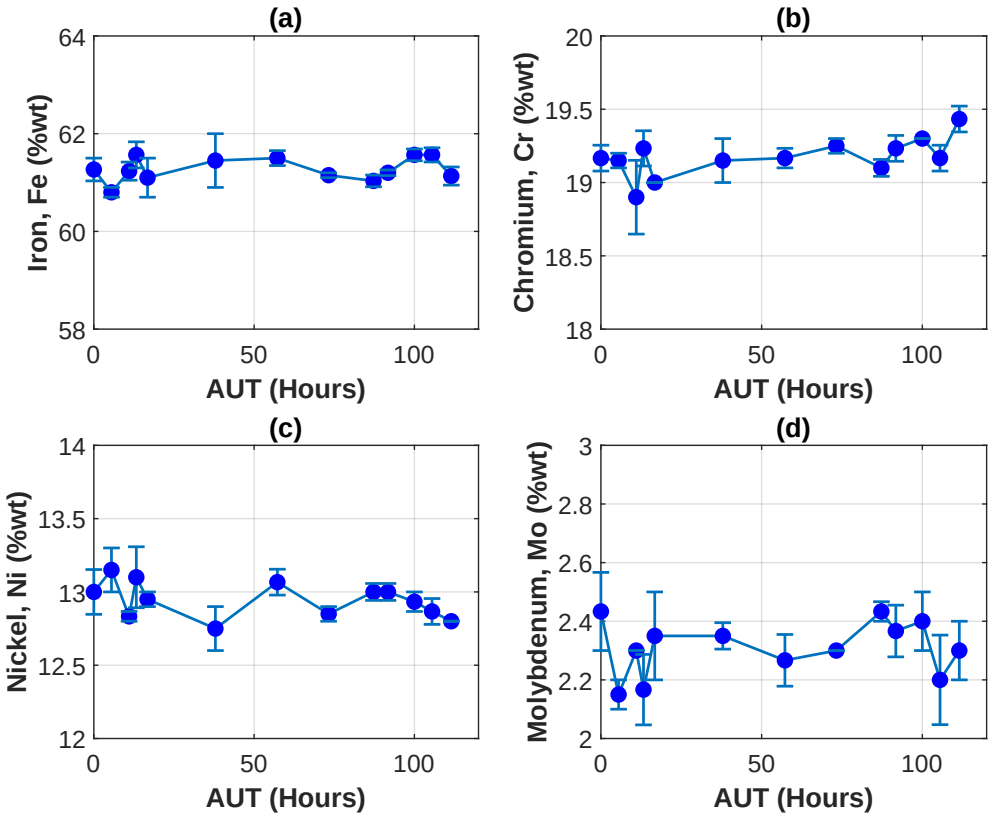

FIGURE 5.2: Effect of powder recycling on the chemical composition of (a) Iron, (b) Chromium, (c) Nickel and (d) Molybdenum.

5.4.1.2 Powder Phase Characterisation

The characteristics of the powder particles influences the microstrucure of the as-built L-PBF parts (Averyanova, Bertrand, and Verquin, 2010). As such, XRD analysis was conducted to assess if the powder recycling process impacts the

phase characteristics of the powder particles. The XRD results presented in Figure 5.3 show the primary phases of the 316L powder used in this thesis, captured at four Average Use Times (*AUT*). The virgin powder sample shown in Figure 5.3 by the black line provides a baseline for an unprocessed sample of 316L stainless steel powder. The position and width of the peaks in the graph indicate single phase Face Centre Cubic (FCC) structure is present, similar to that found in the literature (Gorji, O'Connor, and Brabazon, 2019). Austenite is a γ phase, which contains a unit cell of 3.595 $\mathring{A}$ (Angstrom). The detected phases were located at 43.57°, 50.75° and 74.61°. There was no change observed with the location and width of these peaks in the other powder samples tested.

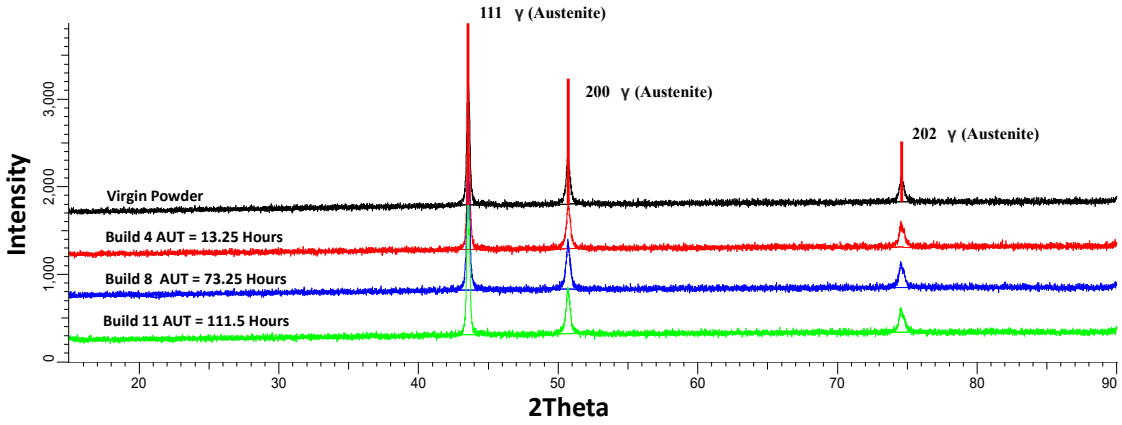

FIGURE 5.3: Effect of powder recycling on the microstructual phases of the powder.

5.4.1.3 Powder Mean Particle Size

Powder particle size affects how the powder material is layered and subsequently melted. A distribution of larger and smaller particles is required to maintain consistent layering and melting during the build process. The powder particle mean size and distribution was determined by laser diffraction. The effect of powder recycling, on the mean powder particle size is shown in Figure 5.4. An increase in the mean particle size was observed as the *AUT* increases.

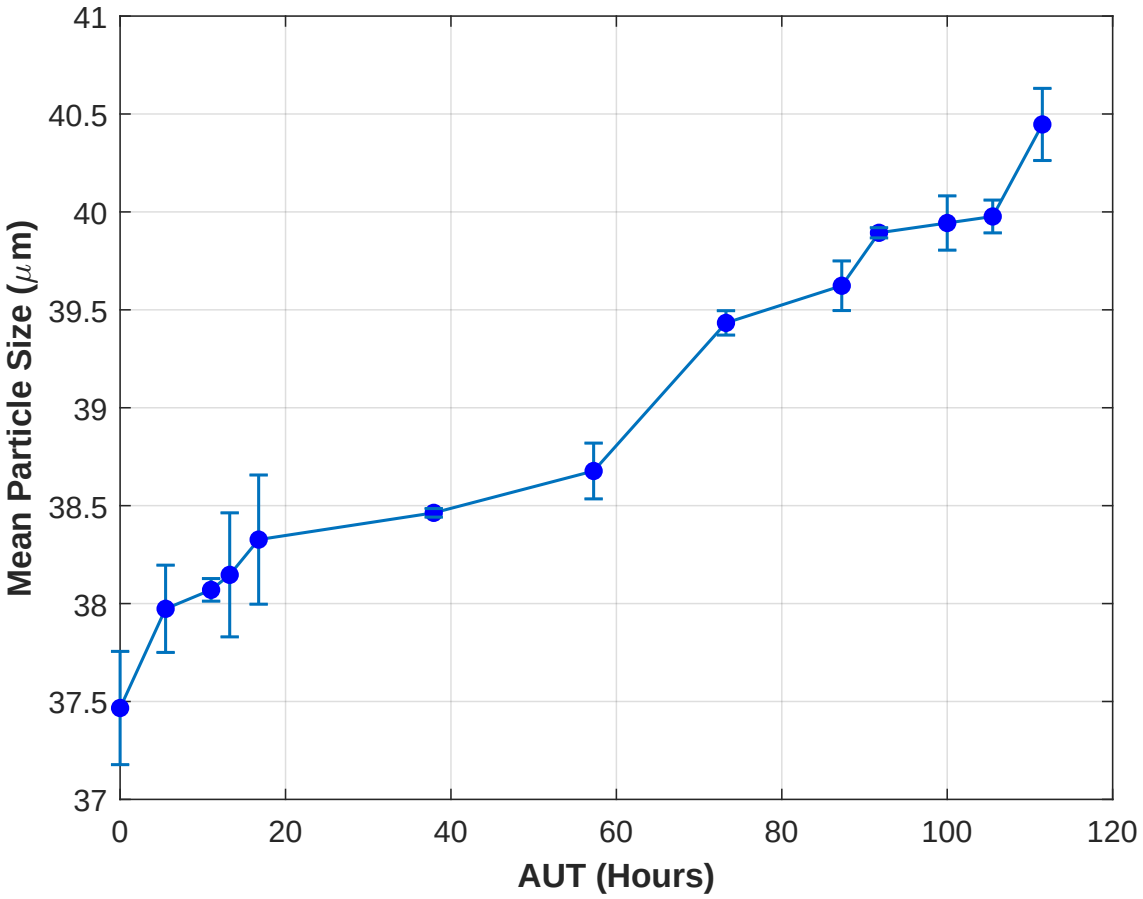

FIGURE 5.4: Effect of powder recycling on mean particle size.

5.4.1.4 Powder Morphology

Powder morphology was evaluated primarily through a consideration of particle circularity using Equation 4.3 as described in Chapter 4. The morphology of individual particles affects powder flowability, where the less circular the particle, the more difficult it will be to flow, thus, affecting the consistency and repeatability of the layering process. Circularity was assessed through image analysis of the SEM images captured. The effect of powder recycling, on powder morphology, i.e. circularity, is presented in Figure 5.5. A decrease in the powder circularity was observed as the powder is recycled and the accumulated build time increases.

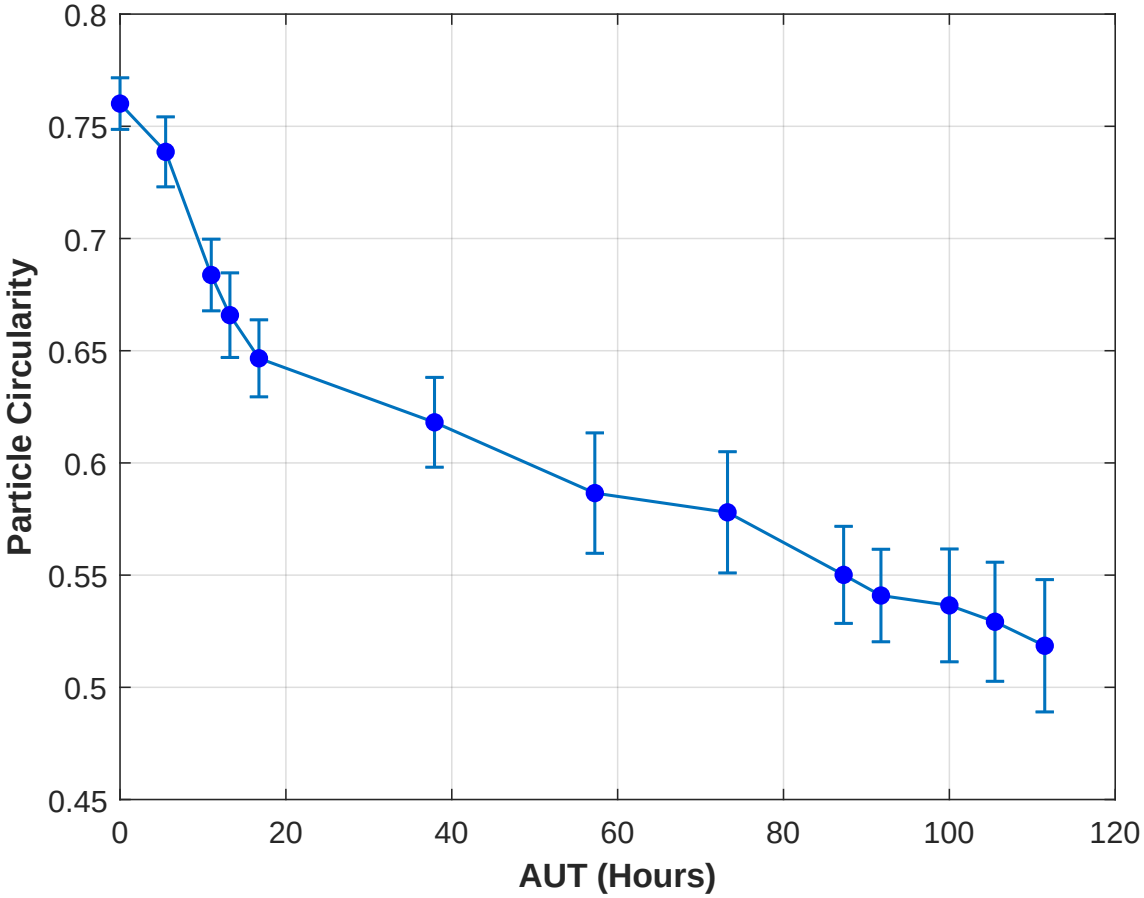

FIGURE 5.5: Effect of powder recycling on powder morphology (circularity).

5.4.1.5 Powder Density

The apparent and tapped density of the powder affects how the powder bed is produced. Figure 5.6 shows both the apparent and tapped density of the powder increases with the *AUT*, powder recycling. The increase in powder density is attributed to the increasing particle size and change in reduction in the number of small particles present in powder batches. This was shown by the increase in mean particle size in Figure 5.4. The apparent density is the density of the powder uncompacted and the tapped density is the density of the compacted powder, both of which provide an indication of how the powder bed is produced.

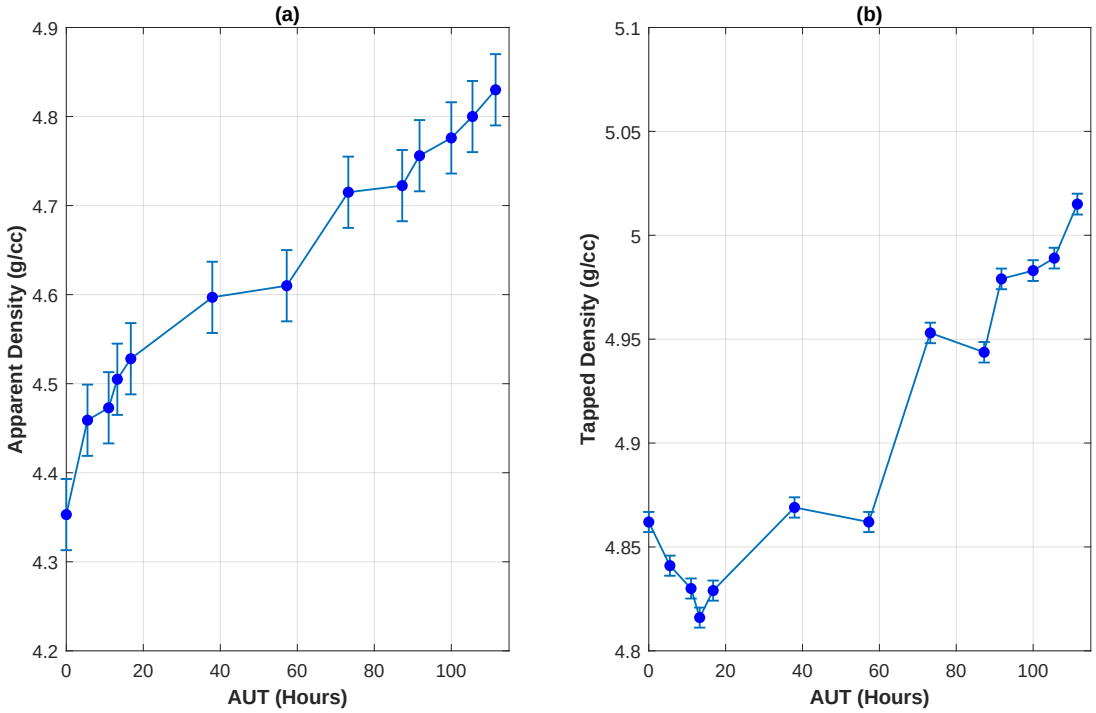

FIGURE 5.6: Effect of powder recycling on (a) powder apparent density and (b) Tapped Density.

5.4.1.6 Skeletal Powder Density

The skeletal powder density is determined through helium pycnometry. The skeletal density of the powder is assumed to be the density of a fully dense part with no discernible porosity. Figure 5.7 shows the skeletal density of the powder remained within 0.03 g/cc of the virgin powder. This shows that there was no discernible change in the skeletal density as a result of the increasing *AUT*.

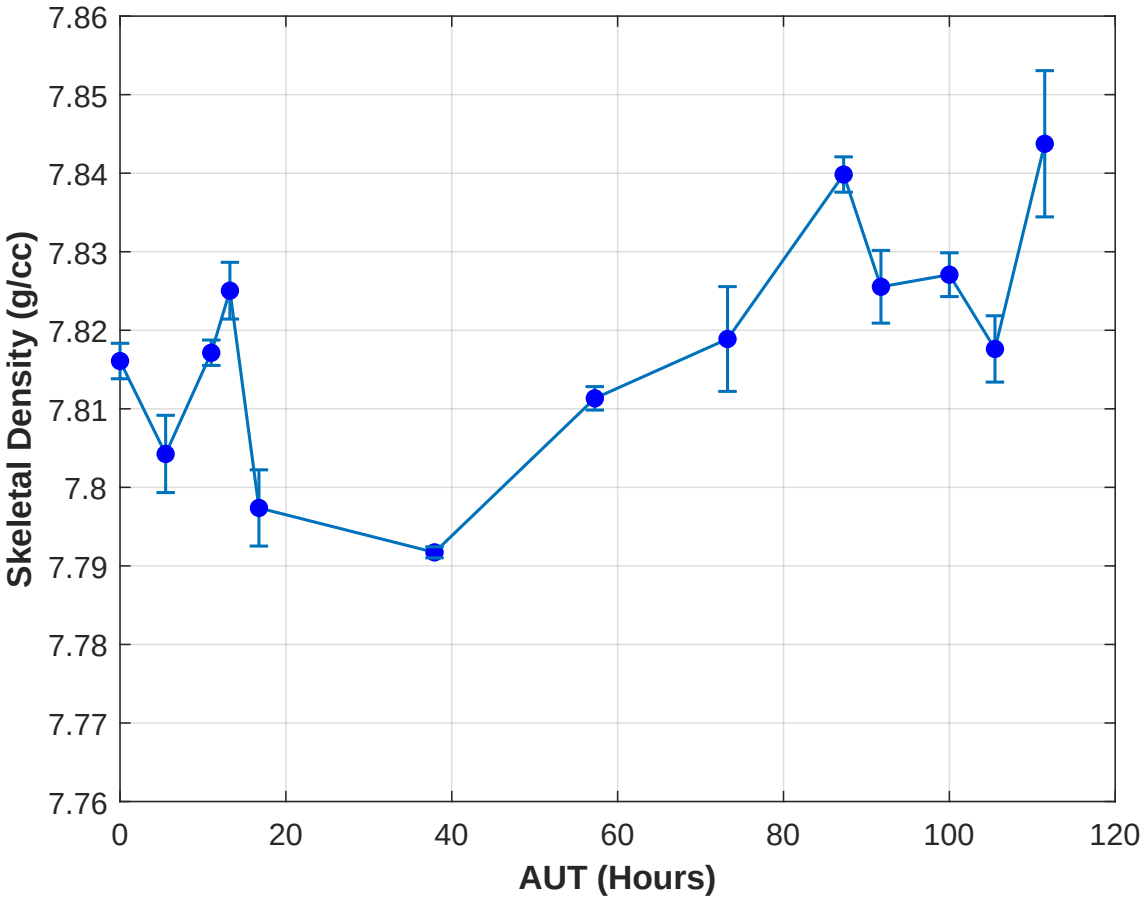

FIGURE 5.7: Effect of powder recycling on the skeletal density of the powder.

5.4.1.7 Powder Flowability

Figure 5.8 shows the effect of the *AUT* on the Hausner ratio of the recycled powder. It is expected that there would be a change in the flow behaviour of the powder due to a change in the powder particles circularity (see Figure 5.5) and an increase in the mean particle size (see Figure 5.4). Figure 5.8 shows a decrease in the Hausner Ratio measured, therefore, the powders ability to flow is increasing as the *AUT* increases. The increased flowability of the powder can negatively impact the quality of the manufactured parts. Highly-flowable powders with very minor resistance to flow (HR = 1) can result in poor powder layers being deposited. Resulting in a decrease in the density of the manufactured parts (Zielinski et al., 2017). Some ability of the powder to resist flow is an important feature in the consistent deposition, and generation of a dense powder layer within the L-PBF process. This will ensure consistent and repeatable laser melting.

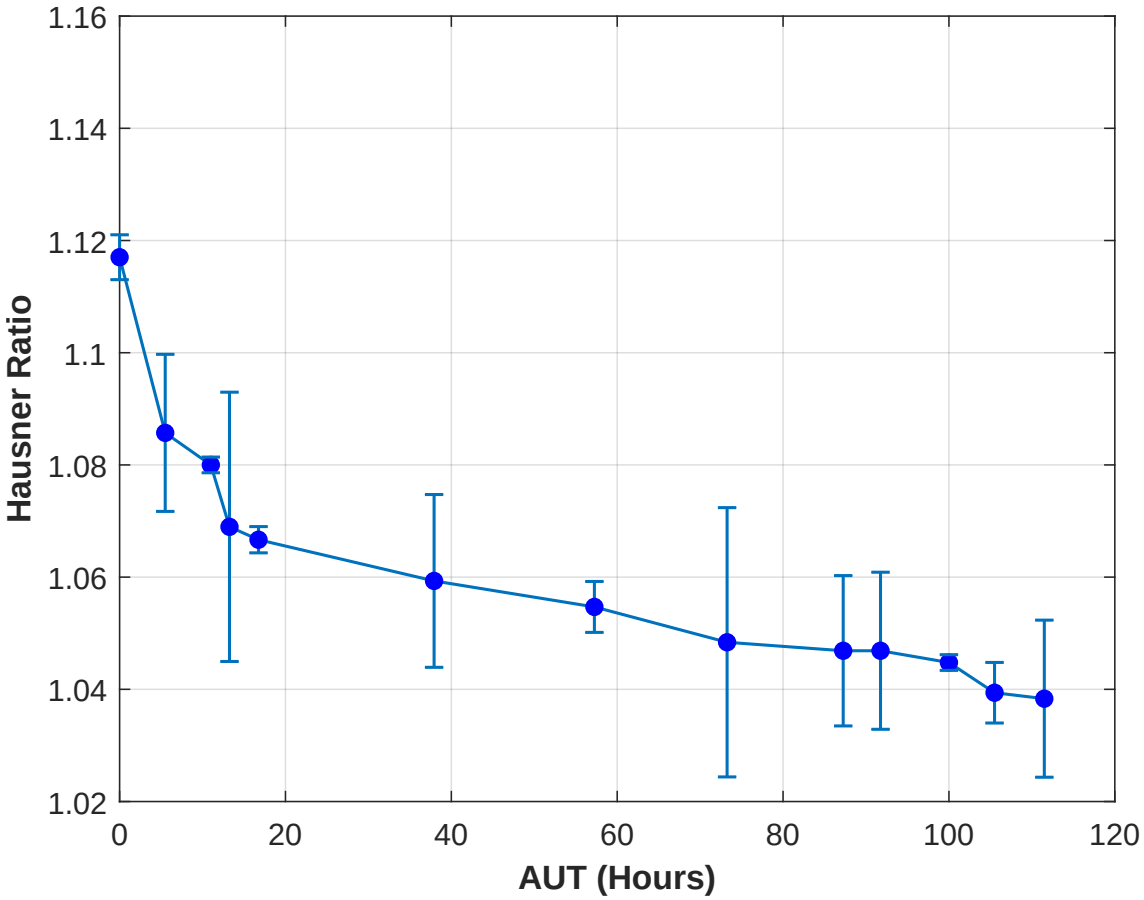

FIGURE 5.8: Effect of powder recycling on powder flowability.

5.4.2 Part Quality Assessment

The assessment of the part qualities in this study enables the changes observed in the feedstock powder to be related to the final as-built part qualities. Changes in the part qualities will be related and correlated with the changes observed in the powder material in a later section of this chapter.

5.4.2.1 Dimensional Accuracy

Dimensional accuracy of the parts produced (Figure 4.9) was assessed and the maximum difference, in *mm*, from the designed dimension was recorded. This was assessed through the use of CNC optical measurement. The effect of the accumulated build time on the dimensional accuracy, i.e. the maximum difference from the designed dimensions, is shown in Figure 5.9. The result shows that as the *AUT* increases, due to powder recycling, the maximum difference from the designed dimension also increased.

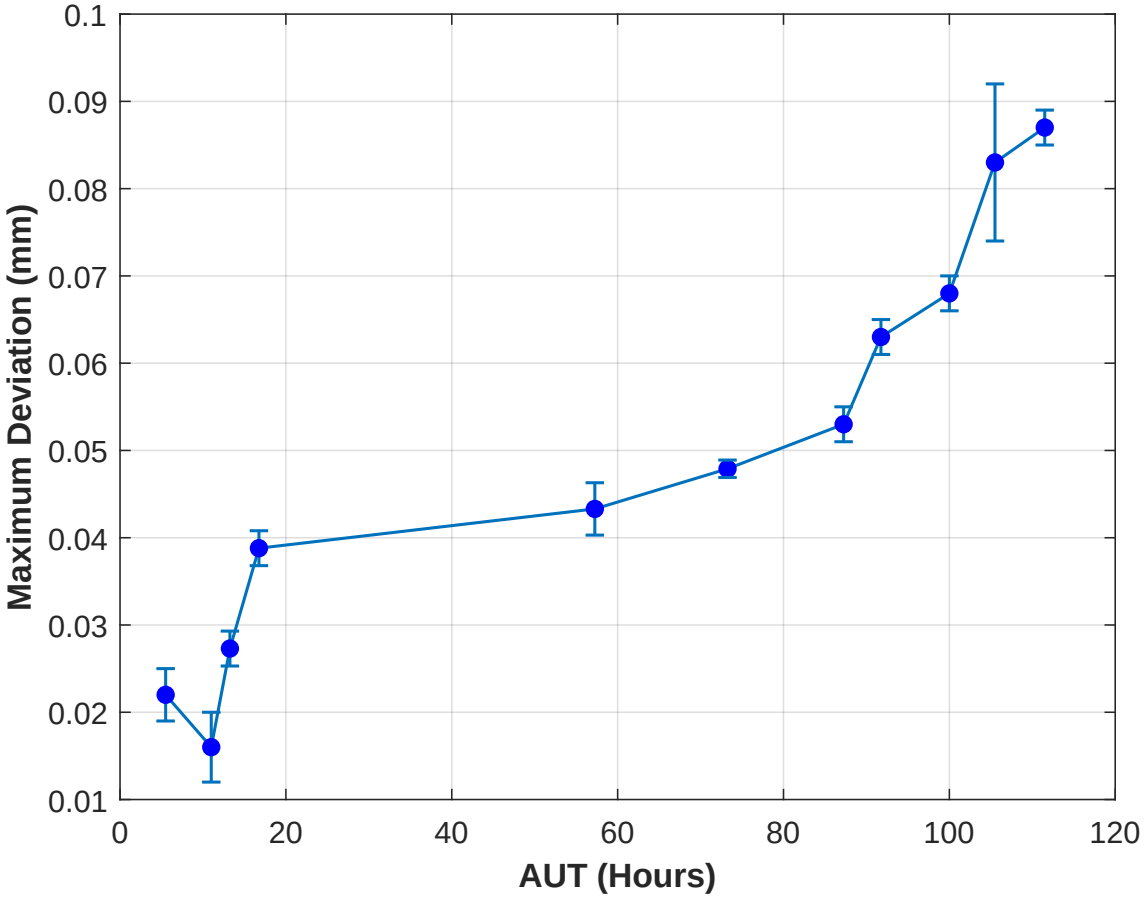

FIGURE 5.9: Effect of powder recycling on maximum difference in part dimensions

5.4.2.2 Part Hardness

The part hardness for 316L built components is specified in the powder data sheet as 89 HRB (EOS GmbH, 2014). The measured part hardness remained within $\pm$ 5% of this specified hardness from the data sheet regardless of the recycling stage. These results, Figure 5.10 show that there was no significant change in the hardness of the parts manufactured with recycled powders.

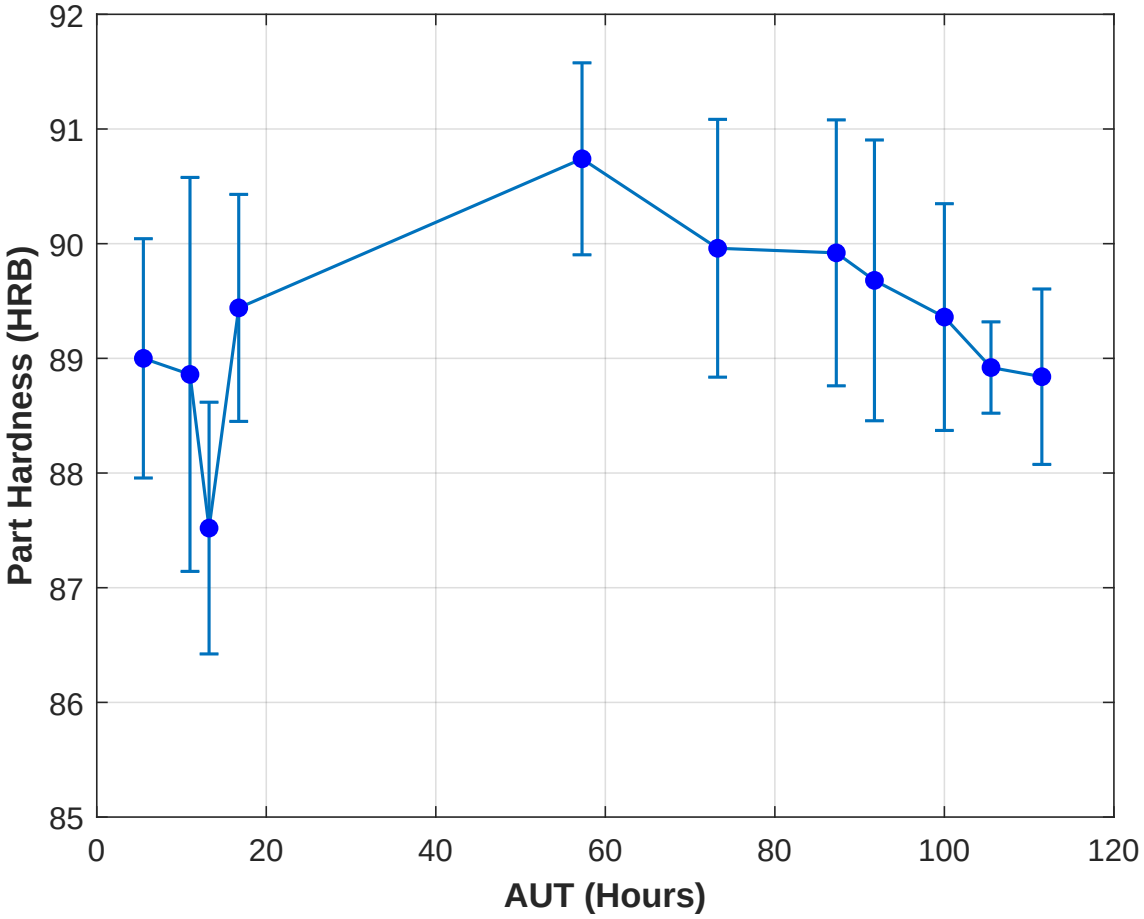

FIGURE 5.10: Effect of powder recycling on the part hardness

5.4.2.3 Surface Roughness

Surface roughness for as-built parts using 316L powder is expected to be 13 $\pm$ 5 μm, as stated in the powders data sheet (EOS GmbH, 2014). Surface roughness was assessed using focus variation. The effect of accumulated build time due to powder recycling on the surface roughness of the as-built overhang part is presented in Figure 5.11. The surface roughness, Ra, increased with the increase in the number of powder recycling stages.

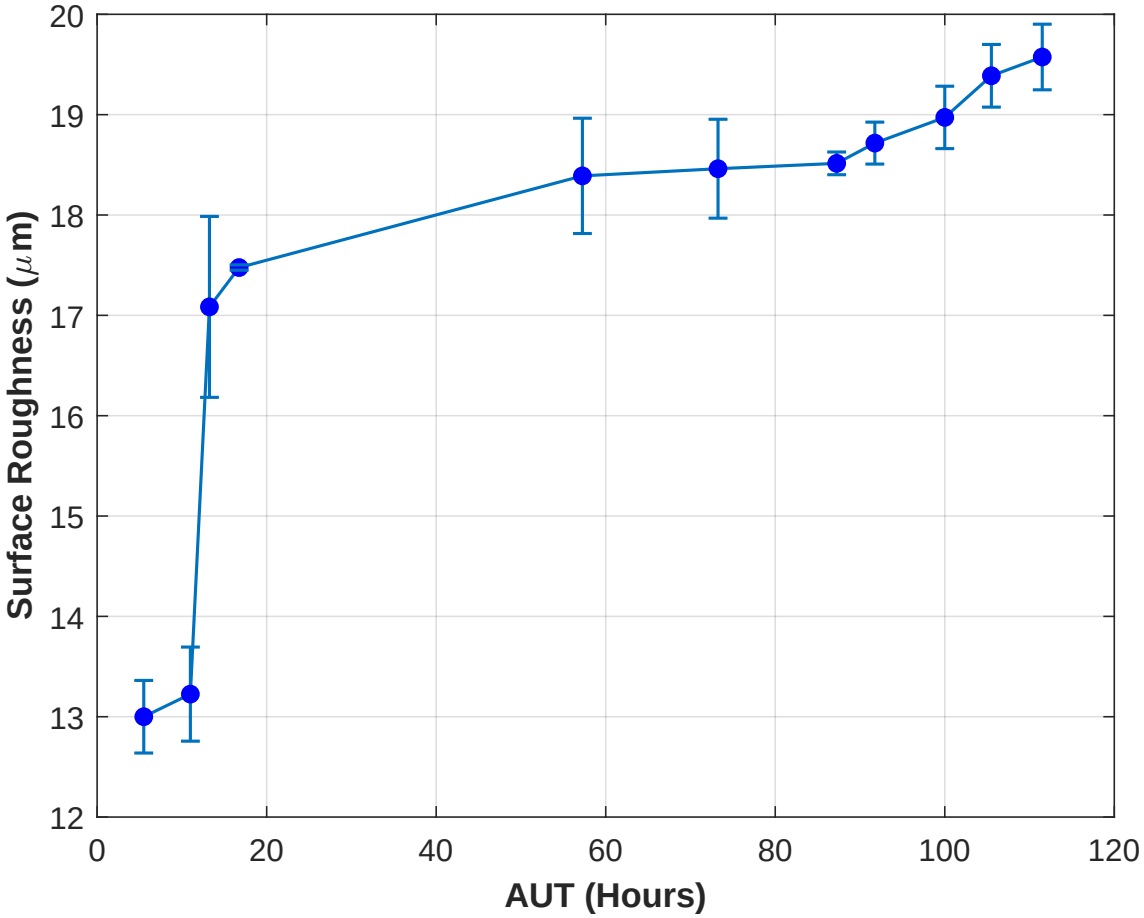

FIGURE 5.11: Effect of powder recycling on part surface roughness

5.4.2.4 Part Density

Part density for as built 316L parts is 100%, as stated in the powder manufacturer data sheet (EOS GmbH, 2014). The part density was assessed through micro-sectioning and image analysis of the quantity and size of pores presented in the micro-section. The effect of accumulated build time (powder recycling) on as-built part density is presented in Figure 5.12. The results show as the *AUT* increases, the as-built part density decreased.

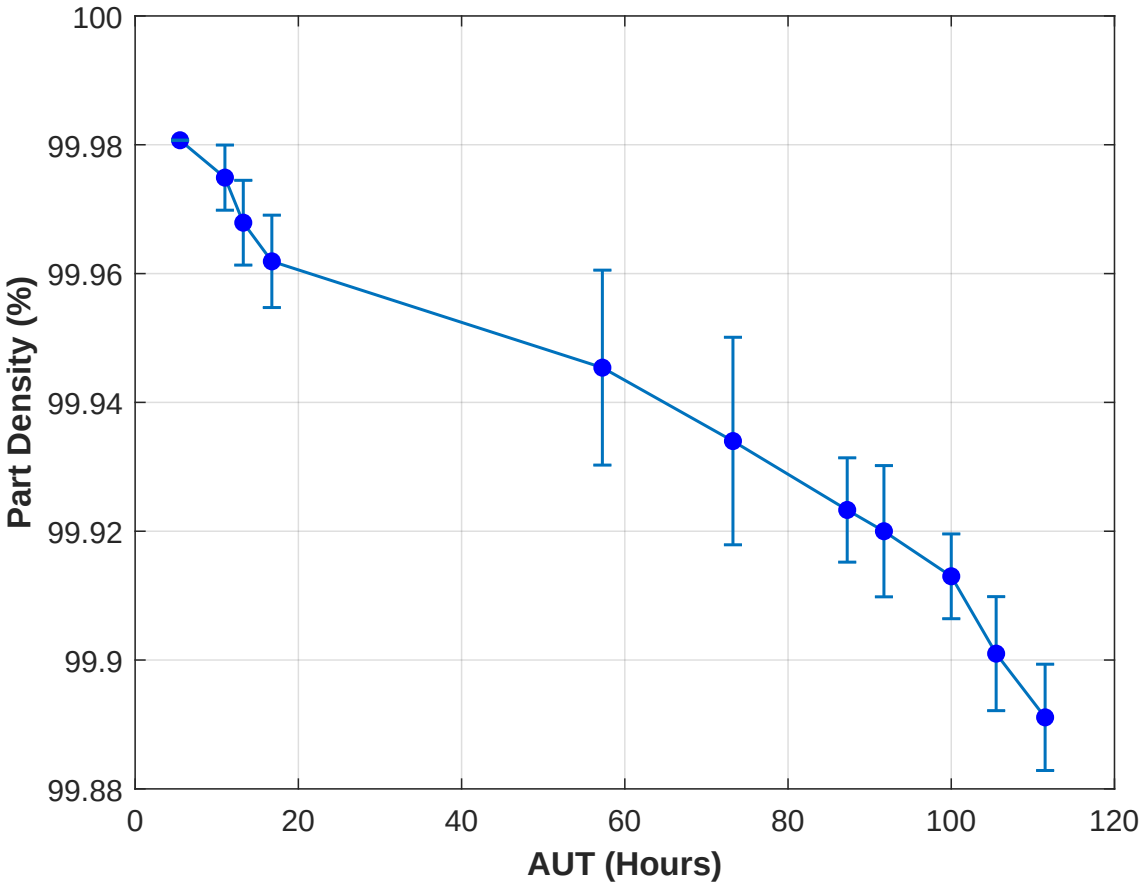

FIGURE 5.12: Effect of powder recycling on as-built part density

5.4.2.5 Phase Analysis Composition

The effect of increasing *AUT* on the resulting microstructure of the manufactured parts is illustrated by the optical micrographs in Figure 5.13. These optical microscope images show the melt pools formed by the L-PBF process, with clear pool boundaries visible between the layers as well as to adjacent melt pools. Figure 5.13 displays the expected microstructures for L-PBF 316L parts.

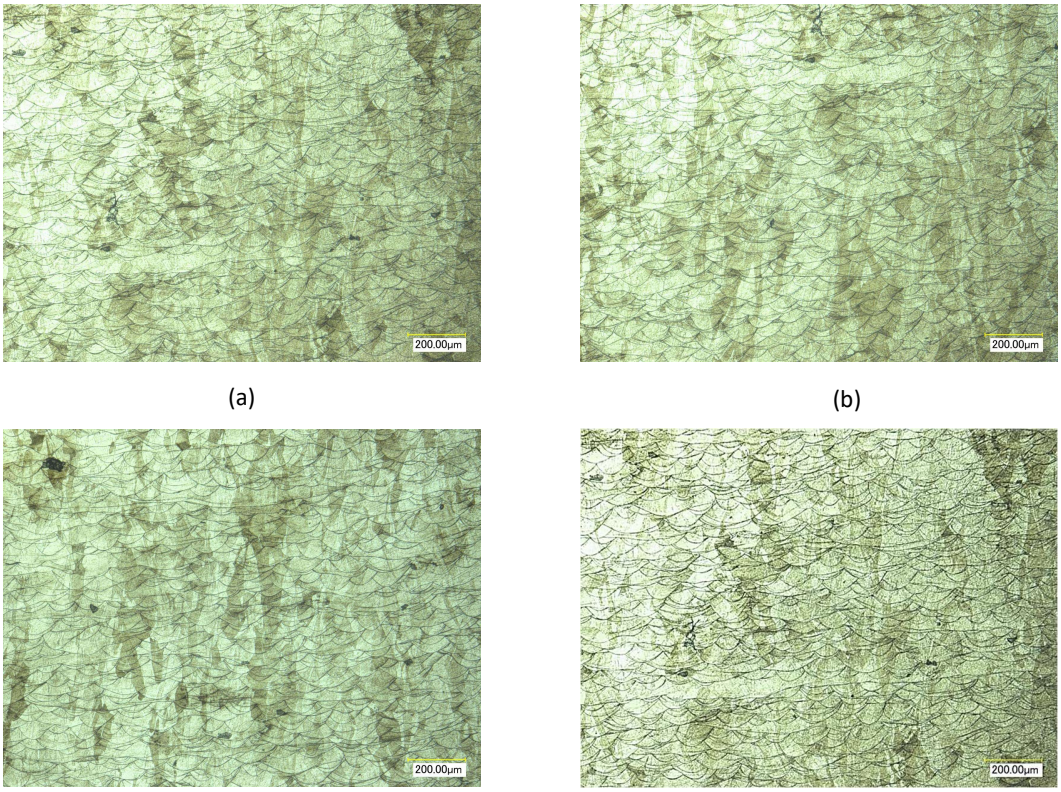

FIGURE 5.13: OM Images (magnification x200) of the etched microstructure to demonstrate the melt pools boundaries formed at different AUTs (a) AUT = 5 hours, (b) AUT = 13.25 hours, (c) AUT = 73.25 hours and (d) AUT = 111.5 hours

To accompany the optical microscope (OM) images further SEM imaging was completed. Figure 5.14, highlights the single-phase microstructure present within a single melt pool. Columnar grains with a transition to cellular grains are present within the melt pools. These cellular grains are present closer to the melt pool boundaries in the heat affected zone (HAZ). The samples all contain coarse columnar grains, which are regarded as consisting of single-phase sub-grains. The OM and SEM images confirm that the increasing AUT of the powder material did not have a significant effect on the microstructure of the manufactured samples, also demonstrated by the XRD analysis presented in Figure 5.3.

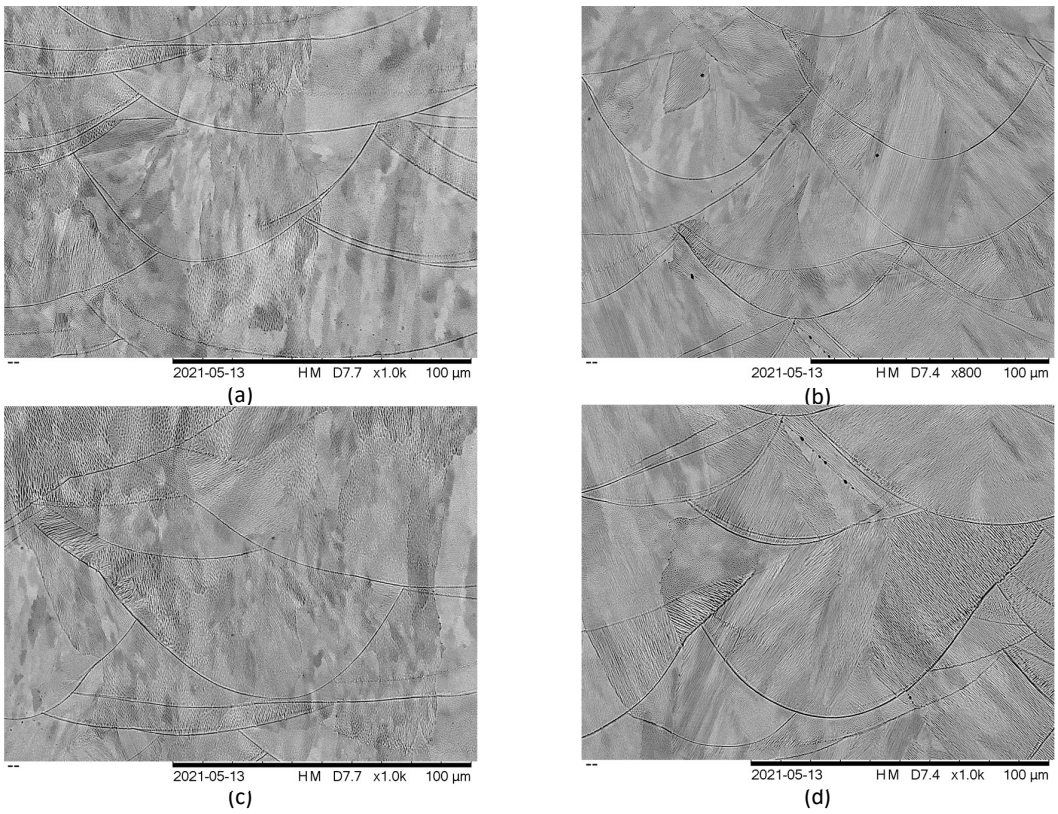

FIGURE 5.14: SEM Images (magnification x1000) of the etched microstructure at different AUT's (a) AUT = 5 hours, (b) AUT = 13.25 hours, (c) AUT = 73.25 hours and (d) AUT = 111.5 hours.

5.4.3 Influence of Powder Characteristics on Part Qualities

Relating the changes in the powder characteristics to the resulting part qualities allows for a greater understanding of how the characteristics of the powder affects the built parts. The analysis presented here investigates the effect of the increasing particle size on the part density as well as showing the effect of the decreasing circularity of particles on the as-built surface roughness. Figure 5.15 and Figure 5.16 shows that the change in the part qualities, specifically, part density and surface roughness can be attributed to the corresponding changes in the mean particle size and morphology of the powder. Often, part density and surface roughness are critical part qualities required by designers, particularly in industries such as medical device and aerospace. Therefore, the influence of raw material properties on the resultant part characteristics is important for the manufacturing of high-quality parts.

Figure 5.15, relates the observed increase in mean particle size, as presented in Figure 5.4, to the decrease in part density, also presented in Figure 5.12. Figure 5.15 shows that as the mean particle size increased the part density decreased. This is attributed to the change in the powder layering process due to differences in the mean particle sizes. A linear regression line was fitted to the graph (shown in red). There is a strong correlation between the increasing mean particle size and the decreasing part density resulting in an R^2 value of 0.955.

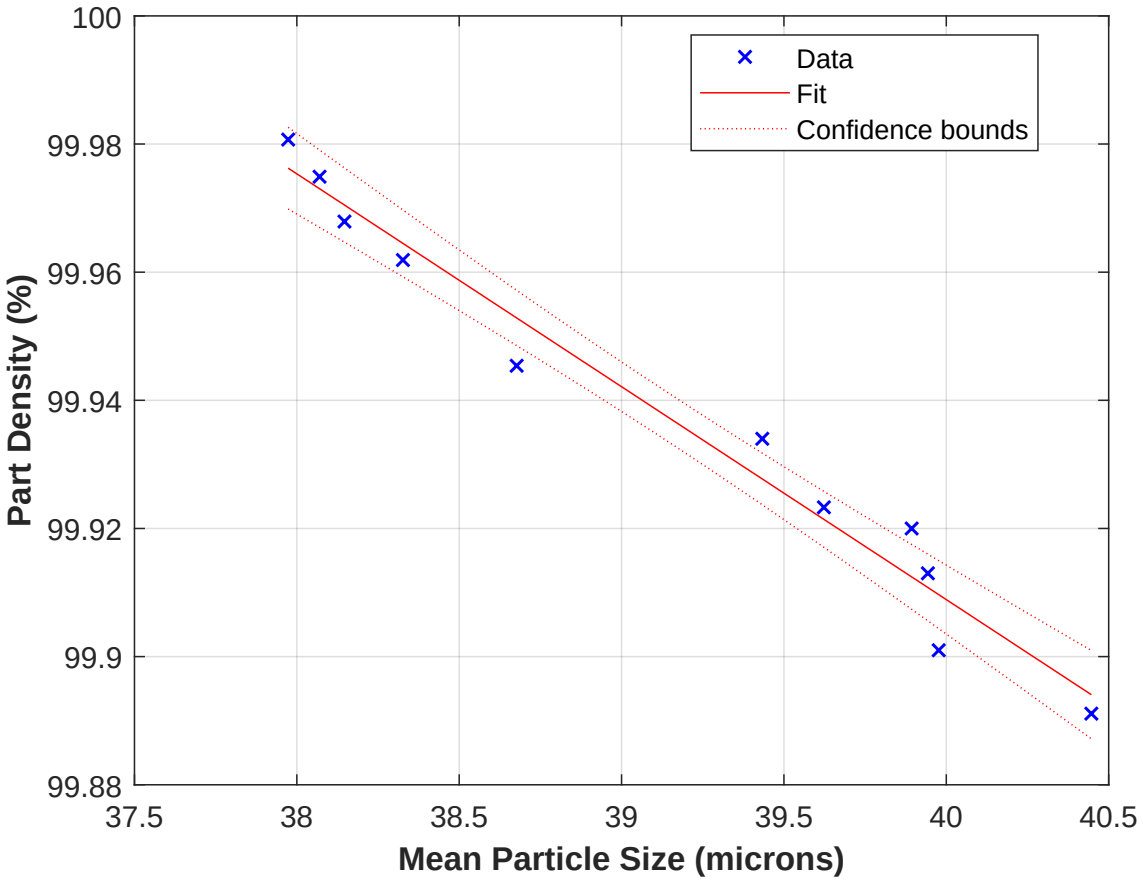

FIGURE 5.15: Correlation of the Mean Particle Size (μm) and Part Density (%) with linear regression fitted (red)

Surface roughness is often a critical feature of a manufactured part due to the relationship between surface roughness and component performance. The difficulty in post-processing some complex features, possible with metal AM, requires the desired surface finish to be produced in process (Shamvedi et al., 2017). Figure 5.16, relates the deterioration in the powder morphology, Figure 5.5 and the increase in the surface roughness, Figure 5.11. Figure 5.16 shows that the decreasing circularity of the particles leads to an increase in the surface roughness of the as-built overhanging surface. A linear regression line was fitted to the graph (shown in red). There is a strong correlation between the increasing mean particle size and the decreasing part density resulting in an R^2 value of 0.828.

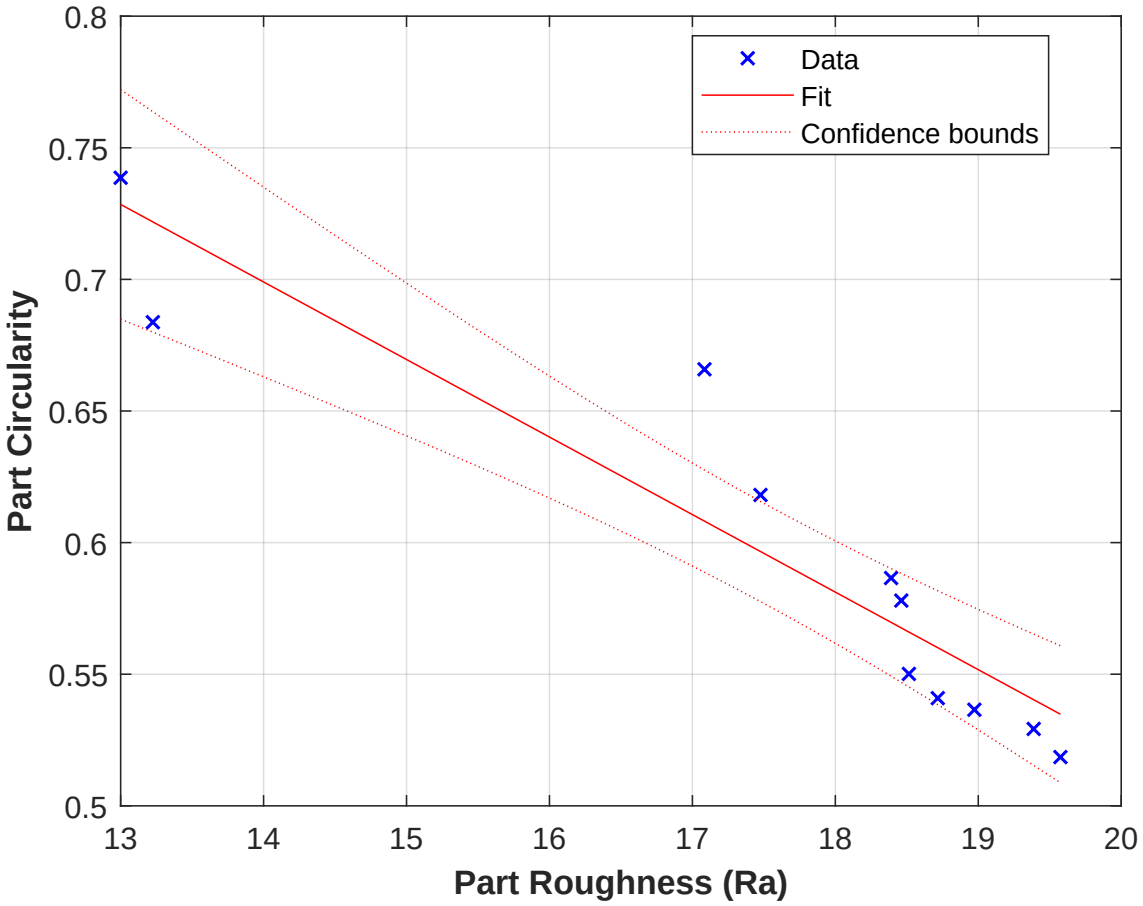

FIGURE 5.16: Correlation of the Powder Morphology (circularity) and the Surface Roughness(Ra) with linear regression fitted (red)

5.5 Discussion

The recycling process led to changes in the powder characteristics. The chemical composition of the powder in bulk form showed no significant change in the wt% of all elements, with all values remaining within the specifications for the powder. This allows for the material to be used for the duration of the recycling process. Any significant deviation in the chemical composition of the powder, due to the recycling process would effect the as-built components. This would open the question if the powder recycling process is worth while.

The mean particle size increased with the increased powder recycling. Smaller powder particles tend to be melted first in the laser interaction, this leaves the larger particles for use in future builds. This causes the larger particles to be recycled for future builds. The re-coater blade used for the layering process will also ensure that the larger particles (those greater than the layer thickness) are dragged across the build plate into the overflow region.

The powder morphology in terms of the circularity of the particles decreased with increased recycling. Particles are less circular compared to the virgin powder due to the inclusion of particles which contain agglomerates as a result of partial melting of adjacent particles in the L-PBF process. An example of some of the

agglomerated particles observed in the recycled powder can be seen in Figure 5.17, these particles shown are clearly not circular in shape.

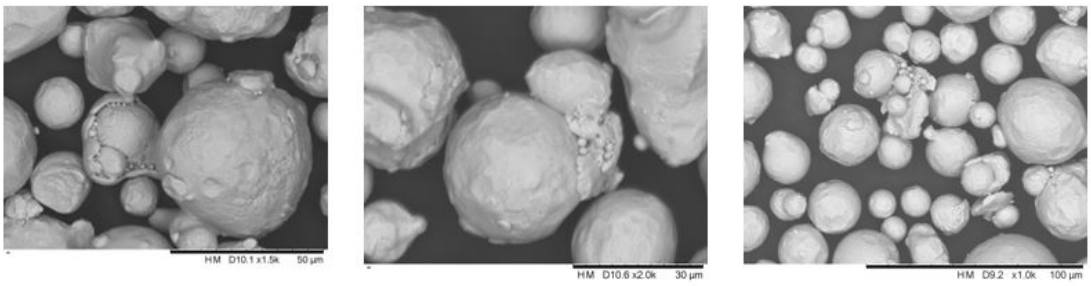

FIGURE 5.17: Examples of agglomerated particles

The dimensional accuracy of the designed parts showed an increasing deviation from the designed dimensions. This is shown in Figure 5.9 where the increased recycling of the powder material leads to an increase in the maximum deviation from the designed dimension. This increase is greater than the specification for the dimensional accuracy of the material, which is given as $\pm$ 20-50 μm (EOS GmbH, 2014). The measured dimensions of the parts produced a maximum deviation of 90 μm from the designed dimensions.

Assessment of the part hardness concludes that there was no significant effect of powder recycling on the resulting hardness of the as-built parts. The hardness remained within $\pm$ 5% of the stated hardness value of 89 HRB from the material data sheet (EOS GmbH, 2014).

The surface roughness of the parts increased with increased powder recycling, as shown in Figure 5.11. The as-built surface roughness of the overhang structure increased beyond the specification of 13 $\pm$ 5 μm (EOS GmbH, 2014), after 57 hours of accumulated build time. This is caused by a combination of the increased mean particle size and a decrease in the circularity of the powder particles, as is shown in Figure 5.16. This is further discussed in the following paragraphs.

The part density decreased with the increased powder recycling, as seen in Figure 5.12. The expected density of the material is 100% (EOS GmbH, 2014). It is observed that as the powder recycling increases the density of the parts decreases. This is seen through an increase in the quantity and size of pores imaged in the micro-sections. This density decrease is certainly detrimental for many industries where parts of high density are required.

The increasing mean particle size on the part density produced a strong relationship, as shown in Figure 5.15. The reduction of smaller particles leads to an increase in the voids and pores produced in the layering process. This results in the decrease in density. Figure 5.18 (a) illustrates that with the greater presence of small particles in the virgin powder the deposition of powder results in layer with fewer voids present. Figure 5.18 (b) illustrates that the recycled powder material, when deposited on the layer results in voids due the larger

mean particle size. This introduction of voids in the layering process is translated into pores and voids in the as-built part.

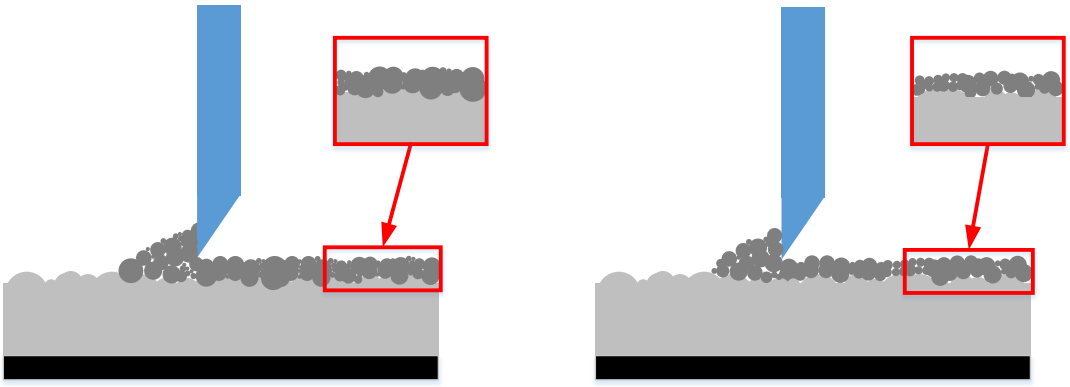

FIGURE 5.18: Powder layering process for (a) virgin powder and (b) recycled powder

The decreasing circularity influenced the surface roughness of the overhang parts. As the surface roughness of the parts is dominated by the presence of partially melted particles on the surface of the parts, the shape of the particles will affect the resulting surface roughness. The larger mean particle size also influences this feature. Figure 5.19 depicts the effects on the changes in the powder particle size and morphology (SEM powder images) on the surface roughness of the parts produced at various stages (0, 57.25 and 111.5 accumulated build hours) of the powder recycling. The decreasing powder circularity and increasing mean particle size is related to the increasing surface roughness.

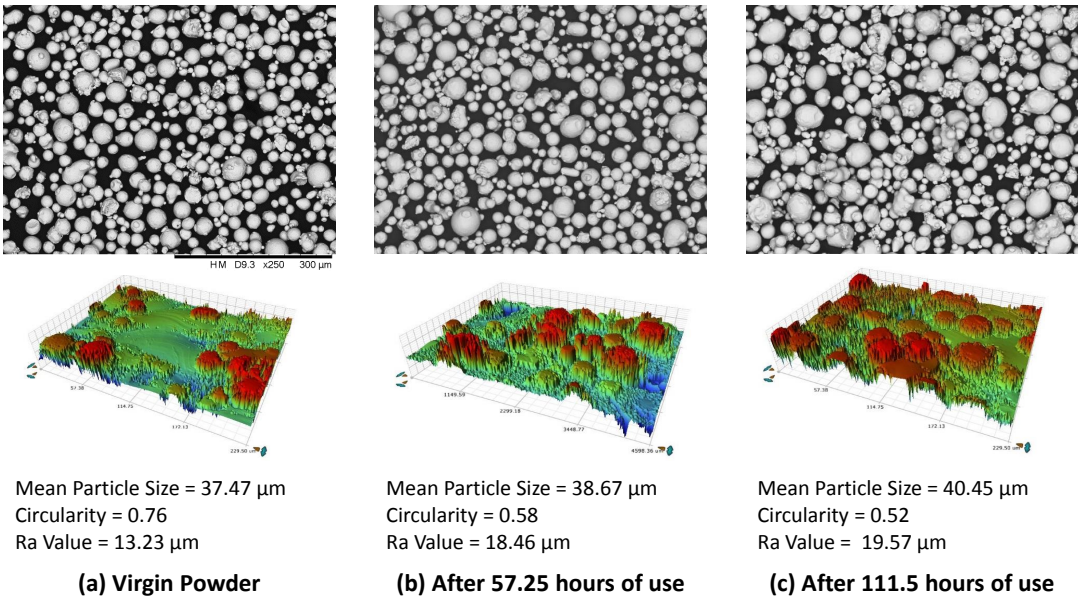

FIGURE 5.19: Effect of Powder Characteristics on the Surface Roughness (Ra) at different stages of powder recycling (0, 57.25 and 111.5 accumulated build hours)

5.6 Conclusion

The results from this research show that the continued recycling of powder material has an effect on the powder characteristics and the resulting part qualities. The mean particle size of the powder increases with the number of powder reuses, indicating that smaller particles are being melted by the process leaving larger particles for subsequent builds. The particles also become less circular, suggesting a change in morphology due to the partial melting of smaller powder particles to larger particles causing agglomerates to form. The results show that there was no significant change found in the powder chemical composition throughout the recycling process.

The analysis of part qualities showed that the maximum difference of part dimensions from the specifications increases with the increased powder use. The surface roughness of the parts increased with the number of powder reuses, indicating that the presence of larger particles in the powder affects the surface roughness. The hardness of the parts remains consistent with the expected value. Part density decreases with the number of powder reuses, indicating that an increase in mean particle size produces increased porosity in the built parts.

These results allow for a greater understanding of the effect that powder recycling has on the powder and the parts built. This will enable a more controlled use of recycled powder materials as well as allowing for higher utilisation of powder batches.

6 Powder Rejuvenation

Powder recycling enables the powder material in L-PBF to be used further, powder rejuvenation is a process that can further the life cycle of the powder material. The previous chapter provides an understanding of effect the recycling process has on the powder and parts in the L-PBF process. The aim of this chapter is to continue that study through a powder rejuvenation process. The rejuvenation process requires the mixing of new virgin powder with a batch of powder which has been through multiple recycling stages.

Consisting of two sections, this chapter, presents an initial study and an extended study. The first investigates the effect of different powder mixing ratios on the bulk powder properties, while the second studies the impact of mixing virgin and recycled powder at a 50:50 ratio on the powder characteristics and the resulting part properties. Powder rejuvenation is completed typically because either the quantity of powder in the recycled batch is lower than the amount required to continue processing or the bulk powder properties have deteriorated beyond a specific point. The results from the tests are presented before being discussed in detail in the discussion section of this chapter.

6.1 Materials and Methods

The core material for this study was EOS Stainless Steel 316L as outlined in Section 4.1.1. This powder is a commonly applied stainless steel powder for the medical device, aerospace and auto-mobile industries (EOS GmbH, 2014). The virgin powder material will be new as-received powder of 20kg quantity and the recycled powder will have been cycled through the L-PBF process for a total *AUT* of 112 hours in a quantity of 19kg.

The characteristics of the rejuvenated powder as it is repeatedly processed in the L-PBF process were determined as outlined in Table 6.1. These methods are described in detail in Chapter 4 of this thesis.

TABLE 6.1: Powder Characterisation Methods

Characteristic	Method
Powder Chemical Composition	Scanning electron Microscopy (SEM) and Energy Dispersive X-Ray (EDX)
Particle Size	Laser Diffraction
Particle Morphology	SEM Imaging and Image Analysis
Powder Skeletal Density	Helium Pycnometry
Powder Bulk Density	Hall Funnel
Powder Flowability	Hausner Ratio

A baseline virgin powder sample was taken as a reference point for the studies presented. Further powder samples were assessed after each build, as discussed in Section 5.3. The sample was taken after sieving the un-melted powder using a 63 μm sieve, as shown in Figure 6.1. The sieving process was conducted to remove any potential contaminants. It is a standard practice for a range of L-PBF machines to complete this sieving process post-build. This ensures that any oversized particles or contaminants are removed from the powder batch prior to the next build. The powder sample was then tested using the methods outlined above in Table 6.1.

The test samples that were used to determine the initial effect of powder recycling in Chapter 5, were also used in this study. Resulting part qualities were assessed using the methods outlined in Table 6.2. The samples were manufactured on an EOS M280 system with default processing parameters for 316L stainless steel, as specified in the previous chapter, Section 4.2. All test specimens were assessed in their as-built state, without post-processing, such as heat treatment or surface finishing.

TABLE 6.2: Part Quality Assessment Methods

Part Quality	Method
Dimensional Accuracy	CNC Coordinate Measuring Machine
Hardness	Rockwell Hardness (Scale B)
Surface Roughness	Focus Variation Surface Measurement
Part Density	Micro-sectioning and Image Analysis

6.1.1 Powder Rejuvenation

Powder rejuvenation is a process that can be applied to further extend the usable life of a recycled batch of powder in the L-PBF process. As previously discussed powder recycling allows for increased utilisation of feedstock material in the L-PBF process. The recycling process can be repeated until one of two limitations is reached;

1. the powder quantity becomes too low to continue building.
2. the characteristics of the powder material are causing the resulting part qualities to be out of specification. Depending on the final part requirements these powder characteristics may be chemical composition, particle morphology or powder flowability. A discussed in previous sections these characteristics influence the resulting part qualities such as part density, mechanical properties and surface roughness.

If either of these limitations occur, a powder rejuvenation process may be deployed to maximise utilisation of the costly powder material. The powder rejuvenation process consists of mixing recycled powder material with virgin powder to increase the quantity of the powder available and improve the bulk characteristics of the powder material. Figure 6.1 depicts the powder-recycling loop and how this proposed powder rejuvenation process fits into the recycling methodology. As shown in Figure 6.1, the powder rejuvenation process begins after a powder sample fails the powder monitoring tests. If the characteristics of the powder sample and the manufactured parts meet the pre-defined specifications, i.e., a "pass", the powder recycling loop continues. Alternatively, if either the powder or manufactured parts do not meet these predefined specifications, virgin powder is added to the recycled powder and mixed. The powder recycling loop outlined in Figure 6.1 is initiated again.

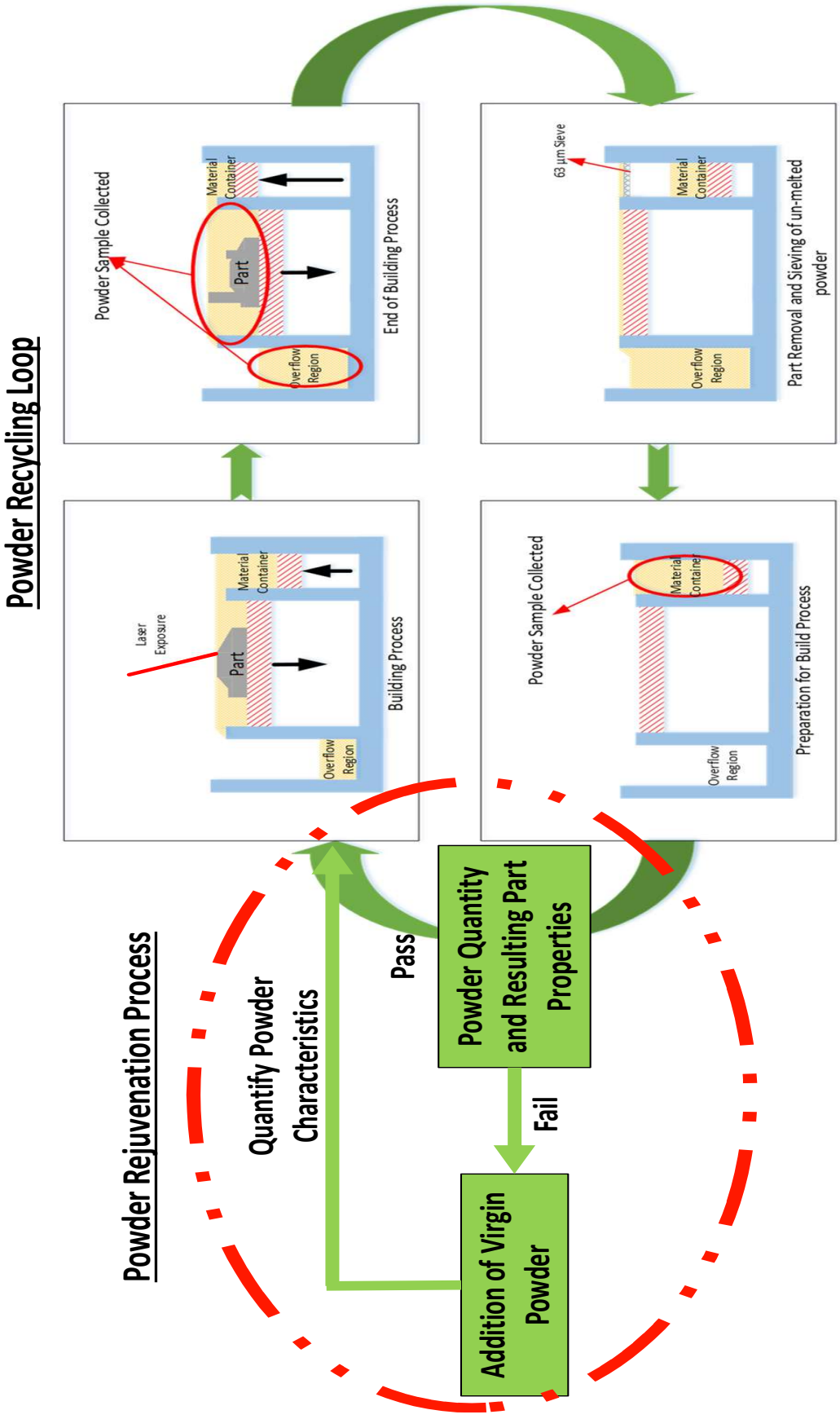

FIGURE 6.1: Schematic of the powder recycling process with the powder rejuvenation loop added.

A total of 17 build cycles were completed in this study with both the powder and manufactured parts being sampled and analysed after each build using the methods presented in this section. These aforementioned pre-defined specifications are determined by the required specification of the part being manufactured and the final application of the part. Ultimately, the user determines the specification they require. The specifications may be a particular mean particle size range, powder morphology, flowability or a combination of these powder characteristics.

To determine the effect of the powder rejuvenation process on the powder material an initial study was performed to assess the effect of different ratios of virgin and recycled powder material on the bulk powder characteristics. The powder was mixed at different ratios, as shown in Table 6.3. Some of these ratios have been proposed in previous research as methods to offset the changes in powder characteristics due to the powder recycling process (Clayton and Deffley, 2014; Strondl et al., 2015). Effects are shown of these mixing ratios on the bulk powder characteristics in the following results sections.

TABLE 6.3: Powder Mixing Ratios

Sample ID	Virgin Ratio	Recycled Ratio	Source
A	100%	0%	
B	0%	100%	
C	75%	25%	(Clayton and Deffley, 2014)
D	66%	33%	
E	50%	50%	(Clayton and Deffley, 2014)
F	33%	66%	
G	25%	75%	(Clayton and Deffley, 2014)
H	5%	95%	(Strondl et al., 2015)

6.2 Results and Discussion

The aforementioned experiments were conducted over a period of 6 months which resulted in a total of 17 separate L-PBF builds accumulating a total of 180 build hours on the powder material. After each build a sample of powder was extracted from the EOS M280 and stored in sealed container prior to characterisation. The sealed container ensured that the exposure to oxygen and moisture was minimised. Testing was then conducted in the order presented by the results sections below.

The results presented below show the effect of powder recycling (i.e. Average Use Time (*AUT*)) on the powder characteristics and the part qualities. Each data point on the following graphs represents a powder sample, taken at the end of a L-PBF build. The error bars presented in all graphs are representative of the standard error of the mean, calculated using Equation 4.12.

6.2.1 Effect of powder mixing ratio on the bulk powder characteristics

The powder material was initially mixed into small quantities in order to determine the effect of this mixing process on the bulk characteristics of the powder. The ratios used are outlined in Table 6.3 above. The characteristics of the virgin and recycled powder, sample ID A and B respectively, are outlined below in Table 6.4.The characteristics, of Sample B, show the effect of powder recycling as previously studied in Chapter 5. The resulting characteristics of the mixed powder batches are presented in the following sections.

TABLE 6.4: Initial powder characteristics for virgin and recycled powder.

Sample ID	A	B
AUT	0 Hours	112 Hours
Mean Particle Size	36.45 μm	38.813 μm
Particle Circularity	0.741	0.578
Apparent Density	4.393 g/cc	4.533 g/cc
Tapped Density	4.730 g/cc	4.986 g/cc
Hausner Ratio	1.118	1.177

6.2.1.1 Powder Chemical Composition

The chemical composition of the mixes of powder material was found to conform to the chemical composition of the 316L stainless steel powder as specified by the manufacturer (EOS GmbH, 2014). Figure 6.2 presents the results from the EDX maps conducted on each sample. This presents the weight percentage of the most prominent chemical elements of each of the mixed powder batches. The results show that regardless of the quantity of virgin to recycled powder mixed the composition remains within specification for the 316L powder. This highlights that there were no contaminants within the powder, which if present can affect the composition of the manufactured parts.

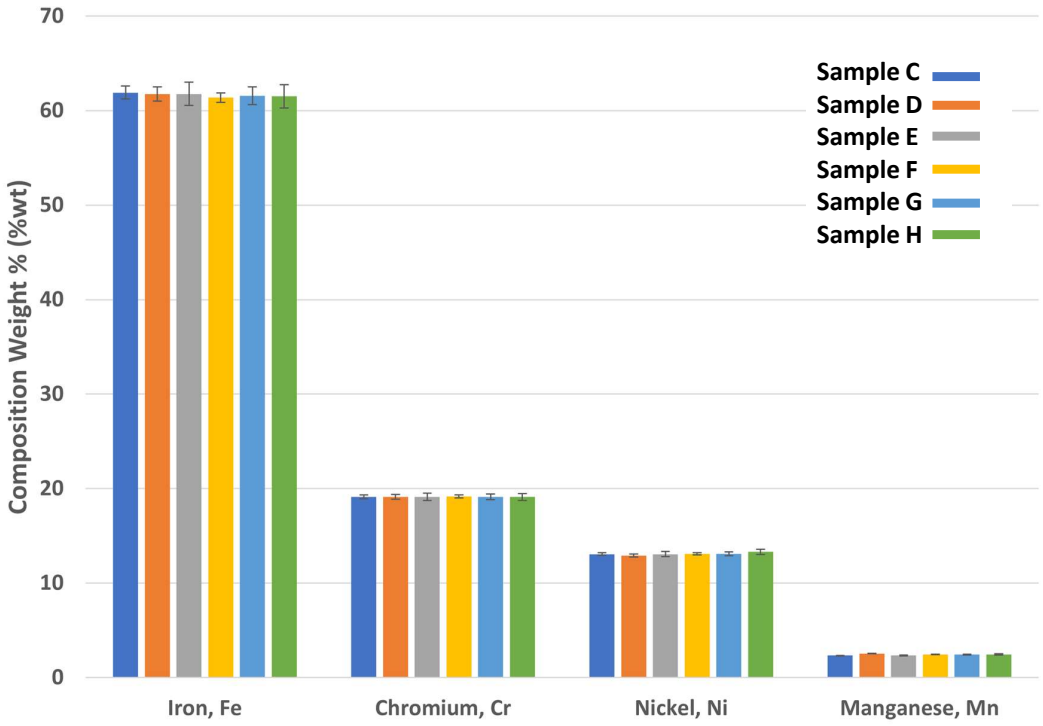

FIGURE 6.2: Powder chemical compositions after mixing.

6.2.1.2 Powder Particle Size

Larger particles in the batch affect the way the powder behaves within the L-PBF process, impacting the flowability and packing density of the powder. Therefore, it is preferential to have powder particles that are closer to the mean particle size of the virgin powder received from the powder supplier. Figure 6.3 shows the mean particle size of the powder material for each of the powder mixes described in Table 6.3. The samples show that those with a higher proportion of recycled powder have a larger mean particle size. For example, Sample C, the 75:25 ratio mix, has the lowest mean particle size. This is closest to that of the mean particle size of the virgin powder, 36.45 μm, outlined in Table 6.4.

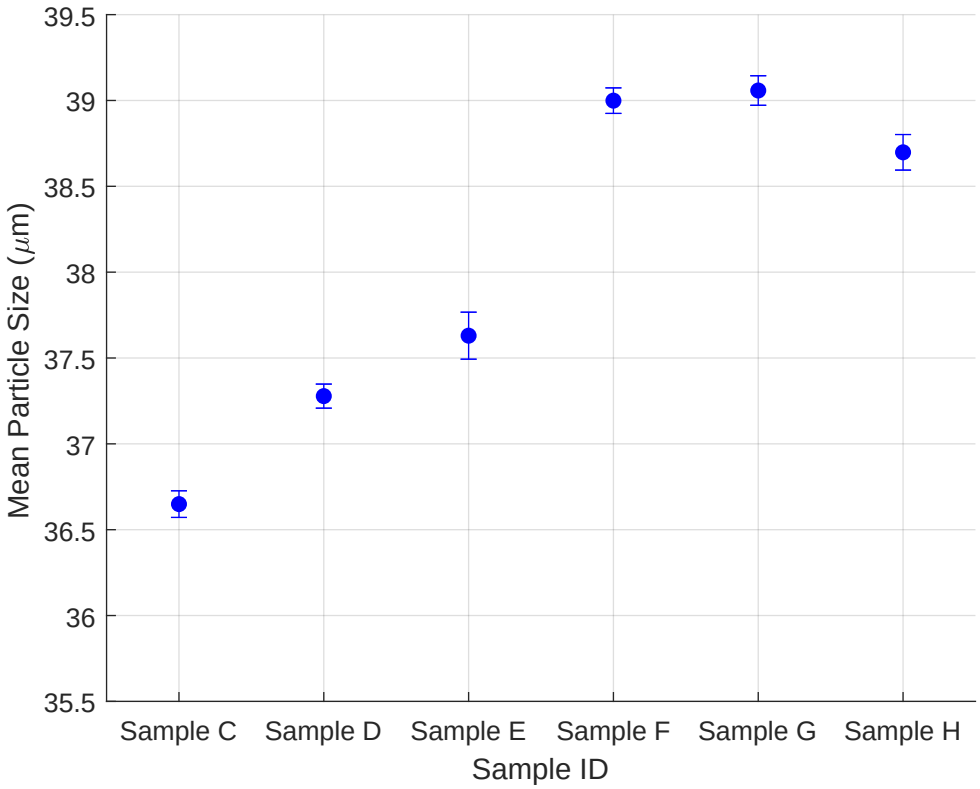

FIGURE 6.3: Mean Particle Size after powder mixing.

6.2.1.3 Powder Morphology

The morphology of the powder material, as described by the particle circularity, of each of the powder mixes is shown in Figure 6.4. An increase in the quantity of recycled powder in the powder mixes is seen here to result in the presence of less circular particles in the powder batch. Therefore, the particles are more irregular in shape which can affect the flow behaviour of the powder, thus affecting the powder packing density in the L-PBF process.

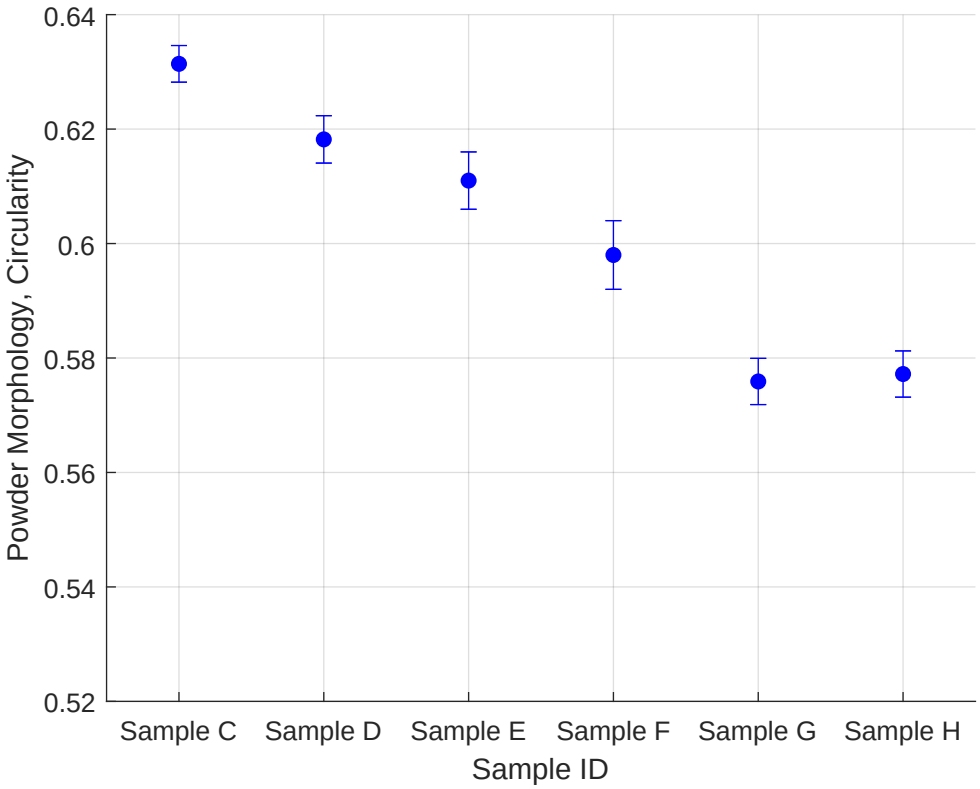

FIGURE 6.4: Powder Morphology, circularity, for the powder mixes.

6.2.1.4 Powder Density

Figure 6.5 shows the apparent and tapped density of each of the powder mixes studied. The apparent and tapped density both affect the flow and the compressibility of the powder. These two factors directly impact the quality of the powder bed during the powder deposition process in L-PBF; this, in turn, effects the properties of the parts that are manufactured. These measures of density are indicators to how well the powder can pack, an important characteristic in ensuring an evenly packed powder bed. The powder flowability is also affected by these characteristics as shown in the following section.

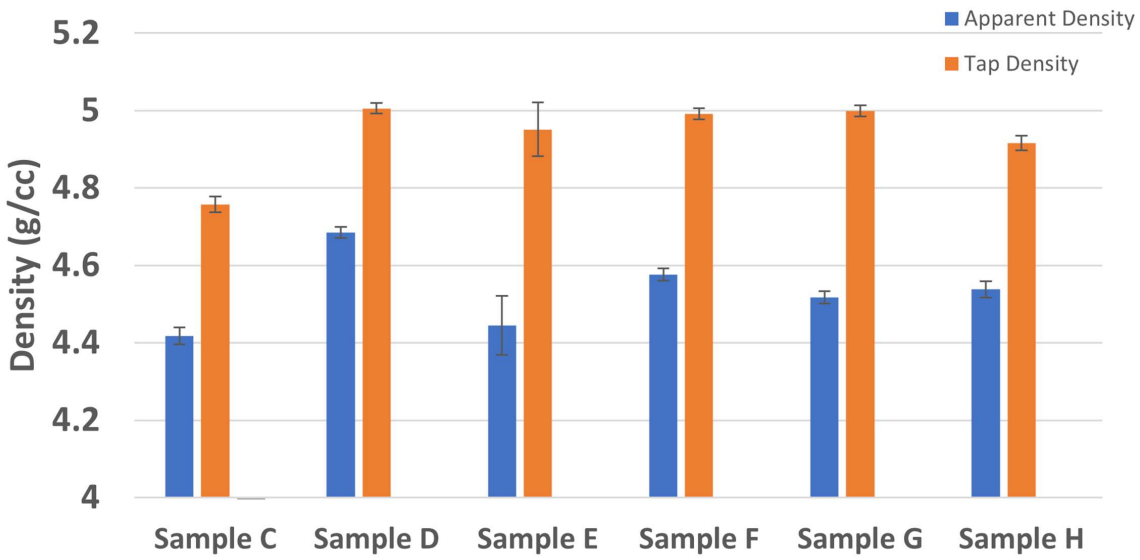

FIGURE 6.5: Apparent and Tapped Density for the powder mixes.

6.2.1.5 Powder Flowability

The powder flowability is a vital characteristic in terms of understanding how the powder will behave in the re-coating process; the Hausner ratio is used to quantify this characteristic. The effect of the powder mixing process on the flowability of the batch is shown in Figure 6.6. The flowability of the powder material is affected by the size and shape of the powder particles. The smaller and less circular powder particles will not flow as well as larger, more circular particles. This is due to the larger inter-particle forces that are caused by the increased surface area of the smaller and less circular particles. These increased inter-particle forces, due to Van der Waals forces (Spierings et al., 2015) causes a resistance to flow within the powder batch, which results in a lack of powder deposition in the recoating process. This highlights the importance of high degree of powder flowability in the L-PBF process. It is important to note here that good flowability can also negatively impact the powder deposition process in L-PBF, this is discussed further in later sections.

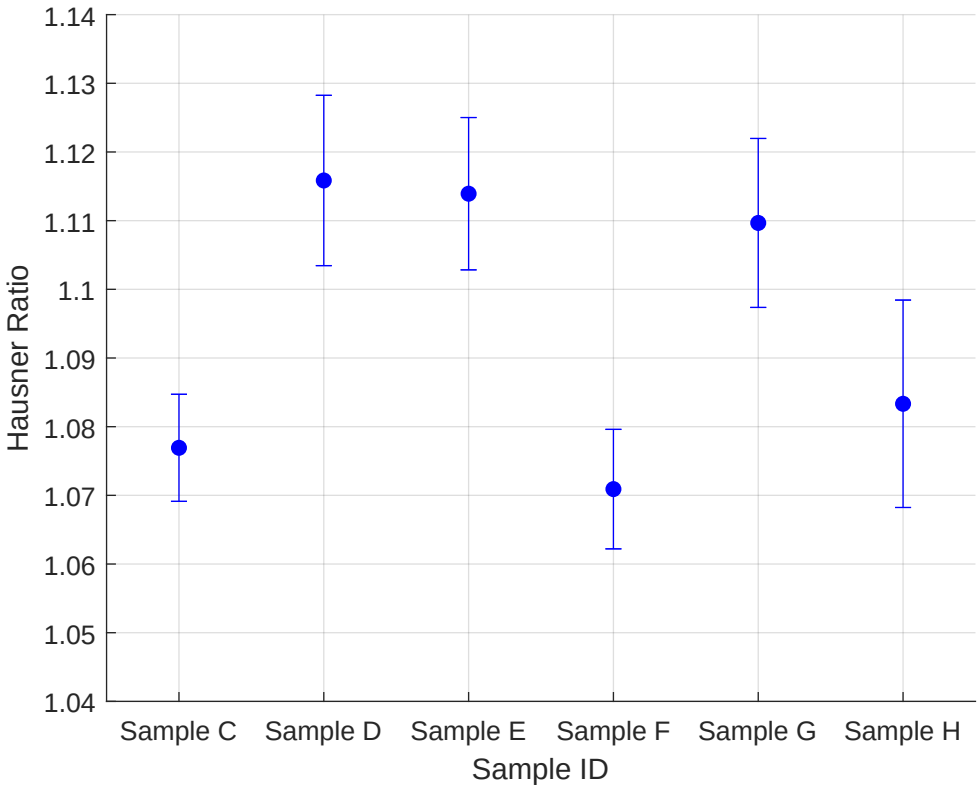

FIGURE 6.6: Effect of the powder mixes on the flowability of the powder as indicated by the Hausner Ratio.

6.2.2 Effect of powder recycling on the rejuvenated powder characteristics

With the understanding in how the resulting powder characteristics are affected by the ratio of virgin to recycled powder used presented in the previous sections, it is important to study how this rejuvenated powder performs in the L-PBF process. The following sections present the results of the powder recycling process on a batch of rejuvenated powder which consists of 50% virgin powder and 50% recycled powder, Sample E (50:50).

A total of 17 build cycles, resulting in an average use time (*AUT*) of greater than 300 hours on the rejuvenated powder batch was completed. The results show a change in the powder characteristics and the resulting part properties with an increase in use, indicated by the *AUT*. Each data point presented in the following graphs represents a powder sample or manufactured part that was tested.

6.2.2.1 Powder Chemical Composition

As previously stated the chemical composition is a very important characteristic to quantify for each powder sample. As a result of this the chemical composition was the first characteristics to be quantified after each samples was collected. This was to ensure that during the recycling process no inclusions or contaminants

had been introduced into the powder batch. The primary elements of the powder composition, Iron (Fe), Chromium (Cr), Nickel (Ni) and Molybdenum (Mo) are shown in Figure 6.7. The weight percentage of these elements within the powder batch remain consistent with the expected composition as per EOS GmbH, 2014 throughout the 17 builds studied. These results confirmed that the recycling process of the rejuvenated powder, in this study did not introduce any contaminants into the powder batch. These may negatively affect the properties of the manufactured samples (Averyanova, Bertrand, and Verquin, 2010).

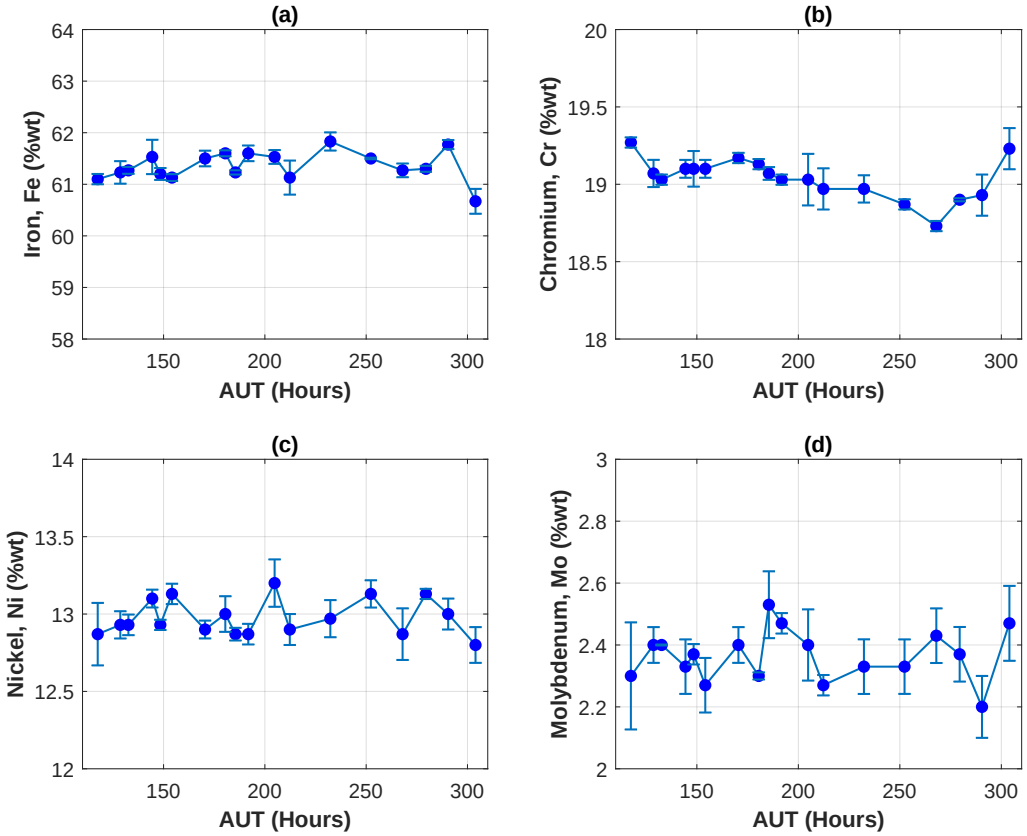

FIGURE 6.7: The effect of the *AUT* (powder rejuvenation) on the powder chemical composition (a) Iron, (b) Chromium, (c) Nickel and (d) Molybdenum.

6.2.2.2 Powder Phase Characterisation

The microstructure of the powder particles influences the microstrucure of the as-build L-PBF parts (Averyanova, Bertrand, and Verquin, 2010). The effect of the *AUT* on the phases present within the powder samples is shown in the XRD analysis results in Figure 6.8. These samples had a corresponding *AUT* of 128.7, 180.5, 232.3 and 304 hours respectively. XRD results for a virgin powder sample is also included as a baseline of the expected phases. The XRD results shows an overlap between the virgin powder and rejuvenated powder samples, with the peaks associated with an austenitic stainless-steel present. The peaks indicate a

single-phase Face Centre Cubic (FCC) structure present for all samples. Austenite is a γ phase, which contains a unit cell length of 3.595 Å (Armstrong). The phases detected were located at 43.57°, 50.75° and 74.61° and there was no change in the location or width of these peaks presented in the graph. This confirms that as the rejuvenated powder batch is recycled, there was no effect on the phases present within the powder material. This indicates that the microstructure present within the manufactured samples will remain consistent. The XRD analysis confirms that the recycling and rejuvenation processes applied in this work did not negatively impact the phase and crystallinity of the powder material as *AUT* increases.

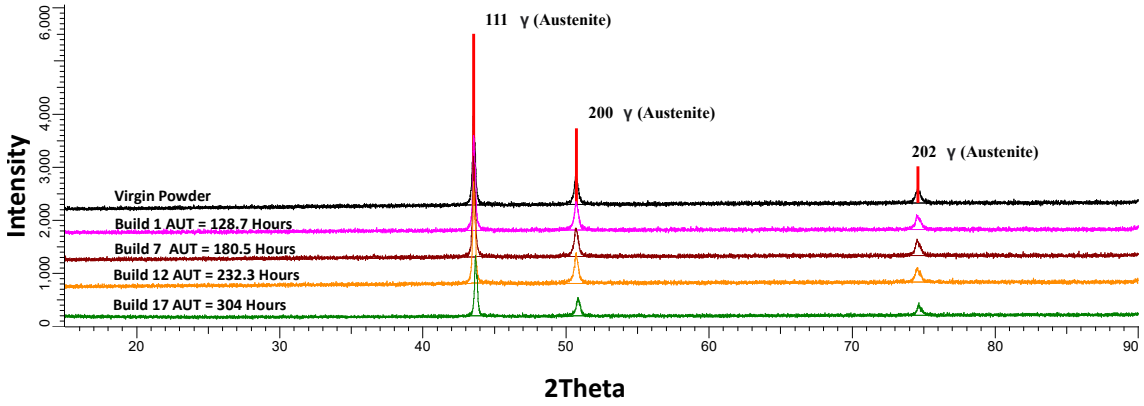

FIGURE 6.8: Effect of powder rejuvenation and subsequent recycling (average use time) on the microstructual phases of the powder.

The results presented in Figure 6.8 are consistent with the results shown in previously in Figure 5.3. This results highlights that both the recycling process, presented in Chapter 5, and rejuvenation process, presented here, do not have an negative effect on the phase composition of the powder.

6.2.2.3 Powder Particle Size

The effect of the powder recycling process, as denoted by an increase in the *AUT* of the powder, on the mean powder particle size is presented in Figure 6.9. As the rejuvenated powder use increases, there is a clear increase in the mean particle size of the powder batch, this is consistent with the previous study presented in Chapter 5. This change is due to the ease at which the smaller powder particles are melted during the selective laser melting process. These smaller particles tend to be drawn into the laser melting zone more readily, while larger particles remain in the powder batch for future builds, resulting in an increase in the mean particle size. This reduction in the quantity of smaller particles should result in an increase in the flowability of the powder as the Van der Waals forces are decreased.

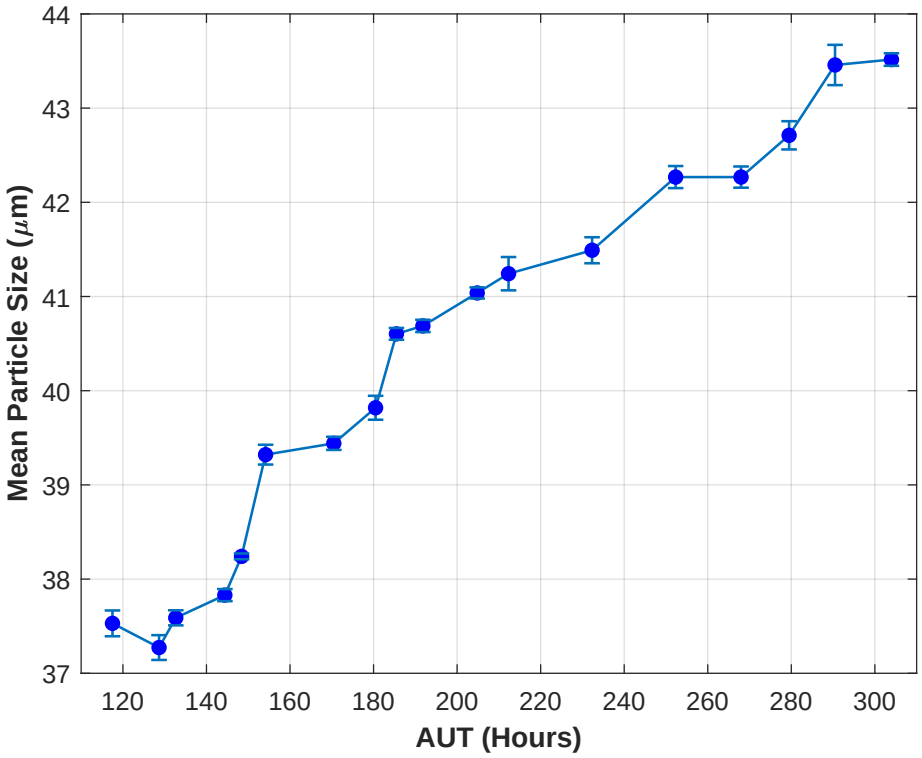

FIGURE 6.9: The effect of the *AUT* (powder rejuvenation) on the mean powder particle size.

6.2.2.4 Powder Morphology

The effect of increasing the *AUT* for the rejuvenated powder on the morphology of the powder particles is shown in Figure 6.10. The results show a deterioration in the powder particle morphology with respect to the *AUT* as shown by a decrease in the circularity of powder particles. This is as a result of the increase in the number of agglomerated particles present within the batch due to the increased powder use. Examples of these agglomerated particles can be seen in Figure 6.11. As the rejuvenated powder was used repeatedly the larger and smaller particles agglomerate forming these highly irregular shaped particles. These particles have a low circularity value which results in the decreasing circularity shown in Figure 6.10.

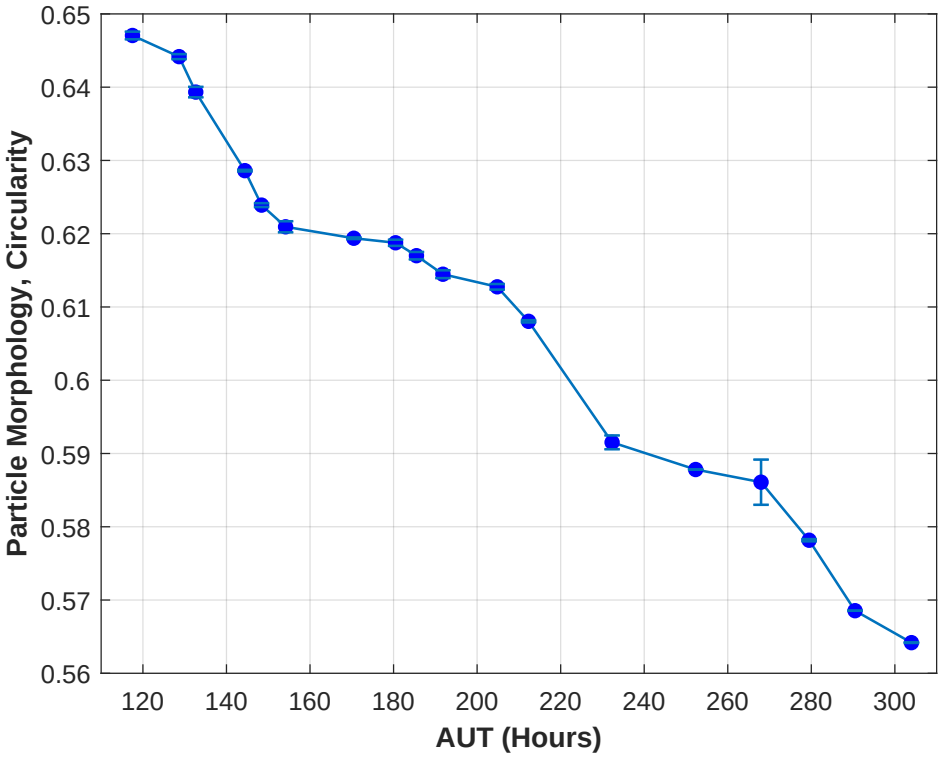

FIGURE 6.10: The effect of the *AUT* on the circularity of the powder particles.

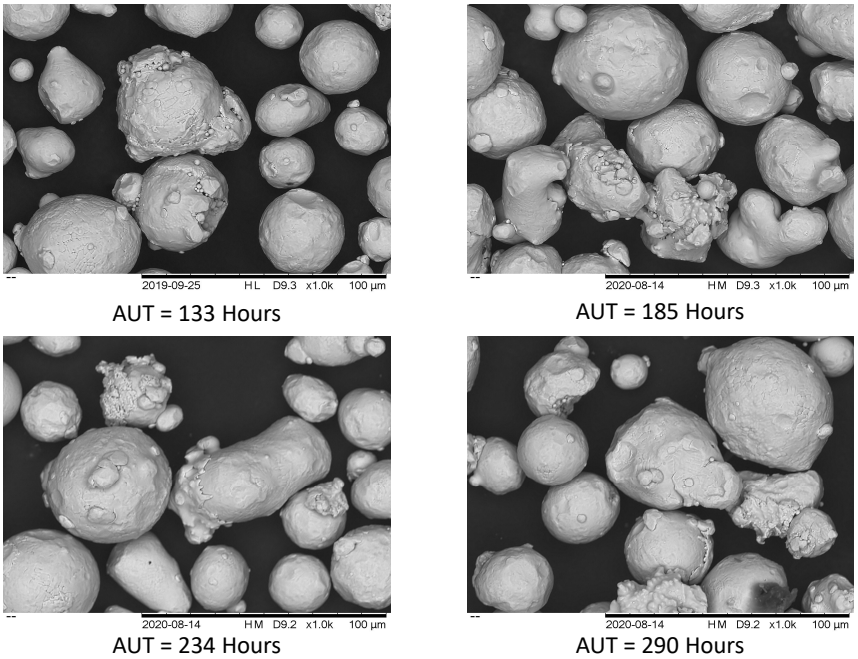

FIGURE 6.11: Examples of agglomerated and irregular shaped powder particles found in the rejuvenated powder at different stages of the study.

6.2.2.5 Powder Density

As with the powder recycling study the apparent and tapped density of the powder affects how the powder bed is produced. Figure 6.12 shows both the apparent and tapped density of the powder increased as the build time, powder recycling, increases. The increase in density is explained by the continued reduction in the number of smaller particles present in powder batches as shown in Figure 6.9. The apparent density is the density of the powder un-compacted and the tapped density is the density of the of the compacted powder, both of which provide an indication of how the powder bed is produced and how the powder will behave in a flowing state.

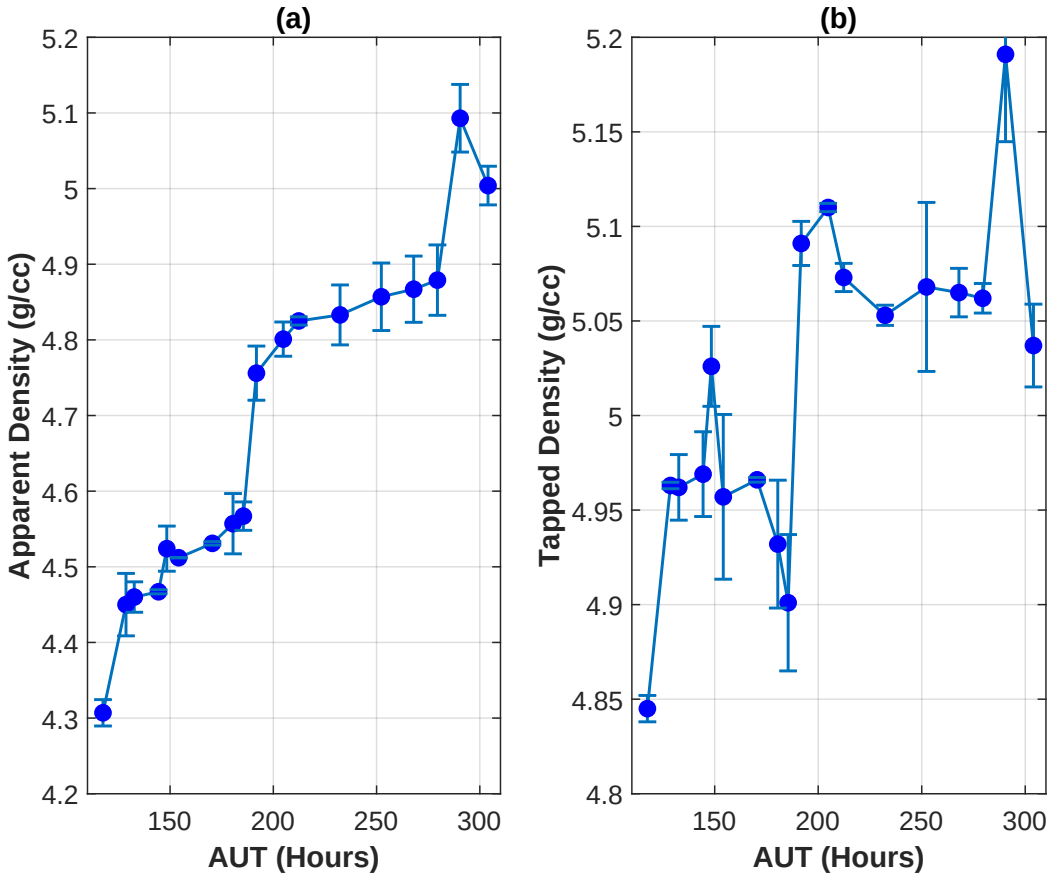

FIGURE 6.12: The effect of the *AUT* on both the (a) apparent density and (b) tapped density of the powder.

6.2.2.6 Powder Skeletal Density

This increase in agglomerated particles leads to an increase in intra-particle porosity, i.e. porosity which is internal to the powder particles. This can contribute to a decrease in the final part density produced. Figure 6.13 shows the skeletal density of the powder material; the skeletal density of the powder

remained consistent across the duration of the rejuvenation study. This result shows that the intra-particle porosity does not increase as the powder is reused, despite the clear increase in the quantity of irregularly shaped and fractured particles, as demonstrated in Figure 6.11. The consistent skeletal density across the powder samples shows that despite the particles displaying a more irregular shape there is still no porosity within the individual particles.

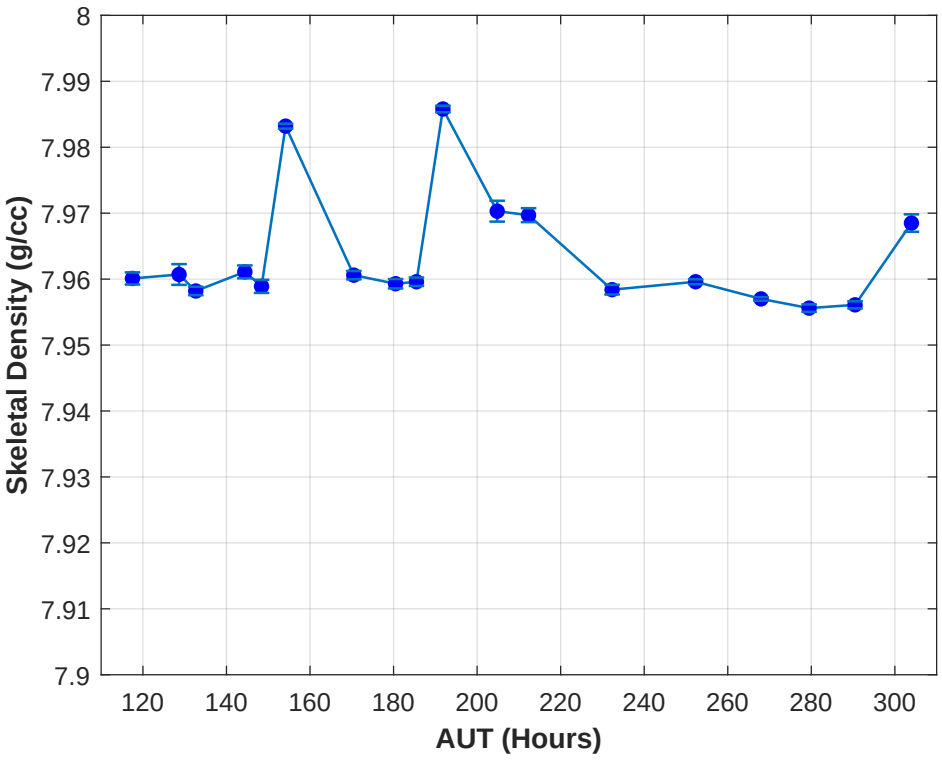

FIGURE 6.13: The effect of the *AUT* on the skeletal density of the powder.

6.2.2.7 Powder Flowability

Figure 6.14 shows the effect of the *AUT* on the Hausner ratio of the rejuvenated powder. The Hausner Ratio is used to indicate the flowability of the powder. This characteristic is affected by the particle size and shape. Therefore, it was expected that there would be a change in the flow behaviour of the powder due to a reduction in the powder particles circularity (see Figure 6.10) and an increase in the mean particle size (see Figure 6.9). As expected Figure 6.14 shows a decrease in the Hausner Ratio measured, therefore, the powders ability to flow increases as the *AUT* increases. The increased flowability of the powder can result in negative effects on the quality of the manufactured parts. Highly-flowable powders with very minor resistance to flow (HR = 1) can result in poor powder layers being deposited and, therefore, lead to a decrease in the density of the manufactured parts (Zielinski et al., 2017). Some ability of the powder to resist flow is an

important feature in the consistent deposition, and generation of a dense powder layer within the L-PBF process. This will ensure consistent and repeatable laser melting.

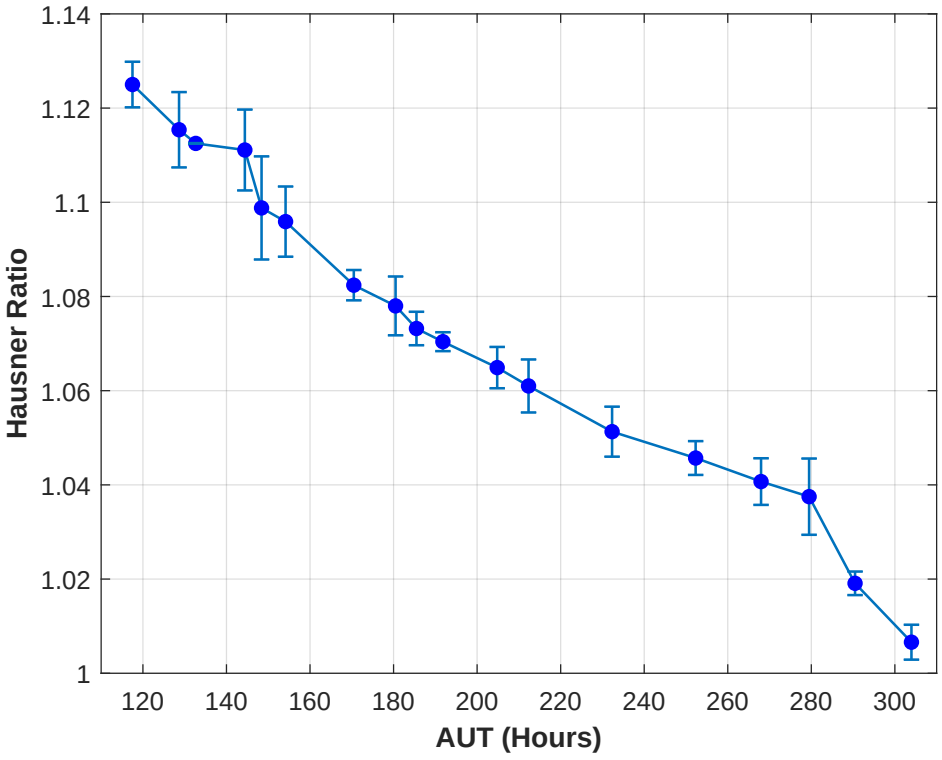

FIGURE 6.14: The effect of the *AUT* on the flowability, as indicated by the Hausner Ratio of the powder.

6.2.3 Effect of the use of rejuvenated powder on the part properties

The properties of the parts produced by the L-PBF process are greatly influenced by the characteristics of the feedstock powder material for each build. With an understanding of how the powder characteristics change after multiple uses, shown in the previous section, it is important to assess the potential effects on the parts produced.

6.2.3.1 Dimensional Accuracy

The effect of the increasing average use time (*AUT*) on the dimensional accuracy is shown in Figure 6.15. The results showed an increasing deviation from the designed dimension over the increasing *AUT* of the rejuvenated powder batch. This indicates that the recycled process of this powder batch had a negative effect on the dimensional accuracy of the manufactured parts. The measured change in the dimensions can be attributed to the increase in the mean particle size. Similar

results were also found by Cooke and Slotwinski, 2012. This increase in the deviation of the dimensions of the manufactured parts results in the requirement for increased post-processing such as machining, to achieve the dimensional accuracy that may be required in the final part.

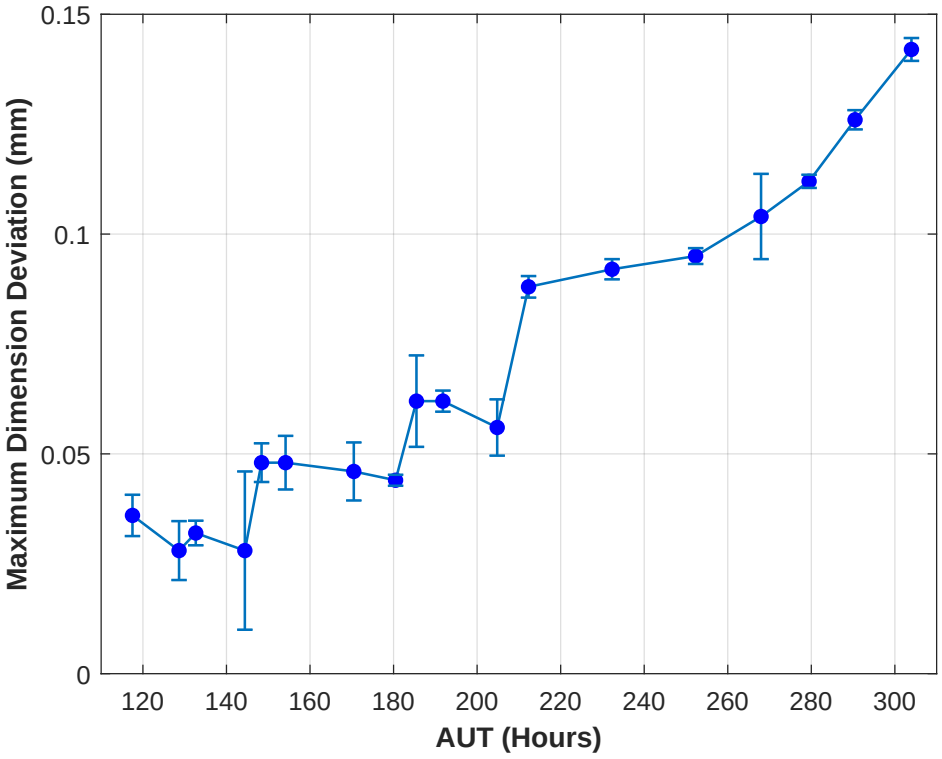

FIGURE 6.15: Effect of *AUT* of the rejuvenated powder batch on the resulting dimensional accuracy of the as-built parts.

6.2.3.2 Surface Roughness

Figure 6.16 shows the measured surface roughness of the samples manufactured as the powder batch was used, increasing *AUT*. This shows the increase in the Ra value of the measured surfaces which in turn depicts a deterioration of the surface finish of the samples, in the as manufactured state, as the rejuvenated powder batch is used repeatedly. This increase in the surface roughness of L-PBF manufactured parts is attributed to the increase in the mean particle size of the powder batch. This relationship is explored in detail in a later section of this chapter.

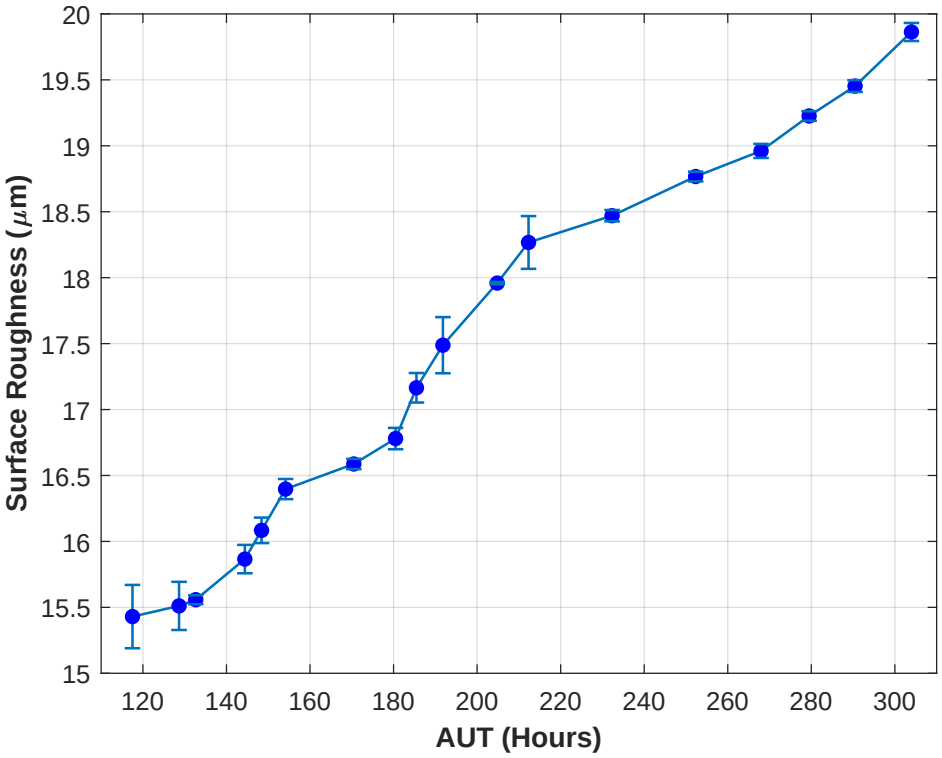

FIGURE 6.16: Effect of *AUT* of the rejuvenated powder batch on the resulting surface roughness of the as-built parts.

6.2.3.3 Hardness

The stated hardness of the 316L material is 89 HRB, as per the material data sheet (EOS GmbH, 2014). Figure 6.17 shows the hardness of the samples manufactured. The results show that the average hardness of the samples remained constant at 89 HRB $\pm$2 HRB as the rejuvenated powder use increases. This highlights that, despite the changes in the powder characteristics shown in the previous section, there was no observed effect on the part hardness. A negative change in the measured part hardness would suggest that this powder rejuvenation and subsequent recycling process has an effect on the mechanical properties of the as-built parts.

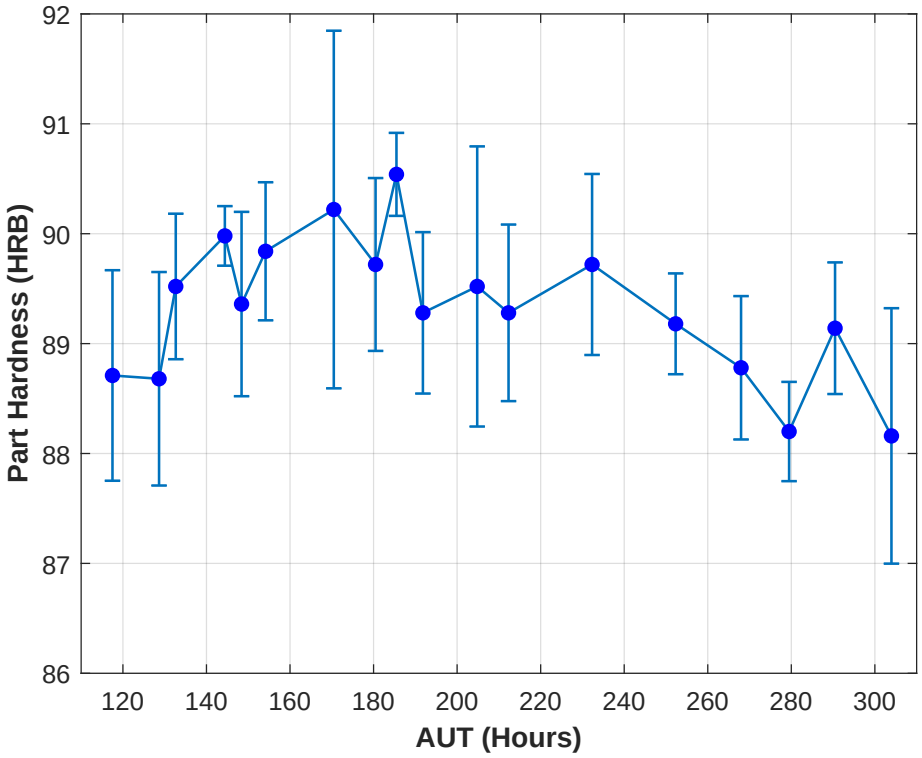

FIGURE 6.17: Effect of *AUT* of the rejuvenated powder batch on the resulting part hardness of the as-built parts.

6.2.3.4 Part Density

The effect of *AUT* of the rejuvenated powder on the manufactured part density is shown Figure 6.18. The part density decreased as the *AUT* of the rejuvenated powder batch increases. This decrease in the density is caused by the increase in the quantity and size of the pores observed in the micro-sections of the manufactured samples. This decrease in density, shown in Figure 6.18, can also be related to the changes observed in the mean particle size of the powder due to the rejuvenation and recycling process. Larger particle sizes result in less dense manufactured parts (Spierings, Herres, and Levy, 2011), with the presence of smaller particles benefiting the resulting part density (Sukal, Palousek, and Koutny, 2018). This relationship is explored in detail in a later section of this chapter.

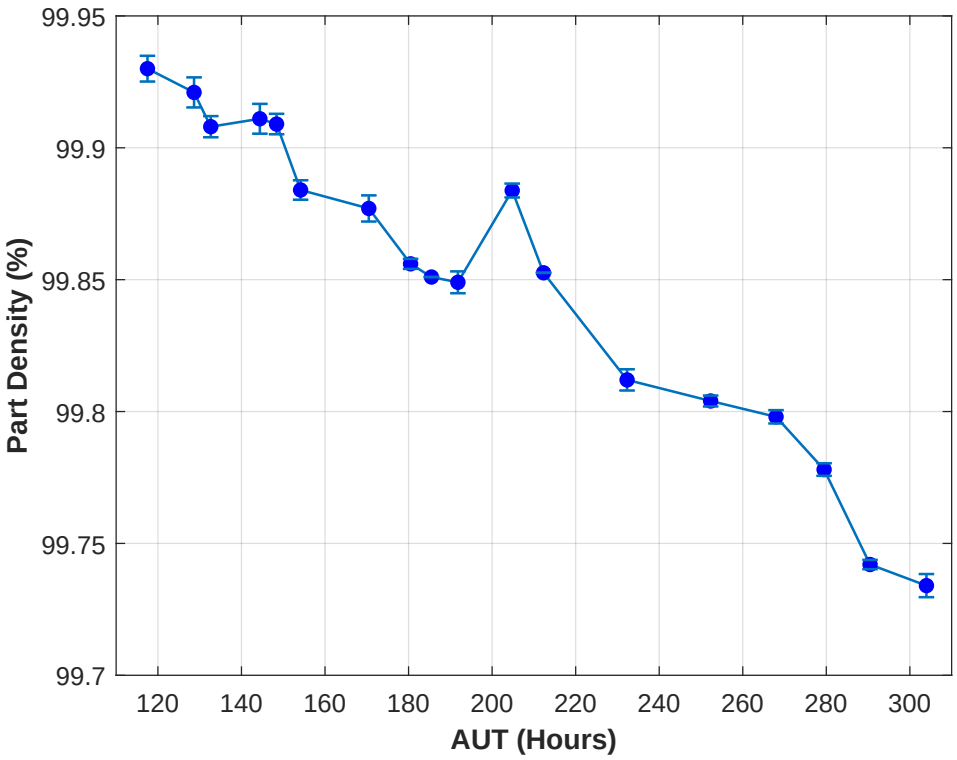

FIGURE 6.18: Effect of *AUT* of the rejuvenated powder batch on the resulting part density of the as-built parts.

6.2.3.5 Part Phase Characteristics

Figure 6.19 presents the optical microscopy (OM) images of the phase characteristics of the manufactured parts as a result of the increasing *AUT*. These OM images show the expected microstructures for L-PBF 316L in four as-built parts in the Z direction. The melt pools formed in the laser processing of the powder material, with clear melt pool boundaries visible between layers as well as adjacent laser melt tracks can be seen in the OM images presented.

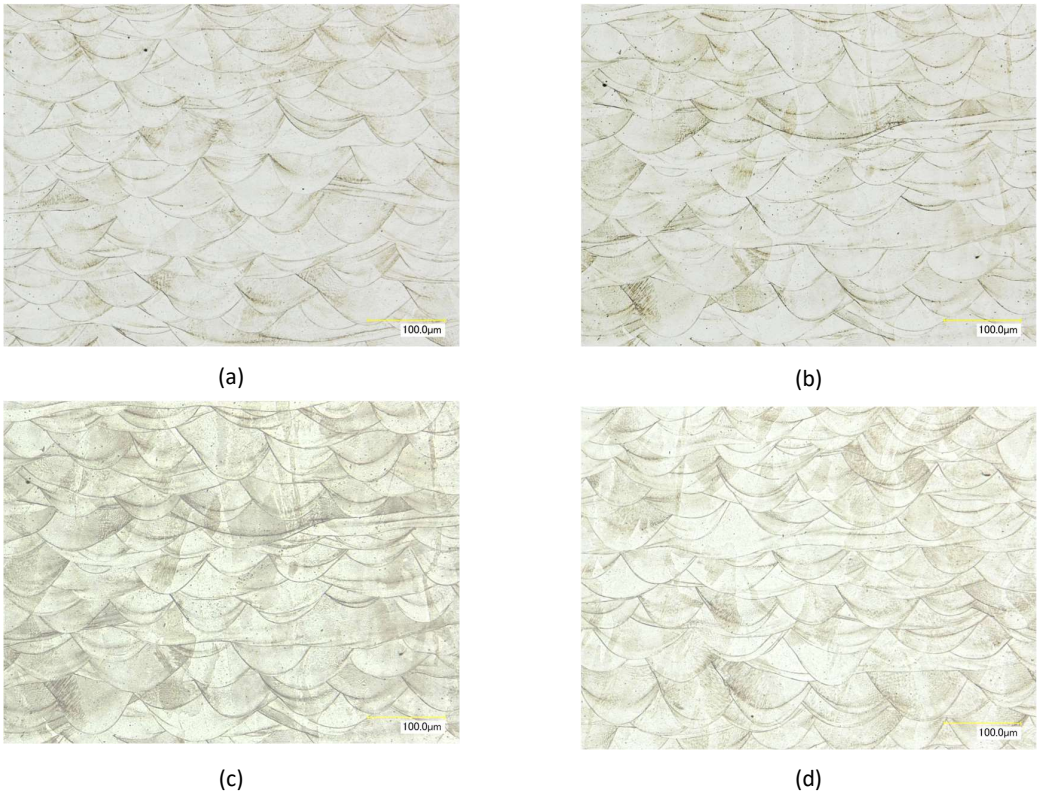

FIGURE 6.19: OM Images (magnification x500) of the etched microstructure to demonstrate the melt pools boundaries formed at different AUTs (a) AUT = 128.7 hours, (b) AUT = 180.5 hours, (c) AUT = 232.3 hours and (d) AUT = 304 hours

Further SEM imaging of the etched microstructures, shown in Figure 6.20, highlight the single-phase microstructure present within the melt pool of the samples. There is a presence of columnar grains within the melt pool with a transition to cellular grains, shown closer to the melt pool boundaries in the heat affected zone (HAZ). The samples all contain coarse columnar grains, which are regarded as consisting of single-phase sub-grains. These columnar grains have some crystallographic orientation within the melt pools as highlighted in Figure 6.21. Similar findings of these grain orientations were found for all analysed samples.

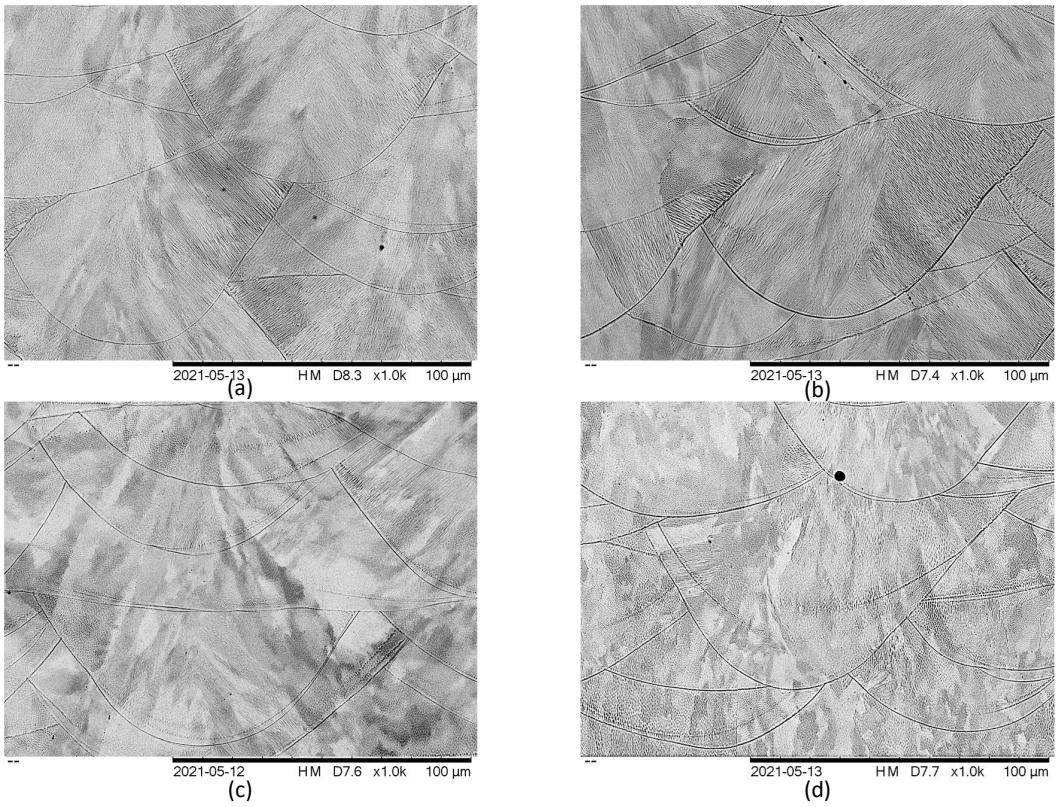

FIGURE 6.20: Figure 27: SEM Images (magnification x1000) of the etched microstructure at different AUT's (a) AUT = 128.7 hours, (b) AUT = 180.5 hours, (c) AUT = 232.3 hours and (d) AUT = 304 hours.

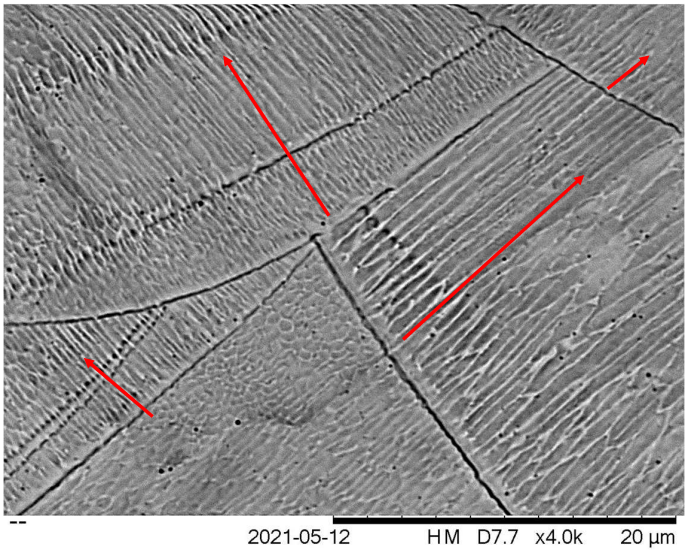

FIGURE 6.21: SEM Image (x4000) of the grain structure and orientation of the coarse grains present within the microstructure.

The microstructural analysis conducted confirms that the increasing *AUT* of the powder material does not have a significant effect on the microstructure of the

manufactured samples. As shown by the XRD analysis in Figure 6.8, despite the increasing *AUT* of the powder, the material maintains a single austenite phase throughout the rejuvenation process and this remains constant in the manufactured samples.

6.2.4 Influence of powder characteristics on the part properties

It is well understood that the characteristics of the raw powder material influence the resulting manufactured part properties (Sutton et al., 2016a; Sartin et al., 2017). As shown in the results section above and the previous chapter the changes in the powder characteristics due to the average use time or the accumulated build time effect the as built part properties. In order to understand the effects of each of the powder characteristics on the part properties, Surface Roughness and Part Density, a main effects plot was generated to study which of the powder characteristics contribute the most to the changes observed in these part properties, shown in Figure 6.16 and Figure 6.18. Main effects plots for all of the powder characteristics against the Surface Roughness and part Density were generated in order to screen the powder characteristics influencing the two part properties. Table 6.5 shows the factors, powder characteristics, and responses, part properties, used to generate the main effects shown in Figure 6.22.

TABLE 6.5: Main Effect Plots : Factors and Responses

Factors	**Responses**
Mean Particle Size	Surface Roughness
Powder Morphology	Part Density
Powder Skeletal Density	

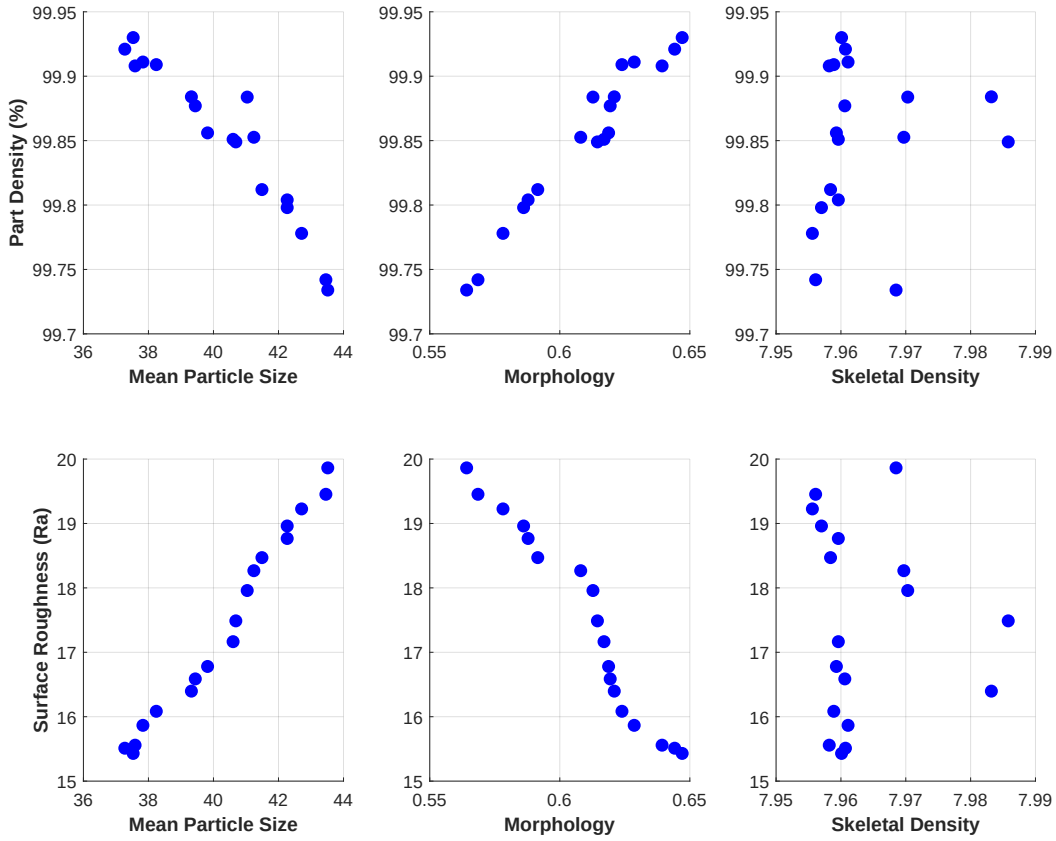

FIGURE 6.22: Main Effects plot between the powder characteristics and part qualities as outlined in Table 6.5

As we can see from the above the mean particle size and morphology are the dominant powder characteristics in contributing to the change in the surface roughness and part density. As the mean particle size is the more accessible characteristics of these two powder characteristics, in terms of the ease of quantifying it, the relationships produced as a result of the interaction between the mean particle size and part qualities are explored in the following sections.

6.2.4.1 Surface Roughness

The increase in surface roughness as depicted by Figure 6.16 can be correlated with the increase in the mean particle size as the rejuvenated powder is used repeatedly. This relationship is presented in Figure 6.23. There is a strong correlation, R^2 = 0.976, between the change in the mean particle size of the powder and the resulting part surface roughness. The surface roughness of L-PBF manufactured parts is influenced by large powder particles present in the powder batch. These larger particles are melted to the surface of the parts resulting in this increased surface roughness.

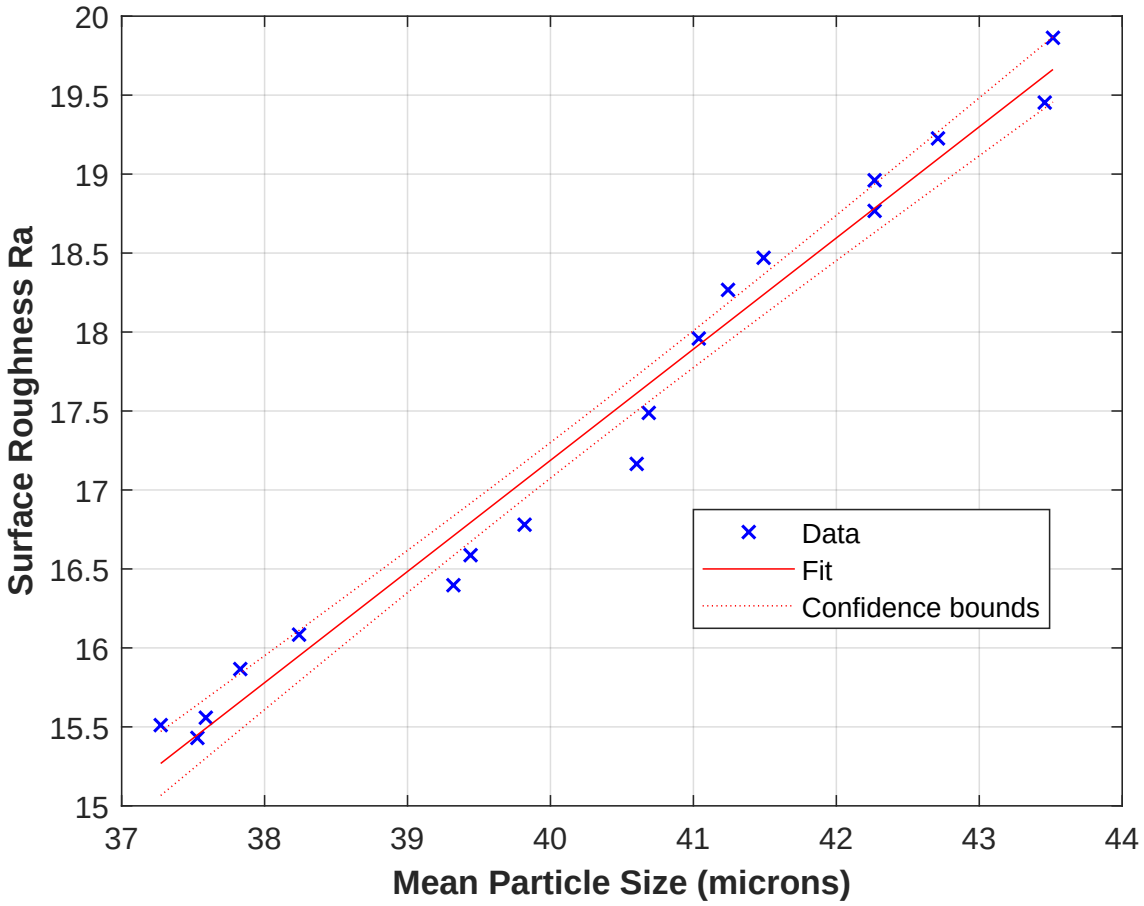

FIGURE 6.23: Relationship between the mean particle size of the powder and the surface roughness of the part.

6.2.4.2 Part Density

The decrease in density, shown in Figure 6.18, can be related to the changes observed in the powder characteristics due to the rejuvenation and recycling process. There is a strong linear relationship, $R^2 = 0.963$, between the increase in the mean particle size and the decrease in the part density measured. This relationship is shown in Figure 6.24 below. This increase in the particle size affects the density of the powder bed that is deposited in the L-PBF process and thus effecting the resulting part density. A larger mean particle size results in a reduction in the quantity of smaller particles present in the powder batch. These smaller particles, while having a negative effect on the flowability of the powder, improve the packing of the powder material. Smaller particles orientate themselves within the spaces and gaps between the larger size particles producing a highly packed powder bed resulting in more dense manufactured parts. The reduction of part density observed in Figure 6.18 can be attributed to the increase in the mean particle size of the powder batch, shown in Figure 6.9.

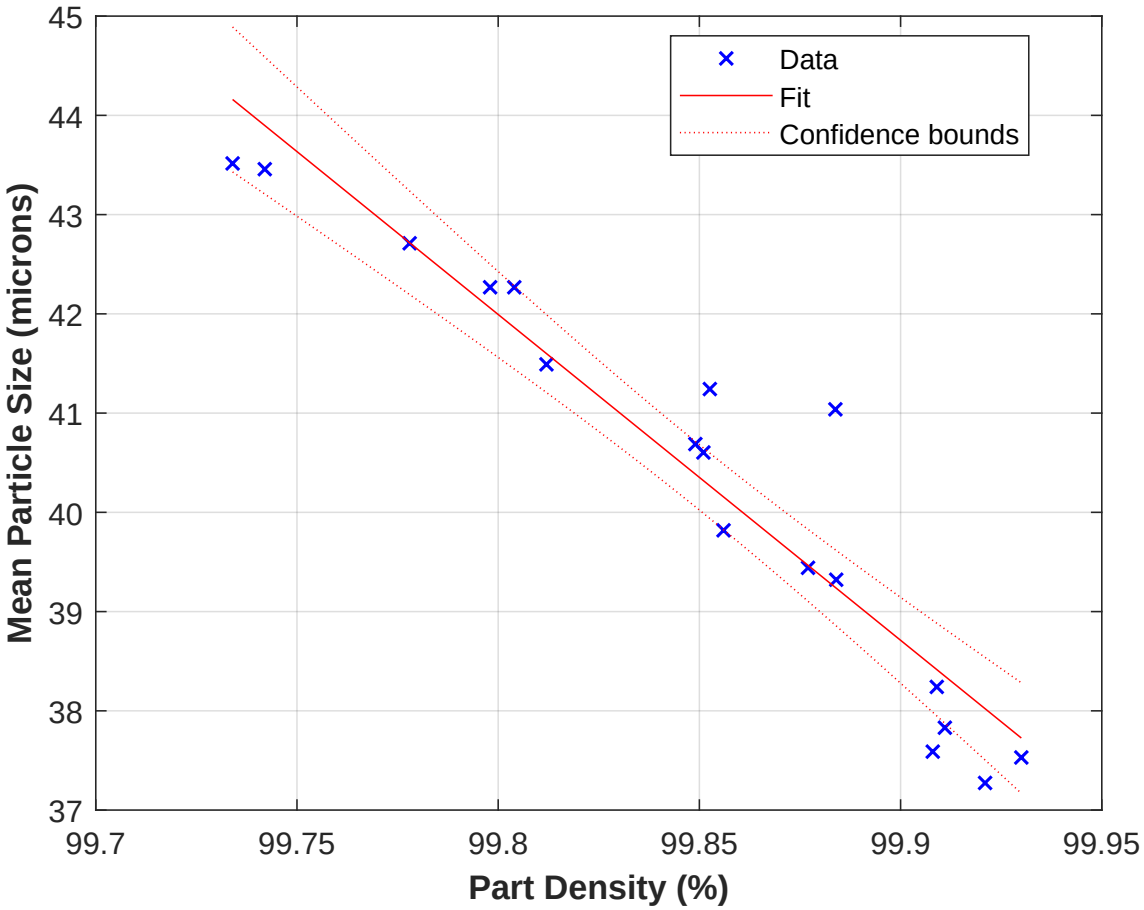

FIGURE 6.24: Relationship between the mean powder particle size and the manufactured part density.

6.3 Conclusions

The data presented in this chapter illustrates the impact of a "top-up" powder rejuvenation process applied to 316L stainless steel material in laser powder bed fusion. An initial study to determine the effect of mixing recycled and virgin powder material at different ratios led to a 50:50 powder mixing ratio. This regime was implemented for a total of 17 builds accounting for over 300 build hours. The effects of average use time, *AUT* on the powder characteristics and on the additively manufactured part characteristics were investigated. Key conclusions from this chapter are as follows:

- The mixing ratio of recycled powder material to virgin powder material determines the resulting powder batch properties, which are a function of the characteristics of both the recycled and virgin powder batches. It was found that as the proportion of virgin powder increased, the mean particle size decreased, the morphology of the powder batch became more circular and the flowability decreased. It was found that an ideal mixing proportion increased the quantity of material available for manufacturing while also restoring the powder characterises similar to the initial virgin powder properties.

- As the rejuvenated powder was used, the powder characteristics deteriorated in terms of size and shape of the particles. Mean particle size increased and the particles became less circular caused by an increased quantity of agglomerates and fractured particles within the powder batch. These were a result of the increased *AUT*. This resulted in improved powder flowability with increased powder use in the AM process.
- The changes observed in the powder characteristics, due to powder reuse, negatively influenced the manufactured part properties. This was observed as a decrease in the dimensional accuracy of the manufactured parts, with increased surface roughness and internal porosity. It was found that the dominant powder characteristic contributing to these measured changes in the surface roughness and the part density was the mean particle size.
- There was no significant change detected in the microstructure of the powder material as the powder was re-used. This, in turn, did not affect the microstructure of the as-built parts. As expected, γ FCC austenitic phases were found in both the powder material and manufactured samples at different stages of the recycling and rejuvenation process.
- The powder rejuvenation process is a viable solution to increase utilisation of a powder material for laser powder bed fusion. While there are observed changes in both the powder material as well as the manufactured part properties, with knowledge of these changes a successful rejuvenation process can be applied to increase raw material utilisation and reduce the wastage of the un-melted powder material.

7 Empirical Relation Development

Powder recycling and further rejuvenation has been shown in the previous chapters to extend the usable life of a powder material within the L-PBF process. These processes however, do impact the output part properties as shown. The aim of this chapter is to build a series of empirical models that can be used to predict the resulting part density and surface roughness from the input powder properties. This chapter begins with an outline of context in which the development of predictive models can be justified. It then applies the multiple linear regression method outlined in Chapter 4, using average use time, mean particle size, circularity and skeletal density. It then describes the development of part density and surface roughness models and closes with an evaluation of the developed models. The models enable the L-PBF user to input known powder characteristics and to calculate an expected part density and surface roughness.

7.1 Background

Like many manufacturing processes, the L-PBF process is highly dependent on a range of different input factors. This combination of varying input factors and the characteristics of the L-PBF process itself affects the resulting output properties. The input factors for the L-PBF process include but are not limited to the following:

- Input powder properties such as composition, particle size, and powder density.
- Laser processing parameters such as laser power, scan speed and spot size.
- Processing conditions such as inert processing gas, chamber temperature and oxygen content
- CAD geometries such as overhang features, lattice structures and thin walls.

Varying any of the above factors can impact the resulting output from the L-PBF process. These may include but are not limited to the following (Bian, Thompson, and Shamsaei, 2015) :

- Mechanical properties
- Chemical composition
- Micro-structural properties
- Surface properties

This research is an evaluation of the impact of recycled and rejuvenated metal powders on the resulting part properties. Figure 7.1 conveys a simplified Input-Process-Output diagram for the L-PBF process identifying some of the potential input metal powder characteristics. The diagram combined with the results presented in the previous chapters illustrates the relationships between the various elements in the L-PBF process, and specifies some of the key input and output properties. The knowledge of these interactions can be utilised to develop prediction tools for the outcome of the L-PBF process.

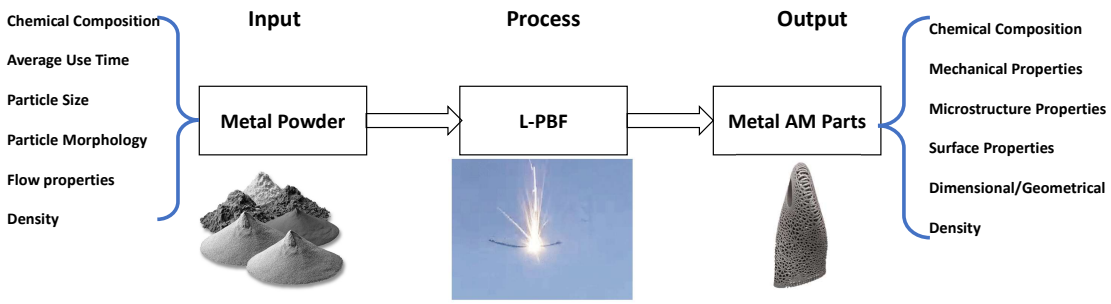

FIGURE 7.1: Input-Process-Output diagram for the L-PBF process.

In this chapter, the development of two empirical relationships, is described based on the data collected from in the powder recycling and rejuvenation studies. These models take the characteristics of the input powder material and enable the prediction of the resulting part density and surface roughness. These models can be used as an indication into the expected part density and surface roughness for a given powder batch.

7.2 Model Selection

The developed models are multiple linear regression models generated using Minitab Statistical Software. This method is described in detail in Chapter 4. The first step of the development of the empirical models was to assess the range of variables that may influence the Part Density and Surface Roughness. This was completed through the use of an exploration matrix plot. The dependant properties were chosen as they were shown in Chapter 5 and Chapter 6 to have had the strongest relationship with the evolving powder characteristics. The exploration plot was used to determine the strengths of the relationships between the part density and surface roughness and the powder characteristics. The powder characteristics that were used in this study are as follows:

- Average Use Time *(AUT)* - A description of the amount of time the powder has been used within the AM process. (See description of *AUT* in Chapter 4)
- Mean Particle Size (MPS) - The mean particle size present within the powder batch.

- Particle Circularity - The average circularity of the particles within the powder batch.
- Skeletal Density - The density of a sample of powder consolidated to represent the final part density, skeletal density can identify porosity within powder particles which can translate to porosity in the as-built part.

Other powder characteristics that are presented in this thesis were omitted from the model development process as they are characteristics that are derived from the above powder characteristics. The strength of the relationship between the dependent variable, part density and the independent variable was determined by a series of scatter plots. These are seen in Figure 7.2 below the absolute Pearsons correlation coefficient is also displayed on each of the graphs. This value will indicate the strength of the relationship between the plotted variables. The higher the Pearson correlation coefficient value, i.e. closer to 1, the stronger the relationship is between the plotted variables.

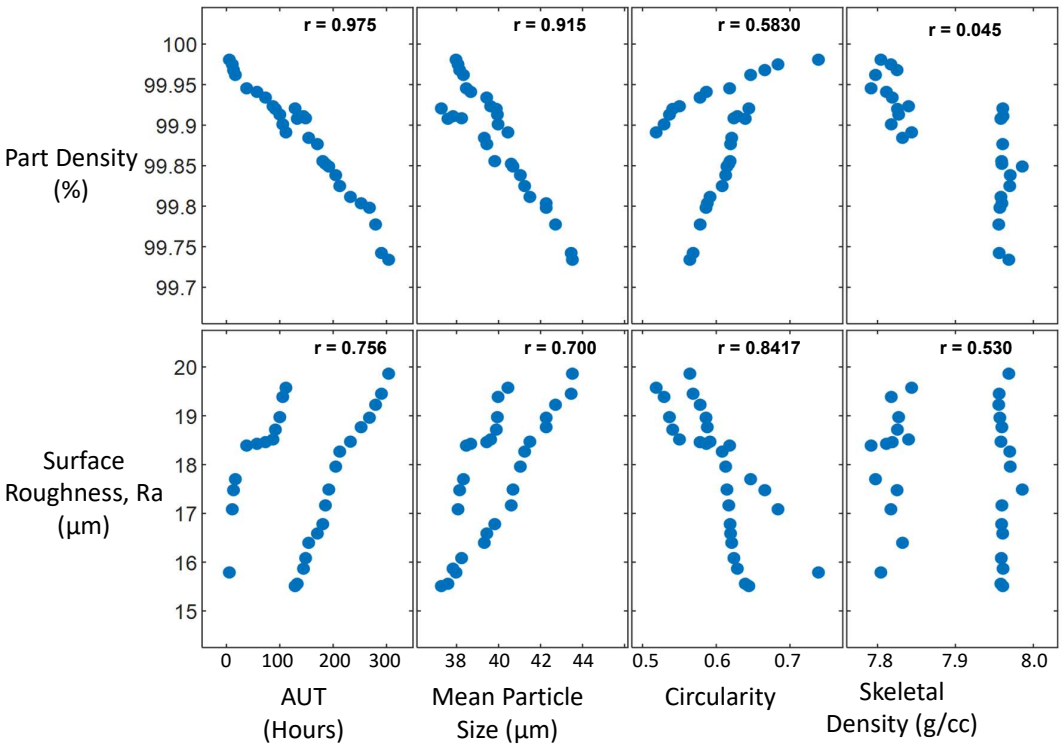

FIGURE 7.2: Matrix plot of powder characteristics and part properties.

From the above matrix plot of the most influential powder characteristics for each of the dependent variables of Part Density and Surface Roughness can be identified and used to predict the as-built part properties. A summary of the most influential powder characteristics for the built part properties are detailed in Table 7.1 below.

TABLE 7.1: Summary of Interactions

Part Property	Powder Characteristics	Correlation Coefficient
Part Density	Average Use Time	0.975
	Mean Particle Size	0.915
Surface Roughness	Average Use Time	0.756
	Mean Particle Size	0.700
	Circularity	0.841

The aim of the matrix plot in Figure 7.2 was to eliminate those powder properties that do not highly correlate with the as-built part properties. With that objective in mind the impact of each of those identified powder characteristics in the empirical model are investigated in the following sections. With the information from the correlation coefficients as well as the matrix plot the multiple linear regression models for part density and surface roughness can be developed and verified.

7.2.1 Part Density Model

This section presents, evaluates and confirms the accuracy of an empirical model that can be used to provide an indication as to the expected part density from a given batch of powder. The model is based on the results that are presented in Table 7.1. The *AUT* of the powder batch and the mean particle size (MPS) of the powder correlated strongly with the Part Density. The model was generated using Minitab multiple linear regression (MLR) model function to provide the following equation.

$$PartDensity = \beta_0 - \beta_1 AUT - \beta_2 MPS \tag{7.1}$$

Where the *y*- intercept term $\beta_0 = 100.466$, and the slope coefficients for the variables AUT, β_1, and Mean Particle Size, β_2, are 0.000526 and 0.01276 respectively. The resulting model is as follows:

$$PartDensity = 100.466 - 0.000526 AUT - 0.01276 MPS \tag{7.2}$$

In order to assess if the inferences that were drawn from Figure 7.2 and Table 7.1 are correct the variables need to be assessed in terms of the significance to the model. These statistics are shown in Table 7.2. The coefficient of determination (R-Squared) is a metric that is also used to explain the variation of in the independent variables (Powder Characteristics). The higher the R-squared value for the model the more of the change in part density can be explained by the model. The p-value was the test statistic, used to assess if the inclusion of the powder characteristics in the model are statistically significant. In order for the inclusion to be considered statistically significant the p-value for the powder characteristics is required to be less than 0.05. The final metric that was used to

confirm the significance of the developed model is to assess the Variance Inflation Factor (VIF). This is a measure of the multicollinearity of the variables in the model (See Chapter 4 for more detail). A high, greater than four, VIF value would indicate that the variables are highly collinear, meaning that the model inputs are interacting with one another.

TABLE 7.2: Part Density Model Summary Statistics

Source	R-Squared	P-Value	VIF
Model	98.79%	0.00	-
AUT		0.00	2.6
Mean Particle Size		0.00	2.6

From the statistics that are displayed in Table 7.2 the significance of the model can be determined. The R-Squared for the model is high, highlighting that the model is significant and that the observed variation in the part density can be explained by the model developed. The p-values also show that the inclusion of the *AUT* and Mean Particle size in the model is statistically significant as the p-value is below 0.05. Finally the VIF is used to ensure that the powder characteristics do not exhibit multicollinearity. This would be shown in a VIF value of greater than 4.

The assumptions for a MLR model must be met by each model. These assumptions are described in detail in Chapter 4, and can be summarised as follows:

- Plot of the residual values vs. the fitted values for the model is normally distributed around a mean of 0.
- The residuals are normally distributed.
- Plots of the residuals against the inputs display no significant trend.
- Plots of the residuals and the powder characteristics omitted in the exploratory stage.

These plots are displayed in Figure 7.3 below which enable the model to be verified using the above assumptions. The data presented in the graphs in Figure 7.3 can be used to assess the assumptions for a MLR model. Figure 7.3 (a) shows the residual errors from the model plotted against the models fitted values. The assumption with this test is that plot displays no significant trend and that the data has a mean of approximately 0 (actual mean = 0.0006). The plot confirms that this is the case for the model developed.

Figure 7.3 (b) is a histogram plot of the models residuals. This plot confirms the assumption that a histogram of the residuals will be normally distributed, as shown by the approximate bell shape to the plot shown.

The next assumption that was tested is that the residuals from the model do not display any specific trend with the input variables to the model. It is clear from

Figure 7.3 (c) and (d) that there is no significant or clear trend when the residuals are plotted against the input variables.

The final assumption that needs to be tested for the MLR model is the assumption that there are no clear trends with the residuals and the variables that were omitted in the initial exploration stage. These plots are shown in Figure 7.3 (e) and (f) and it is clear that there is no trend displayed in the data. With the graphs displayed in Figure 7.3 confirm that the developed MLR model meets the assumptions required for a MLR model.

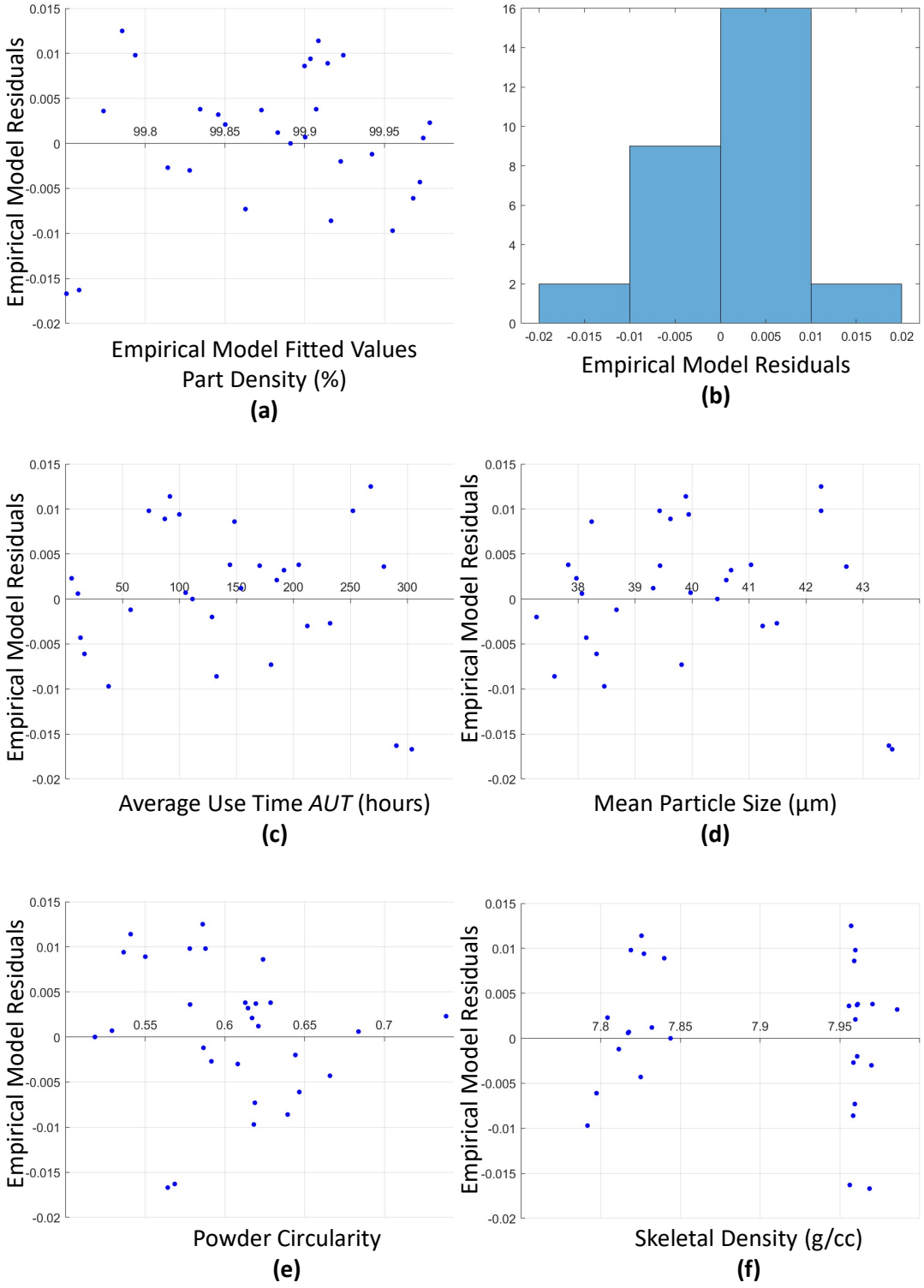

FIGURE 7.3: Part Density Multiple Linear Regression Assumption Tests.

With the assumptions of MLR models met by the developed model, Equation 7.2, the predicted values can be plotted against the observed part density. Figure

7.4 presents the fitted values which are calculated from Equation 7.2 and the observed data from the powder recycling and rejuvenation study.

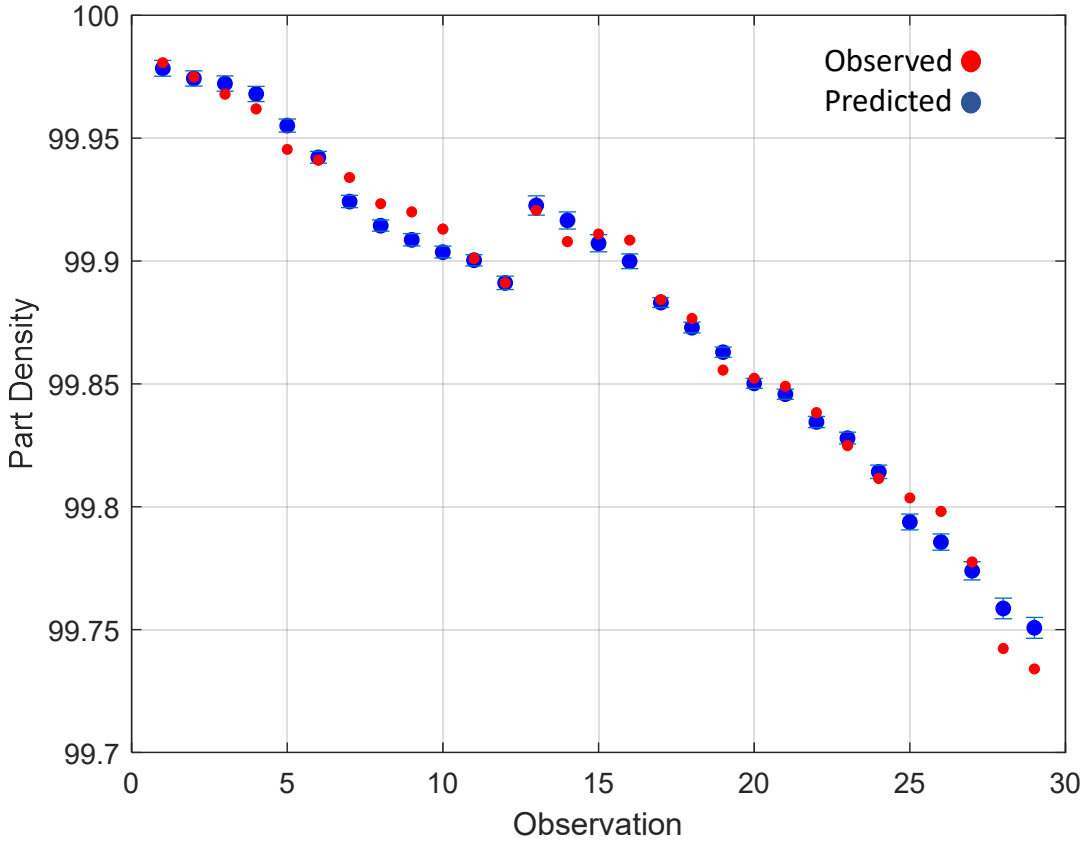

FIGURE 7.4: Part Density Model Fitted values and Observed Values.

It is evident from Figure 7.4 above that the fitted values that are calculated by the developed model shown in Equation 7.2 is capable of predicting the resulting part density by utilising the powder characteristics identified in Table 7.2. The developed model predicts the part density of the as built parts within an accuracy of $\pm$ 0.015 % of the observed part density.

7.2.2 Surface Roughness Model

This section presents an empirical model that can be used to provide an indications as to the expected surface roughness from a given batch of powder. The model is based on the results that are presented in Table 7.1 which show that both the *AUT* of the powder batch, the mean particle size (MPS) of the powder and the particle circularity correlated highly with the measured surface roughness.

$$SurfaceRoughness = \beta_0 - \beta_1 AUT - \beta_2 Circularity + \beta_3 MPS \tag{7.3}$$

Where the y- intercept term $\beta_0 = -7.02$, and the slope coefficients for the variables AUT, β_1, Mean Particle Size, β_2, and Particle Circularity, β_3, are 0.01274, 12.31 and 0.8537 respectively. The resulting model is as follows:

$$SurfaceRoughness = -7.02 - 0.01274AUT - 12.31Circularity + 0.8537MPS \tag{7.4}$$

The inferences that are drawn from Figure 7.2 and Table 7.1 provide the characteristics that are included in Equation 7.4. The models statistical summary is displayed in 7.3, which is used to assess if the inclusion of the selected powder characteristics contribution to the developed model is statistically significant. As previously outlined for a powder characteristic to be statistically significant in the model the p-value is required to be less than 0.05, the coefficient of determination (R-Squared) should be high and there should be minimal multicollinearity in the variables in the model as shown by a low Variance Inflation Factor (VIF). The model statistics are shown in 7.3 below.

TABLE 7.3: Surface Roughness Model Summary Statistics

Source	**R-Squared**	**P-Value**	**VIF**
Model	93.64%	0.00	0
AUT		0.00	2.61
Circularity		0.00	1.58
Mean Particle Size		0.00	3.08

The statistics presented in Table 7.3 can confirm the significance in the developed model, this is shown with the high R-Squared value of 93.64%. This means that 93.64% of the variation in the measured surface roughness can be explained by the developed model. The variables used within the model then need to be tested. The p-value and VIF value are used to assess this. For the powder characteristics used in this model, the *AUT*, Circularity and Mean Particle Size, the p-value was below 0.05 indicate that their inclusion in the developed model is statistically significant. The final test was to confirm that there is no multicollinearity between the variables. All VIF values for the powder characteristics included in the model are less than 4, confirming the initial assumption that there is no multicollinearity between the model's variables.

The next stage was to assess if the assumptions made in developing a MLR model are being met. These assumptions test are displayed in Figure 7.5 below allowing the model to be verified against the assumptions for MLR.

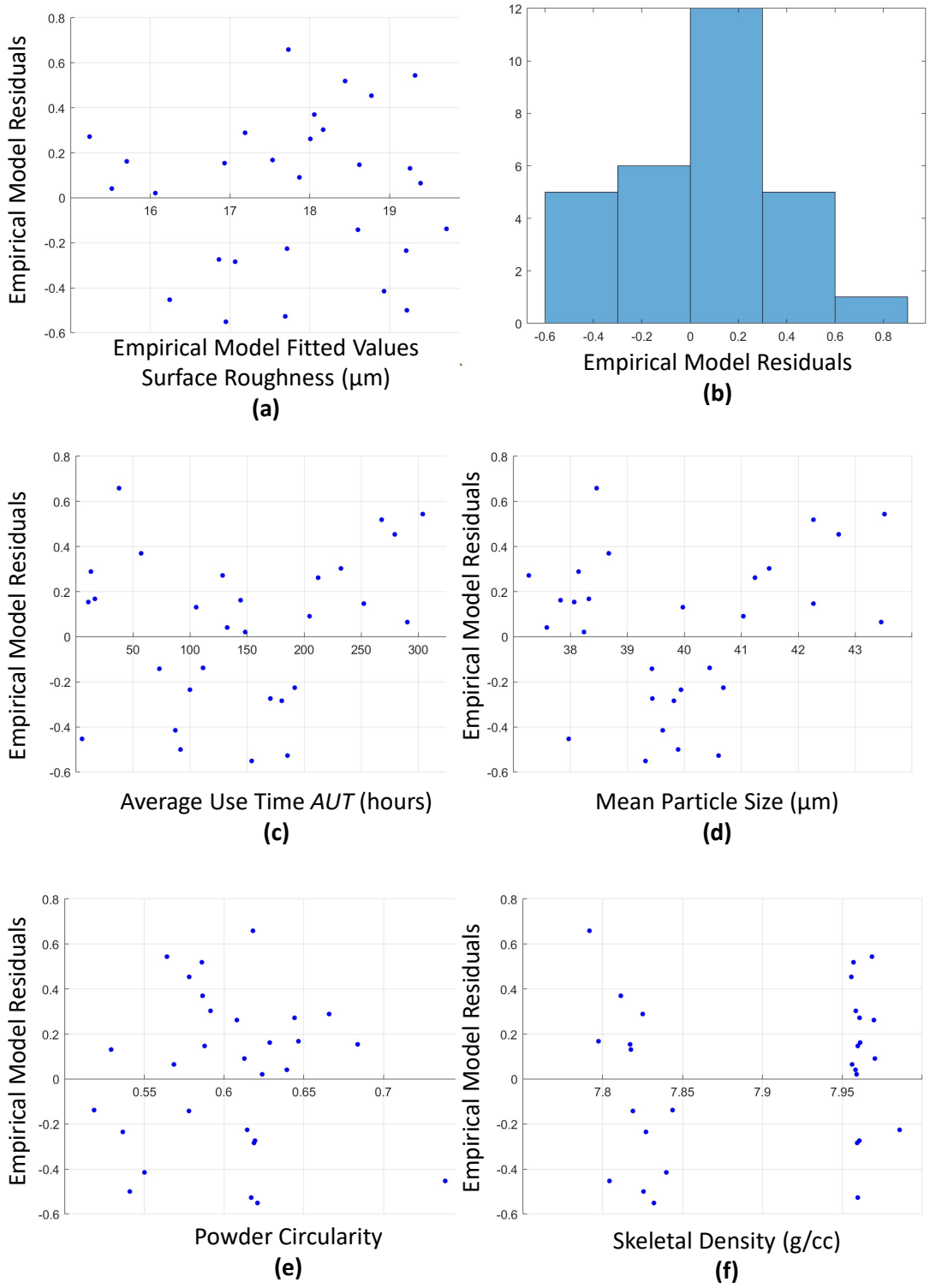

FIGURE 7.5: Surface Roughness Multiple Linear Regression Assumption Tests.

The data presented in Figure 7.5 in summary confirm that the developed model displayed in Equation 7.4. Figure 7.5 (a) displays that there was no trend between

the residual errors from the model and the fitted values, the mean of the residuals is approximately 0 (actual mean = 0.03128). Figure 7.5 (b) shows that residuals generated by the model are normally distributed confirmed by the approximate bell shaped curve generated in the histogram. Figure 7.5 (c), (d) and (e) show that there was no obvious trend between the models residuals and the input variables for the model.

Finally, Figure 7.5 (f) also show that there was no clear trend generated when the residuals from the model are plotted against the powder characteristic omitted from the model in the initial matrix plot and correlation study shown in Figure 7.2. With the assumptions of a MLR model met by the developed model the fitted surface roughness values from the model can be plotted against the observed surface roughness. The fitted values and observed surface roughness values are plotted in Figure 7.6.

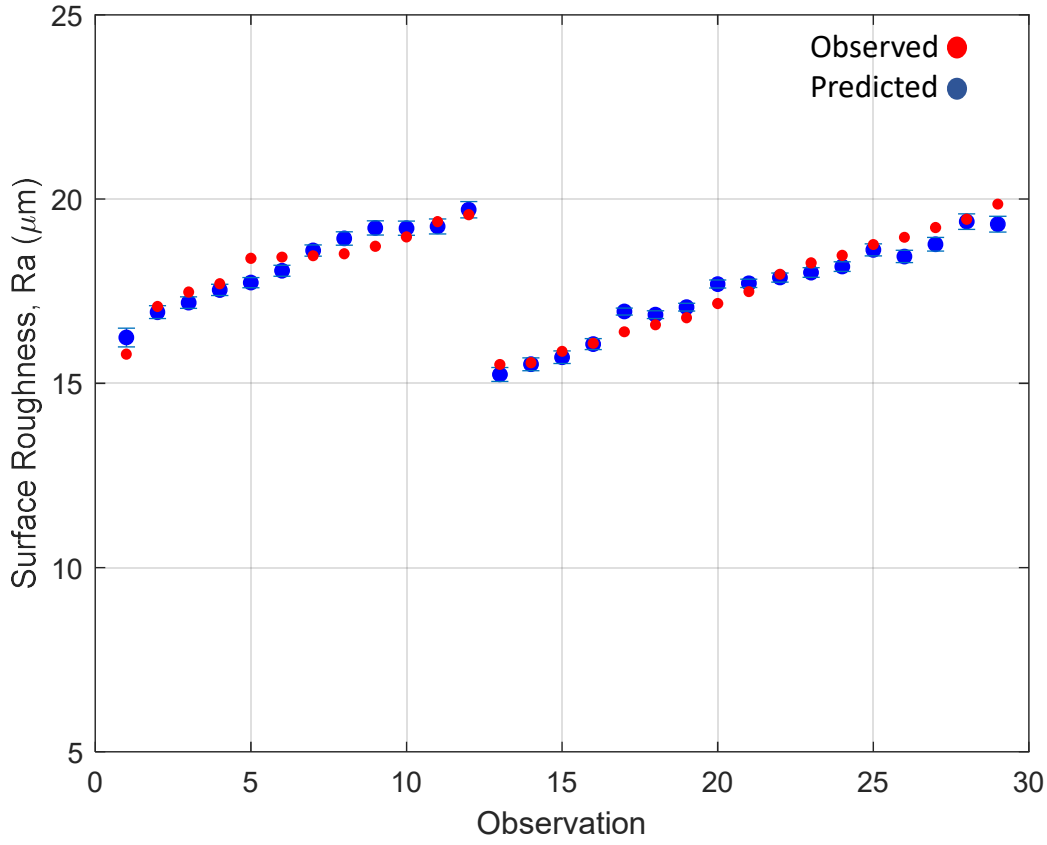

FIGURE 7.6: Surface Roughness model Fitted Values and Observed Values.

From Figure 7.6 above it is evident that the fitted values that are calculated by the developed model shown in Equation 7.4 is capable of predicting the resulting surface roughness by utilising the powder characteristics identified in Table 7.2. The developed model predicts the part density of the as-built parts within an accuracy of 0.5 μm Ra of the observed surface roughness.

7.3 Discussion

The models presented in this chapter allow for the Part Density and Surface Roughness of metal AM parts to be predicted based on the characteristics of recycled powder. To summarise, the models that have been developed are as follows:

$$PartDensity = 100.466 - 0.000526AUT - 0.01276MPS \tag{7.2}$$

$$SurfaceRoughness = -7.02 - 0.01274AUT - 12.31Circularity + 0.8537MPS \tag{7.4}$$

This chapter proposes two empirical multiple linear regression models for the prediction of the part density and surface roughness of manufactured components from the L-PBF process. The models predict the expected outcome for a 316L powder on an EOS M280 machine as the powder ages throughout the powder recycling process. The models utilise input powder characteristics including *AUT*, circularity and mean particle size, which can be determined prior to printing, to predict the manufactured part properties. A summary of the main findings are as follows:

- The initial exploration plot, Figure 7.2, with accompanying Pearson correlation coefficients confirmed that the mean particle size and *AUT* produced the strongest correlation with the observed part density. The resulting model was developed with these two input variables which met all of the requirements for an MLR model. The model shown in Equation 7.2 is capable of predicting 98.79% of the changes observed in the part density, and to within 0.02% of the observed density values.
- For the surface roughness model, Figure 7.2 illustrated that the powder *AUT*, mean particle size and circularity had the strongest linear relationships with the observed surface roughness of the L-PBF parts. The developed surface roughness model met all the requirements for an MLR model, resulting in a model that can predict 93.64% of the changes observed in the surface roughness, and to within 0.5 μm of the observed surface roughness.

These developed empirical models will enable L-PBF operators to characterise the powder material prior to a build and use these quantified characteristics to estimate the expected manufactured part properties, namely part density and surface roughness. Further work will investigate developing similar models to enable the prediction of other output properties, such as mechanical and dimensional properties. This can enable a shift towards zero-defect L-PBF manufacturing.

8 In-situ Process Monitoring

Having previously evaluated the powder recycling and rejuvenation processes, and empirically modelled the relationships between the powder characteristics and the resultant part properties, the next step is to apply these relationships to the L-PBF process. This was achieved by the development of an in-situ monitoring system that can identify defects in the powder layering process. This chapter presents the development, installation and testing of a standalone in-situ monitoring system with accompanied image analysis capabilities. The system allows for the real time standalone monitoring of the L-PBF process. The monitoring system will identify a range of defects and alert the machine operator as and when they occur. Allowing, the operator to make a judgement as to the corrective action required to minimise the effect of defects in a L-PBF build. The defects of interest all occur within the powder layering process. A series of studies are presented which show the operation of the monitoring system and its capability in identifying the desired defects.

8.1 Summary of Defects of Interest

As described earlier in Section 3.5 there are four defects of interest for this defect detection system. These all occur with the powder deposition phase of the L-PBF process and can be summarised as the following:

- Re-coater Hopping: A powder distribution defect as a result of vibration in the re-coater arm leading to ripples in the powder bed.
- Re-coater Streaking: A defect resulting typically from damage to the re-coater blade causing ridges in the powder distribution.
- Super Elevation: A defect resulting from a part protruding above the active build height.
- Incomplete Spreading: A defect resulting in insufficient powder being deposited across the build platform.

8.2 System Aims

With the constraints discussed previously in Section 4.6 in mind the aims of the in-situ defect detection system can be summarised to the following:

1. Suitable to operate in the build chamber environment of the EOS M280 with an elevated temperature, low humidity and inert atmosphere.

2. To operate in a standalone manner from the normal operation of the EOS M280.
3. Be capable of identifying the defects of interest, particularly those mentioned in Section 8.1.
4. Operate in parallel with the build process, to allow an operator to be notified of the occurrence of any defect.

8.3 Operational Workflow

The installed camera system captures two images per layer of a build. Figure 8.1 (a) shows the first captured image which is of the newly deposited powder layer. Figure 8.1 (b) shows the second image captured per layer which is an image of the build platform after laser exposure.

FIGURE 8.1: Images captured by the installed monitoring system (a) after powder deposition and (b) after laser exposure.

As previously discussed the location of the installed trigger sensors utilise the position of the re-coater arm to capture these images. The captured images are then saved to an external hard drive which is connected to the camera controller unit. The controller unit labels these images by date, time and image number. This can allow for post build validation of the images. The stored images are then passed to the developed line segment detection tool, discussed in the following section, which runs in R Statistical Software (R Development Team, 2019). This tool then conducts the line segment detection and plots the results. An additional anomaly detection tool is used to observe the detected line segments and alert the operator when an anomalous number of line segments is detected. These tools are explained in detail in the following section.

The captured images are passed through a developed image analysis code. This code has the capability of reading in the captured images from the camera and performing the required analysis. The main tools and description of how the code operates is discussed further in this section of the chapter. In order to achieve the

desired output from the monitoring system the developed code will be capable of the following:

1. Read images from camera controller.
2. Perform required image manipulation to prepare images for line segment detection.
3. Complete image analysis - Line segment detection (LSD).
4. Store and track results from the line segment detection to identify when defects have occurred.

8.3.1 Code Description

The high level description of the operation of the image analysis code is displayed in the flowchart in Figure 8.2. The descriptions shows the flow and operation of the developed code.

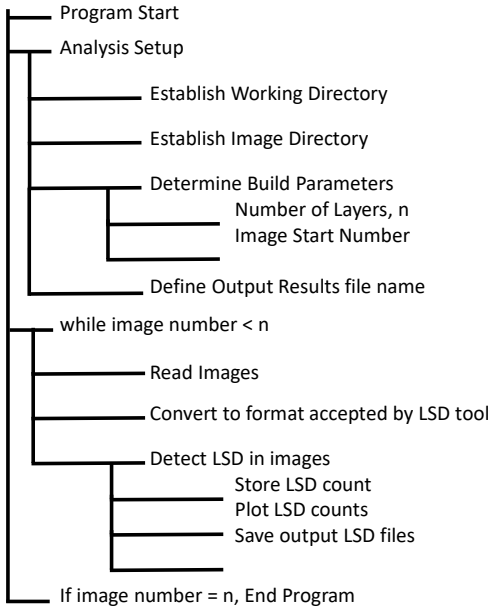

FIGURE 8.2: Pseudo code description of the defect detection code operation and flow.

A simplified version of the pseudo code description of the image analysis code is shown in Figure 8.3, this provides a high level description of the code and its functions. In order for the code to carry out the required image analysis a series of image analysis packages within R Statistical Software (R Development Team, 2019) are used. These libraries are discussed in the following paragraphs with the aim to provide an in-depth understanding of the inner workings of the developed code.

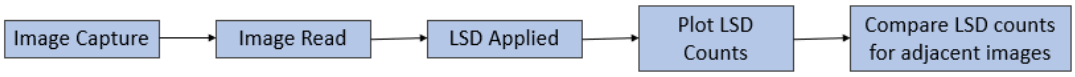

FIGURE 8.3: Flow chart of image defect detection code operating process.

pixmap

As discussed early in this chapter the output image file format of the installed system is a bitmap, .bmp, format. The pixmap library allows R statistical software to import and read bitmapped images. The pixmap functions allow for the developed code to read and import the capture images from their storage directory to the analysis code. Thus, allowing for the image analysis tools to be applied.

Magick

Magick is an open source library with the standard R statistical software package. This library allows for common image manipulation tasks to be completed on a batch or series of images. The library supports a series of image file formats and manipulation tasks, such as image cropping, scaling as well as allowing filters to be applied to images. This will prepare the images for the line segment detection process which is discussed next.

image.LineSegmentDetector

The image.LineSegmentDetector library is a machine learning technique that utilises the method of Line Segment Detection (LSD) (Gioi et al., 2012). LSD is a method which detects locally straight contours in images. These line segments are areas within an image where the grey level between adjacent pixels is changing fast from light to dark or vice versa. This change in grey value is used to detect the edges or contours of different regions in an image. An example of the detected line segments is shown in Figure 8.4. The red lines displayed are the segments detected, these segments sit along the outer edges of the parts being built where there is a high contrast between the melted layer and surrounding powder bed. This change in contrast identifies the edges of the parts built.

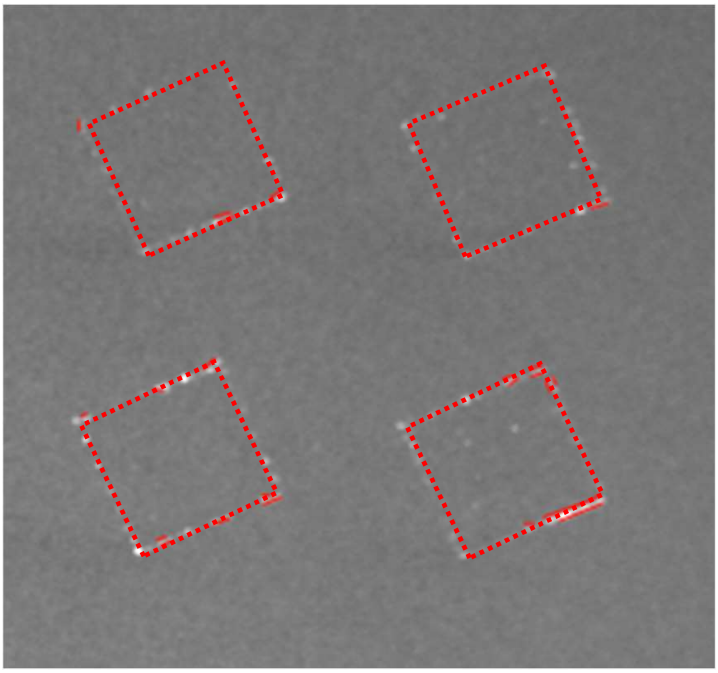

FIGURE 8.4: Line segment detection tool, shown in red, applied to a captured image.

The LSD library is used within the code to detect the number of line segments present within a captured image. As previously described the camera system captures two images per build layer, the first captures the powder deposition and the second captures the result of the laser exposure. Isolating the images that are captured of the new powder layer and applying the LSD tool. Any changes in the number of detected line segments may be the result of an defect present in newly deposited powder layer.

ggplot

To allow for the plotting of the counted line segments the ggplot library is used within the R Statistical software. The library allows for the control and plotting of gathered data, in this case the number of line segments detected. The library allows for a live plot of the detected segments during a build to be output. This plot of the detected line segments can be monitored allowing an operator to identify any sudden changes and make the required adjustments to the build to prevent a defect developing.

8.4 Examples of Defect Detections

A number of test builds were completed in order to demonstrate the installed system and developed code capability to detect the occurrence of the defects described previously in Chapter 3.5.

8.4.1 Short Feeding

As previously mentioned incomplete spreading or short feeding is a common defect that can occur in a L-PBF build. Short feeding is a lack of powder deposition on the parts being produced resulting in the multiple laser exposures to a part. In this study, multiple builds consisting of two sets of four $10mm^2$ cubes were manufactured. The parts were positioned on the build plate in the locations as shown in Figure 8.5. The images of the two sets (Set 1 and Set 2 in Figure 8.5) of cubes were then cropped as shown in Figure 8.5, before being analysed using the line segment detection and anomaly detection scripts.

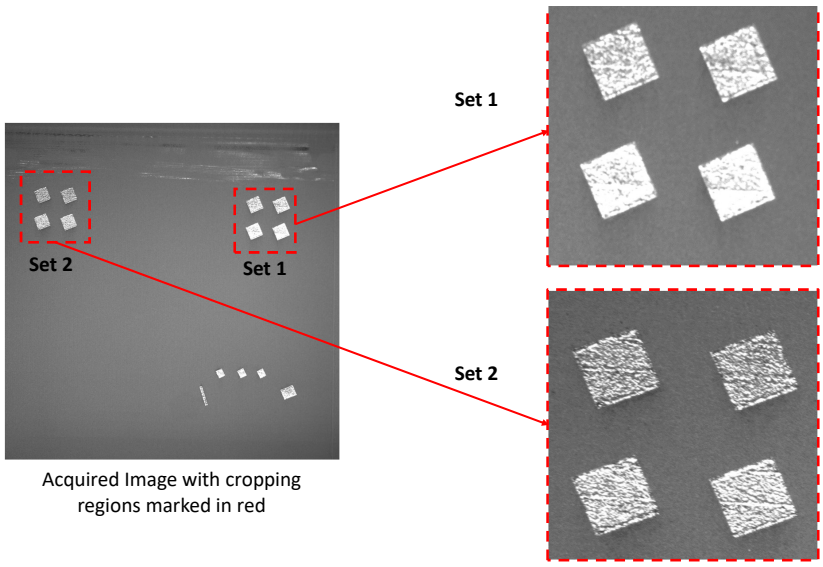

FIGURE 8.5: Cropping Regions for Set 1 and Set 2 of parts.

Set 1 is the control set of samples which are built without any deliberate defects. Set 2 is deliberately subjected to some short-feeding of powder during the build between the build height of 4.5 mm and 6.5 mm. The short feeding was induced by reducing the volume of powder that is fed to the re-coater blade before a new layer of powder is deposited. This resulted in a region on the cubes in Set 2 with a shortage of powder deposited. This lack of deposited powder results in the re-melting of previous layers causing voids and delamination in the part. The damage to the final part due to the short-feeding is presented in Figure 8.6. This type of damage can have a detrimental effect on a part, if not detected within two or three layers of the start of the short-feeding.

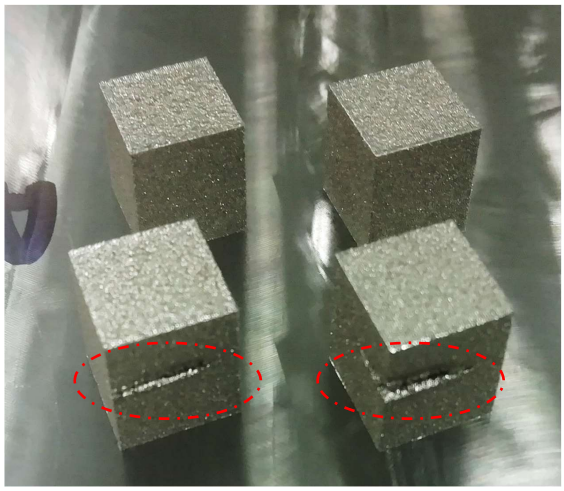

FIGURE 8.6: Set 2 parts - with damage due to short-feeding highlighted.

The short-feeding was applied by reducing the amount of powder that is deposited on the build plate. This is controlled by the re-coating percentage, which can be explained as a percentage of the volume of the build area. Typical re-coating parameters, 1.2 times the layer thickness multiplied by the area of build platform, was used for the study. This ensures that the entire build plate is covered by the new powder layer. The short-feeding of powder was created through the reduction of the re-coating parameters to 80%, for layers between the heights of 5 mm and 6 mm. This created an area on Set 2 of the cubes which received a reduced amount of powder during the re-coating stage.

For example, images that capture unusual lines or patches of powder can be seen on the build plate. Figure 8.7 (a) shows a typical image where a consistent layer of powder was deposited correctly on Set 2 parts prior to the introduction of short-feeding. Figure 8.7 (b) shows an example of where short-feeding has occurred on these parts. This can be seen as an area on the part where there is no deposited powder, which exposes the previously melted layer. Typically, two to three problem layers can cause a defect in the built part.

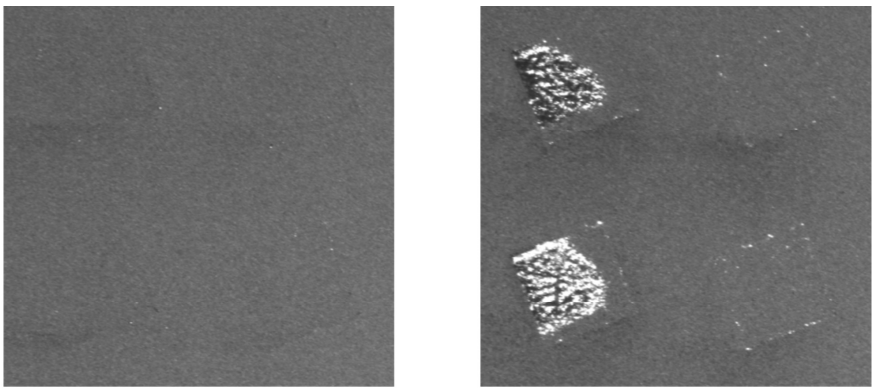

FIGURE 8.7: In-situ camera images showing (a) an example of correct powder distribution on the cubes in Set 2 after re-coating and (b) an example of short-feeding resulting in insufficient powder being deposited on the cubes in Set 2.

The line segment detection tool has been used to identify this issue of short feeding, shown in Figure 8.8. When the short feeding of powder begins, the area with a lack of powder will show an increase in the number of line segments detected. This is indicated by a spike in the plot of the number of line segments per image, as shown in Figure 8.8. The anomaly detection tool is then used to track any deviation in the quantity of line segments detected and then inform the machine operator of the increase in the line segments detected.

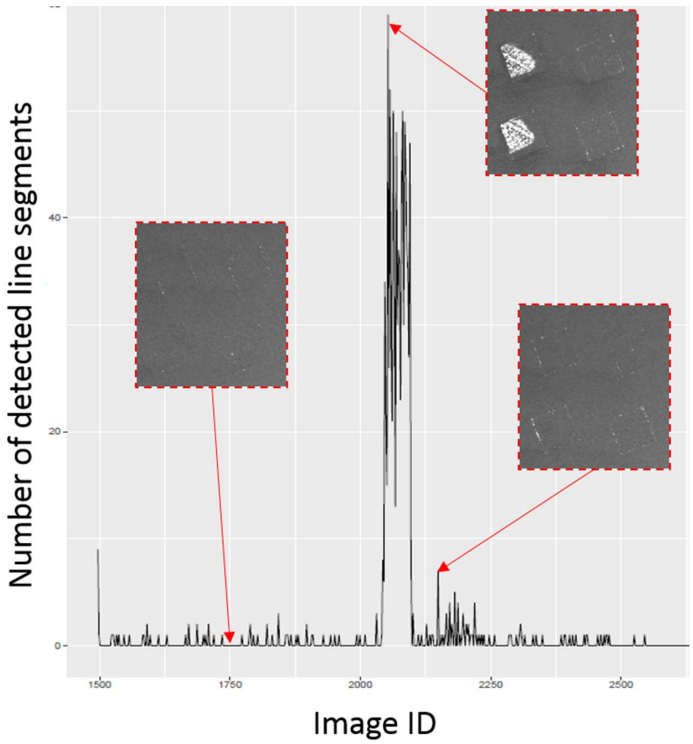

FIGURE 8.8: Line segment detection tool output with corresponding Set 2 build images.

In Figure 8.8 it is clear from the number of line segments detected where a defect has begun to develop. The spike in the graph occurs 5.4 mm (Image ID 2041) into the build process. The deliberate short feeding of powder has reduced the quantity of powder deposited on the build plate, leaving an area on the parts without new powder. This exposes the previously melted layer which is then re-melted by the laser. This issue of short feeding can be rectified by operator intervention, if noticed in time. The operator can, once the defect has been identified, increase the quantity of powder fed to the re-coater blade. This intervention was applied in the study after 6.0 mm (Image ID 2101) of the build by increasing the amount of powder fed to the re-coater blade. This is shown in Figure 8.8 by a decrease in the line segments detected as the powder deposition recovers (Image ID 2130).

8.4.2 Re-coater Streaking

As previously discussed the re-coater streaking defect is a result of a damaged re-coater blade. The defect results in an uneven distribution of the new powder layer. Causing regions of ridges in the powder bed, the regions of damage to the re-coater blade is where these ridges occur. A example of the result of this defect to the powder bed is shown in Figure 8.9.

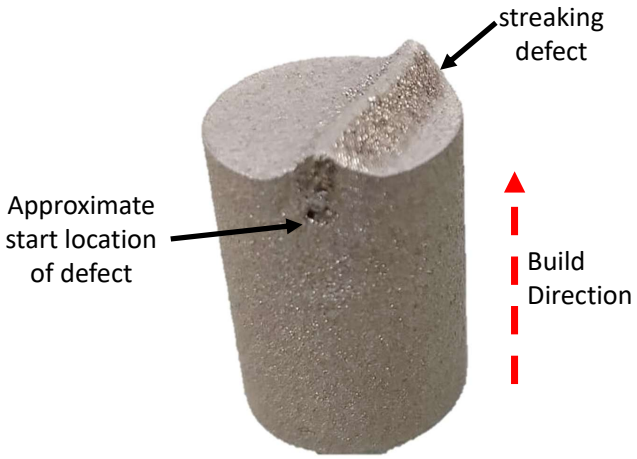

FIGURE 8.9: Image of damaged part due to the onset of re-coater streaking.

This uneven distribution of powder leads to areas on the build plate with varying powder layer thickness, which effects the quality of the manufactured part. Figure 8.9 shows the effect of the re-coater streaking defect on the parts manufactured. It is clear from the image the defect is present on the top surface of the part. Figure 8.10 shows the captured images in the early layers of the development of the defect. The highlighted regions show the effect of the re-coater streaking leading to the damage shown in Figure 8.9.

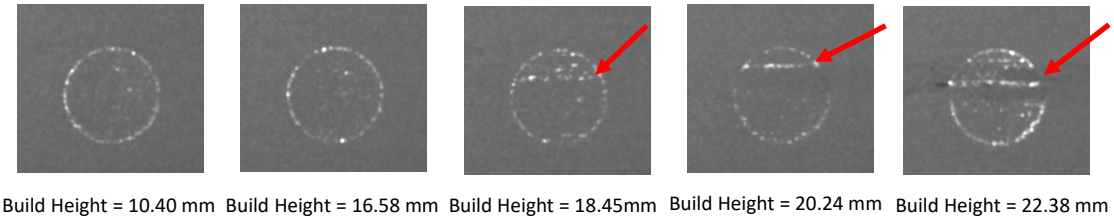

FIGURE 8.10: Development of the defect in images due to re-coater streaking.

Non-destructive testing (NDT), such as x-ray micro-computed tomography (XMT) can be used here identify the internal damage to the sample as a result of the observed defect. The XMT analysis can also be used to verify the location of the defect and determine its starting height. This can be cross referenced with the output LSD plot from the defect detection code.

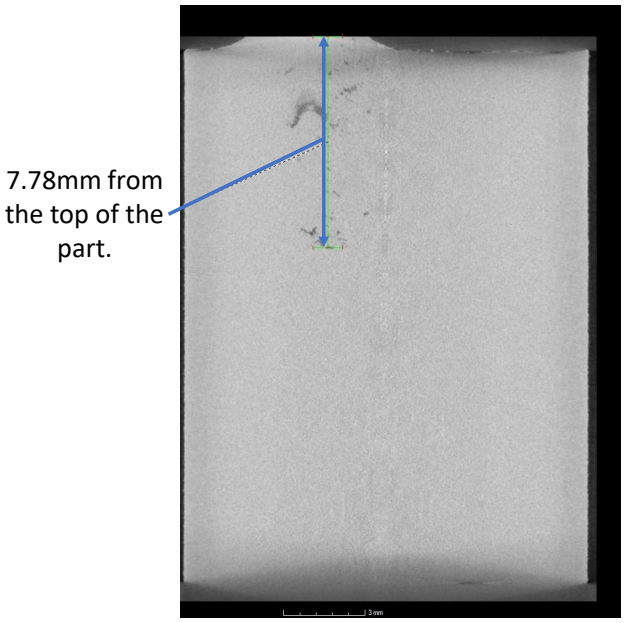

FIGURE 8.11: X-ray μCT Image of the re-coater streaking defect, indicated the internal porosity resultant from this defect.

The corresponding LSD plot is shown in Figure 8.12. This shows that a peak in the number of line segments presented in the images captured during the build was detected around image number 1240. This would correspond to approximately 24.8 mm into the build, based on 2 images per layer at a 40 μm layer height. The XMT analysis also shows the impact of this defect on the integrity of the internal material of the part. This is shown in Figure 8.11 where internal porosity and voids can be seen as a result of the re-coater streaking defect occurring.

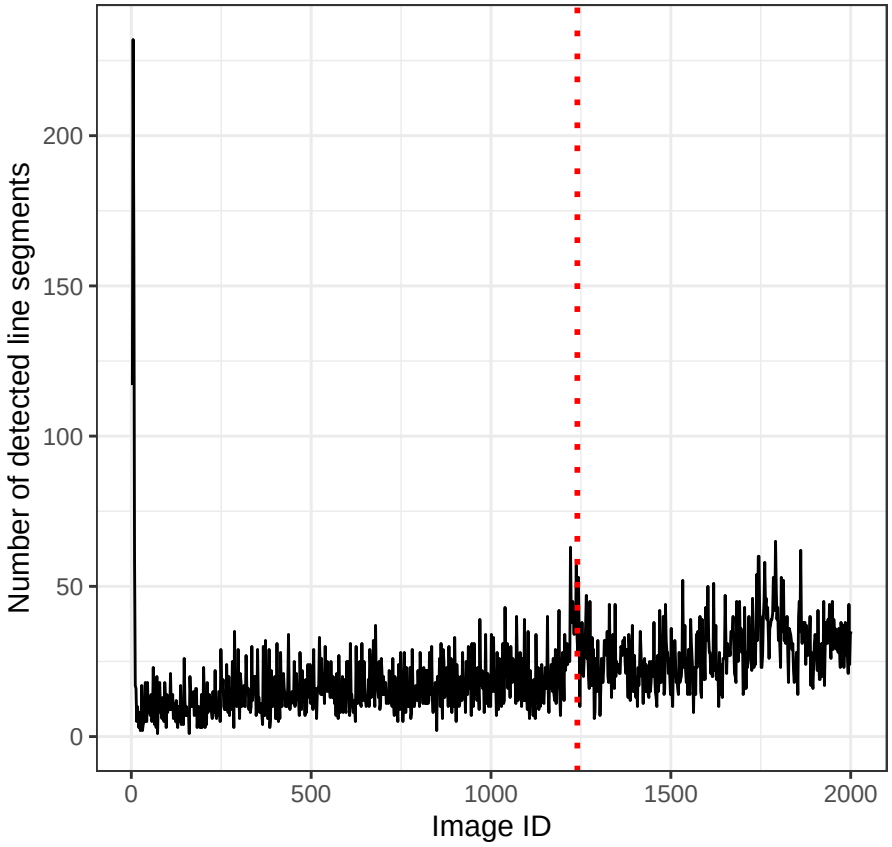

FIGURE 8.12: LSD Plot of build where the Re-coater Streaking defect has been detected.

The results presented here demonstrate the capacity of the developed and installed defect detection system to identify the defect of re-coater streaking and the effects that defect has on the as-built part. The CT analysis was also capable of identifying the internal defects present within the part as a result of the re-coater streaking. These internal defect affect the mechanical properties of the as-built part. The ability to detect this defect in the early layers of its occurrence will allow the operator to take the necessary action in the build settings to minimise the impact the defect will have.

8.4.3 Elevated Edges

Elevated edges are a defect in which the rapid heating and cooling rate in the L-PBF process causes the unconstrained edges of components to warp or deflect. This results in theses edges being visible after the new powder layer is added. This can result in areas of the part being exposed to the laser without a powder layer present. This can result in over melting and in some extreme cases lead to damage to the re-coater blade which can contribute to the aforementioned re-coater streaking. The ability to detect when this defect occurs can assist in the management of this defect through parameter optimisation particularity for the laser scanning settings. An example of how this defect may look in the L-PBF process is shown in Figure 8.13. This figure shows the newly deposited powder

layer, as the images progress, the elevated edges of the component can clearly be identified.

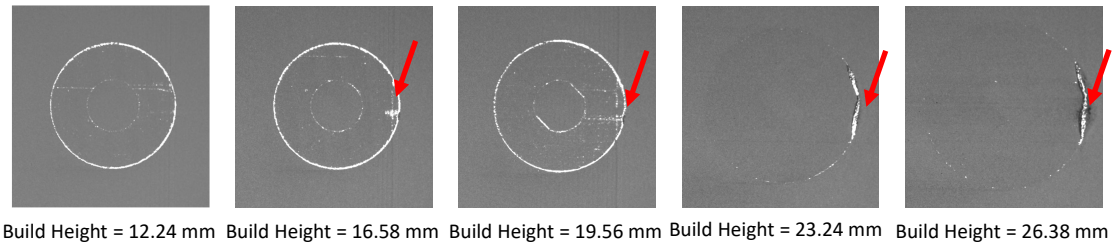

FIGURE 8.13: Captured Images of the elevated edges defect developing.

The LSD tool can be used to identify this defect in the same manner as it was deployed to detect the lack of powder deposition defect. The LSD tool identifies a change in the intensity value of the adjacent pixels due to the exposed metal edges protruding through the powder layer. A LSD plot of the development of this defect is shown in Figure 8.14. Accompanying images identify the development of the defect with their associated image number for reference. As these edges are now elevated, powder is not deposited resulting in the exposure of the previously melted layer.

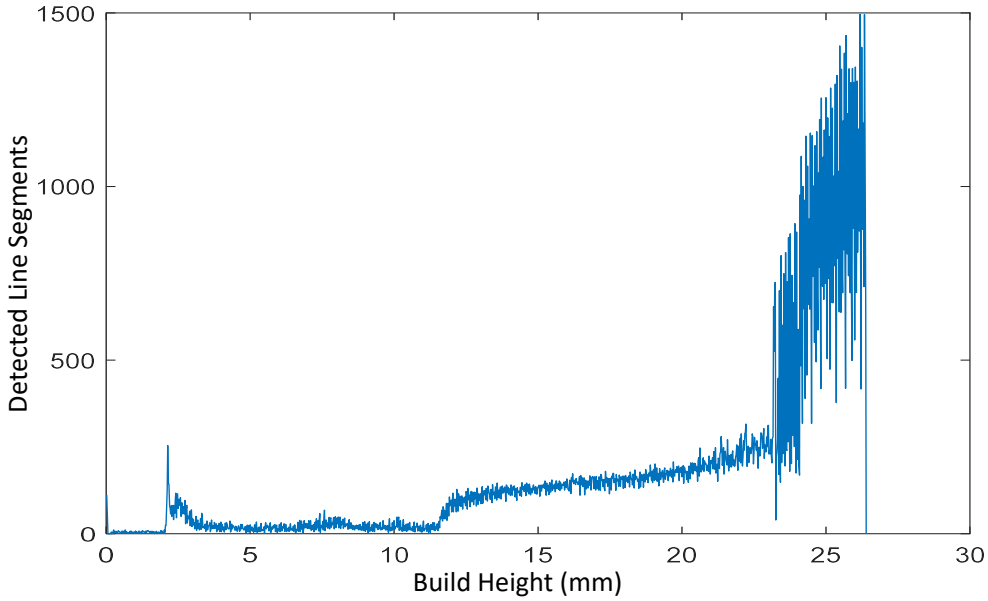

FIGURE 8.14: LSD Plot of build where the elevated edges defect has been detected.

Once again the results presented demonstrate the capability of the installed imaging system and accompanying defect detection code in detecting the occurrence of elevated edges. The ability to detect elevated edges can enable to operator to make the necessary adjustments in the scanning parameters to

minimise their effect on the remainder of the build. Figure 8.15 shows an example of the outcome of a build in which elevated edges resulted in the overall failure of the build.

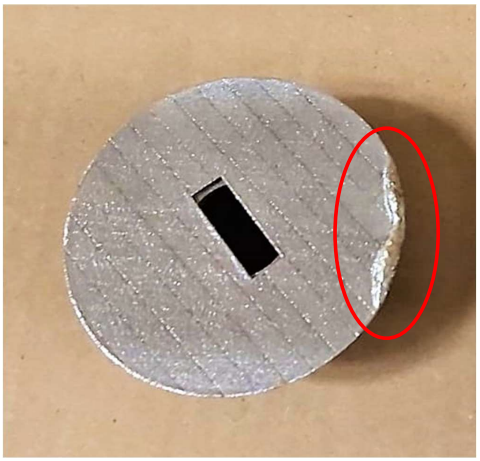

FIGURE 8.15: Damage to cross section of a Turbine component as a result of elevated edges. Elevated edge is highlighted in the red.

8.5 Conclusions

This chapter describes the development and application of a standalone in-situ monitoring and image analysis system applied to a L-PBF system. The system has been installed within an EOS M280 L-PBF machine and has proven to be successful in the identification of the four defects described in Section 8.1. The system identifies defects within the powder deposition stage of the L-PBF process. Many of the flaws and defects presented within the L-PBF process can be directly related to the interactions between the re-coater blade and the powder bed (Scime and Beuth, 2018), hence, the importance for monitoring this stage of the process.

The use of in-situ monitoring can assist L-PBF to reduce the manufacturing costs associated with the occurrence of defects in the L-PBF. The identification of defects as early as possible in the L-PBF process can allow for effective repair strategies to be applied. This may reduce the impact of the identified defect. The presented system and methodology can be used as a tool in the shift of the L-PBF process towards a zero-defect manufacturing process (Colosimo and Grasso, 2020).

9 Conclusion

Metal additive manufacturing opens new possibilities for a range of industrial sectors, especially those operating within the low volume, high value manufacturing space. Before these benefits can be applied, however, a deeper understanding of the L-PBF process as a whole is required. While there are many areas of research within the L-PBF process, this thesis focuses on the process of recycling powder material as well as the development of a standalone monitoring process to identify defects within the L-PBF process. This chapter will summarise the work completed, the implications it may have in the research area and providing some areas for future work.

9.1 Summary of Findings

In Chapter 1 some background to the research area was established. The funding agency IMR and research centre SEAM were introduced as well as their link and interest in the proposed research. This enabled the research questions and aims to be detailed. The subsequent chapters lend themselves to working towards achieving these research aims through a series of studies. A list of the relevant publications and dissemination opportunities as a result of this work are also presented.

In Chapter 2, the metal AM processes were introduced alongside some current examples of the technology at work. These applications are from within the high value, low volume industries such as; medical device, aerospace and dental. These industries require, due to regulations, stringent control over their manufacturing process in order to ensure defects are minimised. This involves having a greater understanding and knowledge of the entire process and the materials used. As with traditional manufacturing processes the process, its inputs and outputs are monitored. This is to ensure they remain within the acceptable standards for that product or industry. In order for metal AM to reach the same level of maturity these relationships need to be fully investigated.

In Chapter 3 the current state of the art is presented, focusing on the additive manufacturing powders, their characteristics and the implications these have on the output of the L-PBF process. It was found that the feedstock material characteristics greatly impact the output from the L-PBF process. Research to date has been focused on the characteristics of virgin powder material with little research investigating the effects of reusing powder material. Powder recycling can be used to to increase yield of the costly powder. The research completed

around the powder recycling process has shown the impact of the powder material on the parts produced by the L-PBF process.

The ability to monitor the AM process and identify the occurrence and severity of defects can lead to increased adoption of the AM process. Four common defects occurring in the powder deposition phase, are defined and presented. Methods to monitor these forms of defects often take a static monitoring approach, observing snapshots of the process. Many of the presented monitoring solutions require the system to be integrated into the operation of the L-PBF machine limiting its applicability to older equipment. A standalone monitoring approach that can be integrated into the process with minimal interference to the operation of the L-PBF process is desirable.

In Chapter 4, the material for this project, a 316L stainless steel powder, was introduced as well as the methodologies that are applied throughout the subsequent chapters. This included the series of powder characterisation techniques used as well as the methods used to determine the quality of the parts manufactured. The relevant statistical methods required to present and investigate this data was also discussed in detail. Methods for the standalone in-situ monitoring of the L-PBF process was also presented detailing the considerations for the developed system as well as the required equipment. The installation of the system is presented with the locations of the required equipment within the L-PBF machine highlighted. The aim of this chapter was to detail the tools required to complete the studies presented in Chapter 5, Chapter 6, Chapter 7 and Chapter 8.

In Chapter 5 the design and implementation of an investigation into the powder recycling process was presented in order to provide a deeper understanding of its impact on the powder itself and the parts that are produced. A single powder batch was repeatedly used through a total of 12 build cycles culminating in a total of 112.5 build hours. The build hours were determined using a method presented by Denti et al., 2019, namely Average Use Time (AUT). Both the powder characteristics and the resulting part properties were tracked and evaluated throughout the 12 build cycles, and the following results were found:

- For the duration of the powder recycling study there was no observed change in the powder chemical composition.
- The mean particle size increased as the powder recycling process continued. This was due to the ease at which the smaller particles are being used within the process. Due to their smaller size they are able to fill voids and gaps in previously melted layers as well as being pulled into the melt pool during the melting process.
- The shape of the particles deteriorated over the powder recycling process. As the powder recycling process continued particles exhibit a more fractured morphology. This was monitored through the use of a shape descriptor know as Circularity. As powder recycling increased this circularity value decreased.

- The flowability of the powder batch improved despite the decrease in circularity of the powder particles. This can be attributed to the reduction in the quantity of smaller particles present in the powder batch, smaller particles can resist the flow of the material.

As a result of these changes in the powder characteristics the resulting part properties are affected.

- The analysis of the part dimensions showed that the maximum difference in the part dimensions from the specifications increased as the powder is used. This change in the part property is highly related to the increased particle size resulting in larger particles adhering to the surface of L-PBF parts.
- The hardness of the manufactured samples remained within a standard deviation of the expected 89 HRB for 316L Stainless Steel. This provides a good indication for other mechanical properties, such as tensile strength or fatigue, remaining within their expected values despite the changing raw material.
- Part density is a property that is closely observed by L-PBF users. Most industrial users require a high part density in order to meet specification. A reduction in the part density as the *AUT* on the recycled powder increased was observed. One of the influential factors here is the reduction in smaller particles which can be used to fill voids in the powder layer increasing the density of the deposited powder.
- The surface roughness increased significantly as the powder properties change in the recycling process. This can be attributed to a combination of the increasing proportion of larger particles present in the powder batch as well as the deterioration of the particle morphology.
- There was no significant change detected in the phase characteristics of the powder material as the powder was re-used. This, in turn, did not affect the micro-structure of the as-built parts. As expected, FCC austenitic phases were found in both the powder material and manufactured samples.

The powder was recycled until the quantity remaining was insufficient for further samples to be manufactured and characterised.

The work completed in Chapter 6 builds on the powder recycling aspect with a process described as powder rejuvenation. This process enables a batch of powder for the L-PBF process to be utilised further through either:

- topping up the powder to maintain a constant quantity, or,
- through the addition of virgin powder once the quantity of powder has reached an unusable level

An initial study with the aim of identifying which ratio of recycled powder to virgin powder found that a mix of 50% virgin powder and 50% recycled powder restored the properties of the powder batch to an acceptable standard. The study concluded that the mixing ratio was highly influential on the bulk powder characteristics of the batch. It was found that as the ratio of virgin powder

increased, the mean particles size decreased, the morphology of the powder batch became more circular and the flowability decreased.

Once the most acceptable powder ratio was determined in the initial study the rejuvenated powder batch was then used within the L-PBF process in a similar manner to the work presented in Chapter 5. The powder characteristics and part qualities were characterised through a series of 17 builds culminating in a total *AUT* of 300 hours. Similar to the findings in the recycling study, it was found that the powder characteristics changed as the rejuvenated powder was recycled. These changes can be summarised as:

- As the rejuvenated powder was used in the L-PBF process, the powder properties deteriorated in terms of size and shape. The mean particle size increased and particles became less circular. This was caused by increased agglomerates and fractured particles within the powder batch. This resulted in improved powder flowability.

These changes in the powder properties heavily influenced the part qualities with the following qualities that were measured showing deterioration:

- The changes in powder characteristics due to powder reuse negatively influenced the manufactured part properties. This was observed as a decrease in the dimensional accuracy of the manufactured parts, with increased surface roughness and porosity. It was found that the dominant powder characteristic contributing to the change in the surface roughness and the part density was the mean particle size.
- There was no significant change detected in the micro-structure of the powder material as the powder was re-used. This, in turn, did not affect the micro-structure of the as-built parts. As expected, FCC austenitic phases were found in both the powder material and manufactured samples at different stages of the recycling and rejuvenation process.

The work completed in Chapter 5 and Chapter 6 provided an insight into how the L-PBF process affects the powder characteristics as well as the manufactured part properties after being exposed to the a powder recycling and rejuvenation process. Both of which enable the usability of the costly powder material to be extended. The results also provide an understanding for the relationship between the powder characteristics, as it is being recycled, and the resulting manufactured part qualities. These findings were leveraged in Chapter 7 to develop a series of empirical relations between the changing powder characteristics and the part properties. Two empirical models were developed for the part density and surface roughness using the multiple linear regression (MLR) method. The part density and surface roughness were selected due to their high correlation with the changing powder properties initially explored in the discussion section of Chapter 5 and 6.

Multiple linear regression models were developed for the prediction of part density and surface roughness from a combination of the powder characteristics. The results of the process of developing the models can be summarised in the following:

- Scatter plots revealed that the changes in the part density observed in the previous studies correlated highly with the changing particle size as well as the increasing powder use time.
- The part density model met the requirements for an MLR model and had the capability to predict 98.79 % of the changes observed in the part density.
- The increased surface roughness was also shown to be highly correlated with increased powder use time, changing particle size and morphology.
- The surface roughness model met the requirements for an MLR model and had the capability to predict 93.64 % of the changes observed in the surface roughness.

These developed empirical models will enable L-PBF operators to characterise the powder material prior to a build and use these quantified characteristics to estimate expected manufactured part properties. The three studies presented in this thesis (Chapter 5, 6 and 7) highlight the effect of the powder material in the L-PBF process. The powder recycling and rejuvenation processes in tandem with the developed models will provide the opportunity to reduce the waste generated by the L-PBF process and increase the utility of the powder material.

Chapter 8 presented a standalone monitoring system for retrofitting into an EOS M280 L-PBF machine. The developed system identifies defects through capturing an image before and after each powder layer has been deposited. This image is then subjected to a developed image analysis tool to identity anomalies within the powder bed. Detected defects are used to notify a machine operator, the operator then can use the information to determine the best course of action for rectifying the defect. This standalone defect detection system allows for legacy L-PBF systems to have monitoring capabilities retrofitted without affecting the operation of the machine. Monitoring systems are used in every manufacturing process to reduce the number of defects and monitor the overall process output to increase yield, this same principle is applied here to a L-PBF machine increasing its applicability in today's data driven world. The developed system is capable of identifying a number of different defects that can occur in the powder deposition phase of the L-PBF process.

The following section of this chapter will look further into the implications of the work presented in this thesis.

9.2 Implications of the Work

The work completed in this thesis provides a deeper understanding of the L-PBF process with the ultimate aim of the knowledge generated being used to de-risk and strengthen the adoption of L-PBF processes within industrial sectors.

The work presented in Chapter 5 and Chapter 6 provided a deeper understanding of the process of metal powder recycling and rejuvenation for 316L powder. It was understood, from the literature, that this process impacts the powder properties and resulting part qualities. The studies, presented in this thesis

further this understanding. The impact of powder characteristics on the finished part properties is highlighted. The powder characteristics exhibited significant changes as the powder is used and repeatedly exposed to the L-PBF process. These observed changes in the powder directly translated into the part properties produced.

Chapter 7 quantifies this dependency through the development of empirical models. The models developed can then be applied to increase the utilisation of the powder material by allowing L-PBF operators to input the characteristics of a powder batch namely; *AUT*, mean particle size and circularity, and receive a prediction of the expected part density and surface roughness. If the expected output is not within the required output parameters the operator can then ensure that either a different batch of powder is used or any necessary post processing required is available. The models provide the L-PBF community an ability to further extend the life of a costly powder batch.

Chapter 8 presented a standalone in-situ monitoring system for the L-PBF process. While in-situ monitoring is now a standard feature on many new L-PBF machines, the EOS M280 does not have this capability. As such this monitoring process was developed coupled with the empirical models developed in Chapter 7 is another tool for L-PBF operators. The monitoring process enables an on-going assessment of the powder layer deposition process throughout a L-PBF build. Defects are identified and are used to alert the machine operator. The standalone aspect of the developed system ensures that the limited processing power of the on-board computer is not being strained during the monitoring process. The system has been developed in a way as to allow it to be retrofitted to any L-PBF and operate in the same manner as presented here. With the high number of in-process defects occurring in the powder deposition phase of the L-PBF process, the ability to identify these defects, alert an operator and therefore enable the process to be adjusted accordingly to suit, is highly valuable.

The work presented in this thesis is targeted towards ensuring that the L-PBF process can move towards a zero-defect manufacturing process, thus increasing its utility and acceptance across other manufacturing industries worldwide. To achieve this the work has provided the ability to:

- Link the relationship between powder recycling and rejuvenation processes to the resulting powder characteristics.
- Understand how the characteristics of these powder materials impact the resulting L-PBF manufactured parts.
- Nominally predict the performance of a powder batch through the use of the empirical models developed in Chapter 7.
- Observe and react to defects in the powder deposition phase of the L-PBF process as a result of powder characteristics.

These will ensure that the manufacturing process can be used as a zero defect process, by providing an understanding of the implications of the input characteristics as well as ensuring that any potential defects are capture in time.

9.3 Future Work

There are a few points that can be considered as by a means to continue the work presented in this thesis:

- While the work presented in Chapters 5 and 6, was conducted on a 316L powder the same methodology applied can be used to study other metal powder used in the L-PBF process such as Titanium, Nickel and Aluminium alloys. This would create a greater understanding as to how these materials would react to the powder recycling process.
- The powder recycling and rejuvenation study could be further strengthened by the inclusion of more mechanical properties of the components produced in the L-PBF process. Further samples should be manufactured to assess the tensile and compressive properties as well as the fatigue properties of the parts manufactured using recycled powder material.
- The accuracy of the empirical models developed in Chapter 7 can be improved through further validation. This would require powder characteristics to be input in to the developed models prior to conducting a L-PBF build. The output properties of the parts produced can then be quantified and compared to the properties predicted by the models. The results from this testing can be used to increase the accuracy of the developed models.
- Extending the capabilities of the defect detection system to quantify the severity of the identified defect in process. As mentioned in Chapter 3 defects in the L-PBF process may be evident in a singe layer and then rectify themselves for the remainder of the build. The ability to assess and quantify the impact the occurrence of this defect would assist L-PBF operators in their decision making. This would require the severity of different forms of identified defects to be quantified, post process through mechanical testing or similar. From there the defect detection algorithm can be improved to further incorporate these findings and notify L-PBF operators of the potential outcomes from the observed defect.

9.4 Closing Remarks

This thesis has presented a series of works to increase the applicability and utility of the metal AM process. The costly metal powders required for the L-PBF process have been investigated in terms of their ability to be recycled, and rejuvenated, through the process. The focus of which being how the characteristics of the powder was affected by the process and the effect on the resulting manufactured part properties. The ability to complete this process can lead to reduction in the overall cost of adopting the L-PBF process. Further to that the understanding developed through these studies has led to the development of empirical models to predict the resulting properties from the L-PBF process from a given batch of powder material. As with all manufacturing process the L-PBF process can produce defects, the process of detecting these defects as they

occur leads to a reduction in waste from the process. The developed monitoring system enables defects in the powder deposition phase of the L-PBF process to be identified, enabling the L-PBF operator to respond accordingly.

In bringing together these issues it is intended the work will help to promote a more complete and sophisticated understanding of the metal AM process, generate insight into the ongoing development of the metal AM technology, and pave the way towards a more competitive and responsive metal AM market.

A Defect Detection Code

Line Segment Detection Code

```
rm(list=ls()) # remove everything from memory
# Set working directory on the machine reading the images from the camera laptop
setwd("D:/01102020/USB/SD2/cv-x/image/SD1_001")
setwd("~/Documents/SEAM/")
########### LOAD LIBRARIES AND FUNCTIONS ###################
source("seamfunctionspq.R")
imagedir="CAM1/"
# These are inputs to the real-time plotting
num_layers_in_build = 2550
# number of odd layers (powder bed rather than post laser firing)
n = num_layers_in_build / 2
# set up a dataframe to store the results in
df_odd = data.frame(layer_number = 1:n, lsd_count = runif(n))
window = 10
# number of first image of this build
start_here = 1
# number of last image of this build
end_here = 5000
# turn cropping on =1 or off =0
cropyn = 0
# define a file to write output to
res_date=format(Sys.time(), "%d-%b-%Y-%H.%M")
res_file=paste(res_date,"_results.csv",sep="")
for (i in start_here:end_here){
 f <- tempfile(fileext = ".pgm")
 # Search for the image coming off the camera
 read = try(Sys.glob((paste(imagedir, "*0000", i, "_*", sep=""))))
 # If the image hasn't been created yet, pause for a few seconds and try again.
 while(is.na(read[1]) == 1){
  print(paste("Attempting to load image",i))
  read = try(Sys.glob((paste(imagedir, "*0000", i, "_*", sep=""))))
```

```
   # Pause for 5 seconds before reattempt to load image file.
   Sys.sleep(5)} # Can change this delay to see less frequent output.
  x <- image_read(read)
  # convert to format required by line segment detection software
  x <- image_convert(x, format = "pgm", depth = 8)
  rm(read)
  image_write(x, path = f, format = "pgm")
  image <- read.pnm(file = f, cellres = 1)
  if(cropyn == 1){
     image_to_crop = image_read(f)
     image_crop(image_to_crop,"400x400+200+200")
     image_cropped = image_crop(image_to_crop,"400x400+200+200")
     # write out to pgm format for use with image_line_segment_detector
     image_write(image_cropped, path = f, format = "pgm")
     # read back in pgm format
     image <- read.pnm(file = f, cellres = 1)
     # detect line segments
     linesegments <- image_line_segment_detector(image@grey * 255)
   }else{
     linesegments <- image_line_segment_detector(image@grey * 255)}
   res_layer = linesegments$n
   # output lsd count to screen
   print(paste("The line segment count for image", i , "is", res_layer))
   # output lsd count to a file
   write.table(t(c(i,linesegments$n)),res_file,sep="
",append=TRUE,row.names=FALSE,col.names=FALSE)
   # output result to a simple real time plot
   df_odd$lsd_count[i]= res_layer
   plot(df_odd$layer_number,df_odd$lsd_count,type='l',xlim=c(1,i),xlab='Image ID',ylab='Number of
detected line segments')
   Sys.sleep(9) }
# Code to automatically save a nice plot at the end of the build with a timestamp.
p=ggplot(data = res_dframe_prepost, aes(x = layer_number, y =lsd_count))+
```

```
  geom_line() +
  xlab('Image ID') +
  ylab('Number of detected line segments') +
  ggtitle('Bad Turbine Build (every second layer, odd)') +
  ggtitle(paste('LSD counts')) +
  expand_limits(y=c(0,73))
 p + theme_bw()
st=format(Sys.time(), "%Y-%m-%d_%H%M")
ggsave(paste("rplot_",st, ".pdf", sep = ""))
```

Line Segment Detection Functions

```
library(magick)
library(image.LineSegmentDetector)
library(pixmap)
library(ggplot2)
############ FUNCTION TO LSD A BATCH OF IMAGES ##########################
lsd_images<-function(start_here,end_here,dir){
 res=rep(numeric(),end_here)
 res_date=format(Sys.time(), "%d-%b-%Y-%H.%M")
 res_file=paste(res_date,"_results.csv",sep="")
 for (i in start_here:end_here){
  f <- tempfile(fileext = ".pgm")
  read=Sys.glob((paste(dir,"*0000",i,"_*",sep="")))
  x <- image_read(read)
  x <- image_convert(x, format = "pgm", depth = 8)
  image_write(x, path = f, format = "pgm")
  image <- read.pnm(file = f, cellres = 1)
  linesegments <- image_line_segment_detector(image@grey * 255)
  res[i-(start_here-1)] <- linesegments$n
 write.table(t(c(i,linesegments$n)),res_file,sep=",append=TRUE,row.names=FALSE,col.names=FALSE)
 }
 return(res)
}
```

Bibliography

Abdelrahman, Mostafa, Edward W. Reutzel, Abdalla R. Nassar, and Thomas L. Starr (2017). "Flaw detection in powder bed fusion using optical imaging". In: *Additive Manufacturing* 15, pp. 1–11. ISSN: 22148604. DOI: 10.1016/j.addma.2017.02.001.

Abdelwahed, M., S. Bengsston, R. Casati, A. Larsson, and M. Vedani (2021). "L-PBF Processing of Steel Powders Produced by Gas and Water Atomization". In: *BHM Berg- und Hüttenmännische Monatshefte* 166.1, pp. 40–45. ISSN: 0005-8912. DOI: 10.1007/s00501-020-01071-1.

Abd-Elghany, K. and D.L. Bourell (2012). "Property evaluation of 304L stainless steel fabricated by selective laser melting". In: *Rapid Prototyping Journal* 18.5, pp. 420–428. ISSN: 1355-2546. DOI: 10.1108/13552541211250418. URL: http://www.emeraldinsight.com/doi/10.1108/13552541211250418.

Abràmoff, Michael D., Paulo J. Magalhães, and Sunanda J. Ram (2004). "Image processing with imageJ". In: *Biophotonics International* 11.7, pp. 36–41. ISSN: 10818693. DOI: 10.1117/1.3589100. arXiv: 1081-8693.

Ahmed, Farid, Usman Ali, Dyuti Sarker, Ehsan Marzbanrad, Kaylie Choi, Yahya Mahmoodkhani, and Ehsan Toyserkani (2020). "Study of powder recycling and its effect on printed parts during laser powder-bed fusion of 17-4 PH stainless steel". In: *Journal of Materials Processing Technology* 278.August 2019, p. 116522. ISSN: 09240136. DOI: 10.1016/j.jmatprotec.2019.116522. URL: https://doi.org/10.1016/j.jmatprotec.2019.116522.

Allen, Terence (1997). *Particle Size Measurement*. Ed. by Brian Scarlett and Genji Jimbo. Fifth. Vol. 1. London: Chapman and Hall, p. 525. ISBN: 978-94-010-6673-0. DOI: 10.1007/978-94-009-0417-0. arXiv: arXiv:1011.1669v3. URL: http://link.springer.com/10.1007/978-94-009-0417-0.

Anderson, Iver E., Emma M.H. White, and Ryan Dehoff (2018). "Feedstock powder processing research needs for additive manufacturing development". In: *Current Opinion in Solid State and Materials Science* 22.1, pp. 8–15. ISSN: 13590286. DOI: 10.1016/j.cossms.2018.01.002. URL: https://doi.org/10.1016/j.cossms.2018.01.002.

Ardila, L. C., F. Garciandia, J. B. González-Díaz, P. Álvarez, A. Echeverria, M. M. Petite, R. Deffley, and J. Ochoa (2014). "Effect of IN718 recycled powder reuse on properties of parts manufactured by means of Selective Laser Melting". In: *Physics Procedia* 56.C, pp. 99–107. ISSN: 18753892. DOI: 10.1016/j.phpro.2014.08.152. URL: http://dx.doi.org/10.1016/j.phpro.2014.08.152.

Averardi, Alessandro, Corrado Cola, Steven Eric Zeltmann, and Nikhil Gupta (2020). "Effect of particle size distribution on the packing of powder beds: A critical discussion relevant to additive manufacturing". In: *Materials Today*

Communications 24.January, p. 100964. ISSN: 23524928. DOI: 10.1016/j.mtcomm.2020.100964. URL: https://doi.org/10.1016/j.mtcomm.2020.100964.

Averyanova, M., P. Bertrand, and B. Verquin (2010). "Effect of initial powder properties on final microstructure and mechanical properties of parts manufactured by selective laser melting". In: *Annals of DAAAM and Proceedings of the International DAAAM Symposium*. Vol. 21. 1, pp. 1531–1532. ISBN: 9783901509735. URL: http://www.engineeringvillage.com/blog/document.url?mid=cpx_b784c2d1478e720776M4b8d10178163125&database=cpx.

Baitimerov, Rustam, Pavel Lykov, Dmitry Zherebtsov, Ludmila Radionova, Alexey Shultc, and Konda Gokuldoss Prashanth (2018). "Influence of powder characteristics on processability of AlSi12 alloy fabricated by selective laser melting". In: *Materials* 11.5, pp. 1–14. ISSN: 19961944. DOI: 10.3390/ma11050742.

Bajt Leban, Mirjam, Miha Hren, and Tadeja Kosec (2023). "The microstructure, mechanical and electrochemical properties of 3D printed alloys with reusing powders". In: *Scientific Reports* 13.1, pp. 1–17. ISSN: 20452322. DOI: 10.1038/s41598-023-28971-9. URL: https://doi.org/10.1038/s41598-023-28971-9.

Balbaa, M. A., A. Ghasemi, E. Fereiduni, M. A. Elbestawi, S. D. Jadhav, and J. P. Kruth (2021). "Role of powder particle size on laser powder bed fusion processability of AlSi10mg alloy". In: *Additive Manufacturing* 37.May 2020, p. 101630. ISSN: 22148604. DOI: 10.1016/j.addma.2020.101630. URL: https://doi.org/10.1016/j.addma.2020.101630.

Beal, Maxime, Mohamed Nour Azzougagh, Jérémie Pourchez, Philippe Bertrand, Elodie Cabrol, Hocine Si-Mohand, and Francois Xavier Keller (2023). "Effect of powder reuse on physical, chemical and toxicological properties of 6061-Zr aluminum alloy processed by Laser Powder Bed Fusion (L-PBF)". In: *Materiaux et Techniques* 111.1. ISSN: 17783771. DOI: 10.1051/mattech/2023013.

Benson, Jeffrey Malcolm and Ettienne Snyders (2015). "the Need for Powder Characterisation in the Additive Manufacturing Industry and the Establishment of a National Facility". In: *The South African Journal of Industrial Engineering* 26.2, p. 104. ISSN: 22247890. DOI: 10.7166/26-2-951. URL: http://sajie.journals.ac.za/pub/article/view/951.

Bhushan, Bharat (2000). *Surface roughness analysis and measurement techniques*, pp. 49–119. ISBN: 9780849377877. DOI: 10.1201/9780849377877-10.

Bian, Linkan, Scott M. Thompson, and Nima Shamsaei (2015). "Mechanical Properties and Microstructural Features of Direct Laser-Deposited Ti-6Al-4V". In: *Jom* 67.3, pp. 629–638. ISSN: 15431851. DOI: 10.1007/s11837-015-1308-9.

Boes, J., A. Röttger, W. Theisen, C. Cui, V. Uhlenwinkel, A. Schulz, H. W. Zoch, F. Stern, J. Tenkamp, and F. Walther (2020). "Gas atomization and laser additive manufacturing of nitrogen-alloyed martensitic stainless steel". In: *Additive Manufacturing* 34.February, p. 101379. ISSN: 22148604. DOI: 10.1016/j.addma.2020.101379. URL: https://doi.org/10.1016/j.addma.2020.101379.

Brika, Salah Eddine, Morgan Letenneur, Christopher Alex Dion, and Vladimir Brailovski (2019). "Influence of particle morphology and size distribution on the powder flowability and laser powder bed fusion manufacturability of Ti-6Al-4V alloy". In: *Additive Manufacturing* 31.November 2019, p. 100929. ISSN: 2214-8604. DOI: 10.1016/J.ADDMA.2019.100929. URL: https://doi.org/10.

1016/j.addma.2019.100929https://www.sciencedirect.com/science/article/pii/S2214860419311868.

Cantor, Brian (2020). *The Equations of Materials*. DOI: 10.1093/oso/9780198851875.001.0001. URL: https://doi.org/10.1093/oso/9780198851875.001.0001.

Carroll, P. A., A. J. Pinkerton, J. Allen, W. U. H. Syed, H. K. Sezer, P. Brown, G. Ng, R. Scudamore, and L. Li (2006). "The effect of powder recycling in direct metal laser deposition on powder and manufactured part characteristics". In: *Proceedings of AVT-139 Specialists Meeting on Cost Effective Manufacture via Net Shape Processing. NATO Research and Technology Organisation*. 2006, pp. 1–8. URL: http://eprints.lancs.ac.uk/59645/.

Chuang, Chihpin Andrew, Syed Saahir Shahab Ahmed, Peter Kenesei, Jonathan Almer, and Dileep Singh (2021). "High-Energy X-ray Tomographic Analysis of Precursor Metal Powders (Ti-6Al-4V) Used for Additive Manufacturing". In: *Journal of Materials Engineering and Performance* 30.1, pp. 610–616. ISSN: 1059-9495. DOI: 10.1007/s11665-020-05341-4. URL: http://link.springer.com/10.1007/s11665-020-05341-4.

Clayton, Jamie and Rob Deffley (2014). "Optimising metal powders for additive manufacturing". In: *Metal Powder Report* 69.5, pp. 14–17. ISSN: 00260657. DOI: 10.1016/S0026-0657(14)70223-1. URL: http://linkinghub.elsevier.com/retrieve/pii/S0026065714702231.

Clayton, Jamie, Doug Millington-Smith, and Brian Armstrong (2015). "The Application of Powder Rheology in Additive Manufacturing". In: *Jom* 67.3, pp. 544–548. ISSN: 15431851. DOI: 10.1007/s11837-015-1293-z.

Colosimo, Bianca Maria and Marco Grasso (2020). "In-situ monitoring in L-PBF: Opportunities and challenges". In: *Procedia CIRP* 94.March, pp. 388–391. ISSN: 22128271. DOI: 10.1016/j.procir.2020.09.151. URL: https://doi.org/10.1016/j.procir.2020.09.151.

Conner, Brett P., Guha P. Manogharan, Ashley N. Martof, Lauren M. Rodomsky, Caitlyn M. Rodomsky, Dakesha C. Jordan, and James W. Limperos (2014). "Making sense of 3-D printing: Creating a map of additive manufacturing products and services". In: *Additive Manufacturing* 1, pp. 64–76. ISSN: 22148604. DOI: 10.1016/j.addma.2014.08.005. URL: http://dx.doi.org/10.1016/j.addma.2014.08.005.

Cooke, April and John Slotwinski (2012). "Properties of metal powders for additive manufacturing: A review of the state of the art of metal powder property testing". In: *Additive Manufacturing Materials: Standards, Testing and Applicability*, pp. 21–48. ISSN: 9781634833035. DOI: 10.6028/NIST.IR.7873. URL: http://www.scopus.com/inward/record.url?eid=2-s2.0-84956672640&partnerID=tZOtx3y1.

Cordova, Laura, Ton Bor, Marc de Smit, Mónica Campos, and Tiedo Tinga (2020). "Measuring the spreadability of pre-treated and moisturized powders for laser powder bed fusion". In: *Additive Manufacturing* 32.April 2019, p. 101082. ISSN: 22148604. DOI: 10.1016/j.addma.2020.101082. URL: shttps://doi.org/10.1016/j.addma.2020.101082.

Cordova, Laura, Mónica Campos, and Tiedo Tinga (2019). "Revealing the Effects of Powder Reuse for Selective Laser Melting by Powder Characterization". In:

Jom. ISSN: 1047-4838. DOI: 10.1007/s11837-018-3305-2. URL: http://link.springer.com/10.1007/s11837-018-3305-2.

Cordova, Laura, Cindy Sithole, Eric Macía Rodríguez, Ian Gibson, and Mónica Campos (2023). "Impact of powder reusability on batch repeatability of Ti6Al4V ELI for PBF-LB industrial production". In: *Powder Metallurgy* 66.2, pp. 129–138. ISSN: 17432901. DOI: 10.1080/00325899.2022.2133357. URL: https://doi.org/10.1080/00325899.2022.2133357.

Cox, E.P. (1927). "A Method of Assigning Numberical and Percentage Values to the Degree of Roundness of Sand Grains". In: *Journal of Paleontology* 1.3, pp. 179–183.

Craeghs, Tom, Stijn Clijsters, Evren Yasa, and Jean-Pierre Kruth (2011). "Online quality control of selective laser melting". In: *Solid Freeform Fabrication Proceedings*, pp. 212–226. URL: http://utwired.engr.utexas.edu/lff/symposium/proceedingsarchive/pubs/Manuscripts/2011/2011-17-Craeghs.pdf.

Dawes, Jason, Robert Bowerman, and Ross Trepleton (2015). "Introduction to the Additive Manufacturing Powder Metallurgy Supply Chain". In: *Johnson Matthey Technology Review* 59.3, pp. 243–256. ISSN: 20565135. DOI: 10.1595/205651315X688686. URL: http://openurl.ingenta.com/content/xref?genre=article&issn=2056-5135&volume=59&issue=3&spage=243.

Dejene, Naol Dessalegn and Hirpa G. Lemu (2023). "Current Status and Challenges of Powder Bed Fusion-Based Metal Additive Manufacturing: Literature Review". In: *Metals* 13.2. ISSN: 20754701. DOI: 10.3390/met13020424.

Denti, Lucia, Antonella Sola, Silvio Defanti, Corrado Sciancalepore, and Federica Bondioli (2019). "Effect of Powder Recycling in Laser-based Powder Bed Fusion of Ti-6Al-4V". In: *Manufacturing Technology* 19.2, pp. 190–196. ISSN: 12132489. DOI: 10.21062/ujep/268.2019/a/1213-2489/MT/19/2/190. URL: https://arl.ujep.cz/arl-ujep/cs/detail-ujep_us_cat-0270432-Effect-of-powder-recycling-in-laserbased-powder-bed-fusion-of-Ti6Al4V/.

Dungkratok, C, N Srisukhumbowornchai, Kittichai Fakpan, M Morakotjinda, N Tosangthum, O Coovattanachai, R Krataitong, A Daraphan, B Vetayanugul, and R Tongrsri (2005). "Analysis of Tin Powder Production Using a Pilot Gas Atomiser". In: *The 19th Conference of mechanical Engineering Network of Thailand*. November 2014.

Džugan, Jan, Zbyšek Novy, Zbyšek Nový, Jan Džugan, and Zbyšek Nový (2017). "Powder Application in Additive Manufacturing of Metallic Parts". In: *Powder Metallurgy*. InTech Open. Chap. 8, pp. 183–197. DOI: http://dx.doi.org/10.5772/66874. URL: http://www.intechopen.com/books/powder-metallurgy-fundamentals-and-case-studies/powder-application-in-additive-manufacturing-of-metallic-parts.

Engeli, Roman, Thomas Etter, Simone Hövel, and Konrad Wegener (2016). "Processability of different IN738LC powder batches by selective laser melting". In: *Journal of Materials Processing Technology* 229, pp. 484–491. ISSN: 09240136. DOI: 10.1016/j.jmatprotec.2015.09.046. URL: http://dx.doi.org/10.1016/j.jmatprotec.2015.09.046.

EOS GmbH (2014). *Material Data Sheet EOS StainlessSteel 316L*. Munich.

Everton, Sarah K., Matthias Hirsch, Petros Stravroulakis, Richard K. Leach, and Adam T. Clare (2016). *Review of in-situ process monitoring and in-situ metrology for metal additive manufacturing*. Nottingham. DOI: 10.1016/j.matdes.2016.01.099.

Fedina, Tatiana, Jesper Sundqvist, John Powell, and Alexander F.H. Kaplan (2020). "A comparative study of water and gas atomized low alloy steel powders for additive manufacturing". In: *Additive Manufacturing* 36.April, p. 101675. ISSN: 22148604. DOI: 10.1016/j.addma.2020.101675. URL: https://doi.org/10.1016/j.addma.2020.101675.

Fischer, Felix Gabriel, Niklas Birk, Leroy Rooney, Lucas Jauer, and Johannes Henrich Schleifenbaum (2021). "Optical process monitoring in Laser Powder Bed Fusion using a recoater-based line camera". In: *Additive Manufacturing* 47, p. 102218. ISSN: 22148604. DOI: 10.1016/j.addma.2021.102218. URL: https://doi.org/10.1016/j.addma.2021.102218.

Foster, B.K., E W Reutzel, A R Nassar, B T Hall, S W Brown, and C J Dickman (2015). "Optical, layerwise monitoring of powder bed fusion". In: *Solid freeform fabrication proceedings*, pp. 295–307. ISBN: 9788578110796. DOI: 10.1017/CBO9781107415324.004. arXiv: arXiv:1011.1669v3.

Frazier, William E. (2014). "Metal additive manufacturing: A review". In: *Journal of Materials Engineering and Performance* 23.6, pp. 1917–1928. ISSN: 15441024. DOI: 10.1007/s11665-014-0958-z.

Getto, E., R. J. Santucci, J. Gibbs, R. Link, E. Retzlaff, B. Baker, M. Koul, B. Croom, T. Montalbano, S. Storck, E. Cimpoiasu, and E. Farnan (2023). "Powder plasma spheroidization treatment and the characterization of microstructure and mechanical properties of SS 316L powder and L-PBF builds". In: *Heliyon* 9.6, e16583. ISSN: 24058440. DOI: 10.1016/j.heliyon.2023.e16583. URL: https://doi.org/10.1016/j.heliyon.2023.e16583.

Ghasemi, Asghar and Saleh Zahediasl (2012). "Normality tests for statistical analysis: A guide for non-statisticians". In: *International Journal of Endocrinology and Metabolism* 10.2, pp. 486–489. ISSN: 1726913X. DOI: 10.5812/ijem.3505.

Gioi, Rafael Grompone Von, Jean-michel Morel, Gregory Randall, Rafael Grompone Von Gioi, Jérémie Jakubowicz, Jean-michel Morel, Gregory Randall, Rafael Grompone Von Gioi, Jean-michel Morel, Gregory Randall, Rafael Grompone Von Gioi, Jérémie Jakubowicz, Jean-michel Morel, and Gregory Randall (2012). "LSD: a Line Segment Detector". In: *Image Processing On Line* 2, pp. 35–55. ISSN: 2105-1232. DOI: 10.5201/ipol.2012.gjmr-lsd. URL: http://dx.doi.org/10.5201/ipol.2012.gjmr-lsdhttp://dx.doi.org/10.5201/ipol.2012.gjmr-lsd.

Gokuldoss, Prashanth Konda, Sri Kolla, and Jürgen Eckert (2017). "Additive manufacturing processes: Selective laser melting, electron beam melting and binder jetting-selection guidelines". In: *Materials* 10.6. ISSN: 19961944. DOI: 10.3390/ma10060672.

Gorji, N E, R O'Connor, and D Brabazon (2019). "XPS, XRD, and SEM characterization of the virgin and recycled metallic powders for 3D printing applications". In: *IOP Conference Series: Materials Science and Engineering* 591, p. 012016. DOI: 10.1088/1757-899x/591/1/012016.

Grasso, Marco and Bianca Maria Colosimo (2017). "Process defects and in situ monitoring methods in metal powder bed fusion: A review". In: *Measurement Science and Technology* 28.4. ISSN: 13616501. DOI: 10.1088/1361-6501/aa5c4f.

Grasso, Marco, Vittorio Laguzza, Quirico Semeraro, and Bianca Maria Colosimo (2016). "In-Process Monitoring of Selective Laser Melting: Spatial Detection of Defects Via Image Data Analysis". In: *Journal of Manufacturing Science and Engineering* 139.5, p. 051001. ISSN: 1087-1357. DOI: 10.1115/1.4034715. URL: http://manufacturingscience.asmedigitalcollection.asme.org/article.aspx?doi=10.1115/1.4034715.

Gu, Dongdong (2015). *Laser additive manufacturing of high-performance materials*. Springer US, pp. 1–311. ISBN: 9783662460894. DOI: 10.1007/978-3-662-46089-4. arXiv: arXiv:1011.1669v3.

Haferkamp, Lukas, Livia Haudenschild, Adriaan Spierings, Konrad Wegener, Kirstin Riener, Stefan Ziegelmeier, and Gerhard J. Leichtfried (2021). "The influence of particle shape, powder flowability, and powder layer density on part density in laser powder bed fusion". In: *Metals* 11.3, pp. 1–15. ISSN: 20754701. DOI: 10.3390/met11030418.

Harkin, Ryan, Hao Wu, Sagar Nikam, Justin Quinn, and Shaun McFadden (2020). "Reuse of Grade 23 Ti6Al4V Powder during the Laser-Based Powder Bed Fusion Process". In: *Metals* 10.12, p. 1700. ISSN: 20754701. DOI: 10.3390/met10121700.

Harkin, Ryan, Hao Wu, Sagar Nikam, Shuo Yin, Rocco Lupoi, Wilson McKay, Patrick Walls, Justin Quinn, and Shaun McFadden (2022). "Powder Reuse in Laser-Based Powder Bed Fusion of Ti6Al4V—Changes in Mechanical Properties during a Powder Top-Up Regime". In: *Materials* 15.6, p. 2238. DOI: 10.3390/ma15062238.

He, Xing, Decheng Kong, Yiqi Zhou, Li Wang, Xiaoqing Ni, Liang Zhang, Wenheng Wu, Ruixue Li, Xiaogang Li, and Chaofang Dong (2022). "Powder recycling effects on porosity development and mechanical properties of Hastelloy X alloy during laser powder bed fusion process". In: *Additive Manufacturing* 55.October 2021, p. 102840. ISSN: 22148604. DOI: 10.1016/j.addma.2022.102840. URL: https://doi.org/10.1016/j.addma.2022.102840.

Herrmann, K (2011). *Hardness testing: principles and applications*, p. 261. ISBN: 0-61503-832-9. DOI: 10.1097/00000433-198206000-00020. arXiv: arXiv:1011.1669v3.

Herzog, Dirk, Vanessa Seyda, Eric Wycisk, and Claus Emmelmann (2016). "Additive manufacturing of metals". In: *Acta Materialia* 117, pp. 371–392. ISSN: 13596454. DOI: 10.1016/j.actamat.2016.07.019. URL: http://dx.doi.org/10.1016/j.actamat.2016.07.019.

Hoeges, Simon, Alex Zwiren, and Chris Schade (2017). "Additive manufacturing using water atomized steel powders". In: *Metal Powder Report* 72.2, pp. 111–117. ISSN: 18734065. DOI: 10.1016/j.mprp.2017.01.004. URL: http://dx.doi.org/10.1016/j.mprp.2017.01.004.

Im, Taehyeob, Kopila Gurung, Sebastian Meyers, Antonio Cutolo, Huengseok Oh, Jai Sung Lee, Brecht Van Hooreweder, and Caroline Sunyong Lee (2022). "A new strategy for metal additive manufacturing using an economical water-atomized iron powder for laser powder bed fusion". In: *Journal of*

Materials Processing Technology 308.April, p. 117705. ISSN: 09240136. DOI: 10.1016/j.jmatprotec.2022.117705. URL: https://doi.org/10.1016/j.jmatprotec.2022.117705.

ISO (2016). *ISO 6508-1:2016 Metallic Materials — Rockwell hardness test — Part 1 : Test Method*.

ISO and ASTM International (2021). *ISO/ASTM 52900:2021 – Additive manufacturing — General principles — Terminology*.

Jacob, G., A. Donmez, J. Slotwinski, and S. Moylan (2016). "Measurement of powder bed density in powder bed fusion additive manufacturing processes". In: *Measurement Science and Technology* 27.11, p. 115601. ISSN: 13616501. DOI: 10.1088/0957-0233/27/11/115601. URL: http://dx.doi.org/10.1088/0957-0233/27/11/115601.

Jacob, Gregor, Christopher Brown, Alkan Donmez, Stephanie Watson, and John Slotwinski (2017). *Effects of powder recycling on stainless steel powder and built material properties in metal powder bed fusion processes*. Tech. rep. DOI: 10.6028/NIST.AMS.100-6. URL: http://nvlpubs.nist.gov/nistpubs/ams/NIST.AMS.100-6.pdf.

Jacob, Gregor, Christopher U Brown, and Alkan Donmez (2018). "The Influence of Spreading Metal Powders with Different Particle Size Distributions on the Powder Bed Density in Laser-Based Powder Bed Fusion Processes". In: *NIST Advanced Manufacturing Series*, pp. 100–17. DOI: 10.6028/NIST.AMS.100-17. URL: https://doi.org/10.6028/NIST.AMS.100-17.

Jacobsmühlen, J, S Kleszczynski, S Dorian, G Witt, and Computer Vision (2013). "High Resolution Imaging for Inspection of Laser Beam Melting Systems High Resolution Imaging for Inspection of Laser Beam Melting Systems". In: *Instrumentation and Measurement Technology Conference (I2MTC), 2013 IEEE International*, pp. 707–712.

Jillavenkatesa, A, S Dapkunas, and L Lum (2001). *Particle-size characterization*. Tech. rep. 1, p. 164. DOI: 682901795.

Kanko, Jordan A., Allison P. Sibley, and James M. Fraser (2016). "In situ morphology-based defect detection of selective laser melting through inline coherent imaging". In: *Journal of Materials Processing Technology* 231, pp. 488–500. ISSN: 09240136. DOI: 10.1016/j.jmatprotec.2015.12.024. URL: http://dx.doi.org/10.1016/j.jmatprotec.2015.12.024.

Kellens, K, E Yasa, Renaldi, W Dewulf, Jean-Pierre Kruth, and J.R Duflou (2011). "ENERGY AND RESOURCE EFFICIENCY OF SLS/SLM PROCESSES". In: *Solid Freeform Fabrication 2011: Proceedings of the 22th Annual International*, pp. 281–293. DOI: 10.1080/01402390.2011.569130. URL: http://www.tandfonline.com/doi/abs/10.1080/01402390.2011.569130%5Cnhttp://proxy.library.upenn.edu:2195/doi/abs/10.1080/01402390.2011.569130.

Kellner, Tomas (2015). *The FAA Cleared the First 3D Printed Part to Fly in a Commercial Jet Engine from GE*. URL: https://www.ge.com/reports/post/116402870270/the-faa-cleared-the-first-3d-printed-part-to-fly-2/ (visited on 10/09/2018).

Kinsella, Mary E (2008). *Additive Manufacturing of Superalloys for Aerospace Applications*. Tech. rep.

Kirchner, A., B. Kloeden, B. Weissgaerber, and B. Kieback (2016). "Powders for additive manufacturing". In: *World PM2016*. ISBN: 9781899072484. DOI: 10.1186/cc3927.

Klar, Erhard and Prasan K. Samal (2007). *Powder Metallurgy Stainless Steels : Processing, Microstructures, and Properties*. A S M International, p. 243. DOI: 10.1361/pmss2007p023.

Land, William S., Bin Zhang, John Ziegert, and Angela Davies (2015). "In-Situ Metrology System for Laser Powder Bed Fusion Additive Process". In: *Procedia Manufacturing* 1, pp. 393–403. ISSN: 23519789. DOI: 10.1016/j.promfg.2015.09.047. URL: http://www.sciencedirect.com/science/article/pii/S2351978915010471.

Lanzutti, A., F. Sordetti, R. Montanari, A. Varone, E. Marin, F. Andreatta, S. Maschio, E. Furlani, M. Magnan, E. Vaglio, E. Pakhomova, M. Sortino, G. Totis, and L. Fedrizzi (2023). "Effect of powder recycling on inclusion content and distribution in AISI 316L produced by L-PBF technique". In: *Journal of Materials Research and Technology* 23, pp. 3638–3650. ISSN: 22387854. DOI: 10.1016/j.jmrt.2023.02.017. URL: https://doi.org/10.1016/j.jmrt.2023.02.017.

Lee, Dong Kyu, Junyong In, and Sangseok Lee (2015). "Standard deviation and standard error of the mean". In: *Korean Journal of Anesthesiology* 68.3, pp. 220–223. ISSN: 20057563. DOI: 10.4097/kjae.2015.68.3.220.

Li, Ruidi, Jinhui Liu, Yusheng Shi, Li Wang, and Wei Jiang (2012). "Balling behavior of stainless steel and nickel powder during selective laser melting process". In: *International Journal of Advanced Manufacturing Technology* 59.9-12, pp. 1025–1035. ISSN: 02683768. DOI: 10.1007/s00170-011-3566-1.

Liu, Bochuan, Ricky Wildman, Christopher Tuck, Ian Ashcroft, and Richard Hague (2011). "Investigaztion the effect of particle size distribution on processing parameters optimisation in selective laser melting process". In: *22nd Annual International Solid Freeform Fabrication Symposium - An Additive Manufacturing Conference*. October 2015, pp. 227–238.

Lott, Philipp, Henrich Schleifenbaum, Wilhelm Meiners, Konrad Wissenbach, Christian Hinke, and Jan Bultmann (2011). "Design of an optical system for the in situ process monitoring of Selective Laser Melting (SLM)". In: *Physics Procedia* 12.PART 1, pp. 683–690. ISSN: 18753884. DOI: 10.1016/j.phpro.2011.03.085. URL: http://dx.doi.org/10.1016/j.phpro.2011.03.085.

Lu, Chao, Ruihua Zhang, Mengzhi Xiao, Xiaohong Wei, Yan Yin, Yuebo Qu, Hui Li, Pengyu Liu, Xiaopan Qiu, and Tieming Guo (2022a). "A comprehensive characterization of virgin and recycled 316L powders during laser powder bed fusion". In: *Journal of Materials Research and Technology* 18, pp. 2292–2309. ISSN: 22387854. DOI: 10.1016/j.jmrt.2022.03.125. URL: https://doi.org/10.1016/j.jmrt.2022.03.125.

– (2022b). "A comprehensive characterization of virgin and recycled 316L powders during laser powder bed fusion". In: *Journal of Materials Research and Technology* 18, pp. 2292–2309. ISSN: 22387854. DOI: 10.1016/j.jmrt.2022.03.125. URL: https://doi.org/10.1016/j.jmrt.2022.03.125.

Lutter-Günther, Max, Christian Gebbe, Tobias Kamps, Christian Seidel, and Gunther Reinhart (2018). "Powder recycling in laser beam melting: strategies,

consumption modeling and influence on resource efficiency". In: *Production Engineering* 12.3-4, pp. 377–389. ISSN: 18637353. DOI: 10.1007/s11740-018-0790-7. URL: http://dx.doi.org/10.1007/s11740-018-0790-7.

Manfredi, D., F. Calignano, E. P. Ambrosio, M. Krishnan, R. Canali, S. Biamino, M. Pavese, E. Atzeni, L. Luliano, P. Fino, and C. Badini (2013). "Direct Metal Laser Sintering: An additive manufacturing technology ready to produce lightweight structural parts for robotic applications". In: *Metallurgia Italiana* 105.10, pp. 15–24. ISSN: 00260843. DOI: 10.1016/j.jallcom.2016.10.285.

Mani, Manesh, Brandon M. Lane, Shaw C. Feng, Shawn P. Moylan, Alkan Donmez, and Ronnie Fesperman (2016). "A review on measurement science needs for real-time control of additive manufacturing metal powder bed fusion processes". In: *International Journal of Production Research* 55.5, pp. 1400–1418. ISSN: 1366588X. DOI: 10.1080/00207543.2016.1223378.

Manriquez-Frayre, J.A and D.L. Bourell (1990). "Selective laser sintering of binary metallic powder". In: *Proceedings of the Solid Freeform Fabrication Symposim*, pp. 99–106. URL: http://utwired.engr.utexas.edu/lff/symposium/proceedingsArchive/pubs/Manuscripts/1990/1990-09-Frayre.pdf.

McCann, Ronan, Muhannad A. Obeidi, Cian Hughes, Éanna McCarthy, Darragh S. Egan, Rajani K. Vijayaraghavan, Ajey M. Joshi, Victor Acinas Garzon, Denis P. Dowling, Patrick J. McNally, and Dermot Brabazon (2021). "In-situ sensing, process monitoring and machine control in Laser Powder Bed Fusion: A review". In: *Additive Manufacturing* 45.April. ISSN: 22148604. DOI: 10.1016/j.addma.2021.102058.

Miao, Guanxiong, Wenchao Du, Zhijian Pei, and Chao Ma (2022). "A literature review on powder spreading in additive manufacturing". In: *Additive Manufacturing* 58.May, p. 103029. ISSN: 22148604. DOI: 10.1016/j.addma.2022.103029. URL: https://doi.org/10.1016/j.addma.2022.103029.

Moghimian, Pouya, Thomas Poiri, Mahdi Habibnejad-korayem, Javier Arreguin, and Jens Kroeger (2021). "Metal powders in additive manufacturing : A review on reusability and recyclability of common titanium , nickel and aluminum alloys". In: 43.March. DOI: 10.1016/j.addma.2021.102017.

Moylan, Shawn, John Slotwinski, April Cooke, Kevin Jurrens, and M. Alkan Donmez (2013). "Lessons learned in establishing the NIST metal additive manufacturing laboratory". In: ISSN: 0960-1643. DOI: 10.6028/NIST.TN.1801. URL: http://nvlpubs.nist.gov/nistpubs/TechnicalNotes/NIST.TN.1801.pdf.

Mussatto, Andre, Robert Groarke, Aidan O'Neill, Muhannad Ahmed Obeidi, Yan Delaure, and Dermot Brabazon (2021). "Influences of powder morphology and spreading parameters on the powder bed topography uniformity in powder bed fusion metal additive manufacturing". In: *Additive Manufacturing* 38.November 2020, p. 101807. ISSN: 22148604. DOI: 10.1016/j.addma.2020.101807. URL: https://doi.org/10.1016/j.addma.2020.101807.

Neef, A., V. Seyda, D. Herzog, C. Emmelmann, M. Schönleber, and M. Kogel-Hollacher (2014). "Low coherence interferometry in selective laser melting". In: *Physics Procedia* 56.C, pp. 82–89. ISSN: 18753892. DOI: 10.1016/j.phpro.2014.08.100.

O'Leary, Richard, Rossi Setchi, Paul Prickett, Gareth Hankins, Nick Jones, Richard O Leary, Rossi Setchi, Paul Prickett, Gareth Hankins, and Nick Jones (2015). "An Investigation into the Recycling of Ti-6Al-4V Powder Used Within SLM to Improve Sustainability". In: *SDM'2015: 2nd International Conference on Sustainable Design and Manufacturing , (2015)*, pp. 14–17. ISBN: 0904-213X. DOI: 10.1016/j.surfcoat.2006.07.216.

Pagani, Luca, Marco Grasso, Paul J. Scott, and Bianca M. Colosimo (2020). "Automated layerwise detection of geometrical distortions in laser powder bed fusion". In: *Additive Manufacturing* 36.July, p. 101435. ISSN: 22148604. DOI: 10.1016/j.addma.2020.101435. URL: http://dx.doi.org/10.1016/j.addma.2020.101435.

Park, H S, N H Tran, and D S Nguyen (2017). "Development of a predictive system for SLM product quality". In: *IOP Conference Series: Materials Science and Engineering*. Vol. 227, p. 012090. DOI: 10.1088/1757-899X/227/1/012090. URL: http://stacks.iop.org/1757-899X/227/i=1/a=012090?key=crossref.c0cfb82e8a66d36b1aeae741c6a23919.

Pinkerton, Andrew J. and Lin Li (2005). "Direct additive laser manufacturing using gas- and water-atomised H13 tool steel powders". In: *International Journal of Advanced Manufacturing Technology* 25.5-6, pp. 471–479. ISSN: 02683768. DOI: 10.1007/s00170-003-1844-2.

Popov, Valadamir V., Alexander Katz-demyanetz, Andrey Garkun, and Menachem Bamberger (2018). "The effect of powder recycling on the mechanical properties and microstructure of electron beam mPowder recycling effect in Electron Beam Melting of Ti-6Al-4V specimens". In: *Additive Manufacturing*. DOI: 10.1016/j.addma.2018.06.003.

Popovich, Anatoliy and Vadim Sufiiarov (2016). "Metal Powder Additive Manufacturing". In: *New Trends in 3D Printing*, pp. 215–236. ISBN: 9789537619343. DOI: 10.5772/63337. arXiv: 0803973233. URL: http://www.intechopen.com/books/new-trends-in-3d-printing/metal-powder-additive-manufacturing.

R Development Team (2019). *R: A Language and Environment for Statistical Computing*. Vienna.

Reilly, James (2006). *Using Statisics*. 1st. Dublin: Gill and Macmillian, p. 180.

Sames, W. J., F. A. List, S. Pannala, R. R. Dehoff, and S. S. Babu (2016). "The metallurgy and processing science of metal additive manufacturing". In: *International Materials Reviews* 61.5, pp. 315–360. ISSN: 17432804. DOI: 10.1080/09506608.2015.1116649. URL: http://www.tandfonline.com/doi/full/10.1080/09506608.2015.1116649.

Santecchia, Eleonora, Stefano Spigarelli, and Marcello Cabibbo (2020). "Material reuse in laser powder bed fusion: Side effects of the laser—metal powder interaction". In: *Metals* 10.3, pp. 1–21. ISSN: 20754701. DOI: 10.3390/met10030341.

Sartin, B, T Pond, B Griffith, W Everhart, L Elder, E Wenski, C Cook, D Wieliczka, W King, A Rubenchik, S Wu, B Brown, C Johnson, and J Crow (2017). "316L Powder Reuse for Metal Additive Manufacturing". In: *Proceedings of the 28th Annual International Solid Freeform Fabrication Symposium*, pp. 351–364. URL:

https://sffsymposium.engr.utexas.edu/sites/default/files/2017/Manuscripts/316LPowderReuseforMetalAdditiveManufacturing.pdf.

Schade, C T, T F Murphy, and C Walton (2014). "Development of atomized powders for additive manufacturing". In: *2014 World Congress on Powder Metallurgy and Particulate Materials, PM 2014*, pp. 215–225. ISBN: 0985339764. DOI: 10.1111/imj.12580. URL: https://www.scopus.com/inward/record.uri?eid=2-s2.0-84945896244&partnerID=40&md5=2702b2490ff4241477ee089e65babe55.

Schueren, B. Van Der and J.P. Kruth (1995). "Powder deposition in selective metal powder sintering". In: *Rapid Prototyping Journal* 1.3, pp. 23–31. ISSN: 1355-2546. DOI: 10.1108/13552549510094241.

Scime, Luke and Jack Beuth (2018). "Anomaly detection and classification in a laser powder bed additive manufacturing process using a trained computer vision algorithm". In: *Additive Manufacturing* 19, pp. 114–126. ISSN: 22148604. DOI: 10.1016/j.addma.2017.11.009. URL: http://dx.doi.org/10.1016/j.addma.2017.11.009.

Scime, Luke, Derek Siddel, Seth Baird, and Vincent Paquit (2020). "Layer-wise anomaly detection and classification for powder bed additive manufacturing processes: A machine-agnostic algorithm for real-time pixel-wise semantic segmentation". In: *Additive Manufacturing* 36.July, p. 101453. ISSN: 22148604. DOI: 10.1016/j.addma.2020.101453. URL: https://doi.org/10.1016/j.addma.2020.101453.

Scipioni Bertoli, Umberto, Gabe Guss, Sheldon Wu, Manyalibo J. Matthews, and Julie M. Schoenung (2017). "In-situ characterization of laser-powder interaction and cooling rates through high-speed imaging of powder bed fusion additive manufacturing". In: *Materials and Design* 135, pp. 385–396. ISSN: 18734197. DOI: 10.1016/j.matdes.2017.09.044. URL: https://doi.org/10.1016/j.matdes.2017.09.044.

Seyda, V., N. Kaufmann, and C. Emmelmann (2012). "Investigation of Aging Processes of Ti-6Al-4 v Powder Material in Laser Melting". In: *Physics Procedia* 39, pp. 425–431. ISSN: 18753892. DOI: 10.1016/j.phpro.2012.10.057. URL: http://dx.doi.org/10.1016/j.phpro.2012.10.057.

Shamvedi, Deepak, Oliver McCarthy, Eoghan O'Donoghue, Paul O'Leary, and Ramesh Raghavendra (2017). "Improved Performance of 3D Metal Printed Antenna through Gradual Reduction in Surface Roughness". In: *2017 International Conference on Electromagnetics in Advanced Applications (ICEAA)*. Vol. 6. Verona, pp. 669–672.

Singh, Sunpreet, Seeram Ramakrishna, and Rupinder Singh (2017). "Material issues in additive manufacturing: A review". In: *Journal of Manufacturing Processes* 25, pp. 185–200. ISSN: 15266125. DOI: 10.1016/j.jmapro.2016.11.006. URL: http://dx.doi.org/10.1016/j.jmapro.2016.11.006.

Slotwinski, J. A., E. J. Garboczi, P. E. Stutzman, C. F. Ferraris, S. S. Watson, and M. A. Peltz (2014). "Characterization of Metal Powders Used for Additive Manufacturing". In: *Journal of Research of the National Institute of Standards and Technology* 119, pp. 460–493. ISSN: 2165-7254. DOI: 10.6028/jres.119.018. URL: http://nvlpubs.nist.gov/nistpubs/jres/119/jres.119.018.pdf.

Slotwinski, John and Shawn Moylan (2014). "Applicability of existing materials testing standards for additive manufacturing materials". In: *Additive Manufacturing Materials: Standards, Testing and Applicability*, pp. 49–66. URL: http://www.scopus.com/inward/record.url?eid=2-s2.0-84956679113&partnerID=tZOtx3y1.

Smolina, Irina, Konrad Gruber, Andrzej Pawlak, Grzegorz Ziółkowski, Emilia Grochowska, Daniela Schob, Karol Kobiela, Robert Roszak, Matthias Ziegenhorn, and Tomasz Kurzynowski (2022). "Influence of the AlSi7Mg0.6 Aluminium Alloy Powder Reuse on the Quality and Mechanical Properties of LPBF Samples". In: *Materials* 15.14. ISSN: 19961944. DOI: 10.3390/ma15145019.

Spears, Thomas G. and Scott A. Gold (2016). "In-process sensing in selective laser melting (SLM) additive manufacturing". In: *Integrating Materials and Manufacturing Innovation* 5.2. ISSN: 2193-9764. DOI: 10.1186/s40192-016-0045-4. URL: http://link.springer.com/10.1186/s40192-016-0045-4.

Spierings, A. B., M. Schneider, and R. Eggenberger (2011). "Comparison of density measurement techniques for additive manufactured metallic parts". In: *Rapid Prototyping Journal* 17.5, pp. 380–386. ISSN: 13552546. DOI: 10.1108/13552541111156504.

Spierings, A. B., M. Voegtlin, T. Bauer, and K. Wegener (2015). "Powder flowability characterisation methodology for powder-bed-based metal additive manufacturing". In: *Progress in Additive Manufacturing* 1.1-2, pp. 9–20. ISSN: 2363-9512. DOI: 10.1007/s40964-015-0001-4. URL: http://link.springer.com/10.1007/s40964-015-0001-4.

Spierings, A.B, N. Herres, and G. Levy (2011). "Influence of the particle size distribution on surface quality and mechanical properties in AM steel parts". In: *Rapid Prototyping Journal* 17.3, pp. 195–202. ISSN: 13552546. DOI: https://doi.org/10.1108/13552541111124770. arXiv: arXiv:1011.1669v3.

Strondl, A., O. Lyckfeldt, H. Brodin, and U. Ackelid (2015). "Characterization and Control of Powder Properties for Additive Manufacturing". In: *Jom* 67.3, pp. 549–554. ISSN: 15431851. DOI: 10.1007/s11837-015-1304-0.

Stryker (2016). *Tritanium Manufacturing Overview*. Tech. rep. New Jersey. URL: http://www.stryker.com/builttofuse/media/assets/TRITA-BR-2TritaniumManufacturingOverviewFINAL.pdf.

Sturm, Logan, Mohammed Albakri, Christopher B Williams, and Pablo Tarazaga (2016). "In-Situ Detection of Build Defects in Additive Manufacturing via Impedance-Based Monitoring". In: *27th Annual International Solid Freeform Fabrication Symposium - An Additive Manufacturing Conference*, pp. 1458–1478.

Sukal, Jan A N, David Palousek, and Daniel Koutny (2018). "THE EFFECT OF RECYCLING POWDER STEEL ON POROSITY AND SURFACE ROUGHNESS OF SLM PARTS". In: *MM Science Journal* March, pp. 2643–2647. DOI: 10.17973/MMSJ.2018.

Sun, Y. Y., S. Gulizia, C. H. Oh, C. Doblin, Y. F. Yang, and M. Qian (2015). "Manipulation and Characterization of a Novel Titanium Powder Precursor for Additive Manufacturing Applications". In: *Jom* 67.3, pp. 564–572. ISSN: 15431851. DOI: 10.1007/s11837-015-1301-3.

Sun, Zhongji, Xipeng Tan, Shu Beng Tor, and Wai Yee Yeong (2016). "Selective laser melting of stainless steel 316L with low porosity and high build rates". In:

Materials and Design 104, pp. 197–204. ISSN: 18734197. DOI: 10.1016/j.matdes.2016.05.035. URL: http://dx.doi.org/10.1016/j.matdes.2016.05.035.

Sutton, Austin T., Caitlin S. Kriewall, Ming C. Leu, and Joseph W. Newkirk (2016a). "Powder characterisation techniques and effects of powder characteristics on part properties in powder-bed fusion processes". In: *Virtual and Physical Prototyping* 12.1, pp. 3–29. ISSN: 17452767. DOI: 10.1080/17452759.2016.1250605.

Sutton, Austin T, Caitlin S Kriewall, Ming C Leu, and Joseph W Newkirk (2016b). "Powders for Additive Manufacturing Processes: Characterization Techniques and Effects on Part Properties". In: *Solid Freeform Fabrication Proceedings*, pp. 1004–1030. DOI: 10.1080/17452759.2016.1250605.

Tan, Jun Hao, Wai Leong Eugene Wong, and Kenneth William Dalgarno (2017). "An overview of powder granulometry on feedstock and part performance in the selective laser melting process". In: *Additive Manufacturing* 18, pp. 228–255. ISSN: 22148604. DOI: 10.1016/j.addma.2017.10.011. URL: http://dx.doi.org/10.1016/j.addma.2017.10.011.

Tang, H. P., M. Qian, N. Liu, X. Z. Zhang, G. Y. Yang, and J. Wang (2015). "Effect of Powder Reuse Times on Additive Manufacturing of Ti-6Al-4V by Selective Electron Beam Melting". In: *Jom* 67.3, pp. 555–563. ISSN: 15431851. DOI: 10.1007/s11837-015-1300-4.

Thijs, Lore, Frederik Verhaeghe, Tom Craeghs, Jan Van Humbeeck, and Jean Pierre Kruth (2010). "A study of the microstructural evolution during selective laser melting of Ti-6Al-4V". In: *Acta Materialia* 58.9, pp. 3303–3312. ISSN: 13596454. DOI: 10.1016/j.actamat.2010.02.004. URL: http://dx.doi.org/10.1016/j.actamat.2010.02.004.

Tofail, Syed A.M., Elias P. Koumoulos, Amit Bandyopadhyay, Susmita Bose, Lisa O'Donoghue, and Costas Charitidis (2018). "Additive manufacturing: scientific and technological challenges, market uptake and opportunities". In: *Materials Today* 21, pp. 22–37. ISSN: 13697021. DOI: 10.1016/j.mattod.2017.07.001. URL: http://www.sciencedirect.com/science/article/pii/S1369702117301773.

Townsend, A., N. Senin, L. Blunt, R. K. Leach, and J. S. Taylor (2016). "Surface texture metrology for metal additive manufacturing: a review". In: *Precision Engineering* 46, pp. 34–47. ISSN: 01416359. DOI: 10.1016/j.precisioneng.2016.06.001. URL: http://dx.doi.org/10.1016/j.precisioneng.2016.06.001.

Traini, T., C. Mangano, R. L. Sammons, F. Mangano, A. Macchi, and A. Piattelli (2008). "Direct laser metal sintering as a new approach to fabrication of an isoelastic functionally graded material for manufacture of porous titanium dental implants". In: *Dental Materials* 24.11, pp. 1525–1533. ISSN: 01095641. DOI: 10.1016/j.dental.2008.03.029.

Upadhyaya, G. S. (1996). *Powder Metallurgy Technology*. Cambridge: Cambridge International Science Publishing, p. 169. ISBN: 9781898326403.

Vafadar, Ana, Ferdinando Guzzomi, Alexander Rassau, and Kevin Hayward (2021). "Advances in metal additive manufacturing: A review of common processes, industrial applications, and current challenges". In: *Applied Sciences (Switzerland)* 11.3, pp. 1–33. ISSN: 20763417. DOI: 10.3390/app11031213.

Vock, Silvia, Burghardt Klöden, Alexander Kirchner, Thomas Weißgärber, and Bernd Kieback (2019). "Powders for powder bed fusion: a review". In: *Progress*

in Additive Manufacturing 0.0, p. 0. ISSN: 2363-9512. DOI: 10.1007/s40964-019-00078-6. URL: http://dx.doi.org/10.1007/s40964-019-00078-6.

Wang, Liyi, Zhijian Tan, Shengxiang Wang, Weiqiang Liu, Jiazheng Hao, Xuekai Zhang, Sihao Deng, Chaoju Yu, Haibiao Zheng, Zhirong Zeng, Huaile Lu, Lunhua He, and Jie Chen (2023a). "Atomization gases dependent mechanical properties in the laser powder bed fusion manufactured 304L stainless steel". In: *Journal of Materials Processing Technology* 316.March, p. 117966. ISSN: 09240136. DOI: 10.1016/j.jmatprotec.2023.117966. URL: https://doi.org/10.1016/j.jmatprotec.2023.117966.

Wang, Xuan, Ying Zhang, Dafan Du, Anping Dong, Baode Sun, Zhiying Chen, Xuewen Zheng, Xiang Wang, Yufei Liu, Jikai Zhou, and Sinuo Kong (2023b). "Evolutionary behavior of Haynes 230 powder during laser powder bed fusion cycle and its effect on the mechanical performance of manufactured parts". In: *Materials Today Communications* 34.October 2022, p. 105384. ISSN: 23524928. DOI: 10.1016/j.mtcomm.2023.105384. URL: https://doi.org/10.1016/j.mtcomm.2023.105384.

Whitehouse, David (2002). *Surfaces and their Measurement*. London: Hermes Penton Science. ISBN: 1903996011.

Wohlers (2023). *Wohlers Report 2023*.

Wohlers, Terry (2018). *Wohlers Report 2018*. ISBN: 978-0-9913332-2-6.

Wong, Kaufui V. and Aldo Hernandez (2012). "A Review of Additive Manufacturing". In: *ISRN Mechanical Engineering* 2012, pp. 1–10. ISSN: 2090-5130. DOI: 10.5402/2012/208760. arXiv: 208760. URL: http://www.hindawi.com/journals/isrn.mechanical.engineering/2012/208760/.

Xiong, Lianghua, Andrew Chihpin Chuang, Jonova Thomas, Timothy Prost, Emma White, Iver Anderson, and Dileep Singh (2022). "Defect and satellite characteristics of additive manufacturing metal powders". In: *Advanced Powder Technology* 33.3, p. 103486. ISSN: 15685527. DOI: 10.1016/j.apt.2022.103486. URL: https://doi.org/10.1016/j.apt.2022.103486.

Yan, Jujie, Xingmin Zhang, Wai-Meng Quach, Ming Yan, Yinghao Zhou, and Ruinan Gu (2019). "A Comprehensive Study of Steel Powders (316L, H13, P20 and 18Ni300) for Their Selective Laser Melting Additive Manufacturing". In: *Metals*. DOI: 10.3390/met9010086.

Yánez, Alejandro, María Paula Fiorucci, Oscar Martel, and Alberto Cuadrado (2022). "The Influence of Dimensions and Powder Recycling on the Roughness and Mechanical Properties of Ti-6Al-4V Parts Fabricated by Laser Powder Bed Fusion". In: *Materials* 15.16. ISSN: 19961944. DOI: 10.3390/ma15165787.

Yoo, Jaehong, Kyutae Han, Younghwan Park, and Changhee Lee (2014). "Effect of silicon on the solidification cracking behavior and metastable carbide formation in austenitic high Mn steel welds". In: *Materials Chemistry and Physics* 148.3, pp. 499–502. ISSN: 02540584. DOI: 10.1016/j.matchemphys.2014.08.053. URL: http://dx.doi.org/10.1016/j.matchemphys.2014.08.053.

Yu, A. B. and J. S. Hall (1994). "Packing of fine powders subjected to tapping". In: *Powder Technology* 78.3, pp. 247–256. ISSN: 00325910. DOI: 10.1016/0032-5910(93)02790-H.

Zegzulka, Jiri, Daniel Gelnar, Lucie Jezerska, Rostislav Prokes, and Jiri Rozbroj (2020). "Characterization and flowability methods for metal powders". In:

Scientific Reports 10.1, pp. 1–20. ISSN: 20452322. DOI: 10.1038/s41598-020-77974-3. URL: https://doi.org/10.1038/s41598-020-77974-3.

Zhao, Yufan, Yujie Cui, Yusaku Hasebe, Huakang Bian, Kenta Yamanaka, Kenta Aoyagi, Takehito Hagisawa, and Akihiko Chiba (2021). "Controlling factors determining flowability of powders for additive manufacturing: A combined experimental and simulation study". In: *Powder Technology* 393, pp. 482–493. ISSN: 1873328X. DOI: 10.1016/j.powtec.2021.08.006. URL: https://doi.org/10.1016/j.powtec.2021.08.006.

Zielinski, Jonas, Simon Vervoort, Hans-Wilfried Mindt, and Mustafa Megahed (2017). "Influence of Powder Bed Characteristics on Material Quality in Additive Manufacturing". In: *BHM Berg- und Hüttenmännische Monatshefte* 162.5, pp. 192–198. ISSN: 0005-8912. DOI: 10.1007/s00501-017-0592-9. URL: http://link.springer.com/10.1007/s00501-017-0592-9.